Scuola Internazionale Superiore di Studi Avanzati - Trieste

Accretion Flows in Active Galaxies

Thesis submitted to the
International School for Advanced Studies, Trieste, Italy
- Astrophysics Sector -
in partial fulfillment of the requirements for the degree of

Doctor Philosophiae

Candidate:

Paola Marziani

Supervisors:

Prof. Dennis W. Sciama
Prof. Massimo Calvani
Prof. Piero Rafanelli

Academic Year 1990/91

SISSA – Via Beirut 2-4 – 34014 TRIESTE – ITALY

Εἰπὲ πόθεν σὺ μετρεῖς χόσμον χαὶ πείρατα γαίης
ἐξ ὀλίγης γαίης σῶμα φέρων ὀλίγον.
σαυτὸν ἀρίθμησον πρότερον χαὶ γνῶθι σεαυτόν,
χαὶ τότ' ἀριθμησήις γαῖαν ἀπειρεσίην.
εἰ δ' ὀλίγον πηλὸν τοῦ σώματος οὐ χαταριθμεῖς,
πῶς δύνασαι γνῶναι τῶν ἀμέτρων τὰ μέτρα;

Aim and Plan of this work

Accretion of matter onto a massive black hole is believed to be the power source of Active Galactic Nuclei (AGN). The idea that its ultimate manifestation is the release of gravitational energy in an accretion disk around the black hole has gained wide acceptance in the scientific community, although many aspects remain open to question. The main reason for this resides in the very limited spatial extent of the central engine producing the power output of AGN, $\lesssim 1pc$*, so that direct resolution of the accretion disk is far beyond our capabilities even in the nearest AGN. Since there is probably not enough supply of matter available in situ in the galactic nucleus, the accretion flow should be triggered in the bulge or in the disk of the galaxy. There is no general consensus as far as the triggering mechanism is concerned. We have thus focussed our investigation on the origin of the accretion flow, and on its ultimate stage – the accretion disk.*

Material at a non–trivial rate of ~ 0.1*–*$10\ M_\odot\ yr^{-1}$ *(depending on the AGN luminosity) should be able to reach the central black hole. It is unclear how the galactic gas can loose its angular momentum, drift toward the center of the galaxy, ultimately reach the central parsec of the active nucleus to provide its fuel. In order to study the relevance of interaction with a close companion galaxy in driving gravitational instabilities able to channel the gas flow toward the active nucleus, we have analyzed at first the frequency of companion galaxies among Seyfert galaxies (Chapter 2). The path of the accretion flow is complicated by the occurrence of dissipative processes which produce not only radial drift of gas, but also enhance the star formation rate, producing a Starburst in the most extreme cases. There is evidence suggesting a link between interaction, bursts of star formation, and fueling of AGN, but it is not clear whether a Starburst is a necessary preliminary for the birth of an AGN. Intermediate objects, which show features of a Starburst as well as of a Seyfert galaxy, and at the same time belong to an interacting system, are ideal laboratories in order to analyze the effects of interaction on the star formation rate and on the gas kinematics, and any connection with the nuclear activity. In Chapter 3, we study in detail the spectroscopic properties of one of these systems, NGC 7592.*

The ultimate stage of the accretion flow is probably to build up an accretion disk. If

the accretion rate is above a critical value, the accretion flow may become geometrically thick, and the radiation emitted would be probably anisotropic. We have pursued a test based on the analysis of the profiles of the broad low ionization profile to search for an unmistakable signature of the accretion disk. This test has been concentrated on some selected best candidates *as well as on a statistical analysis of the emission line profile for a large sample of AGN (Chapter 4). In Chapter 5 we have investigated the effect that anisotropic emission from a thick accretion disk may have on the luminosity function of the AGN, and on the estimate of the central masses.*
In the first Chapter we review some basic aspects of AGN, and we discuss the present status of the art on the problems pointed above. In the concluding remarks (Chapter 6) the original contributions obtained in this work are summarized, and plans for further investigations are discussed.

Acknowledgements

I'm greatly indebted to my supervisors, Profs. D.W. Sciama, M. Calvani, P. Rafanelli, for encouragement and support.
In the course of the last years, I have moreover benefitted of stimulating discussions related to the topics of this works with many astrophycists, among them J.W. Sulentic, C.M. Urry, W. Zheng, J. Acosta-Pulido, P. Grandi, G.Byrd, M. Joly.
The hospitality of the Padova Department of Astronomy and Observatory, where part of this work was done, is gratefully acknowledged.

Contents

Chapter 1

Accretion flows in active galaxies

Abstract – An accretion disk around a supermassive black hole is believed to be the power source of AGN. In this chapter we discuss the current perspective on the possibility that circumnuclear/disk gas can reach the inner parsec of the active nucleus to ultimately build up the accretion disk. We analyze observational evidence and theoretical considerations supporting the existence of the accretion disk, and we suggest the feasibility of a test based on the emission line profiles in order to reveal the accretion disk itself.

1.1 Introduction

Active Galactic Nuclei (AGN) are a very wide and somewhat heterogeneous class of objects, which span several order of magnitudes in bolometric luminosity ($L_{bol} \sim 10^{43} - 10^{48} erg\ s^{-1}$). Nevertheless, there seems to be at least one underlying basic property: the power output of AGN is too large, and emitted in a region of too small size ($d < 0.1\ pc$), to be readily explained even by the most powerful energy release processes involved in the evolutionary stages of normal stars. Although some galaxies with very bright nuclei and a strong emission line spectrum were known since 1943 thank to the work of C. Seyfert, the matter was in a state of lethargy until the discovery of quasars by M. Schmidt in 1963. The identification of the lines observed in the optical spectrum of a stellar–like object, associated with the radio source 3C273 with the Balmer lines redshifted by $z = 0.158$ opened literally a new era in extragalactic astronomy. If the redshift was due to cosmological recession, the luminosity output of this object had to be considered enormous, approximately $L \sim 10^{47}\ erg\ s^{-1}$. Several conflicting models were proposed in the following years, ranging from fine–tuned supernova events, and/or supermassive stars (Colgate and Cameron, 1963; in the most recent form, Terlevich and Melnick, 1987), supermagnetized cores (*e.g.* Kundt, 1987, and references therein), white holes (Ne'eman, 1965), and release of gravitational energy from matter accreting onto black holes (Salpeter, 1964; Zel'dovich and Novikov, 1964). Growing evidence has been collected since then in favour of the last model. It was soon realized that high angular momentum of the gas flowing onto a compact object would lead to the

formation of an accretion disk (*e.g.* Rees, 1984, and references therein), and that the release of gravitational energy via viscous torques in the accretion disk was a very suitable power source for quasars. The last years have seen a steadily increasing effort in order to constrain working mode of the *central engine*, through extensive observations of the emission lines, of the overall continuum and of their variations, the and to search for indirect signatures of the accretion disk. However, observations provide much circumstantial evidence of the presence of the central black hole and of the accretion disk, but a definite probe is lacking as yet (§ 1.6. § 1.7).

A very important point is related to the accreting matter that should build up the accretion disk and accrete the black hole. Since it is very probable that not enough reservoir of matter is available in the galactic nucleus, a flow of gas should be channeled toward the very center of the galaxy from the circumnuclear regions and/or from the galatic disk. The origin and evolution of activity is thus strongly coupled to events occurring on galactic scale (section §1.4). The path the flow has to cover is not easy. The gas has to loose its angular momentum in order reach the central core of the AGN. Gravitational instabilities induced by interaction with a nearby companion galaxy can probably lead to radial flows (§1.4), at least down to $\sim$ 100 *pc* from the very center of the galaxy. Since interaction has also a very direct and strong effect on the star formation rate of galaxies (§1.4.2), gas could be at first consumed in a burst of star formation in the disk or in the circumnuclear region of the *candidate* AGN. It is be necessary to investigate whether interaction, burst of star formation and AGN are causally linked (§1.4.3) in order to clarify in which stage the accretion material is provided to the active nucleus.

In this Chapter, we briefly review at first the basilar properties of the continuum and of the emission line regions of AGN. We then discuss the aspects related to the fuelling problem, and subsequently the observational facts on which our belief of the existence of an accretion disk surrounding a central black hole in the core of AGN is based. A preliminary analysis of the mechanisms of line formations motivates the search (described in Chapter 4) of AGN in which lines are emitted by the accretion disk. Last, we analyze the mechanisms responsible for the anisotropic emission of the radiation field and the most important unified schemes recently proposed for AGN.

1.2 The overall continuum of AGN

A representative continuum for the most fundamental AGN classes is shown in Fig. 2.1. AGN are classified according to the ratio of the radio to optical continuum luminosity, the bolometric luminosity, and the polarization degree of the continuum (for a systematic discussion of the propeties of various AGN classes see Lawrence (1987) and Marziani (1989)). The most remarkable spectral differences are between high polarization objects (*blazars*, only a tiny fraction of total AGN) and *non–blazars* AGN. *Blazars* show a nearly featureless continuum not far from a *canonical* power law $f_\nu \propto \nu^{-\alpha}$, with $\alpha \sim 1$, due to non–thermal emission processes, probably synchrotron radiation. The

strong variability (also a factor ~ 100) suggests that the continuum is relativistically beamed toward us (Angel and Stockman, 1980; Urry, 1990). *Non–blazars* AGN have a small fraction of polarized flux (~ 1 %) and a more complex continuum shape. At least two features are superimposed to a power law emission: (1) the *Big Bump*, spanning from $1\mu m$ to the soft X ray range, that will be extensively discussed in § 1.6, and (2) a far infrared *bump*, at $\lambda \sim 10$–$100\ \mu m$.

Observations of the ionizing continuum are hampered by the interstellar absorption beyond the Lyman limit. The *Big Bump* is constrained on the low frequency side by the flattening of the continuum shape which begins at $\simeq 1\mu m$ and continues up to the Lyman limit; on the high frequency side observations of the continuum have been made for energies $\gtrsim 0.1\ keV$. Between 13.6 eV and 100 eV the continuum is practically unexplored. In the range 0.1–2 keV, observations of AGN with EXOSAT and HEAO-2 are suggestive of complex spectral shapes, variable from object to object (Turner and Pounds, 1989). A simple power–law model of the data (plus a single parameter characterization of photoelectric absorption along the line of sight) gives an acceptable fit to the majority of the cases. In $\gtrsim$ 30 % of the observed objects, best fits were obtained by the inclusion of a soft spectral component in emission (Turner and Pounds, 1989; Warwick *et al.*, 1989; Kruper *et al.*, 1990). Although the shape of the *soft excess* was not well constrained by the data – due to the poor resolution of the EXOSAT Medium Energy camera and of the IPC/MPC counter mounted on HEAO–2 –, Kruper *et al.* (1990) suggested that a thermal model (such as a black body or Bremsstrahlung) gave a significantly better fit than a second power–law component. The SSS spectrometer mounted on HEAO–2 allowed to obtain spectra in the range 0.6 – 4 keV with a resolution of 160 keV. In the very soft X–ray region (0.1–0.5 keV) a steeply falling spectrum is seen, which may be the Wien part of the *Big Bump* spectrum from the accretion disk (Holt *et al.*, 1990; see § 1.6). In the range between 2 and 20 keV, recent data from GINGA (*e.g.* Piro *et al.*, 1991) have shown that the hard X–ray spectra of many AGN is satisfactorily described by the combination of a steep ($\alpha \approx 0.9$) plus a flatter $\alpha \approx 0.6$ power–law component at 10–30 keV, rather than by a power law with spectral index α=0.7 of universal validity among Seyfert galaxies and quasars, as it was commonly believed until 1989 (Turner and Pounds, 1989; Kruper *et al.*, 1990). The power law–spectrum seems to extend up to 100 keV (or even up to γ–rays energies 100 MeV, although only 3C273 has been observed at these energies), without substantial turnover of the spectral shape (Reichert *et al.*, 1985; Turner and Pounds, 1989).

The infrared continuum at the IRAS wavelenghts (12–100 μm) is probably due thermal reradiation by dust heated by the uv radiation emitted either by hot stars or by the active nucleus, plus non–thermal emission direcly arising from the AGN. The relative contribution of the two components varies from object to object. The non–thermal component is probably dominant in quasars and luminous Sey–1, but less luminous Sey–1 and Sey–2 galaxies may have the far–IR emission dominated by thermal emission. We shall return later to this point (§ 1.4.2; *e.g.* Miley *et al.*, 1985, and references therein).

1.3 The Line Emission Regions of AGN

Basically, the optical/uv emission line spectrum of Seyfert galaxies and quasars is characterized by two types of emission lines:

- permitted and semiforbidden lines, with a very broad profiles (typical FWHM span the range $\sim$ 2000–5000 $km\ s^{-1}$; representative FWZI are $1{\cdot}10^4\ km\ s^{-1} \approx$ 0.03 c, with extreme cases reaching $3{\cdot}10^4\ km\ s^{-1} \approx 0.1\ c$; these emission lines are typical of Seyfert 1 nuclei and quasars;

- forbidden lines with narrow profiles (FWHM $\approx 400\ km\ s^{-1}$, with extreme values at 200 $km\ s^{-1}$ and 1200 $km\ s^{-1}$). Forbidden lines are emitted from a wide range of ionization species, comprising O^0, N^+, Fe^{+6}, and in some cases Fe^{+9}, Fe^{+13}.

In Seyfert 2 galaxies, the permitted lines have widths comparable to those of the forbidden lines. *Intermediate* Seyfert galaxies have composite profiles of the permitted lines, with a narrow component superimposed over a broad component. The features of the emission line spectrum have led to single out two distinct emission regions:

1. The *Broad Line Regions* (BLR), which emits the broad permitted lines. There is no spectral diagnostic for both electron temperature T_e and electron density n_e of the BLR. The lack of any strong broad component in the forbidden lines implies that $n_e > 10^7 cm^{-3}$, while the presence of the semiforbidden CIII]λ1909 line with broad profile implies that $n_e \lesssim 10^{9.5} cm^{-3}$.

2. The *Narrow Line Regions* (NLR), where the forbidden lines and the narrow components of the permitted lines are emitted. T_e and n_e can be measured on the basis of several diagnostic line ratios: typical values are $T_e \simeq 10^4\ ^\circ K$ and $n_e \sim 500 - 1000\ cm^{-3}$. The emitting gas is located at $\sim 100 - 1000\ pc$ from the central source of continuum.

Yee (1980) and Shuder (1981) found that the luminosity of the Balmer Lines is proportional to the optical continuum luminosity at $\lambda \approx 4800$ Å, over eight orders of magnitude of the continuum luminosity. This correlation suggests that photoionization by the non–thermal continuum and recombination are the processes which produce the permitted lines. Restricting our discussion to the BLR, the presence of the MgII λ2800 line implies that the emitting gas is optically thick to the Lyman continuum. Under these assumptions, each Lyman continuum photon absorbed by the gas is transformed in radiation of lower energy and in a Lyα photon (see, *e.g.* Osterbrock, 1989). The covering factor f_c, defined as the fractional area of the sky subtended by the gas as viewed from the center, will be given by the ratio of the total Lyα photons to the number of photons emitted in the Lyman continuum: The value of f_c obtained is ≈ 0.1. Observations of high redshift quasars showed that the fraction of the continuum absorbed shortward of the Lyman limit was around 10 %, confirming the previous estimate of f_c.

The ionization parameter Γ is defined as:

$$\Gamma = \frac{\int_{\nu_0}^{\infty} L_\nu d\nu}{4\pi R^2 c n_e} = \frac{density\ of\ ionizing\ photons}{electron\ density} \tag{1.1}$$

where ν_0 is the Rydberg frequency, L_ν is the luminosity at frequency $\nu > \nu_0$ and R is the distance between the BLR gas and the central source of ionizing photons. The observed ratio CIII]/CIV is explained for $\Gamma \approx 0.01$. The knowledge of Γ allows to employ the previous relation for deriving a rough estimate of the BLR distance from the central source: $R \simeq 3 \cdot 10^{18}(L/(10^{46} erg\ s^{-1})^{1/2}\ cm)$, for $\Gamma \approx 0.01$ and $n_e \approx 10^{10}\ cm^{-3}$. Moreover detailed photoionization calculations (discussed in the next section) suggest that the column density is $N_c \sim 10^{22} - 10^{23} cm^{-2}$. The value of N_c, coupled with the electron density deduced above, implies that the size of the emitting element is $r_e \approx 10^{12} cm$, much less than the distance R of the emitting regions from the central source. The ratio of the emitting volume to the total volume (the *filling factor*) is given by: $f_f = f_c N_c / n_e R \sim 10^{-6} \ll 1$. Due to the estimate of a small filling factor and the size of the emitting element r_e smaller than R, the Broad Line flux is often regarded as *the collective emission from a large number of small clouds that fill only a small fraction of the total volume* (Mathews and Capriotti, 1985). The thermal width of a line emitted by a single cloud is $\approx 4\ km\ s^{-1}$; hence at least 10^4 clouds are needed for explaining the observed width of the broad lines. The total number of clouds is probably much larger, since the profiles are generally smooth and do not show any irregularity for time scales of years. This view of the emitting regions is a useful framework, but it is very simplified, and does not account for many observed features (see §1.7).

1.4 Feeding the monster

In principle, a massive black hole should form because of contraction of a star cluster in the very center of a galaxy. The star cluster should evolve to a cluster neutron stars and stellar mass black hole, which may give rise to a central single massive black hole (Rees, 1984; 1991). It is however unclear whether all galaxies did form a massive black hole in their center early after galactic formation. Once the black hole has formed, it can accrete material coming from the galactic bulge, due to stellar winds of a normal type II population. Otherwise, it could be accreted by debris of stars tidally disrupted by the black hole itself. The accreting material could be also provided by the strong mass loss of young stars, or be directly channeled from the the extranuclear regions.

1.4.1 *In situ* production of the accretion flow

In order to sustain the AGN luminosity, the inflow rate able to reach the outer regions of the accretion disk must be $\dot{M} = 1.5 L_{46} \eta_{0.1}^{-1} M_\odot\ yr^{-1}$, where L is in $erg\ s^{-1}$. For $\eta \sim 0.1$, $\dot{M} \sim 1.5\ M_\odot yr^{-1}$ are needed to *feed* an AGN of luminosity $10^{46}\ erg\ s^{-1}$. A population of evolved stars produces $\sim 10^{-11}\ M_\odot\ yr^{-1} \dot{M}_\odot^{-1}$ via mass loss, which is

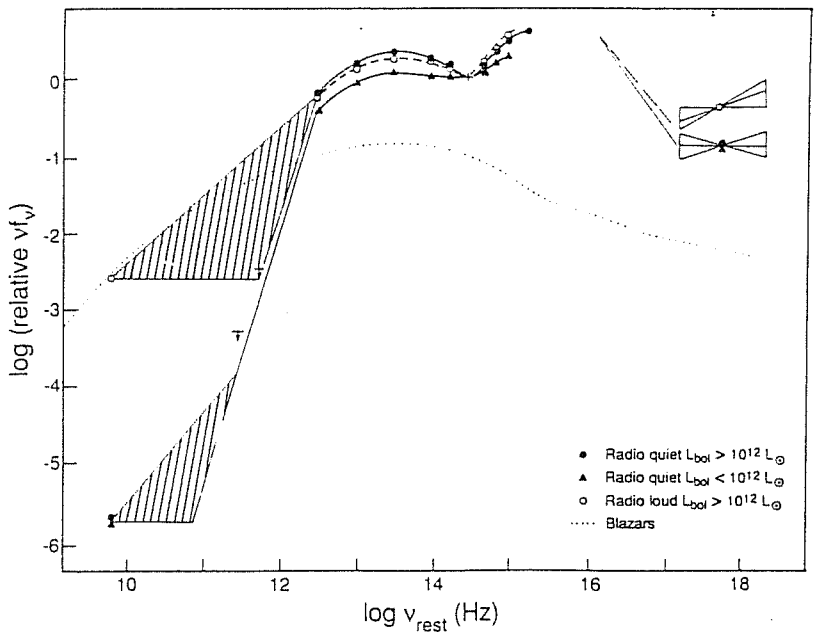

Figure 1.1: *The AGN continuum. From: Sanders et al. (1989)*

woefully inadequate to power even the Seyfert galaxies of lowest luminosity, unless a star cluster of mass $\gtrsim 10^{10}\ M_\odot$surrounds the central black hole.

The central black hole of mass M will dominate the velocity field up to a distance $r_h = gM/V_*^2 = 43 M_6 V_{*,100}^2 pc$, where V_* ($V_{*,100}$ is in units of 100 $km\ s^{-1}$) is the stellar dispersion velocity, and M is units of $10^6\ M_\odot$. At $\approx r_h$ the stellar density increases more with decreasing radius than estrapolating a standard King law (*e.g.* Binney and Tremaine, 1987), and the stellar velocity dispersion increases $\propto r^{-1/2}$. Stars could be tidally disrupted by the black hole within the *tidal radius* $r_T \simeq 1.4 \times 10^18 M_7^{1/3}\ cm \approx 0.45 M_7\ pc \sim 10^{-2} r_h$. If a star has such a low angular momentum that its perigee is within r_T then it must be moving near radially in a small *loss-cone* of semiaperture $\theta_D \simeq (t_{dyn}/t_R)^{1/2}$, where $t_{dyn} = 1.5 \times 10^3 M_8^{-1/2} r$ (r in pc) is the dynamical timescale and t_R is the relaxation time for the cluster (Frank and Rees, 1976). The maximum possible flow is $\dot{M}_{TD} \approx m_* t_{dyn}^{-1}\ M_\odot\ yr^{-1}$, for sperical cluster with nearly isotropic velocity distribution (Shlosman, 1990; Sholsman *et al.*, 1990). The mass converted to gas would be $\sim 2 \times 10^{-5}\ M_\odot\ yr^{-1}$, for a cluster mass of $10^9\ M_\odot$ and a cluster radius of 10 pc. This value is again insufficient, unless the cluster density is so high that the cluster is set in collisional regime. In this case, the cluster should shrink within the radius $r_{coll} \simeq 2.3 \times M_8\ pc$, where V_* is comparable to the escape velocity for typical stars. Stars at $r \lesssim r_{coll}$ cannot deflect themselves without coming so close that they actually collide (Frank and Rees, 1976). In the collisional regime the mass converted to gas should be multiplied by a factor $(\sigma_*/V_*)^4$, (*e.g.* Rees 1984, and references therein; Shlosman *et al.*, 1990). An extremely compact star cluster should be necessary in

order to increase the gas masses to reasonable values, and that star cluster with similar properties have never been observed. For comparison, the stellar density at distance $\sim 1pc$ from the center of the Galaxy is $\sim 10^6\ M_\odot\ pc^{-3}$, and the velocity dispersion of the stars $\sim 120\ km\ s^{-1}$. Furthermore, if the configuration of remnants is compact enough, it could rapidly produce a unique massive object (*e.g.* Shapiro and Teukolsky, 1985).
Conditions could be more favourable if the presence of a *coeval* star cluster is assumed. We will discuss this possibility later (§ 1.4.3).

1.4.2 Accretion flow driven by gravitational instabilities

It is likely that gas is provided from the circumnuclear regions or from the inner disk of the host galaxy. The key point is that, in order to reach the very center of the galaxy gas has to loose most of its angular momentum. Gunn (1979) suggested that exchange of angular momentum can take place between dense gas clouds and a tenuous hot wind driven by supernova blasts, but this process operates over very long timescales, $\gtrsim 10^9\ yr$. Standard viscous processes – which are responsible for angular momentum transport in some cataclysmic variables – can not be scaled up beyond $\sim 1pc$. The radial inflow time for a standard α disk (§ 1.5.1) is $t_{visc} \approx 1.2 \times 10^9 \alpha^{-1} v_2 T_2^{-1} R_{10}\ yr$, where the orbital velocity is $100\ v_2\ km\ s^{-1}$, the distance is $10R\ pc$, and $100\ T_2^\circ K$ is the gas temperature (Shlosman *et al.*, 1989), and it obviously too long to be of any relevance. If self-gravitation becomes important, then the disk would resemble a system of clouds and α will become $\sim t_{dyn}/t_{coll} \lesssim 1$, where t_{dyn} and t_{coll} are the dynamical and the collision timescales respectively, without appreciable shortage of the radial drift time.
In Fig. 1.2 features and/or phenomena relevant for the accretion of matter on the black hole are ordered according to their spatial scales. Three regions can be isolated due to the occurrence of different processes: (1) the *central engine*, where viscous stresses in the accretion disk rule the angular momentum transport; probes for the existence of the accretion disks and the theoretical expectation on disk will be discussed in the second part of this Chapter; (2) a *nuclear* region between the outer edge of the accretion disk ($0.1\ pc$) and $\sim 200\ pc$, (the domain of the inner NLR), where dissipative flows, bar–like instabilities, star formation, photoionization by the active nucleus as well shock driven winds may affect the gas conditions. Qualifying as nuclear all phenomena and features occurring within the inner $\sim 200\ pc$ from the galactic center is more than a matter of convention: as we shall see below, nuclear Starbursts are probably confined within this radius; furthermore, this distance may be the outer radius of the molecular torus hypothized by Antonucci and Miller (1985) (§ 1.9); (3) *extranuclear* regions at $d \gtrsim 200\ pc$ from the nucleus up to the outer edge galaxy disk, where gravitational instabilities may drive inflow of gas. We will consider at first the 3^{rd} region.
There is no general consensus regarding the mechanism able to trigger a radial flow of circumnuclear/disk gas toward the nucleus. Radial flows are not expected to occur in an axially symmetric galaxy under normal circumstances. Non–axisymmetric per-

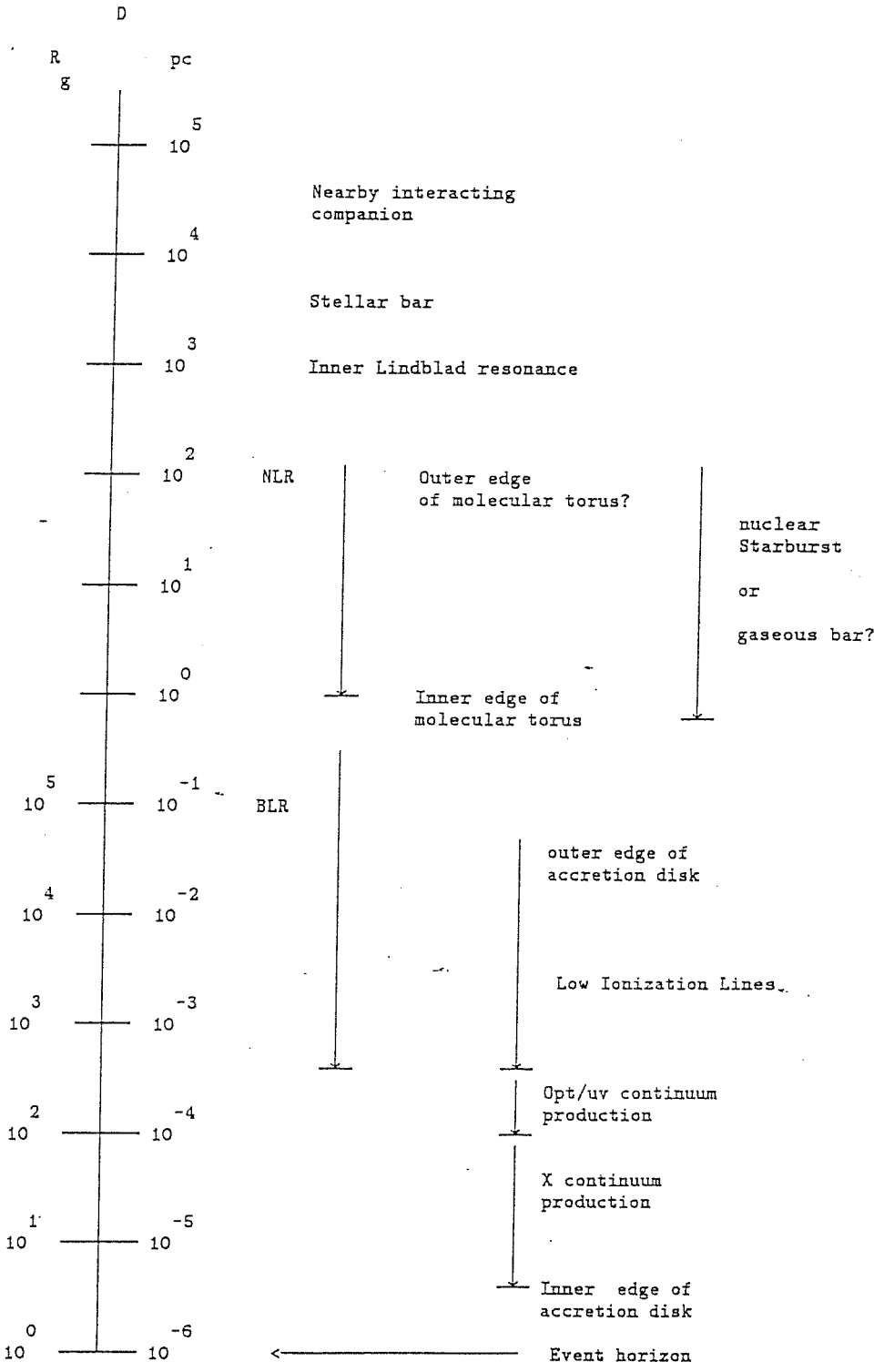

Figure 1.2: Relevant spatial scales for fuelling and energy emission of AGN. Vertical scale is distance from galactic center.

turbations to the gravitational potential are in principle very efficient (Simkin *et al.*, 1980; Norman and Silk, 1983; Shlosman and Begelman, 1988). They can be produced by tidal forces, oval distortion of the disk or bars, and spiral density waves. However, it is difficult to conceive an endogenous mechanism related to the internal dynamics that can operate after $\sim 10^{10} yr$ from galaxy formation as well as in an epoch when galaxy formation was still important (as is the case for the highest redshift quasars observed at $z \approx 4$; *e.g.* Rees, 1991). An esogenous mechanism – as tidal disturbance due to interaction with a nearby galaxy – is in principle much more fashionable (*e.g.* Toomre and Toomre, 1972). Interactions between galaxies are though to be more frequent in the early ages after galaxy formation (Zepf and Koo, 1988; de Robertis, 1985), but are commonly observed at the present age. There are basically two ways in which interaction may act in order to drive inflow of gas toward the galactic nucleus: it may induce bar–like distortion in the potential or it may be able to *strip* gas from a close gas–reach companion. Best conditions for fuelling the material stripped from the companion are in the case the companion disk rotate directly relative to the orbital motion (Toomre and Toomre, 1972; Byrd *et al.*, 1987; Barnes, 1989). Tidal stripping of gas has been suggested for some galaxies of the Arp atlas, in particular Arp 102b (de Robertis, 1985; Stauffer *et al.*. 1983), for UGC 3995A and for NGC 7592 (Rafanelli and Marziani, 1991a). Probably, this process takes place at some stage of a merging or of a close prograde encounter, but little observational attention has been paid to these objects.

The excess of *companions* among Seyfert galaxies (with respect to normal galaxies) early noted by Adams (1977) has been interpreted in support of a connection between interaction and nuclear activity. Dahari (1984) searched on the *Palomar Observatory Sky Survey* plates for nearby companions of Seyfert galaxies (within three diameters of the Seyfert galaxy). He confirmed the *feeling* introduced by Adam's work, and suggested that the percentage of companions was $\approx$ 15 % in comparison to the 3 % of companions found in a control sample of non–active galaxies. Other studies suggest that there is an excess of companions also for quasars (Stockton, 1982; Hutchings *et al.*, 1984): $\approx$ 30 % of 45 low–redshift quasars appear to be currently interacting with a companion galaxy. Although the excess has been questioned in recent times by Fuentes–William and Stocke (1988), our results, reported in Chapter 2, prove that the excess is real, and that *at least* $\simeq 1/5$ of Seyfert galaxies are interacting. The problem here is that most Seyfert galaxies do not show evident sign of gravitational perturbation, and that there is apparently no enhancement (or a marginal enhancement) of the nuclear activity level (emission line luminosity, blue luminosity) in interacting Seyfert galaxies with respect to the non interacting ones (Keel *et al.*, 1985; Dahari and De Robertis, 1988). This result indicates that interaction may act as a *triggering mechanism* for flow of gas which ultimately leads to the nuclear activity, and that other phenomena can be then responsible for the luminosity and working mode of the AGN. The puzzle could be partly solved if the search for companions were coupled with a morphological survey based on broad band images (ideally in the R band and in the near infrared) of a sample of nearby Seyfert galaxies. This point will be discussed in

Chapter 2.

A passing–by companion alters the gravitational potential of the disk of a spiral galaxy introducing a term $\propto \cos(2\vartheta)$, where ϑ is the azimuthal angle of the disk. This perturbation generates a two–arms density wave (Toomre, 1977), which favours orbit crowding, and hence cloud–cloud collision. Molecular clouds collide inelastically, and loose their angular momentum and/or merge to form giant molecular clouds were young associations of stars are formed (among others, Combes and Gerin, 1985; Noguchi and Isibashi, 1986; Noguchi, 1988; Olson and Kwan, 1990). Byrd *et al.* (1986) performed N–body simulations of the tidal effect of a companion in a parabolic orbit on the disk of the *candidate* active galaxy. In order to study the flow into the nuclear region of the galaxy, these authors assumed that inelastic collisions set disk particles onto smaller orbits, and recorded how many particles were thrown into orbits crossing the central *dowel* of the coordinate grid. An important finding of Dahari's work (1984) is that systems in which the separation was comparable to the angular diameters of the components of the system were more frequently found ($\approx$ 7 %) among Seyfert galaxies than among normal galaxies ($\approx$ 1 %). This *strong interaction level* is matched by the required level for rapid global instability and significant nuclear inflow. Byrd *et al.* (1987) estimated the gas inflow rate as a function of time, and found that there is *latency* period of $2 - 3 \times 10^8 yr$ before the maximum inflow rate is obtained. Episodes of maximal gas inflow last $\lesssim 10^8$ for an inflow rate $\gtrsim 1.5\ M_\odot\ yr^{-1}$, so that some interacting galaxies may suffer of *gas starvation* as well as isolated galaxies. Hearnquist (1989) performed simulations using an hybrid N–body and hydrodynamical code in order to account for the behaviour of both the gaseous and stellar component. He examined the case of merging of a gas rich galaxy with a compact companion of smaller mass (1/10). This study agrees with the less elaborate simulations of Byrd *et al.*: strong interaction leads to the accumulation of a substantial gas mass ($\gtrsim 10^9\ M_\odot$for a gas rich galaxy) in the inner few hundred *pc* of the galaxy. It is interesting to note that the disk/halo ratio may influence the driving of strong inflow motions. According to Ostriker and Peebles (1973) the development of global bar–like instabilities is inhibited if a massive halo is present; numerical simulations indeed suggest that the inflow rate may be lower if the halo mass is higher (Byrd *et al.*, 1987).

Hydrodynamical numerical simulations (Hearnquist 1989; Olson and Kwan, 1990) suggest that interaction may enhance the rate of cloud–cloud collision. In order to analyze further the fate of the accretion flow it is necessary to take into account that the most direct effect of cloud–cloud collision is to form giant molecular clouds ($M \sim 10^6\ M_\odot$), where associations of young stars form. As a result, the rate of star formation can greatly increase (up to a factor $\sim$ 100). We observe indeed nuclear and extended Starbursts are produced by interaction. Galaxies showing Star Formation Rates (SFR) which can not be sustained over the age of the galaxies will be designated in the following as *Starburst* galaxies (*e.g.* Balzano, 1983; Weedman, 1983). At variance with AGN, they show a nuclear spectrum typical of low–ionization HII regions, suggesting that hot stars are responsible for the line emission in these objects, although the most energetic Starbursts have a power output comparable to those of quasars.

Interaction and Star Formation

Larson and Tinsley (1978) early showed the dispersion in the U–B and B–V colors of the Vorontsov–Velyaminov (1959) galaxies is larger than for the galaxies of the Hubble atlas (Sandage, 1963), and interpreted this effect as due to bursts of star formations occurring on timescales shorter or comparable to the dynamical timescale of the interaction. A more unambiguous indicator of Star formation is the Hα luminosity, which is directly related to the number of ionizing photons emitted by massive OB stars. Once the Initial Mass Function (IMF) is assumed (for instance a modified Salpeter IMF, $\Psi(m) \propto m^{-1.4}(0.1 \leq m \leq 1 M_{\odot}, \Psi(m) \propto m^{-2.5}, 1 \leq m \leq 100\ M_{\odot})$, the H$\alpha$ luminosity is directly proportional to the Star Formation Rate $SFR(\geq 10 M_{\odot}) = 1.42 \times L(H\alpha)_{42} h^{-2}\ M_{\odot} yr^{-1}$, and $SFR(total) = 8.9 \times L(H\alpha)_{42} h^{-2}\ M_{\odot} yr^{-1}$, where $L(H\alpha)_{42}$ is the Hα luminosity in units of $10^{42}\ erg\ s^{-1}$. The modified Salpeter IMF reproduces the broad band colors and the Hα emission of a large sample of spiral and irregular galaxies studied by Kennicutt (1983). Uncertainties in the SFR estimates are rather large, because of frequently underestimate of the internal extinction and of the poorly known shape of the IMF. For instance, the choice of a Miller–Scalo IMF would enhance the SFR by a factor $\simeq 3$ (Bushouse, 1987). Furthermore, UBV and Hα luminosity constrain at best the *high mass* star formation, but set poor constrains on the low mass part of the IMF. It is at present unclear whether the Salpeter and Miller–Scalo IMF are appropriate for energetic Starburst, or whether a deficient number of low mass stars is being produced (Gehrz *et al.*, 1983). IRAS fluxes are measured on bands centered at $12, 25, 60, 100 \mu m$. They allow to roughly constrain the emission mechanism at these wavelength. In the case the far–IR flux has a thermal origin, it depends upon the energy reradiated by dust associated with star forming regions, and hence it can be related to the SFR. The use of the IRAS fluxes solves the problem associated with reddening, but due to the low spatial resolution of IRAS, the SFR can be estimated only for the whole galaxy or for the interacting system in most cases. The average SFR deduced from IRAS data is higher by a factor of ~ 10 than the SFR deduced from Hα. As shown in Chapter 3, the discrepancy may be easily reduced if proper account is taken of the spatial extent of the Hα emission and if the Hα are adequately corrected for extinction. Fig. 1.3 shows the global SFR per unit area, as deduced from the Hα emission, for a sample of pairs of interacting galaxies exhibiting features unmistakably associated with strong tidal interaction, and a sample of isolated unperturbed galaxies. Since SFR strongly increases along the Hubble sequence, and for Sc galaxies it can be comparable to that of Starburst galaxies (Kennicutt and Kent, 1983; Kennicutt, 1983; AKennicutt *et al.*, 1989), it is necessary to have a control sample matching the morphological types (if it possible to deduce it also when tidal distortion operate) of the interacting sample. The response varies enormously from object to object; clearly, orbital parameters of interacting system are most important in the analysis of the effect of the encounter. The average enhancement is moderate, $\approx$ 2–3 if we compare isolated and interacting galaxies having roughly the same morphological type (Kennicutt, 1987). It is important to note that the most powerful Starbursts (far infrared $L \gtrsim 10^{11} L_{\odot}$) are observed nearly

exclusively in strongly interacting or merging galaxies (Soifer *et al.*, 1987; Joseph and Wright, 1985). Starburst can be spread over the galaxy disk on *kpc*–sized scales (De Robertis and Shaw, 1988). Bushouse (1987) and Kennicutt *et al.* (1987) found however a strong tendency for the SFR to be higher in the nucleus than in the disk regions of Starburst galaxies.

Star Formation in Seyfert Galaxies

Analysis of nuclear and circumnuclear star formation in active galaxies is in principle a difficult task, since star formation events can be masked by the presence of a luminous active nucleus. Rings of HII regions around nearby active and Starburst nuclei have been revealed at distances 1–3 *kpc* from the nuclei. These rings are probably located at the inner Lindblad resonances of stellar orbits, where orbit crowding may favour collision between molecular clouds. Best examples among Sey–2 galaxies are NGC 1097, NGC 4303, NGC 4321 (Keel, 1987). For most Markarian galaxies these structures would not be revealed from ground based observations due to their proximity to the nucleus. Nevertheless, several diagnostic tools have revealed that enhanced star formation is taking place in the circumnuclear or even in the nuclear regions of active galaxies.

A powerful diagnostic for revealing the star formation is based upon emission line ratios. Sey–2 galaxies, and generally speaking emission region photoionized by an AGN continuum, can be distinguished from Starburst galaxies by the weakness of the low ionization lines such as [NII]$\lambda\lambda$6548,6583, [SII]$\lambda\lambda$6716,6731 and [OI]λ6300, since the [SII] and [OI] emission lines arise in a region of the emitting clouds where hydrogen is partly ionized. This zone is created by the hard X–ray continuum emitted by an AGN but is nearly absent where the ionization source is provided by the thermal continuum of OB stars. Veilleux and Osterbrock (1987) proposed *diagnostic diagrams* which are built from the line ratios [OIII]λ5007/Hβ versus [NII]λ6584/Hα, [OI]λ6300/Hα, and [SII]$\lambda\lambda$6717,6731/Hα able to distinguish between thermally and non–thermally ionized regions. Veron *et al.* (1981) were able to infer the presence of HII–regions regions in the nuclei of the Sey–1 galaxies NGC 7469 and NGC 7582 by the analysis of the different width of the of Hβ and [OIII]$\lambda\lambda$4959,5007 emission lines, in a fashion similar to that described in Chapter 3 for NGC 7592. Employing long–slit spectra of sufficient high resolution ($\lesssim$ 2 Å), it was possible to resolve a low–ionization *Starburst* component and a high–ionization component, with strong [OIII]$\lambda\lambda$4959,5007 emission, in the circumnuclear regions of NGC 7469, Mkn 315 (Wilson *et al.*, 1986) and Mkn 423 and Mkn 739 (Rafanelli *et al.*, 1991). Radio maps at 6 and 20 cm obtained with the *Very Large Array* published by Ulvestad and Wilson (1984a,b), reveal that the high ionization gas is often associated with jet–like radio structures (Whittle *et al.*, 1986; Wilson, 1988). Presence of low–ionization emission regions is associated with a *diffuse*, blob–like radio emission surrounding the nucleus. The steep radio spectrum suggest that the *diffuse* emission is be related to a circumnuclear Starburst. Prominent emission feature due to gas and dust are observed in the 8–13 μm spectra of Starburst galaxies, as well as

in Seyferts where a circumnuclear starburst has been revealed. It is however thank to the IRAS survey that the extent of the connection between star formation and AGN has been emphasized. Rodriguez–Espinoza *et al.*(1987) suggested that a large fraction of the emission at far–IR wavelengths of Seyfert galaxies is produced by heated dust associated with star formation regions around the active nucleus. Indeed, an analysis of the spectral indexes $\alpha(60,25)$ and $\alpha(100,60)$ in a two–colors diagram shows that there is a wide overlapping region where Starburst galaxies, Sey–2 and Sey–1 galaxies are present. In these cases, much of the infra–red emission observed by IRAS from Seyfert galaxies may be due to an extended, non–nuclear component, dust heated by hot stars or by the nonthermal continuum of the AGN. The SFR also correlates with the surface density of molecular gas. Sey–2 galaxies have an excess of CO while Seyfert 1 galaxies do not. The great majority of Sey–2 galaxies populates the overlapping region. The available evidence from IRAS colors and luminosity suggest that Sey–2 galaxies are characterized by a star formation rate higher than that of galaxies of the corresponding morphological types (*e.g.* Kennicutt, 1990, and references therein). However, since Sey–1 and Sey–2 are partly located in a region of the two color diagram where no starburst galaxies are found, star formation does not provide the dominant contribution in all Seyfert galaxies. Wilson (1988) has shown that galaxies having diffuse radio morphology or with evidence of circumnuclear starburst nearly completely fall in the region occupied by Starburst galaxies in the far–infrared two colors diagram. The most remarkable *intermediate objects* (Mkn 315, NGC 1068, NGC 7469, NGC 7582, NGC 7592, NGC 6764, NGC 5728, Mkn 231, NGC 1365; Wilson, 1987, and references therein) have composite nuclear spectra showing emission lines with a Starburst and a non–thermally ionized component, probably associated with the NLR of the active nucleus (see also Chapter 3). We have done an analysis of the morphology (on images of our archive) and of the galactic environment (on the *Palomar Observatory Sky Survey* prints) of these objects. Seven out of nine galaxies belong to interacting systems (the exceptions being NGC 1365 and NGC 1068). It is interesting to note that McKenty (1989) compared the IRAS colors for a sample of non–interacting and interacting Seyfert galaxies selected from the Markarian lists. He found that the IRAS colors of *interacting Seyferts* span the same range of the IRAS colors of non–Seyfert (*i.e* starbursting) Markarian galaxies.

We have shown in the previous sections that interaction is probably the main responsible in triggering Starbursts, and reviewed that a nuclear Starburst can be related to the birth and to the fuelling of an active nucleus. Now we argue that intermediate Starburst/AGN occur preferentially in interacting systems. At this point, we should analyze whether gravitational instabilities are able to fuel directly the AGN or whether the fuelling is provided as a consequence of the Starburst. Preliminary considerations will be made in the next section; this problem will be also discussed in the last section of Chapter 3.

1.4.3 The nuclear flow

The scenario presented here suggests that the origin and the evolution of activity is controlled by events on galactic scale. To be honest numerical simulations demonstrate that a large gas mass $\lesssim 10^9\ M_\odot$ can be brought in the inner $\lesssim 200\ pc$ of the galaxy, but the fate of the gas on scales between 0.1 *pc* and 100 *pc* is very uncertain. Most uncertain is how the gas releases its residual angular momentum. A thin accretion disk is an efficient mechanism for the angular momentum transfer in the innermost regions of AGN, but a viscous disk at a distance of a few hundred *pc* cannot be scaled down, unless the viscosity parameter α is $\gg 1$ (Shlosman *et al.*, 1990). Cloud–cloud collision in a circumnuclear ring may lead to further infalling of molecular gas (in dissipative flow), and to build up a thick torus at radii between 1–100 *pc*. Otherwise, triaxial perturbations in the core of a galaxy containing a central massive black hole can very substantially increase the fuelling rate. If gas is $\gtrsim$ 20 % of the dynamical mass (as in the case of the powerful Starburst Arp 220), it can be channeled toward the nucleus by a bar–like instability operating on scale of a few hundred parsec (Shlosman *et al.*, 1989). Bars can not cross the Lindblad resonances, but barred structures may be present inside and outside the resonances. The tidal disruption rate of stars near a central black hole may be consideraby enhanced during a merger with a smaller companion. This can be due to scattering of stars into loss–cone orbits by the perturbing gravitational field of the intruding galaxy (Roos, 1981). The fuelling rate is enhanced to $\dot{M} \approx 0.45\rho_7 V_{*,200} M_7^{4/3}$, where ρ_7 is the stellar mass density in units of $10^7\ M_\odot pc^{-3}$. This value is sufficient to power all but the most luminous AGN. The relevance of the mechanism is however limited since nuclear activity does not occurr *only* in merging galaxies. Otherwise, if the companion also contains a massive black hole, it will settle in the core of the merged stellar system because of dynamical friction. A *binary* configuration of two black holes of comparable masses $\sim 10^8\ M_\odot$, can be sustained for a time $\tau \gtrsim 10^8 yr$ with a separation of $\sim 10^{-1} pc$, before gravitational radiation lead to coalescence into a single black hole (Begelman *et al.*, 1980).

An evolutionary link between Starburst and AGN?

Given the tight connection between star formation of nuclear activity, the emission line properties of Sey–1 and particularly of Sey–2 galaxies have been explained as due to hot stars by several authors (Shklowskii, 1960; Harwit and Pacini, 1975; Terlevich and Melnick, 1985). The enhancement of the SFR observed in Sey–2, and the many observational evidences linking star formation with interaction and nuclear activity, suggest that at least for Seyfert galaxies, this idea should be taken into serious account. In its most recent acception (Terlevich and Melnick, 1985; 1988) the NLR are explained as HII-regions photoionized by high mass ($M \gtrsim 25\ M_\odot$) stars in an advanced evolutionary stage where outer layers have been removed leaving an high temperature core ($T \sim 100,000° K$). These stars will spend the He burning phase near to the He *Zero Age Main Sequence*, and their continuum spectrum would be able to photoionize the surrounding gas and produce a Sey–2 spectrum instead of an HII spectrum. The broad

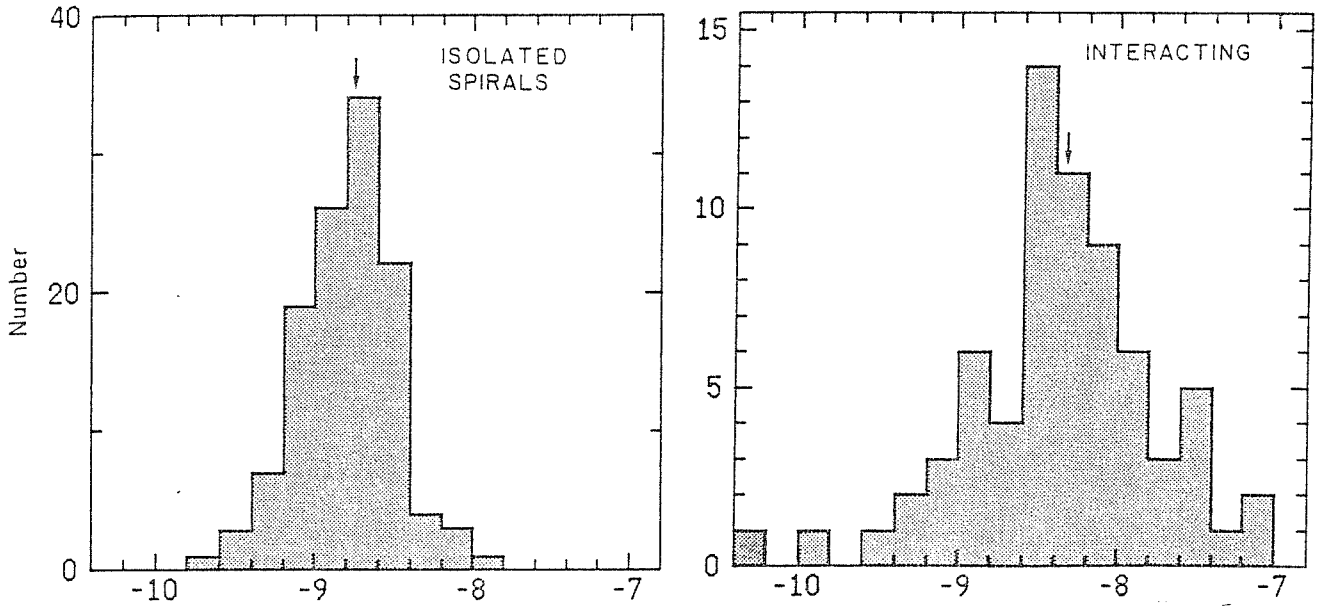

Figure 1.3: *Star Formation Rate per unit area ($M_\odot\ yr^{-1}pc^{-2}$) in isolated and interacting galaxies. From: Bushouse (1987).*

Balmer lines observed in Sey–1 are accounted for if lines are emitted by type II supernovae. The discovery of two supernovae with optical line spectra undistinguishible from that of a Sey–1 galaxy (Filippenko, 1989), implies that supernovae *may* be responsible for *part of* continuum and line emission in *some* Sey–1 galaxies. A supernova rate of 1–2 $SN\ yr^{-1}$ is required to match the timescale observed for variation in the emission line of Sey–1 galaxies. NGC 5548 underwent an increase of optical luminosity accompanied by the appearance of strong HeII λ4686 with line wing broader than the Balmer lines. This *flare–like* variations can be interpreted as evidence of infall in an accretion event (Peterson and Ferland, 1986; Peterson, 1987), as well as due to a type II supernova event (Terlevich and Melnick, 1988). To be fair, at present the supernova interpretation for the variation in NGC 5548 can not be ruled out. The ambiguity can be solved by a close comparison of the temporal evolution of Supernovae (particularly that with a parent star of Wolf–Rayet type, a few of which are known at present) and the spectral variation of AGN.

There is convincing evidence that Starburst and AGN are related, but there is also more convincing evidence that star formation is not the whole part of the story. Star formation models are unable to explain beaming collimation of radio jets, the radio morphology of powerful radio galaxies. Moreover, apart from classical arguments, which are not directly applicable to Seyferts, we believe that it is very difficult to explain, for a model involving line emission supernovae, the remarkable stability (over more than then years) of substructures observed in the emission line profiles of some Sey–1 galaxies (for instance Akn 120 and IC 4329a, Marziani *et al.*, 1991; Chapter 4 and § 1.7.3). The problem is whether a Starburst phase should *necessarily* precede the

birth of an AGN, because gas supply is provided by the Starburst, or whether the gas flow (or part of it) is able to reach directly to accretion disk.

Molecular gas in a torus could be the reservoir of matter for a burst of star formation, but gas could be also channelled directly to the outer regions of the accretion disk. Begelman and Krolik (1986) suggested that the obscuring matter responsible for the occultation of the BLR to the line of sight in some Sey–2 galaxies takes the form of a torus of compressed molecular clouds. This suggestion was based indeed on the observation of a rather strong burst of star formation in the circumnuclear regions of NGC 1068. These authors have shown that the balance between cloud evaporation and dissipative inflow occurs when the inner edge of the torus is located at $r \approx 1\ pc$ from the center of the galaxy. Cloud–cloud collision allows to dissipate the gravitational energy and lead to an inward flow of matter at a rate $\dot{M} \sim 1 - 2\ M_\odot\ yr^{-1}$(Begelman and Krolik, 1988), provided that new material can be fed at the outer edge of the torus, which should be located at $\sim 200\ pc$ from the nucleus.

The formation of the black hole itself could be a consequence of a Starburst. Feldman *et al.* (1982) have found that the average radial velocity dispersion for a number of Starbursts is $\sigma_r \approx 70\ km\ s^{-1}$. Since Starbursts follow the extrapolation of the law $L \propto \sigma^4$ found for HII regions (Terlevich and Melnick, 1981), the Starburst could be considered as a giant self gravitating HII complex not in equilibrium with the potential of the galactic bulge. Assuming a typical dimension of a nuclear starburst of $\sim 100\ pc$, the decoupling between the Starburst and the Population II stars in the nuclear bulges of spiral galaxies would allow the concentration of a large mass of remnants in a small volume $\lesssim 1pc$, whose ultimate fate is probably to form a black hole. If there is a sufficient supply of gas then the AGN phase could begin (Weedman, 1983).

Once a mass of $M \gtrsim 10^9\ M_\odot$has been accumulated in a radius of few hundred pc, the fragmentation of the gas into massive molecular clouds and the orbital decay due to gas drag then occurs in a $10^6 yr$ time scale (Norman and Scoville, 1988). The final fate of the gas is to build up a star cluster of a few tens parsec by dynamical friction on a time–scale of $10^7 - 10^8\ yr$. Scoville and Norman (1988) have proposed that the broad emission line clouds in active galaxies are ionized mass–loss envelopes of giant stars whose line widths are due to the orbital motion in the massive cluster. If there is already a $10^9\ M_\odot$ black hole waiting for gas in the center of the galaxy, the luminosity due to accretion would become higher by a factor $\gtrsim 10$ than that due to the stellar cluster soon after $\sim 10^7 yr$. Otherwise $\sim 10^8 yr$ would be needed to form the $10^9\ M_\odot$ black hole at a mass loss rate of $\sim 10\ M_\odot\ yr^{-1}$. A possible objection to this model is that the massive starburst would leave a very large mass concentration $\gtrsim 10^{10}\ M_\odot$ in the inner few tens of parsecs of a galaxy.

On the other side, star formation could be a *a consequence* of the nuclear activity. Jets can certainly trigger star formation, since jet pressures are high compared to interstellar medium pressures, and produce an effect of cloud–cloud collision. Intense star formation has been observed where jets lose collimation and intensity (*e.g.* Keel, 1987 and references therein), but the *global* star formation rate is weakly affected. Since we are considering systems in which a *Starburst* is occurring, we think that

the question should be addressed this way: interaction is able to drive gas in the nuclear region of galaxies as well as to trigger nuclear and extensive Starbursts; thus are non–thermal activity and Starburst induced independently, or are they causally linked? Many heuristic indications suggest – if a causal link exists – that the connection should be in the sense of an evolution from Starburst to AGN. Although the *existence* of intermediate objects favours an evolutionary link, the late evolution of a Starburst is unclear: Starbursts of large spatial extent would give rise to strong galactic winds driven by supernova explosions would leave a large region free of gas, thereby depriving the AGN from gas (Heckman *et al.*, 1990).
In order to set the way interaction/AGN/SF are connected, it is necessary to have an age estimator for the Starburst and/or for the interaction phase. This can be done matching the observed morphology with N–body simulation for pairs of galaxies, which would also allow to study the orbital parameters of the encounter and its influence upon the star formation. A more difficult approach is based on the observation of the Hα, Hβ, Hγ, G–band absorption features coupled with the Balmer emission line diagnostic of the Lyman continuum. When the massive stars evolve through the red giant phase they produce abnormally deep CO absorption in the galaxy spectrum, as observed in NGC 253, M82 and NGC 6240 (*e.g.* Rieke, 1987). These feature are strongly dependent on stellar age, and can thus serve – for a given initial mass function – as rough *clocks* for tracing the star formation history. In the case of an aging burst, an age estimator is provided by the shape of the radio continuum (Condon *et al.*, 1982; Ulvestad, 1982). To our knowledge, this study has not been done as yet. In Chapter 3 the detailed study of an *intermediate* Starburst/AGN is presented, and its implications are analyzed.
In the following sections, the main concern will be to find an ultimate probe of the existence of the accretion disk around a massive black hole. Current arguments are based on the features of the continuum; we will rather be oriented to a *kinematical* signature due to the keplerian velocity field of the rotating disk.

1.5 Looking for (thick) accretion disks.

1.5.1 Basis facts on disks

Thin disks

The main problem of accretion of circumnuclear and disk gas onto the central core if the release of angular momentum. If gas is able to reach the inner $0.1 - 1$ *pc*, and if its angular momentum per unit mass exceeds $\sqrt{12}R_g c$ the infalling gas can reduce its angular momentum via viscous torques before it can cross the event horizon. In this case, the formation of an accretion disk is expected.
Theoretical expectations for steady disks are based upon the following assumptions:

1. the disk is able to radiate most of the released binding energy; this is equivalent to the conditions that the disk is geometrically thin, that is the disk height is $H(R) \ll R$ at each radius R.

2. the circular velocity v_ϕ of the disk is very close to its keplerian value, $v_\phi = (GM/R^3)^{1/2}$. Keplerian motion implies differential rotation, which reflect the presence of shear viscosity, i.e. transport of angular momentum in the radial direction. Shakura and Sunyaev (1973) introduced the phenomenological parameter $\alpha = \lambda_{turb} v_{turb}/c_s H$, where λ_{turb} is the scale size of the turbulent motion ($\approx$ H), and v_{turb} is the turbulent velocity ($v_s \lesssim c_s$). Hence, the thin disk assumption is consistent with the condition $\alpha < 1$.

The equations of the disk structure can then be integrated to find an analytical solution for the temperature, the surface density, the disk height the opacity as a function of the distance R from the black hole (Shakura and Sunyaev, 1973; Frank *et al.*, 1985). Integral properties of the disks depend upon M, $\dot{M}$, but not (or only weakly) upon α. For instance the disk luminosity is $L_{disk} = GM\dot{M}/2R_{in}$, where $\dot{M}$ is the accretion rate and R_{in} is the inner radius of the disk, located at the marginally stable orbit $R_{in} = 3R_g = 6GM/c^2$, where R_S is the Schwarzshild radius. The efficiency of mass to energy conversion ranges from $\eta = 0.057$ for a non-rotating hole to a maximum of $\eta \simeq 0.4$ for a Kerr black hole surrounded by a prograde disk. The spectrum emitted by the a geometrically thin, optically thick disk can be approximated by the expression:

$$L_\nu \propto \nu^{1/3} \exp(-h\nu/kT_b) \tag{1.2}$$

where T_b is the temperature at $R \approx 5R_g$. The temperature as a function of R is given by (e.g. Shakura and Sunyaev, 1973; Frank *et al.*, 1985):

$$T_b \approx 1.6 \cdot 10^5 \left(\frac{L}{10^{46} erg\ s^{-1}}\right)^{1/4} \left(\frac{R}{5R_g}\right)^{-1/2} \left(\frac{M}{10^8 M_\odot}\right)^{-1/2} {}^\circ K \tag{1.3}$$

From these equations we infer that T_b decreases as the black hole M increases: this has the important consequence that the emitted spectrum becomes softer for larger black hole masses.

Thick disks

The accretion rate cannot increase indefinitely without influence on the accretion mode. There is a limiting luminosity at which the outward radiation pressure on free electrons balances the gravitational attraction, and accretion is stopped. This limiting luminosity is called the *Eddington luminosity*, which in the case of spherical accretion is given by:

$$L_E = \frac{4\pi GMm_p c}{\sigma_T} \simeq 1.3 \cdot 10^{38} \frac{M}{M_\odot}\ erg\ s^{-1} \tag{1.4}$$

where m_p is the mass of the proton and σ_T the cross–section for scattering Thomson (*e.g.* Frank *et al.*, 1985).
Shakura and Sunyaev (1973) suggested that the hottest, innermost regions of the accretion disk should be dominated by radiation pressure. In this case the main source

of opacity should be electron scattering. The global structure of the accretion disk is controlled by the ratio $\dot{m}$ of the accretion rate $\dot{M}$ to the critical accretion rate $\dot{M}_{Edd} = L_{Edd}/\eta c^2 = 0.2 M_8\ M_\odot\ yr^{-1}$. If the Eddington ratio is $\dot{m} \gtrsim 1$ the accretion flow is unable to cool, since the electron scattering opacity increases as the Eddington ratio itself, $\tau_{es} \propto l\rho \propto \dot{m}$ (*e.g.* Begelman, 1985). If luminosity approaches the Eddington luminosity the disk inflates to form a radiation pressure supported torus, whose height is given by (Frank *et al.*, 1985):

$$H \simeq \frac{3R_{in}}{4\eta}\frac{\dot{M}}{\dot{M}_{crit}}[1-(\frac{R_{in}}{R})^{1/2}] \tag{1.5}$$

More generally the shape of a thick disk can be computed once the surface angular momentum per unit mass, the inner edge r_{in} and a suitable equation of state are specified (Madau, 1988). A pair of narrow funnels of aperture angle $\simeq 30°$ aligned with the rotation axis develops (Abramowicz *et al.*, 1980). The radiation field along the rotation axis is greatly enhanced by the multiple scatterings of photons along the funnel walls: radiation pressure in the funnels can potentially accelerate matter to relativistic velocities (up to $\gamma \sim 2$). The stability properties of thick accretion disks are far from being well understood: Papaloizou and Pringle (1984) showed that thick disks are subjects to non–axisymmetric instabilities operating on dynamical timescale. Recent works have taken into account the presence of several stabilizing mechanisms which should be very efficient particularly if the angular momentum distribution is described by a power–law function (Goldreich *et al.*, 1986; Blaes, 1987). Models are however not fully self consistent since the energy generation and transport are not modelled in any detail. Thick disks are a very interesting theoretical construct: they provide a tool for collimating plasma and radiation, for accelerating plasma to relativistic velocity, and a direct explanation for the many observations supporting anisotropic emission of the AGN continuum (Abramowicz *et al.*, 1987; § 1.9). The demand for the existence of thick disks stems also from the super–Eddington accretion rate deduced from the continuum fitting (Sun and Malkan, 1989; Laor, 1990; § 1.8).
Madau (1988) and Acosta–Pulido (1990) have investigated the emitted spectrum from a thick accretion disks. The model of Madau assumes a power–law distribution of the angular momentum, and it is probably *robust*, as far as global instabilities are concerned. The following basic points can be stated:

1. the bolometric luminosity depends strongly upon the viewing angle, e.g. the angle between the rotation axis and the line of sight. Madau (1988) studied a torus for which $L_{bol} \approx 6 L_{Edd}$, M $= 10^8\ M_\odot$, $r_{out} = 500 R_g$. In this case, if the torus would be seen within the opening angle of the funnel, the torus would appear to radiate at a luminosity $\approx$ 20 times larger than the Eddington luminosity. The same disks would seem to radiate near to the Eddington limit when seen edge–on;

2. the shape of the spectrum also depends upon the viewing angle; the spectrum is emitted within the funnel is harder because radiation from the hottest innermost part of the disk is able to escape; it becomes softer as the viewing angle increases;

3. the spectrum emitted becomes softer if the central mass or the outer radius r_{out} increases (the same trend holds also for geometrically thin disks).

1.6 Continuum emission from the accretion disk: the *Big Bump*

The AGN electromagnetic spectrum can be modelled without introducing thermal emission from an accretion disk. One of the most accreditated model is the synchrotron plus inverse Compton interpretation, which is able to satisfactory reproduce the whole spectrum from radio to γ–ray ranges (Jones *et al.*, 1974; Jones and Stein, 1990). At the other extreme, Sanders *et al.* (1989), and Bregman (1991) has suggested that most of the AGN continuum is emitted via thermal processes, with the exception of the radio and of the hard X–ray range. Both views seem too radical, since best fits for the far infrared flux (e.g. $10 - 100\mu m$) and for the *Big Bump* are obtained if the features are thermal in origin, but assuming that an underlying power–law continuum is present (Spinoglio and Malkan, 1989). Since the discovery of the *Big Bump* is a milestone in the search of an observational evidence of the accretion disk, we will discuss in this section the evidence supporting the disk origin of the *Big Bump*, and the assumptions (some of which rather *ad hoc*) recently introduced to satisfy several new observational constraints.

The first suggestion that the flattening observed in the continuum spectrum of AGN around 4000 Å and extending in the ultraviolet was due to thermal emission of an optically thick geometrically thin accretion disk was made by Shields (1978). Detailed fits of the continuum were made by Malkan and Sargent (1982) and Malkan (1983) for several AGN. Malkan and Sargent (1982) and Wills *et al.*(1985) showed that the continuum flattening around 4000 Å was due to Balmer continuum, blends of high order Balmer lines, and blends of FeII lines, whose contributions extended down to 2000 Å (the *little Bump*), and that a more prominent feature, the *Big Bump* was detectable from $\sim 1\ \mu m$. Malkan and Sargent (1982) considered in their fits a single temperature black body curve, plus a power law component and the contribution from the *little Bump*. UV data collected by Malkan (1983) allowed to extend the frequency domain over which the continuum could be fitted. The new data were represented at best by a stretched blackbody curve, as emitted by an optically thick geometrically thin accretion disk (eq. 1.2). Although the frequency extension of the continuum was not fully understood at that time, the very good agreement obtained in the model fitting with a black body or a stretched black–body spectrum raised the convinction that a first signature of the accretion disk had been found. In principle, model fitting can provide most important parameters,as M, $\dot{M}$ and the disk inclination i. In practice, due to the difficulty to measure the energy emitted in the *Big Bump* only the accretion rate $\dot{M}$ and $M_{bh}/(\cos i)^{3/2}$ can be tightly constrained (Malkan, 1991). Difficulties arise because little part of the *Big Bump* is accessible for direct observation. The spectrum below 1200 Å in the rest frame of the object has been observed only exceptionally on space–

borne observatories for a few bright quasars of intermediate redshift (Reichert *et al.*, 1988). Although strong blended absorption features affect the continuum shortward of the Lyman limit, there seems to be no cutoff in the spectral shape shortward of 1200 Å. A different method for gaining information about the EUV continuum is to reproduce emission line ratios and fluxes for different shapes of the continuum, and to compare the computed values with the observations. Unfortunately, the strength of most lines depends much more on the ionization parameter than from the shape of the ionizing continuum (Tarter *et al.*, 1969). A sensitive tool are only the very high ionization recombination lines (as OVIλ1034, HeIIλ1640), which are dependent upon the shape of the continuum just beyond the ionization edges of the ions producing the lines, but which are not easily observable. Krolik and Kallman (1988) computed the emerging emission line spectrum for a *pure* power–law spectrum, and for a power law continuum plus a thermal component peaked at $kT_b = 10\ eV$ and 80 eV. The observed mean value of the ratio HeIIλ1604/Lyα $\sim$ 0.01 (Veron–Cetty *et al.*, 1981) for Seyfert galaxies compares with the predicted value for the power–law plus a 10 eV thermal component, HeIIλ1604/Lyα $\sim$ 0.02, while the 80 eV component leads to a ratio which is too large (HeIIλ1604/Lyα $\sim$ 0.06 – 0.11). This suggests that the *Big Bump* may peak at energies close to 10 eV. Clavel and Santos-Lleo (1990) used the large variations observed in the line and continuum emission of the Sey–1 galaxy F9 to infer the position of the turnover frequency of the *Big Bump*. These authors showed that the spectrum needs to steepen considerably at 1 Ryd in order to explain the variations of the Lyα/CIVλ1549 ratio given by the ultraviolet and X–ray continuum variations.

On the high energy side, the *Big Bump* is probably connected to the ultra–soft X–ray excess or even with the soft X–ray excess, extending respectively up to energies $\sim$ 0.1 keV and $\sim$ 2 keV. The connection is supported by the evidence of variability in the soft X–ray range uncorrelated with the hard part of the spectrum, suggesting that the soft X–ray excess is emitted by a distinct component (Turner and Pounds, 1989). Furthermore, BL objects, which do not have the *Big Bump*, also lack the soft X excess (e.g. Urry, 1988, for a review). If the *Big Bump* extends up to 0.1–2 keV the maximum temperature of the disk should be $\sim 10^6\ ^\circ K$, with the unkind drawback that the disk should radiate at a Super–Eddington rate. Bechtold *et al.* (1987) suggested that the electron scattering influenced the continuum opacity in the innermost parts of the disk. Electron scattering is able to produce a flattening in the high energy tail of the stretched black body spectrum, without increasing the maximum temperature T_b of the disk (Bechtold *et al.*, 1987; Czerny and Elvis, 1987). Sun and Malkan (1989) employed non LTE stellar atmosphere models in order to account for the electron scattering opacity, and assumed that the disk was rotating around a Kerr black hole. This allowed to solve the problem of the super–Eddington disk luminosity, since the efficiency of accretion is higher for a Kerr black hole than for a non rotating one. Sun and Malkan (1989) were able to fit with very good agreement the overall spectral shape of some quasars and Seyfert galaxies spanning over 6 decades in frequency, from the far infrared to the soft X–ray range (logν $\sim$ 12–18, see Fig. 1.3). Noticeably, their results

compare with the trend obtained from the dynamical estimate of masses and accretion rates: Seyfert galaxies accrete at a sub–Eddington rate, while quasars accrete near or above the Eddington rate.

Important advances on the origin of the continuum have been gained from optical/uv/X monitoring campaigns of some variable Seyfert galaxies, and from the comparison of the variability time scales and amplitudes in the different energy ranges. There is evidence of *no significant time delay* between the variation at optical and UV (1300 Å) wavelengths. Three Seyfert galaxies (NGC 4151, NGC 5548 and F9) and one quasar (3C273) have reliable upper limits to the lag between uv and optical variations. In all cases the variability timescale (estimated as the sound crossing time needed to reach the uv emitting regions from the optical emitting regions) is several order of magnitudes longer than any upper limit of the time lag (Clavel *et al.*, 1990; 1991; Ulrich *et al.*, 1991). The short time delay suggests that the same emission mechanism seen at different wavelength produces the variable part of the uv and optical continuum. In the Shakura-Sunyaev model the optical/uv continuum is produced by the viscous flow in the disk. The time lag expected between optical and uv variations is governed by the radial drift timescale between the optical/uv emission regions which is $t_{vis} \sim$ *several years*. In order to save a disk origin for the optical and uv continuum, it is necessary to suppose that the uv radiation is reprocessed optical radiation. Since most of the disk radiation comes out from the hottest innermost part ($\lesssim$ 20 R_g), light bending may redirect radiation emitted in the inner disk region along the equatorial plane (Netzer, 1991). Otherwise, part of the continuum could be scattered in region at large height above the disk (Dumont and Collin–Souffrin, 1990a). We will return later (Chapter 4) on the latter point.

If the continuum is emitted by a geometrically thin accretion disk it should be highly polarized ($\sim$ 11%; Shields, 1978). Netzer (1991) however stressed that general relativistic effects could lead to a depolarization of the continuum because of the rotation of the polarization plane dependent upon the radius of emission. Since the spectrum emitted at a given frequency includes a contribution from a range of radii (and hence of polarization planes) is less polarized. The computations suggest that the percentage of polarization should be reduced to 2–3 %, a value which is still higher than that observed ($\approx$ 1 %). Laor and Netzer (1989) predict that the increase in absorption opacity near to the Lyman limit should give rise to a strong broad polarization feature.

A thermal component in the spectrum is not necessarily a probe for the existence of an accretion disk: it simply means that there is optically thick gas which is able to absorb the radiation and to reradiate it after thermalization. Guilbert and Rees (1988) proposed that the soft X–ray bump is emitted by very dense optically thick clouds heated by the central source and located at a few gravitational radii ($\sim$ 20 R_g) from the black hole. In the following we will be concerned with the problem of the emission of a line spectrum from an accretion disk.

The discovery of a flattening at energies between 10 and 30 keV add a vary interesting indication in favour of cold and dense matter in the vicinity of the black hole. Indeed, the reflection model (Lightman and White, 1988), which assumes that the composite

X–ray spectrum consists of a direct component and a reprocessed one by cold optically thick matter ($N \gtrsim 10^{24} cm^{-2}$, Piro *et al.*, 1991) can reproduce the spectrum better than other simple models. The observation of a 6.4 keV iron fluorescence line, variable in phase with the 10–20 keV continuum suggests that the hard flatter component may be due to Compton scattering of the softer X–ray continuum by (mostly) neutral iron in cold gas. We believe that a powerful test for the accretion disk will be the Kα line, nearly resolved in the GINGA spectra, which will be resolvable with the next generation of X–ray spectrometers. The very broad profile – when resolved – could provide evidence of rotating matter at a few gravitational radii from the black hole. The importance of this issue is not limited to the understanding of the BLR kinematics, but stems also from the possibility to find evidence for the existence of the disk itself from the analysis of line profiles.

1.7 Line emission from the accretion disk?

1.7.1 Theory of line formation

The observational and theoretical knowledge led to the *heuristic* model described earlier, in which a roughly spherical ensemble of many, small optically thick gas clouds undergoing rapid motion under (for now) unspecified acceleration mechanism, is photoionized by a powerful, non–thermal continuum source. The proportionality between line and continuum emission (Yee, 1980; Shuder, 1981) strongly suggests that photoionization followed by recombination is the main excitation mechanism for the BLR gas. Photoionization explains also why we see high ionization species such as C^{+3} and N^{+4}, while the temperature is not larger than $\approx 2 \cdot 10^4\ ^\circ K$ (*e.g.* Davidson and Netzer, 1979).
In this framework, it is possible (Kwan and Krolik, 1981, hereafter KK; Kwan, 1984) to compute the line emergent flux from a single cloud of given chemical composition under the assumption of plane–parallel geometry. Starting from the illuminated surface of the slab, the ionization, thermal and pressure equilibrium are solved at each point. Simultaneously, the excited state population is also self–consistently computed for the HI, OI, HeI and FeII atoms. The continuum and line radiation transfer is treated computing at each optical depth a mean local escape probability (averaged on the line profile), which measures the probability that in a semi–infinite plane–parallel medium a line photon emitted toward the surface at a point of optical depth τ_0 escapes without undergoing subsequent scatterings. The main physical processes entering the ionization balance are ionization both by radiative and collisional processes. Radiative processes include ionization from the ground state end excited states of HI atoms by incident and diffuse Lyman continuum photons, spontaneous and induced recombination, ionization by incident hard UV and X radiation. Collisional processes involve collisional ionization from HI excited states by thermal electrons, and ionization from the ground state by non–thermal electrons, dielectronic and three body recombination and charge exchange processes (the last four processes were not included in the original KK work). Five

main inputs are necessary: the ionization parameter Γ, the electron density n_e at the illuminated surface of the cloud, the shape of the photoionizing spectrum, the column density and the chemical composition. The final results are reached by fixing the column density at which a set of reliable line fluxes is obtained. Near the illuminated surface of the cloud, the ionizing continuum creates a regions where the hydrogen is completely ionized (HII zone). The ionization structure at larger optical depths of the slab is of basilar importance for understanding the emitted fluxes: proceeding further in the cloud, after the Lyman continuum is exhausted, X–rays ionization of He, H and heavy element becomes the main source of heating. At high energy photoionization of heavy ions can dominate the opacity. X–rays will produce high energy electrons, which loose their energy via the following processes: (1) Coulomb collisions, directly heating the gas, (2) collisional ionization, yielding secondary electrons, (3) excitation of bound levels, especially of H^0, leading to line radiation. If these effects are considered, a *Partially Ionized Zone* (PIZ) develops, with $H^+/H^0 \approx 0.1$ and $T \approx 8000\ ^\circ K$. This zone emits a strong contribution in the Balmer lines, the Mg II λ2800 and the FeII lines and the Balmer continuum (Halpern and Grindlay, 1980; KK).
Photoionization calculations are able to explain the observed high–ionization line ratios within a factor of 2. Particularly the wide range of ionization species observed in the AGN spectrum are readily accounted for: the HII region emits the bulk of the high ionization lines, like CIV λ1549, Lyα, NV, OIV, whether the PIZ allows to have simultaneously the presence of the MgII, FeII.
Despite this success, several problems remain to be solved in order to get a satisfactory agreement with the observations. The most important ones are:

- The FeII problem: photoionization models yield a FeII to hydrogen line ratio about a factor 3 smaller than the average observed one; a better agreement is obtained when very high density ($n_e \geq 10^{12} cm^{-3}$) and large column densities $N_c \approx 10^{25} cm^{-2}$, in order to allow a significant absorption of X–ray radiation in the range between 10 and 200 keV (Collin–Souffrin, *et al.* 1986; Collin–Souffrin, 1988; Wills *et al.*, 1985). It remains unclear whether the strength of the FeII lines can be *entirely* explained by radiation transfer effects in a dense medium, or whether chemical abundances above solar are necessary (Collin–Souffrin, 1986).

- the Lyα and the *energy budget* problems. It is known that the expected value of the ratio Lyα/Hβ, under case B conditions and for density higher than $1.6 \cdot 10^4 cm^{-3}$, where $2s \longleftrightarrow 2p$ levels are collisionally exchanged in spite of the 2–photon continuum (*e.g.* Osterbrock, 1974; Netzer, 1982), is ≈ 34 and decreases at a minimum value ~ 23 to $T \sim 10^4\ ^\circ K$ as $n_e \rightarrow 0$. At sufficiently large optical depth Lyα is thermalized and a significant amount of hydrogen is sustained in excited states. If the heating rate remains appreciable collisional excitation of Hα, Hβ competes against collisional excitation of lines of heavy elements for the available energy. Thus the Balmer lines are enhanced where Lyα is saturated, reducing the Lyα/Hβ ratio from the case B to the observed value ≈ 5. In facts, the KK model and its refinements were able to explain for the first time the very

low ratio Lyα/H$\beta \approx$ 5 observed. This problem remains however unresolved by the KK work, since KK employed a continuum with a too strong X–ray component which is rarely observed. For instance, Zamorani *et al.*, (1981) found a spectral index $\alpha_{ox} \approx 1.3$, which results in a ratio of the flux at 2 keV over the flux in proximity of the Lyman edge $F_\nu(2keV)/F_\nu(Lycont) \approx 6$) times smaller than the KK continuum. Netzer (1985a) noted that a substantial part of the total broad line flux is emitted in the small bump, which is formed by thousand of FeII lines and by Balmer continuum. Taking into account this contribution, Collin–Souffrin and Lasota (1988) suggest that: $< F(Ly\alpha)/F(H\beta) >= 6$, $< F(HIL)/F(Ly\alpha) >= 3$, and $< F(LIL)/F(Ly\alpha) >= 5$. Netzer (1985a,b) stressed that his photoionization calculations provide a value of the $Ly\alpha$ flux which is not too much different from the case B value ($\approx 1 - 1.5$ (Kwan and Krolik, 1981; Kwan, 1984; Mushotzky and Ferland, 1984); hence the problem resides in a selective enhancement of the Balmer line and in the LIL, rather than in a suppression of the Lyα photons. Netzer proposed that also internal reddening plays a major role for explaining the *energy budget* problem of the BLR. It is unclear whether internal reddening in the BLR gas is able to play a role appreciably in affecting the observed line ratios. Although the observed line ratios seem to generally exclude E(B–V) larger than 0.2, it seems more likely that the dust content is strongly variable from object to object. The problem is made difficult by the lack of any reliable reddening indicator for the BLR: only the line ratio HeII λ4686/ λ1640 avoids optical depth effects, but it is very difficult to estimate (Netzer *et al.*, 1985; Grandi 1983). Collin–Souffrin (1986; 1988) pointed out that the presence of reddening would enhance the *Fe II problem.* Present photoionization codes fail in accounting for the observed strength of the optical and UV FeII multiplets with respect both to the Balmer lines and to Lyα. If a substantial reddening affects the observed line ratios, the HIL should be preferentially absorbed, since they are mainly emitted in the UV. The reddening correction would enhance the HIL in comparison to the LIL, but at the same time it would enhance the ratio between the optical FeII strength and Hβ. Thus, the FeII/Hβ problem is worsened by reddening. Although reddening should computed before the observed and theoretical line ratios are compared, it seems unlikely that internal reddening is determinant in solving the *energy budget* problem. The *energy budget* problem is readily accounted for once it is assumed that a substantial fraction ($\sim$ 10%) of the hard X–ray flux ($h\nu >$ 2 keV) is selectively absorbed by the disk, which has column density $N_c \geq 10^{25} cm^{-2}$). On the contrary, the BL clouds ($N_c \sim 10^{22} cm^{-2}$) are transparent to the hard X–ray flux (Collin–Souffrin and Dumont, 1989). This is the physical basis on which line emission from the disk is possible, as discussed below.

- It is difficult to explain the observed spectrum in terms of a unique value of the ionization parameter; very high ionization lines NV λ1240 and OVI λ1034 favour $\Gamma \approx 0.03$, while the CIV/Lyα and CIII]/Lyα favour $\Gamma \approx 0.01$. The strength of

the FeII lines indicates that Γ should be $\ll 0.01 \sim 10^{-4}$.

- The $H\alpha/H\beta \approx 2 - 3.5$ ratio would be better explained if dense, optically thick gas is present. If the density is very high, $n_e \sim 10^{12} cm^{-3}$, then the optical depth on the Paschen continuum would led to the selective suppression of Hα, thus decreasing the Hα/Hβ ratio. At the same time, the CIII] line requires a density $\leq 10^{9.5} cm^{-3}$.

- The presence of optically thin gas is demonstrated by the presence of Lyβ in high redshift quasar spectra, but it is not clear whether optically thin gas emits a considerable contribution to the lines. The OI λ8446 line is emitted via a Bowen fluorescence mechanism by gas very optically thick to Lyα (Elitzur and Netzer, 1985). It has the same profile of Hα, which can be emitted both by optically thin and optically thick gas (Morris and Ward, 1989). Only two objects among the 12 studied by Morris and Ward (1989), Akn 120 and IC 4329A, show profile differences, in the sense that Hβ has a stronger blue wings than OI λ8446. This implies that usually optically thin gas is not present or it follows the same velocity field as the optically thick gas, apart the high velocity gas which emits the line wings.

Further results hint that the observed spectrum cannot be reproduced in terms of a unique emissive medium:

- Gaskell (1982, 1983a) has found that HIL (Lyα and CIVλ1549) are systematically blueshifted by several hundred of $km\ s^{-1}$ with respect to the Balmer lines and to the MgIIλ2800 line. Espey *et al.* (1989) obtained spectra of intermediate to high redshift quasars and confirmed that Lyα and CIVλ1549 are sistematically blueshifted (by $\sim 1000\ km\ s^{-1}$) with respect to the Hα and MgIIλ2800 line/ Ulrich *et al.* (1984) found that various broad lines react to changes in the ionizing continuum with different timescales, providing an other evidence that the excitation level of the emitting gas is kinematically and spatially variable (Mathews and Wampler, 1985; § 1.6).

- Differences in profile width between low–ionization and high–ionization emission lines, and different responses to continuum changes for lines coming from different ionization stages (see *e.g* Osterbrock, 1985; Ulrich *et al.*, 1985; Penston, 1991 for a recent review; § 1.7.4) confirm the need of (at least) two disjoint emitting media of different density and location with respect to the continuum source.

These facts led Collin–Souffrin (1987), Netzer (1985b), Smith and Raine (1980), Mardaljevic *et al.* (1988) to suggest that the BLR is made up of two disjoint emitting media: a dense region, emitting the bulk of the LIL, identified with the accretion disk, and a second region, characterized by the same physical parameter of the standard model, mainly contributing to the HIL.

A correct treatment of the line formation problem in the dense region may therefore require that both high numerical and column densities are taken into account. High numerical densities require an adequate treatment of the excited state population balance for a large number of new ionic species (C^{+2}, C^{+3}, N^{+4}, Si^{+4}, Mg^{+2} (Krolik, 1988b) since more and more ground state transitions are thermalized. High column densities imply an accurate treatment of the line transfer. The mean escape probability may not be valid, since the non-local absorption will affect photons coming from a large number of transitions. In the works of Dumont and Collin–Souffrin –which assume that the dense region is an illuminated part of the disk – the treatment of the line transfer is still based on the mean escape probability formalism. The ionization and excitation equilibria are treated in a simplified way (Collin–Souffrin and Dumont, 1989). This could be adequate for the Balmer lines, but not for the FeII and MgII lines.

1.7.2 Emission line production from the outer regions of accretion disk

The gravitational energy release at distances $R \gg R_g$ is given by: $D(R) \approx 3GM\dot{M}$ $8\pi R^3$ $ergs^{-1}cm^{-2}$. In the SS model, $n_e \lesssim 10^{12}cm^{-3}$ for $R \gtrsim 10^3 R_g$ (Dumont and Collin–Souffrin, 1990a). Integrating over the disk surface for $R > 10^3 R_g$, we get a total disk luminosity $L_{disk} \sim 5 \cdot 10^{40}$ erg s^{-1}, for $L \simeq 0.1 L_{Edd}$ and $M \approx 10^8 M_\odot$. Since the typical energy emitted in Hα is $10^{42} erg$ s^{-1},the emission of the accretion disk can not be responsible for the entire emission in the Balmer lines, unless an additional, external source of heating is present. An additional requirement for the production of emission lines from the disk is that the temperature increases in the vertical direction. The SS model gives the radial behaviour of the central and surfaces temperatures, T_c and T_σ. Both scale as $\propto R^{-3/4}$, but T_σ is always $< T_c$, in the inner region where the disk is optically thick (note that the column density decreases with increasing radius). The inner part of the accretion disk should therefore emit *absorption lines.*

An external radiating source can completely alter the vertical temperature gradient. Therefore, the disk should be able to see part of the ionizing continuum, either directly or after being scattered, for producing emission lines. The first possibility seems unlikely, since the covering factor of the disk should be very small. The second one appears more plausible. Several mechanisms have been proposed in order to account for the reflection of the ionizing radiation toward the disk, among others scattering due to the highly ionized gas above the disk, or reflection by the BL clouds moving over the disk. Collin–Souffrin and Dumont (1990) and Dumont and Collin–Souffrin (1990a) have shown that scattering of the continuum toward the disk can heat a column density of about $10^{25} cm^{-2}$ to a constant temperature of $7 \cdot 10^7$ $^\circ K$. At the radius where the column density becomes lower than $10^{25} cm^{-2}$, the disk becomes optically thin to visible emission and is able to emit a line spectrum. Since the disk column density is very large, the column density of the PIZ depends much more on the shape of the spectrum in the X–ray range rather than on the ionization parameter (Kwan and Krolik, 1979; 1981; Halpern and Grindlay, 1980; Dumont and Collin–Souffrin, 1990a),

and it is expected that the ratio I(HIL)/H(LIL) is $\ll 1$, provided that the continuum follows a flat enough power-law spectrum, with $\alpha \lesssim 1$, *up to 100 keV*. According to the computations of Dumont and Collin Souffrin (1990a) and Collin–Souffrin and Dumont (1989), the scattered X–ray radiation produces a very extended PIZ, which is able to produce the bulk of the LIL, once a suitable model for the external illumination has been provided.
Collin–Souffrin and Dumont (1990a) consider two possibilities:

- the illuminating sources are two point sources located symmetrically at a height A above the black hole; the physical meaning of this model becomes clear if we consider for instance that part of the continuum is reflected by cloud constrained in a jet along the disk axis (*Point Source Model*, PSM).

- disk illumination is provided by a scattering medium above the disk, which redirects part of the ionizing continuum emitted in the innermost part of the disk toward the outer disk region (*Diffusion Model*, DM).

Collin–Souffrin and Dumont (1990b) and Dumont and Collin–Souffrin (1990b) found moreover that the equivalent width of the lines produced by the disk *are in good agreement* and can equal the observed ones. The disk can also give a *partial* contribution to the total line emission, according to the fraction of continuum scattered toward the disk for a fixed bolometric luminosity. The $Ly\alpha/H\alpha$ ratio is smaller than observed ($\sim 0.2 - 0.6$, depending on the illumination model), since Lyα originates in different regions. We shall return to this point in Chapter 4. One strong point in favour of this model is that it solves the *energy budget problem* for the BLR, since the X–ray flux backscattered to the disk is responsible for a strong enhancement of the LIL. The detection of cold optically thick gas in the vicinity of the black hole add further support to this model.
Dumont and Collin–Souffrin (1990b) and Rokaki *et al.*(1991) computed the emission line profiles self–consistenly, that is evaluating radial dependence of the emissivity on the base of a photoionization code.

1.7.3 Line profiles from the accretion disk

One challenge to the BLR models is the variety of emission line profiles and shifts observed among AGN. Quasars tend to have symmetric, logarithmic shaped profiles. The profile does not change during flux variations. Profile shapes among Seyfert galaxies range from flat–topped, bell–shaped, to truly logarthmic profiles. Asymmetries are widely observed, both to the red and to the blue (see Chapter 4 for a more quantitative analysis), with a weak preference for red shifts and red asymmetries. Among radio–loud AGN there are examples of unusually very broad and structured profiles (Miley and Miller, 1979; see again Chapter 4 for a thorough discussion of some of them). Variations (some of which very remarkable, as for instance the disappearing of the broad component in NGC 4151) occur on time–scales of months, and in some cases

of several weeks. Several kinematical and dynamical models have been discussed in the past years: ballistic outflow, outflow driven by radiation pressure, gravitational infall, orbital motions, rotation, turbolence *etc.* (for a review see Mathews and Capriotti, 1985). Logarithmic profiles are reproduced satisfactorily in models assuming that the Balmer lines are emitted by an ensemble of optically thick clouds outflowing under the effect of radiation pressure (Mathews and Blumenthal, 1977; Blumenthal and Mathews, 1979), but this models also predict asymmetric Lyα emission, the contrary of what is observed. The gas in the disk moves approximately at the local keplerian speed. A continuous disk of gas gives very distinctive profiles which, at a first glance, are not commonly observed (*e.g.* Mathews, 1982):

1. the core will be double–peaked, as if the line were self absorbed. This is a direct consequence of the keplerian velocity field and of the finite extension of the disk. Profile substructures do not provide unambiguous supporting evidence for disks: shoulder can for example arise in spherical cloud distribution as a result of irregularities in the radial line luminosity distribution. In this case however the structures should be rather transient and be subject to considerable changes on timescale comparable to the light travel time of the BLR, $\tau_{LT} \simeq 5 \cdot L_{42}(H\beta)^{1/3}/N_9^2 f_f$ *days*, where $L_{42}(H\beta)$ is the Hβ luminosity in units of 10^{42} *erg* s^{-1}. The profiles considered best candidates for disk emission discussed in Chapter 4 show substructures which are long lasting (ten years) with respect to a typical $\tau_{LT} \simeq 10$ *days*.

2. the profile is symmetric and, for non–pathological variations of the emissivity along the radius, the line wings should be smooth;

3. the profile should remain symmetric also during responses to continuum changes (*e.g.* Blandford and McKee, 1982). Response of a keplerian relativistic disk to variations in the continuum has been recently studied by Stella (1990). He suggest that a short-lasted doubling of the continuum could give rise to two features on the opposite sides of the lines, which gradually drift from the line wings to the blue and red horn, without however affecting the profile symmetry.

Asymmetries in line profiles are possible only if:

1. relativistic effects are relevant;

2. the disk is not uniformly illuminated, e.g. the emissivity depends upon the azimuthal angle.

Relativistic disks show an enhanced blue peak because of Doppler boosting and a redshifted line base because of the combined effect of gravitational and transverse redshift: $\Delta v_r = \frac{3}{2} GM/Rc^2$.
Increasing attention has been paid in the most recent year to the possibility that the lines are emitted by the accretion disk. One reason for this is that the size of the inner edge of the BLR is now thought to be much closer to the central black hole (a few

hundred R_g, § 1.7.4) than as estimated on standard photoionization arguments. The second reason is the impressive agreement between the observed Balmer line profiles of Arp 102b and the prediction for line emission from a relativistic disk (Chen *et al.*, 1989), although the profiles of Arp 102b seem to be rather uncommon (*e.g.* § 4.2). Relativistic disk features are observed in the Balmer line profiles of Arp 102b, but they cannot be easily recognized in nearly all AGN.
Dumont and Collin–Souffrin (1990b) and by Rokaki *et al.* (1991) show that profiles computed assuming large disk radii, both in the diffuse and in the point source model are generally single peaked, with shoulders (in the diffuse model) or with a *narrow* core and an underlying broad component (in the point source model). Attempts to fit observed profiles give good agreements near to the line core and in the *intermediate* line wings. The fits are of poor quality at the line center and in the far wings (Rokaki *et al.*, 1991). The profiles of the far wings could be reproduced adding an additional outflowing component to the disk emission (van Gröningen, 1983). This reduces somewhat the apparent disagreement between theory and observation, but a word of caution is issued in Chapter 4.
Recent results on line variability suggest important constraints on the model of the emission region.

1.7.4 Line profile variability

Line profile variability is in principle the most powerful method to gain insight on the geometry and on the velocity field of the line emitting gas. Variations in the ionizing continuum can give rise to substructures in the broad line profiles, if two conditions are met: first, the velocity field of the BLR is ordered; second, the light travel time of the BLR compares with the timescale of the continuum variations. If lines respond to changes in the ionizing continuum, then the light curve of an emission line $L(t)$ is related to the continuum light curve $C(t)$ by the convolution with a transfer function $\Psi(t)$, which depends upon the geometry of the BLR: $L(t) = \int_0^\infty \Psi(\tau)C(t-\tau)d\tau$. The time lag between line and continuum variation is given by the displacement from zero of the maximum of the cross correlation of function between $L(t)$ and $C(t)$ (Gaskell and Sparke, 1986). This provides an estimate of the *inner radius* of the BLR. The convolution equation is valid only if the continuum is emitted by an unique source whose extension is much less than the line emission region. Note that this may be not true if the continuum is also scattered by a medium partly located beyond the inner edge of the disk (§ 1.7, Chap. 4). Ideally, if the signal to noise ratio would be excellent and data would be evenly and densely sampled it should be possible to obtain the two dimensional transfer function $\Psi(v,t)$ from $L(t,v) = \int C(\tau)\Psi(t-\tau,v)d\tau$ and hence to solve for the velocity field of the BLR. From even and dense observations of $C(t)$ and $L(t)$ one could solve at least for $\Psi(t)$. While monitoring campaigns devoted to obtain the $\Psi(t,v)$ are in progress, important results based on the one dimensional transfer function have been recently published.
Clavel (1991) and Clavel *et al.*(1991) examinated the light curves obtained for the most

prominent ultraviolet emission lines for NGC 5548. This provides a very interesting test on the need of different emissive media for the BLR. From a cross correlation analysis it results that the high ionization lines NVλ1240, and Lyα, SiIV+OIV] vary with maximum amplitude and with time delays of 4 and 12 days respectively. The CIVλ1549 line varies with a time lag of 8 days, while the lag is considerably longer for CIII]λ1909 (26 days) and, noticeably, for MgIIλ2798 (34–72 days). The MgIIλ2798 was underwent only a tiny variation in flux ($\lesssim$ 30 %). Roughly the same trend was found to hold for Mkn 335 (Koratkar and Gaskell, 1991) Hβ follows the continuum by $\sim$ 24 days, while the optical and uv continuum have a time lag $\lesssim 2$ *days* (Malkan, 1991). The fair wings are less variable that the line cores, suggesting that they are optically thin to the ionizing continuum.
In NGC 4151, the CIVλ1549 and MgIIλ2798 lines varied strongly, with a time delay short compared to the continuum $\lesssim 4$ *days*, while the CIII]λ1909 lines remained nearly constant (Clavel *et al.*, 1990). Maoz *et al.* (1991) obtained a lag ~ 9 *days* for the Balmer lines. The BLR appear thus to be extremely compact in this object. Variations appeared to be simultaneous in the red and in the blue wings of the lines, and occurring in a timescale shorter than that of the line core, both in NGC 5548 and in NGC 4151. This ruled out the possibility of dominant radial motions in the BLR of these objects, and suggests that the velocity dispersion of the BLR gas increases for decreasing radial distances. Moreover, Horne and Welsh (1991) suggest that Hβ and Lyα originate in disjoint regions since their transfer functions are very different.
These variability results thus confirm that the distance of the BLR from the central source is smaller than assumed in standard photoionization models (Koratkar and Gaskell, 1990), and that the LIL and HIL are emitted in disjoint media.
The onset and the variation of additional BL components is also observed. Ulrich *et al.* (1984) noted in NGC 4151 the presence of two *satellite* components around the CIV λ1549 line, which were visible when the continuum level is low and situated ~ -30 and $\sim$ 40 Å from the center of the CIVλ1549 line. This allows an interesting comparison wih the optical spectrum of SS433, where both a blueshifted and redshifted system of lines is observed (*e.g.* Zwitter *et al.*, 1990, for a recent review). The intensity of the satellite components in NGC 4151 is variable on time scales of months, but do not *strictly* correlate with changes in the continuum. The peak wavelength of the two satellite lines is constant since 1981. (Ulrich *et al.*, 1984; 1985; Clavel *et al.* 1987). This feature bears some resemblance with the presence of two broad components, respectively blueshifted and redshifted by $\sim$ 2000 $km\ s^{-1}$to the center of Hβ, discovered in NGC 5548 by Peterson *et al.* (1987) and Stirpe *et al.* (1988). The flux in both the blueward and the redward component does not seem to be correlated with the continuum variation, but the red component seems to vary in a different way than the blue one (Peterson, 1988). This fact disfavours the suggestion that the two satellite components are emitted in a disk–like geometry (as instead proposed by Stirpe *et al.* (1988)). These components could be otherwise produced and enhanced by trapping of the broad line gas in jet–like geometry by the radio emitting plasma (Blumenthal and Mathews, 1977; Whittle *et al.*, 1988).

1.8 Mass and accretion rate estimates for AGN black holes

The presence of a deep potential well in AGN is suggested by the very broad profiles of the emission lines (Woltjer, 1959) and by the observations of superluminal motions in some radio–loud quasars. Under the assumption of infall, the dynamical mass of the central black hole is $M = v^2 r/2G$, where v is the infall velocity at distance r. Wandel and Yahil (1985), Padovani and Rafanelli (1988) and Padovani (1989) computed the dynamical masses and the Eddington ratios for several Sey–1 galaxies and quasars. Padovani (1989) found a strong dependence of the Eddington ratio on the redshift: Seyfert galaxies radiate at a very sub-Eddington rate ($L/L_{Edd} \sim 10^{-0.8}$), while high redshift quasars are above the Eddington rate ($L/L_{Edd} \sim 10^{0.5}$). Wandel and Yahil (1985) on the contrary suggested that the masses are proportional to the luminosity of the non stellar continuum, and thus that the Eddington ratio is constant and $\ll 1$ for both Seyfert galaxies and quasars. Padovani estimated the mass measuring the the FWZI of the broad Hβ line; this should give the maximum velocity v_{max} reached at the inner boundary of the BLR r_{min}. The estimate of r_{min} was based upon the definition of the ionization parameter Γ: $r_{in} = (N_{ion}/4\pi c(\Gamma n)_{in})^{1/2}$, N_{ion} was obtained from observations of the uv and X–ray continuum, while the product $(\Gamma n)_{in}$ was assumed constant fro all AGN and $\simeq 10^{9.5} cm^{-3}$. Although the latter assumption is very rough, it is qualitatively justified by the similarity of the spectra of Seyfert galaxies and quasars. Severe uncertainties affect both works, but probably the result of Wandel and Yahil is affected by a spurious correlation: they estimated r as $r \approx N_e f_c/f_f n_e$, and the mass $M \propto (L_{H\beta}/n_e f_c N_e)^{1/2} v^2$. They assume that the covering factor is luminosity dependent: $f_c \approx 1$ if $L < 2 \cdot 10^{43} erg\ s^{-1} = L_1$, and $f_c \propto L^{-0.2}$ if $L > L_1$, where L is the continuum luminosity at 4000 Å. This assumption strengthen the correlation between mass and luminosity: since $V \propto L^{0.2}$ (Joly *et al.*, 1985) and $L_{H\beta} \propto L$ (Shuder, 1982), $M \propto L$.

Smaller masses are suggested by X–ray variability. Variation of the luminosity can give an upper limit on the size of the emitting region, $R \lesssim 2c\Delta t$, where Δ is the characteristic time for variability. Assuming that the emitting region for hard X–rays is $\gtrsim 5R_g$ (Lightman *et al.*, 1979), the mass can be estimated from $M(\Delta t) \gtrsim (c^3/10 \cdot 2 \cdot G)\Delta t \approx 10^4 \Delta t M_\odot$ (Wandel and Mushotsky, 1986). GINGA observations have shown that the Seyfert galaxy NGC 6814 is strongly variable on very short timescales (doubling timescale $\lesssim 50$ *sec*; Turner *et al.*, 1991). Since the continuum cannot arise at $R \lesssim 5R_g$, $R_g \sim 10lt - sec$, implying that the central mass $M \lesssim 10^6\ M_\odot$. The findings on X ray variability challenge the current models of continuum emission. X–ray emission is so rapidly variating in some objects that it is not consistent even with single black hole models, suggesting that the emission can be anisotropic. In this case, it is dangerous to deduce the size of the emitting regions from X–ray variability.

1.9 Anisotropic emission and unified schemes

The belief that all AGN are basically the same object but viewed along different line of sights is forcing the way through their intricate taxonomy. Several *unified* schemes have been proposed in the last years. Possible origin of the anisotropic emission are relativistic beaming, shadowing by a dense molecular torus, and intrinsic angular dependence of continuum emission by a thick accretion disk. We will briefly consider the domain of each of these mechanisms in order to introduce the scheme recently proposed by Barthel (1991).

Relativistic beaming permits to explain superluminal motions, rapid variability and one–sided jets. The intrinsic luminosity L is affected by relativistic beaming through $L = [\gamma(1 - \beta\cos\theta^2)]^{-4}\mathcal{L}$, where β is the velocity in units of the speed of light, $\gamma = (1 - \beta^2)^{-1/2}$. θ is the angle between the velocity vector and the line of sight. Thus, the emerging radiation can be enhanced by a factor $\sim 10^4$ if $\vartheta \rightarrow 0°$. Unification schemes based on beaming involve the identification of an unbeamed parent population: the scheme of Orr and Browne (1982) allows to reconduct blazars to radio loud quasars. Browne *et al.* (1982), and Orr and Browne (1982) have suggested that different type of radio loud AGN (namely core dominated and extended radio sources) are explained by a projection effect. In their scheme, the flat spectrum compact core component is emitted by an unresolved symmetrical jet, and is relativistically beamed with a Lorentz factor γ, while the steep spectrum extended component is the emission due to the unbeamed lobes. They define the parameter: R = *Flux density of beamed compact core/Flux density of unbeamed components.* The parameter R depends upon the angle θ between the line–of–sight and the direction of motion of the approaching side of the compact core. According to Orr and Browne (1982) all core dominated quasars have double lobes whose axis are pointing close to the line–of–sight, while all normal double–lobed quasars are just unaligned core–dominated ones.

The parameter R versus the FWHM of Hβ is shown in Fig. 1.4. There is clearly a paucity of very broad profiles at large values of R. The corresponding *narrow* Hβ profiles imply that the line emission is constrained in a plane perpendicular to the radio axis (as in a rotating thin disk). The disk inclinations for the different values of R and Hβ FWHM are shown on the right side of Fig. 1.4. This approach has however been criticized since: (1) the number of core dominated objects is too large to be consistent with the beaming factor $\gamma \approx 5$ found by Browne, and would imply that the beaming is into a large angle ≈ 2 *sterad* (Phinney, 1985); (2) the profiles in radio quite objects (which are viewed in random directions) resemble those in core–dominated galaxies, but never those of galaxies with small R. This would suggest that lobe dominated galaxies have intrinsically unusual profiles (Miley and Miller, 1979). An interesting, albeit indirect confirmation of the interpretation of Wills and Browne (1986) comes from the fact that FeII lines are much weaker in lobe than in core dominated radio galaxies (Phillips, 1978; Wills *et al.*, 1985; Boroson, 1989). Jackson and Browne (1991a,b) found moreover that also the Balmer decrement tends to be flatter if R increases. Noticeably, the ratio Hβ/Hγ is very low for objects with high R, implying that Balmer

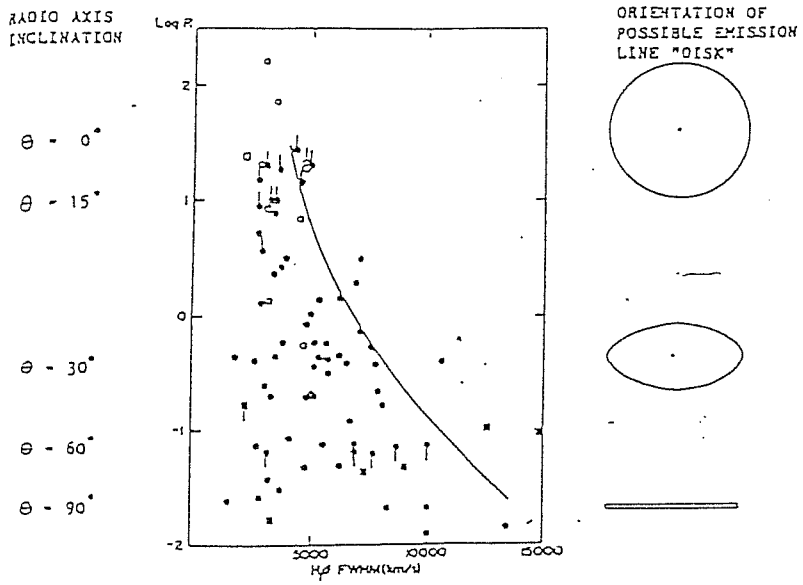

Figure 1.4: *The correlation between the parameter R and the FWHM of Hβ. From: Wills and Wills (1986)*

emission from very dense gas should dominate in this case. Probably, the spread in the correlation is accounted for if two components are present in the BLR: (1) a component with isotropic velocity distribution, which could be in the form of discrete clouds; (2) a flattened (probably associated with the disk), very dense component (Jackson and Browne, 1991b).

Another building block was added by the works of Miller and collaborators. Excluding Blazars and BAL QSOs, AGN typically show a low polarization degree of the optical and UV non–stellar continuum. Polarization of Sey–1 galaxies is $\sim 1\%$, while Sey–2 galaxies have a higher polarization degree $\sim 10 - 20$ % . Moreover, the electric vector is parallel to the radio axis in Sey–1, and nearly perpendicular to it in Sey–2 galaxies (Antonucci, 1983; Miller and Antonucci, 1983). If the radio axis lies close to the axis of a central obscuring disk, scattering material would indeed produce polarization at right angles to the axis of the disk. This result has been extended by the important finding that the spectrum of NGC 1068, the *prototype* Sey–2 galaxy, has a polarized spectrum which is very similar to a Sey–1 type galaxy, with broad permitted lines and FeII emissions. This means that we would infer a much higher optical luminosity NGC 1068 and call it a Sey–1 galaxy, if we would observe it from a direction roughly aligned with the radio axis (Antonucci and Miller, 1985; Miller, 1988, Miller *et al.*, 1991). Subsequent work (Miller and Goodrich, 1990) has shown that nearly half of the Sey–2 galaxies observed by Miller and collaborators have obscured broad lines, which are detected only in polarized light. Miller and Antonucci interpret their data suggesting that in the nuclei of Sey–2 galaxies*a thick disk of absorbing material (most probably dense molecular matter) is located beyond the BLR and restricts the view of the continuum source and of the Broad Line Clouds.* Light emerging above the disk encounters hot electrons which scatter the light of the Broad Line into our line of sight.

The torus opening angle an be estimated from the relative number of Sye–2 and Sey–1 (nearly 6:1): it is 43°, which is equivalent to a ratio between the vertical scale height and the distance from the galactic center $h/r \simeq 0.7$ (Kallman and Krolik, 1988 Miller and Goodrich, 1990).

The detection of extended emission line regions in many Seyfert and Radio galaxies has emphasized the coupling between the active nucleus and its circumnuclear environment. The ionization mechanism of the circumnuclear gas has been proved to be due to direct photoionization from the active nucleus, usually when high ionization degree is observed (Baldwin *et al.*, 1987; Haniff *et al.*, 1988; Corbin *et al.*, 1988; Pogge, 1988), or to *in situ* ionization from young hot stars (see Heckman, 1987), or also b shock–heating, as in NGC 6240 (Fried and Schulz, 1983). Restricting the attention to gas photoionized by the active nucleus, mapping of the high ionization gas in several nearby Seyfert galaxies (through narrow band imaging of the [OIII]$\lambda\lambda$4959,5007 lines) has revealed that it can be located in cone shaped structures, whose apex is pointing at the Seyfert nucleus (Pogge, 1988; see Tadhunter and Tsvetanov, 1989 for the most impressive example, NGC 5252). Wilson *et al.* (1988), and Haniff *et al.* (1988) have suggested that the number of ionizing photons obtained assuming isotropic emission and extrapolating the power–law continuum observed in the optical and uv towards the X–ray range is not sufficient to explain the observed Balmer line luminosity. Wilson (1991) analyzed the extranuclear emission regions for $\sim$ 15 Seyfert galaxies, and found a *photon deficit* by a factor $\gtrsim$ 10 (up to $\sim$ 100) in most objects. In most of these galaxies, it is probable that the ionizing continuum is reddened, but there is in principle no way to estimate the amount of reddening and to verify whether it is not different from that of the emission line regions, casting some doubt on the reality of an *intrinsic photon deficit*. Interstellar dust could also provide a rough collimation source along an axis perpendicular to the galactic plane. This problem has been studied in detail for NGC 1068. Miller *et al.*(1991) suggested that dust cannot provide a collimating source in this case, otherwise a substantial fraction of the ionizing continuum should be absorbed and reradiated in form of an excess of IR emission, which is not observed.

In principle, the luminosity of an AGN should be able to ionize the interstellar medium on kpc–sized scales, provided that enough gas is available. Intrinsic anisotropy of the source may help to explain why in some Seyfert galaxies the NLR appear unresolved, why in several others there is extended high–ionization gas. Detailed photoionization computations for the extended emission line regions have been performed by Acosta–Pulido *et al.* (1990) and by Fosbury *et al.* (1991), which found that thermal emission from a thick disk (whose angular dependence was given by Madau, 1988) allows to reproduce better the observed line ratios than a single power–law. The strong angular dependence of the hardness and intensity of the flux from a thick disk allow to search for changes in the ionization degree in the direction perpendicular to the cone axis. No variations are expected if the collimation is provided by the *thick molecular torus*. Recently, Miller *et al.*(1991), have argued that the central continuum source of NGC 1068 should be intrinsecally anisotropic, with a narrow opening angle (*i.e.* the collimation should not be produced by the molecular torus).

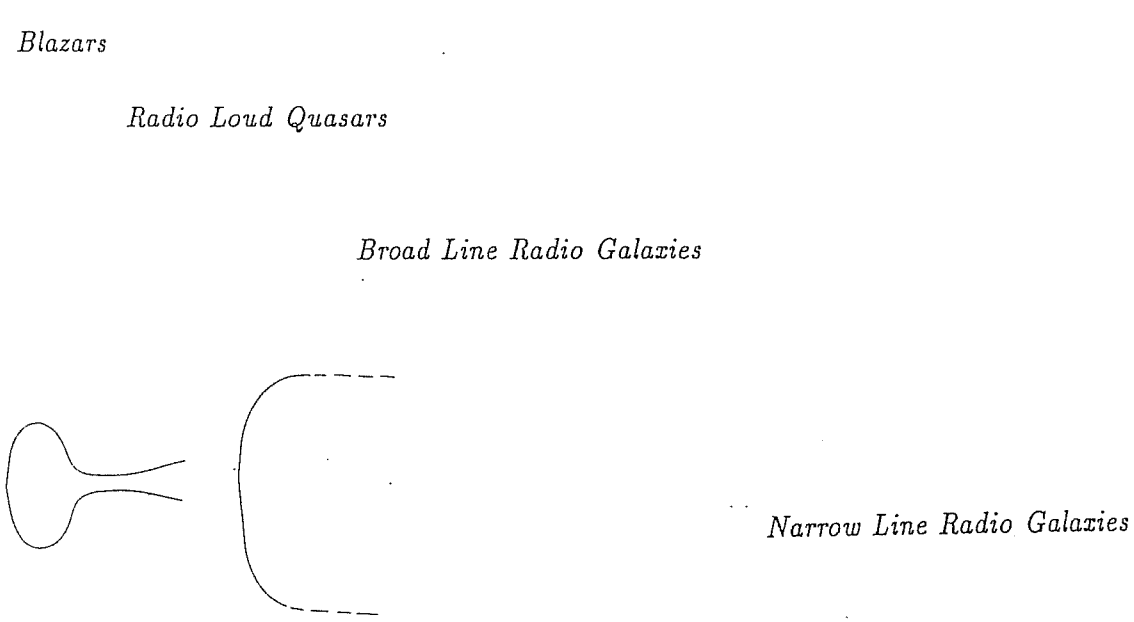

Figure 1.5: *A pictorial view of the unified scheme proposed by Barthel (1991) for radio loud AGN.*

As far as radio loud AGN are concerned, the radio morphology and the parameter R are probably reliable inclination indicators. For radio quiet AGN, it is not clear whether the radio properties of the Sey–1 and Sey–2 galaxies can be used as orientation indicators. If Sey–2 are edge–on Sey–1, According to Ulvestad and Wilson (1984) Sey–1 and 2 have nearly the same surface brightness, but Sey–2 are more extended, and hence more powerful radio sources. The same authors (Ulvestad and Wilson, 1989) suggested in a later work that their result was due to the limitation of the sample analyzed and that Sey–1 and Sey–2 galaxies do not have different radio properties. The *prominence* of the *Big Bump* could provide an estimate of the disk inclination i, but current fits are not able to give an independent estimate of $\dot{M}, M$ and i. *If* FeII lines are emitted in disks, their strength should depend (among many other factors) upon the disk inclination (*e.g.* Collin–Souffrin, 1987). However it is even unclear whether the emission should have its maximum when the disk is seen face on, or whether gravitational focusing should enhance the emissivity when the disk is seen *edge–on* (Laor, 1990; Netzer *et al.*, 1990). It should be interesting to investigate whether there is also a correlation between the radio morphology (or at least the radio power) and the FeII emission in radio quiet objects. If Sey–2 galaxies are edge–on Sey–1 obscured by a geometrically thick torus, an inclination indicator could be represented by the Balmer decrement of the broad component in intermediate Seyfert galaxies (Osterbrock, 1979, 1981; Cohen, 1983). If the *bulk* of the Balmer lines is emitted in the disk, their width should obviously correlate with the disk inclination.

The most comprehensive scheme has been proposed very recently by Barthel (1989;

1991). Blazars are radio–loud AGN viewed nearly pole on, where relativistic beaming operates. At larger viewing angles blazars would be identified as radio loud quasars and BLRG; when seen edge on, the BLR would be obscured by the molecular torus, and these objects would be classified NLRG (see Fig.1.5). It is not clear whether an analogous trend holds for radio–quiet objects too. Barthel (1991) suggested that there is a bimodality between radio loud and radio quiet AGN: radio jets correspond to the outflowing shells of radio quiet *Broad Absorption Line* (BAL) QSOs. If Seyfert galaxies are considered, it seems now certain that some Sey–2 galaxies are edge–on Sey–2, but one must take into account that there is not an analogous of BAL QSOs among these objects. There is evidence that some Seyfert galaxies are seen with the disk oriented nearly pole–on (NGC 4151, Penston, 1991; Akn 120 and IC 4329a, Marziani *et al.*, 1991, and Chapter 4), but their line profiles do not show the strong P Cygni features observed in BAL QSO. Furthermore, the inner edge of the BLR in NGC 4151 is estimated at only $\sim 4lt-days$ from the continuum source. If the line emitting clouds are accelerated outward by radiation pressure, the effect should be maximized in this object, but we do not observe a P Cygni profiles. There is little doubt that the emitting gas in BAL QSOs is outflowing, but the physical conditions in the BAL are probably rather different from those of the non–BAL quasars and in Seyfert galaxies. In order to let this scheme be viable, one should suppose that radio–quiet low–luminosity objects do not have the proper counterpart of BAL QSOs.
It is important to take anisotropy into account. If the intrinsic emission is anisotropic in Sey–1 galaxies (as if the innermost part of the disk are inflated, or if the super–Eddington accretion rate lead to the formation of a radiation torus), estimates of the masses using the dynamical method would be seriously affected. A quasar of $L \sim 10^{47}$ $erg\ s^{-1}$ radiating at its Eddington luminosity could have central masses $\lesssim 5 \cdot 10^7\ M_\odot$ if viewed face on. Selection effect could be introduced in samples otherwise believed to be complete, as the CfA sample of Seyferts used by Padovani *et al.* (1990) to estimate the mass function of Sey–1 galaxies. This problem will be extensively treated in Chapter 5.

This chapter has been partly based on the following works:

1. M. Calvani, P. Marziani, P. Padovani: *(Thick) accretion disks: where are they?*, in *Proceedings of the VIII Italian Symposium on General relativity and Gravitation.* p.169. (Singapore: World Sci. Comp.) M. Cerdonio *et al.*, Eds. 1989.

2. P. Marziani: *Accretion disks in Active Galactic Nuclei: observations versus theory*, *Magister Thesis*, SISSA, 1989.

Chapter 2

The excess of companions among Seyfert galaxies

Abstract – The percentage of Seyfert galaxies with close companions is estimated for all Seyfert galaxies of $z < 0.11$ listed in the 2^{nd} Veron Catalogue. The selection criteria $d < 3D$ and $\Delta m \lesssim 3$ match the distances and the magnitude difference of nearly all ($\simeq$ 90 %) the galaxies belonging to the interacting systems connected by bridges of matter in the Vorontsov–Velyaminov catalogue. We demonstrate that the advantage of our selection criteria is to pick up companions due to a chance alignment at a very low frequency. It is found in a set of 232 Seyfert 1 and 174 Seyfert 2 that the percentage of Seyfert galaxies with physical *companions is $\approx$ 23 %. This value should be compared with the percentage $\approx$ 3 % of companions for non–active galaxies found in large spectroscopic surveys. The significance of the excess of interacting systems among Seyferts is discussed.*

2.1 Introduction

The role that interaction may have in triggering the nuclear activity is as yet not well documented on an observational basis. Numerical simulations suggest, as outlined in Chapter 1, that the the gas distributed in a disk galaxy responds strongly to the tidal field of an approaching companion. The perturbation in the field may lead to a bar–like distortion of the potential (Simkin *et al.*, 1980; Noguchi, 1987; Gerin *et al.*, 1990), which in turn may induce inflow of disk gas and fuel the central engine. It is at present uncertain whether effects related to the internal dynamical evolution of a galaxy can give rise to strong inflow of gas toward the nucleus (Gunn, 1979). Since the pioneering work of Toomre and Toomre (1972), simulations of galaxy interaction have shown instead that even weak interaction–induced instabilities can lead to radial flow of gas (*e.g.* Barnes, 1988; Noguchi, 1988; Hearnquist, 1989). From the observational point of view, the excess of interacting and perturbed systems was noted by Adams (1977), who published large–scale images of most of the nearby Seyfert galaxies known at that time ($\simeq$ 80). More of 10 % of the galaxies he studied had disturbed morphologies, due to jets

or highly distorted main bodies, or showed obvious evidence of interaction, because of a nearby companion of comparable size. The excess of Seyfert galaxies with companions was quantified by Dahari (1984, 1985). In his first work, Dahari considered 103 galaxies up to a redshift $z < 0.030$, with the exclusion of galaxies in rich clusters. Companions of Seyfert galaxies were all galaxies located within a distance $d < 3D$, where D is the diameter of the Seyfert galaxy, measured up to the faintest envelope detectable on the *Palomar Observatory Sky Survey* prints. He defined a control sample of five randomly selected galaxies visible on the same POSS print of each Seyfert galaxy in consideration. The main concern in the choice of the control sample was to ensure that the percentage of optical pairs among the two samples were similar. He found that the percentage of companions were 38 % and 22 % in the Seyfert and in the control sample respectively. The frequency of optical companions (which was estimated following the procedure described in § 2.4.1) was around 20 %. After correction for optical companions, the percentage of interacting Seyfert galaxies was $\sim$ 15 %, in comparison to $\sim$ 3 % of the control sample, suggesting that there is *definite* excess of companions among Seyfert galaxies. More recently, McKenty (1989) compared the environment of $\sim$ 50 Seyferts and Starburst Markarian galaxies. He found that approximately three fourth of both Seyfert and Starburst galaxies have (at least) one nearby companion in a search radius of $\sim$ 10 galaxy diameters. A control sample in which both Seyferts and Starbursts are avoided shows only $\simeq$ 28 % of companions. McKenty did not perform a correction for background galaxies, but if the percentage of optical companions is the same in the three samples, as likely, the excess is highly significant. However, the IRAS color indexes of Seyfert differ when they have a close companion and when they are truly isolated; in the first case, the IRAS colors are very similar to those of Starburst galaxies, suggesting that the presence of close companions is associated more directly to Starburst rather than non–thermal activity. We have addressed this problem in § 1.4.2, and we will treat it again in Chapter 3.

The reality of the excess of interacting systems among Seyferts has been questioned recently by Fuentes–Williams and Stocke (1988, hereafter FWS). These authors searched for companions on a sample of 53 Seyfert galaxies and on a control sample of 37 galaxies within 1 Mpc of projected linear distance. The primary goal of the study of FWS was to determine whether the environment of Seyfert galaxies differed from the environment of a sample of spirals similar to Seyferts in all way but nuclear activity. To this aim, the galaxies of the control sample were chosen in order to (roughly) match the morphological types (as well as the diameters) of the Seyfert sample. Physical companions were assumed to be all galaxies within that radius, and with a diameter $D_{comp} \gtrsim 1/4\ D$. FWS report the percentage of galaxies possessing companions as a function of the projected distance to the nearest companion measured in the number of Holmberg diameters of the central galaxy. At 2.5 Holmberg radii the percentages can be directly compared with those obtained by Dahari. FWS found that the galaxies having a companion are $\approx$ 45 % and $\approx$ 35 % in the sample of Seyfert galaxies and in the control sample respectively. This difference is not really significant, and led FWS that *there is only very marginal evidence that Seyferts possess an excess of comparably*

sized companions.
We will discuss later – in light of the results presented in this Chapter – possible reasons for the discrepancy. We remark here that the importance of determining the frequency of interacting Seyfert galaxies is not limited to the sake of the numbers, but rather stems from the possibility to test whether, and under which conditions, disk or circumnuclear gas can be accreted by the galactic nucleus.

2.2 Method of identification

The only two parameters which can be measured on the blue POSS and ESO prints and used in a comparative way are:

1. the separation d between pairs of galaxies, measured taking as unit the major axis D of the main component. D was measured up to the faintest features visible on POSS prints.

2. an estimate of the difference in magnitude of the two galaxies.

In order to select the pairs of galaxies which are interacting using both these parameters it is necessary to estimate the upper limit to the separation and to the magnitude difference in a sample of pairs or multiple galaxies which:

1. have been initially selected on the POSS prints;

2. are *physical companions*, since they show the effects of a close interaction.

Such a sample is given in the *Atlas of Interacting Galaxies* by B. Vorontsov– Velyaminov (1959; hereafter V–V), which lists 355 interacting galaxies defined as objects *connected by bridges of matter* and selected on the POSS prints. The following data can be easily extracted from the catalogue and from the enclosed atlas:

1. m_A = apparent magnitude of the main component of the interacting system. The main component is defined either as the brighter galaxy or as the central one if the system is multiple;

2. $\Delta m = m_{comp} - m_A$, the magnitude difference between the companion and the main component;

3. $d =$ separation between the components of the system.

The number of interacting V–V galaxies as a function of the magnitude of their principal component (Fig. 2.2) increases up to $m_A \simeq 16$, and shows a rapid decrease for $m_A \gtrsim 16-17$, indicating that systems whose principal component is fainter than 16–17 are likely to be lost, because: (1) $m_{comp} \gtrsim (m_{lim})_{POSS}$; (2) the bridges of matter are fainter than the level of sky noise.

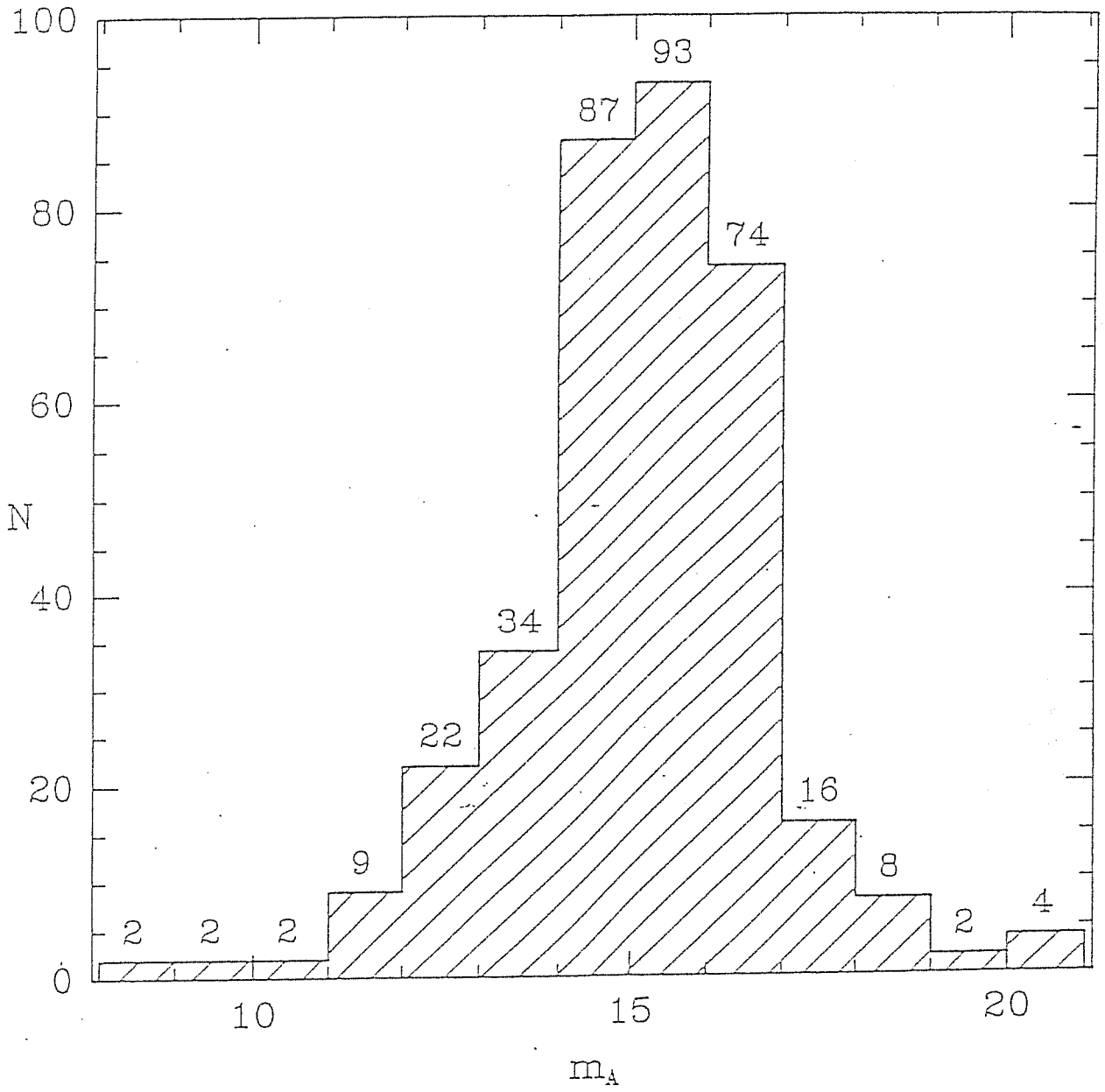

Figure 2.1: *Number of interacting systems per unit magnitude of the principal component m_A for 355 systems reported in the Vorontsov–Velyaminov (1959) catalogue.*

This is confirmed by Fig 2.2. For the different intervals of magnitude of the principal component, the number of companions per unit magnitude (or of the second brightest galaxy if the system is multiple) is reported in the histograms of Fig. 2.2. The number of companions undergoes an abrupt decreases for $m_A \gtrsim 16$; if $m_A \gtrsim 16$ the number of companions with $\Delta m \lesssim 1$ is larger that the number of companions with $1 \lesssim \Delta m \lesssim 3$, indicating that companions with $\Delta m \gtrsim 1$ are frequently lost if $m_A \gtrsim 16 - 17$; and that any direct search for interacting systems connected by bridges of matter in the POSS prints is *strongly* warped for galaxies fainter than 16^m. The V–V catalogue is not designed to give a *complete* sample of interacting galaxies, as for instance the Karashentsév catalogue. Rather, it provides as an atlas in which interacting systems are grouped together according to their peculiar morphologies. We are therefore restricted to the kind of analysis presented above.
The upper limit of Δm can then be derived from Fig. 2.3, which shows that 90 % companions of the 355 V–V objects result to be contained in a circle of radius $3D$, centered on the main component of the system. Hence the conditions to be imposed in our attempt to identify interacting galaxies are:

1. $d \lesssim 3D$;
2. $\Delta m \lesssim 3$.

The choice of the V–V systems as representative of a sample of interacting galaxies, and the selection criteria deduced from their properties, limits the *strength* of the interaction we are considering. Systems in which a component shows bridges of matter are believed to be interacting with less massive companions: $0.1 \lesssim M_{comp} \lesssim 1$; prograde encounters between galaxies of comparable masses instead produce narrow tidal tails and, under certain conditions, a merger in a few dynamical timescales (*e.g.* Schweizer, 1990, for a recent review). *Strongly* interacting objects are likely to be lost, because most galaxies are overexposed in their central parts on the POSS prints, making an analysis of the morphology difficult or impossible. For instance, multiple nucleus galaxies will be probably mis–classified, and unless the conditions listed above are satisfied, they will be considered as single objects.
In the following, we will distinguish between *optical* companions (that is background or foreground galaxies whose location on the sky *nearby* to the galaxy in consideration is due to a chance alignment), and *physical* companion, which are interacting with the galaxy in consideration.

2.2.1 The set of Seyfert galaxies

The selection criteria deduced earlier have been applied to *all* Seyfert galaxies with $z < 0.11$ known at Jan. 1, 1984, and listed in the second edition of *A Catalogue of Quasars and Active Galactic Nuclei* (Veron–Cetty and Veron, 1985, hereafter V85). We considered 232 Sey–1 and 174 Sey–2 out of 310 Sey–1 and 226 Sey–2 listed in the catalogue. These numbers are not strictly coincident with the number of galaxies

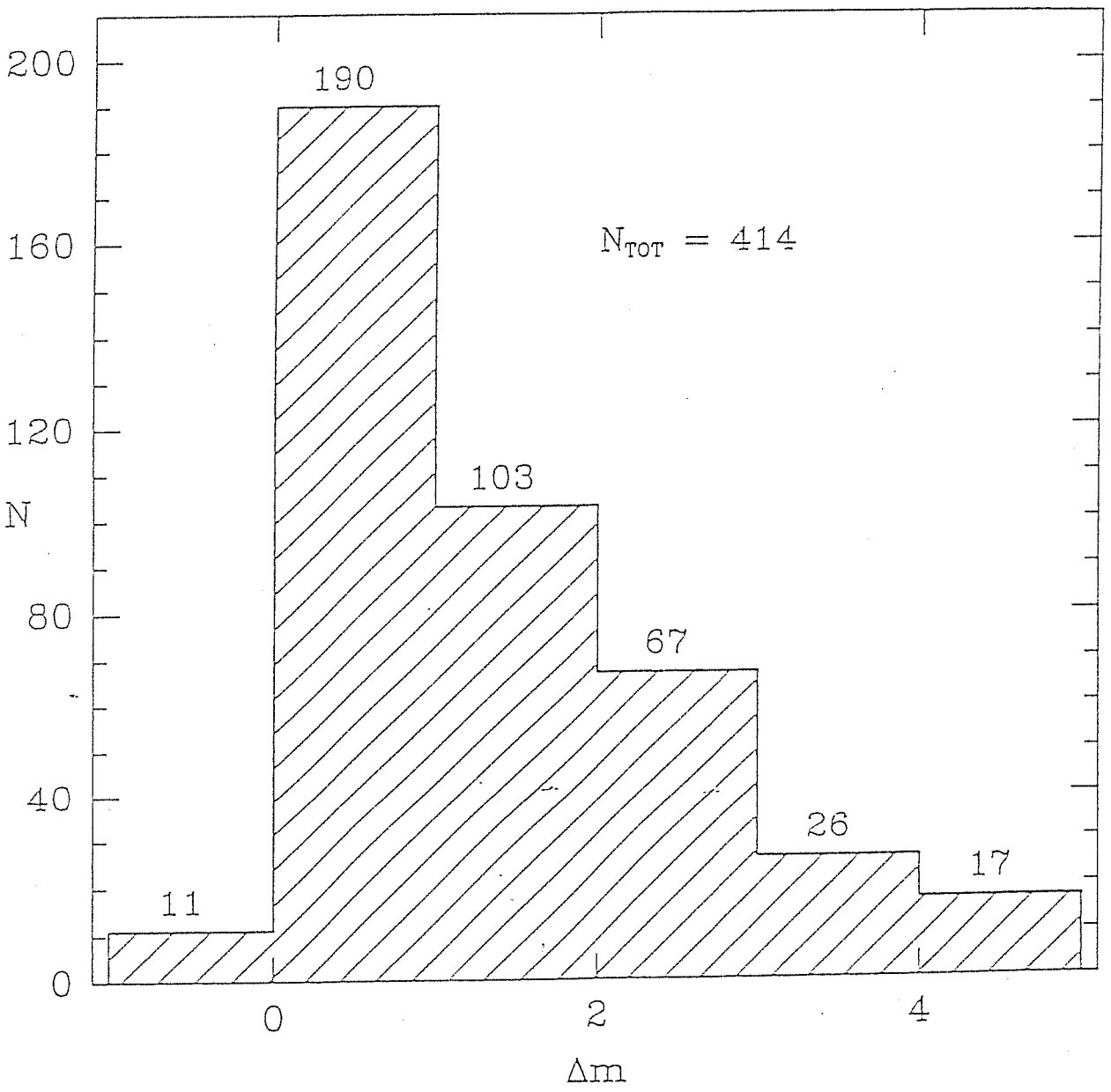

Figure 2.2: *Number of companions as a function of the magnitude difference with the principal component of the interacting system (as defined in the text) for the Vorontsov–Velyaminov galaxies.*

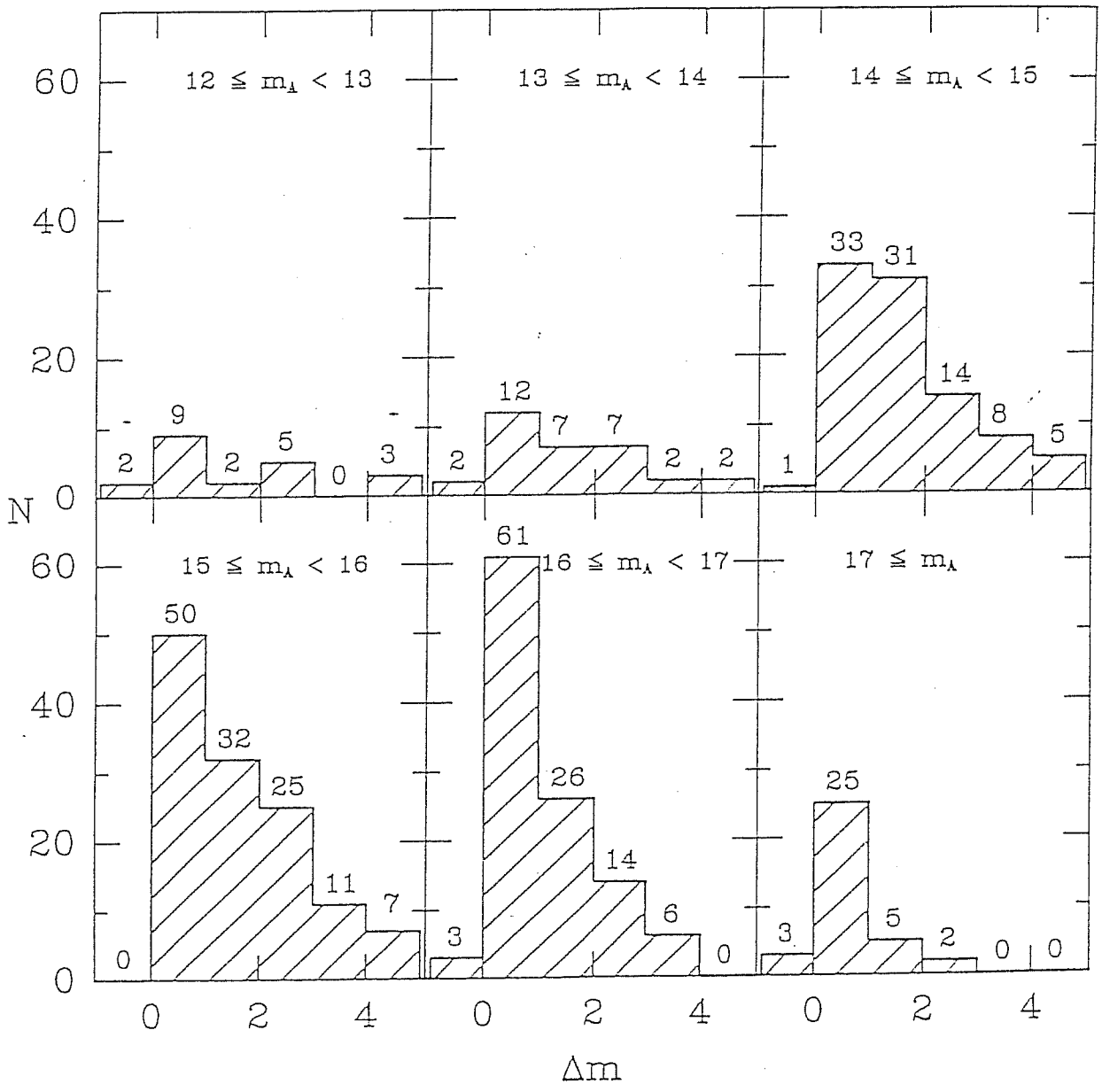

Figure 2.3: *Magnitude difference between companion and principal galaxy of the Vorontsov–Velyaminov sample for different magnitudes of the principal galaxy.*

classified as Sey–1 and Sey–2 in the lists of V85, since a few object listed in the catalogue but without identification of the Seyfert type – or misclassified as nuclear HII regions – were included in our study. Although our sample is the largest employed as yet (§ 2.1), it cannot be regarded as a complete sample, since the V85 catalogue has been not compiled on the basis of a systematic search using uniform criteria, but it is a rather heterogenous list of galaxies. As far as the excess of companions is concerned, this should not influence our results at least for Sey–1 galaxies (see also § 2.4.1, and § 2.4.3).

The surroundings of the Seyfert galaxies were analyzed by view on the blue POSS prints or on the ESO charts. The search for companions was made independently by three persons (P. Rafanelli, G. Tomezzoli and myself). Objects not classified in the same way by all of us were subsequently reanalyzed and discussed.

2.3 Results

Results are summarized in Table 1. The total number of Seyfert galaxies considered, the total number and the percentage of Seyferts with companion are listed as a function of redshift separately for all Sey–1 and Sey–2 with $z < 0.11$ and with $z < 0.11, \delta > -24°$.

The restriction to $\delta > -24°$ is necessary because galaxy counts needed to estimate the frequency of optical companions (see §2.4.1) are available only down to this declination limit. A test for evaluating up to which redshift value the percentage of interacting Seyfert galaxies found with our method is reliable, can be based on the assumption that the expected frequency of interacting Seyferts should be almost the same for different z values. Fig. 2.4 shows the percentages of interacting Seyfert galaxies that we have found as a function of the redshift. The same is shown in Fig. 2.5, but for galaxies with $\delta > -24°$. The flat shape of the distribution of the frequency of interacting Seyfert 1 indicates that their percentage is probably reliable up to $z = 0.05$. The values found for $0.05 \leq z < 0.07$ are quite likely produced by selection effects. One of them could be introduced by the limit of resolution of the POSS prints, which tends to hamper the detection of close companions. The high frequencies obtained for $0.07 < z < 0.09$ are not significant since the number of known Sey–1 galaxies in this redshift range is too small (17). The distribution of Sey–2 galaxies is more difficult to decode. The frequency is constant only up to $z = 0.02$. Up to this limit, the frequency of interacting Sey–2 is approximately the same ($\simeq 23$ %) of Sey–1 galaxies. The observed excess of interacting systems among Sey–2 for $0.02 \leq z < 0.05$ could be due to the fact that many Sey–2 galaxies have been referentially identified within spectroscopic surveys of interacting galaxies or of group of galaxies. It is noteworthy that the apparent magnitude of Sey–1 (Sey–2) galaxies at $z = 0.05$ ($z = 0.02$) derived assuming $M_{Sey1} = -21$ ($M_{Sey2} = -19$) and $H_0 = 75\ km\ s^{-1} Mpc^{-1}$ is ~ 16, namely the magnitude below which our method of selection begins to loose companions.

Table 1

	Seyfert 1						*Seyfert 2*					
Δz	$z < 0.11$			$z < 0.11, \delta > -24°$			$z < 0.11$			$z < 0.11, \delta > -24°$		
	N	N_{int}	F_{int}	N	N_{int}	F_{int}	N	N_{int}	F_{int}	N	N_{int}	F_{int}
$0.000 \leq z < 0.010$	25	6	24 %	19	6	32 %	30	7	23 %	19	5	26 %
$0.010 \leq z < 0.020$	23	5	22 %	19	4	21 %	42	9	21 %	26	7	27 %
$0.020 \leq z < 0.030$	32	6	19 %	29	5	17 %	37	15	41 %	34	15	44 %
$0.030 \leq z < 0.040$	48	9	19 %	43	9	21 %	22	8	36 %	19	7	37 %
$0.040 \leq z < 0.050$	25	6	24 %	24	6	25 %	10	3	30 %	7	2	28 %
$0.050 \leq z < 0.060$	27	4	15 %	24	4	17 %	15	1	7 %	12	1	8 %
$0.060 \leq z < 0.070$	22	2	9 %	22	2	9 %	7	1	14 %	4	1	25 %
$0.070 \leq z < 0.080$	15	2	13 %	13	2	15 %	2	0	0 %	1	0	0 %
$0.080 \leq z < 0.090$	5	1	20 %	5	1	20 %	4	0	0 %	4	0	0 %
$0.090 \leq z < 0.100$	5	1	20 %	5	1	20 %	3	0	0 %	1	0	0 %
$0.100 \leq z < 0.110$	5	0	0 %	4	0	0 %	2	0	0 %	2	0	0 %

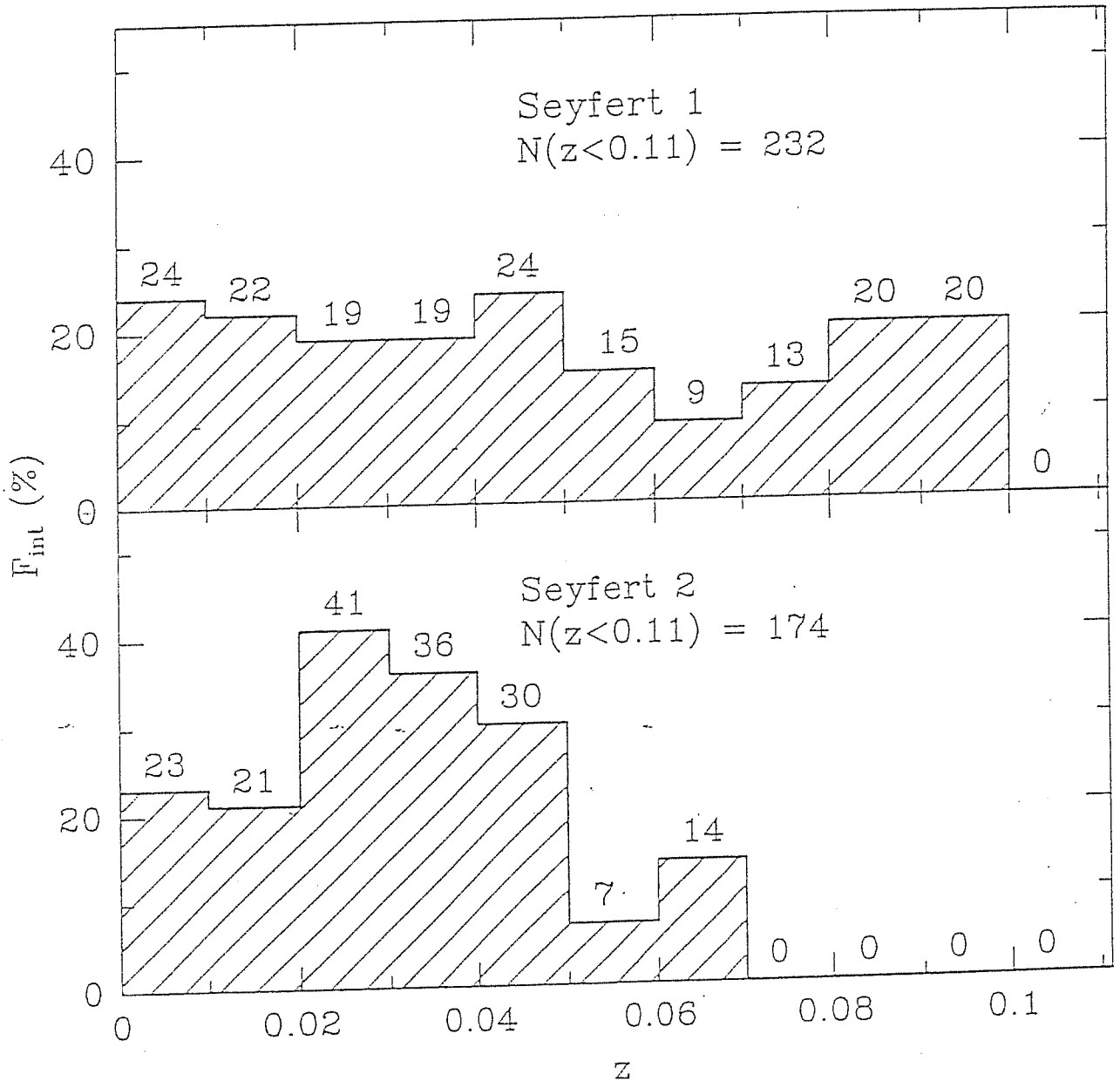

Figure 2.4: *Percentage of interacting Seyfert galaxies with $z < 0.011$ for Sey–1 galaxies (upper panel) and Sey–2 galaxies (lower panel) as a function of redshift z.*

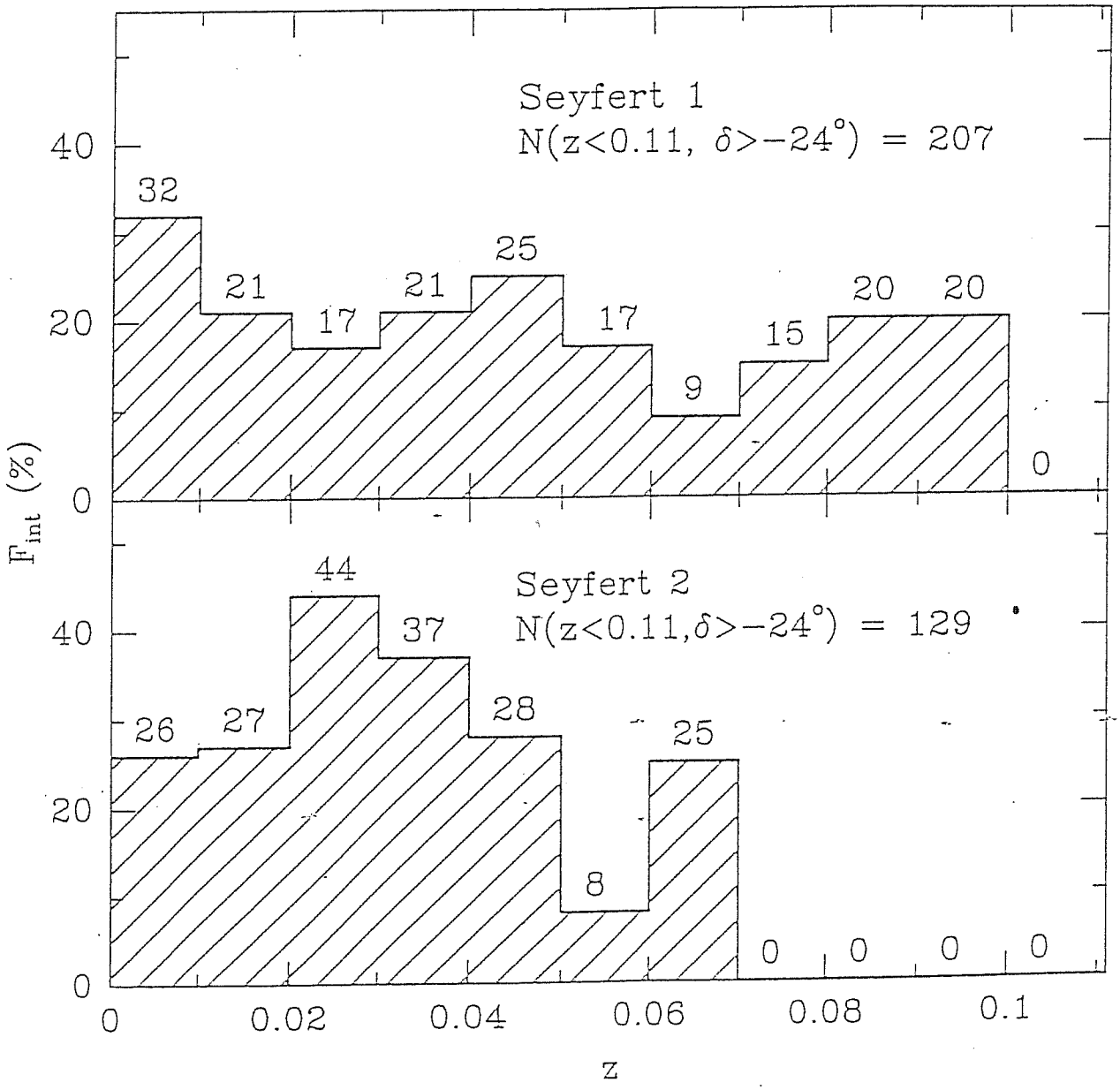

Figure 2.5: *Percentage of interacting Seyfert galaxies with* $z < 0.011$ *and* $\delta > -24°$ *for Sey–1 galaxies (upper panel) and Sey–2 galaxies (lower panel) as a function of redshift* z.

2.4 Analysis

2.4.1 The frequency of optical companions

As outlined in § 2.2.1, our sample of Sey–1 and Sey–2 galaxies selected from the V85 catalogue can not be a complete sample. The following analysis shows that the selection criterium $\Delta m \lesssim 3$ allows anyway a drastic reduction of the expected percentage of optical companions.

The search for an *optical* companion is a random process with probability of success given by the Poisson statistics. We remark that the use of the Poisson statistics is appropriate since we are interested in estimating the number of companions occurring *only* by chance alignment. Even so, our procedure is not strictly correct, because our search radius is much smaller (typically 3 *arcmin*) than the area over which sky counts are averaged. This has little influence on our result, since galaxies located regions of dense clustering are avoided.

For each Seyfert galaxy, we want to know the Poisson probability of having a galaxy located within a search radius S < 3 D_S, and whose magnitude differs by $\Delta m < 3$ from the magnitude of m_S of the Seyfert galaxy itself. The probability is given by

$$P(\Delta m, \alpha, \delta) = 1 - \exp\left[-\pi(S^2 - \frac{1}{4}D_S^2)\int_{m_S}^{m_S+\Delta m} A(m, \alpha, \delta)dm\right] \qquad (2.1)$$

(*cf.* Dahari, 1984, Eq. 1), where A(m,α, δ) is the number density of galaxies per unit magnitude per square degree and S and D_S should be measured in degrees. A(m,α, δ) can be written as A(m, α, δ) = C·$10^{0.6m}$, under the assumptions of negligible intergalactic absorption, uniformity of galaxy distribution, and euclidean space. All conditions are probably met within our redshift limit $z = 0.11$. Nevertheless, companions will probably get lost if $m_{comp} \gtrsim 18.5 - 19$, *e.g.* if $m_{Sey} \gtrsim 15.5 - 16$, since the limiting magnitude of the POSS is $\simeq 19$. The following computation will thus probably *overestimate* the number of expected optical companions.

A(m,α, δ) is related to the number density per square degree $\sigma(\alpha, \delta)$ (which can be obtained by tabulated galaxy counts) by

$$\int_{m_{min}}^{m_{lim}} A(m, \alpha, \delta)dm = \int_{m_{min}}^{m_{lim}} C10^{0.6m}dm = \sigma(\alpha, \delta) \qquad (2.2)$$

where m_{lim} and m_{min} are the limiting magnitudes of the galaxy counts. The constant C can be written in terms of $\sigma(\alpha, \delta)$:

$$C = \sigma(\alpha, \delta)ln10\ 0.6\ 10^{-0.6(m_{lim} - m_{min})} \qquad (2.3)$$

so that we can now write the integral in Eq.(1) as:

$$\int_{m_S}^{m_S+\Delta m} A(m, \alpha, \delta)dm = \sigma(\alpha, \delta)10^{0.6\Delta m}10^{-0.6(m_{lim}-m_{min})} = \sigma^{\star}(\Delta m, \alpha, \delta), \qquad (2.4)$$

where $\sigma^*(\alpha,\delta)$ is the number density of galaxies per square degree whose magnitudes are between m_S and $m_S + \Delta m$. $\sigma^*(\alpha,\delta)$ will not depend upon m_S as long the law $A(m) \propto 10^{0.6m}$ is valid.
The probability of having a companion because of a chance alignment is thus:

$$P(\Delta m,\alpha,\delta) = 1 - \exp\left[-\pi(S^2 - \frac{1}{4}D_S^2)\ 10^{0.6\Delta m} 10^{-0.6(m_{lim}-m_{min})}\sigma(\alpha,\delta)\right] \qquad (2.5)$$

The restriction of the search to $\Delta m < 3$ has a strong effect on the expected number density of galaxies per square degree: $\sigma^*(\alpha,\delta) = \sigma(\alpha,\delta)\ 10^{1.8} 10^{-0.6(m_{lim}-m_{min})}$, which will become $\sigma^*(\alpha,\delta) \approx 6 \times 10^{-3}\ \sigma(\alpha,\delta)$, adopting the limiting magnitudes $m_{lim} = 18.7$ and $m_{min} = 12.0$ estimated for the survey of Shane and Wirtanen.
The average probability of finding optical companions for Sey–1 and Sey–2 is $P(\Delta m,\alpha,\delta) \approx 9 \cdot 10^{-3}$ and $\approx 3 \cdot 10^{-3}$ respectively, far below the *measured* percentage. In order to obtain the upper limit to the expected number of optical companions, it is necessary to compute the probability density function $\Phi(K,N)$, that is the probability of finding K galaxies with companions among N objects. We considered the distribution of probabilities of finding optical companions for the Sey–1 and Sey–2 galaxies of our set, on logarithmic scale, shown in Fig. 2.6[1]
Following the same procedure of Dahari (1984), we compute the binomial density function for each histogram bin, and we convolve together the results obtained for each bin. The resulting $\Phi(K,N)$ are shown in Fig. 2.7 for Sey–1 and Sey–2 galaxies. The upper limit of the number of optical companion is ≈ 5 (≈ 2.5 %) for Sey–1 and ≈ 3 (≈ 2.5 %) for Sey–2, in both cases much lower than the observed frequency of companions. We suggest that the percentage of physical companions is thus (at least) around 20 %. This value should be compared with the frequency of companions found in spectroscopic surveys of normal galaxies, e.g. 3 % (Turner, 1976). We can conclude that *there is a significant excess of interacting systems among Seyfert galaxies, and that the frequency of interacting galaxies is* $\gtrsim$ *20 %.*

2.4.2 Comparison with previous works

In order to compare our results with those of Dahari, we have extracted the interacting Seyfert galaxies with $z < 0.030$ identified with our method. Numbers and frequencies are listed in the table below.

Class	N		N_{int}		F_{int}	
	Dahari	*This work*	*Dahari*	*This work*	*Dahari*	*This work*
Sey–1	44	*80*	12	*17*	27 %	*21 %*
Sey–2	55	*109*	23	*31*	42 %	*28 %*

[1]The differences in probabilities of Sey–1 and Sey–2 galaxies do not reflect a difference in the environment. Since Sey–2 galaxies in our sample have an average lower redshift than Sey–1, the search radius is larger for the Sey–2 (since they will have an average larger angular extent), and hence and hence also the probability of finding a companion will be higher.

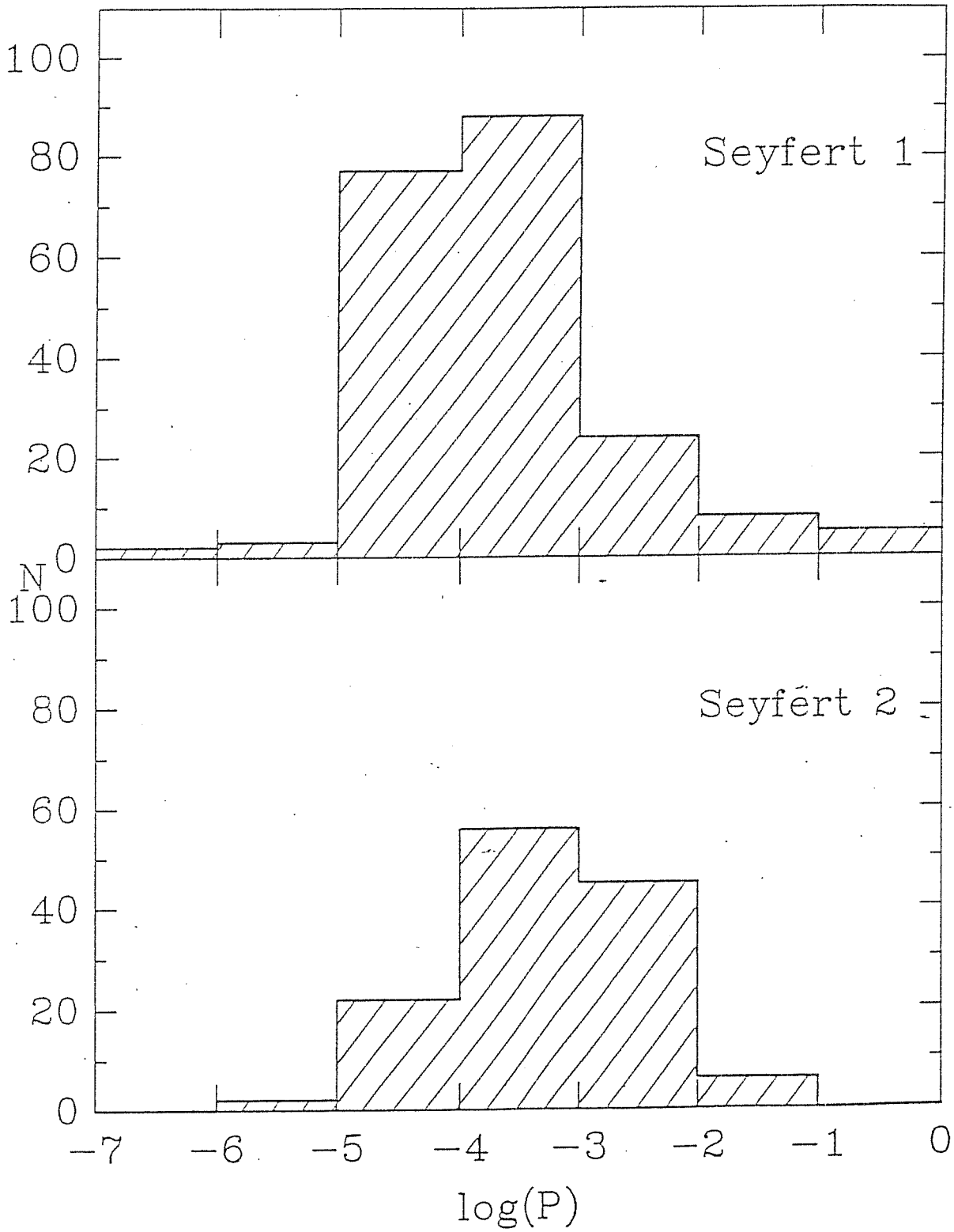

Figure 2.6: *Number of galaxies versus probability of finding a companion. Upper panel: Sey–1 galaxies; lower panel: Sey–2 galaxies.*

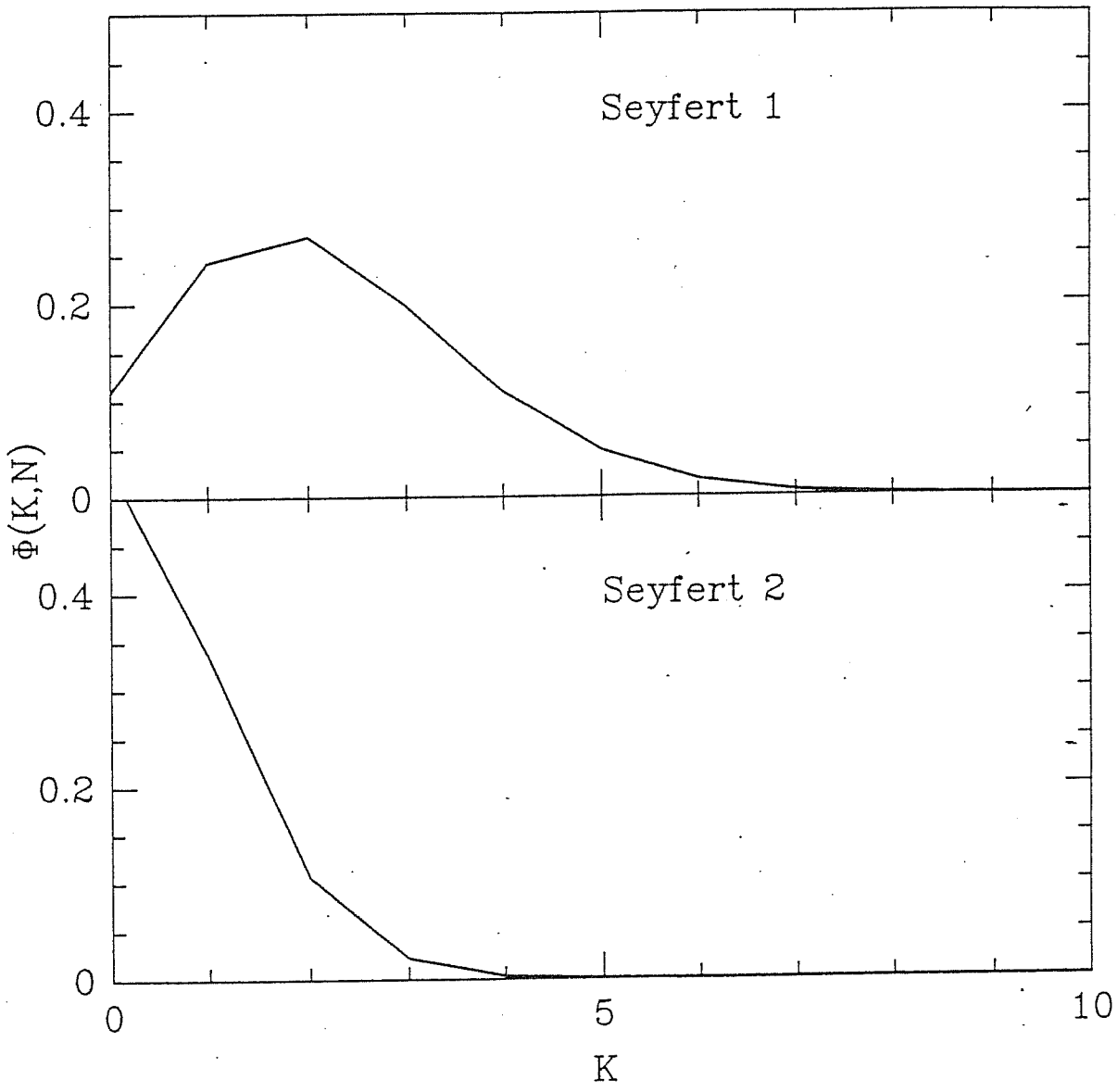

Figure 2.7: *Probability of finding K optical companions in our sample of Sey–1 (upper panel) and Sey–2 galaxies (lower panel).*

The percentages of interacting objects that we have found are lower than those of Dahari and *very close* to the values found by us for $z < 1.1$. Since the percentage of optical companion is negligible with respect to the percentage of companions found in our sample of Seyfert galaxies the conclusions of Dahari (1984, 1985) are strengthened in this work. The avoidance of optical companions is the principal advantage relative to the work of Dahari (1984), who identified $\approx$ 38 % of interacting Seyfert galaxies, but picked up optical companions at a comparable frequency (23 %).
As noted in § 2.1, FWS suggested, at variance with our results and with those of Dahari (1984) and McKenty (1989) that there is no significant excess of interacting systems in Seyfert galaxies. The limit on the diameters $D > 1/4\ D_S$ is a criterion substantially equivalent to that adopted by us on the magnitudes, namely $\Delta m < 3$. The selection of a control sample with matching morphological types is clearly an improvement with respect to our work and that of Dahari. However, it is not clear why such a large discrepancy between the study of FWS the other studies arises. Possible causes include:

1. The control sample of Dahari does not match the distribution in morphological types of Seyfert galaxies. This is probably true, since Seyfert nuclei are host in early–type spiral galaxies (Sa–Sb), while the control sample would also comprise late–type spirals (Sc) and elliptical galaxies. The spectroscopic survey of Turner (1976) suggests that the percentage of physical companions in a large sample of field spiral galaxies is $\lesssim$ 3 %. The percentage of companions within 2.5 Holmberg radii (both for non–active and Seyfert galaxies) found by FWS is in this respect surprisingly high. A possibility is that the percentage of interacting galaxies depends strongly on the morphological type, and is much larger in early–type spirals than in galaxies of different morphological type. Since the percentage should be larger by a factor $\simeq$ 10, this possibility seems unlikely. Moreover, galaxies belonging to a pair tend to have the same morphology, and in the Karashentsev catalogue shows that there is no overabundance of containing Sa or Sb galaxies (Karashentsev, 1972).

2. There is an excess of *faint* companions among Seyfert galaxies, but no (or a less significant) excess as far as *bright* companions are concerned. This explanation was favoured by FWS, but the condition upon the diameter of the companion is roughly equivalent to $\Delta m \lesssim 3$. This condition – although useful for avoiding optical companions – does not mean that we are selecting only extremely close companions, of brightness comparable to that of the Seyfert galaxy: if the companion would be located at the same distance of the Seyfert, $L_{comp} \approx 0.06 L_{Sey}$; or, if the companion would be of the same absolute magnitude of the Seyfert galaxy, it could be picked up to a distance $d_{comp} \simeq 4 \cdot d_{Sey}$.

3. The sample of FWS is too limited in number to draw any un–biased conclusion about the percentage of interacting Seyfert galaxies.

Thus, the discrepancy between FWS and our results remains unclear.

2.4.3 Are the frequencies for Seyfert 1 and Seyfert 2 galaxies really different?

The average density $\sigma(\alpha,\delta)$ for the sky regions of Sey–2 galaxies, $\sigma(\alpha,\delta) \approx 37.2 \pm 1.6$, is very similar to that of Sey–1 galaxies, $\sigma(\alpha,\delta) \approx 39.1 \pm 1.4$. This suggests that Sey–2 and Sey–1 are found in similar environments. Taken at a face value, this would suggest that the excess in the frequency of interacting galaxies among Sey–2 with respect to Sey–1 galaxies is a real effect. It is very interesting that previous studies (Dahari, 1984; Mc Kenty 1989) also found that the percentage of interacting Sey–2 galaxies is larger than that of Sey–1 galaxies. It is known that most of Starburst galaxies belong to interacting systems. This result is intriguing since Sey–2 galaxies seem to be somewhat more directly linked to Starburst galaxies than Sey–1 (*e.g.* Chapter 1), but it may be deeply affected by the search methods used in the discovery of new Seyfert galaxies. While Sey–1 galaxies have been identified mainly using homogeneous selection criteria in surveys covering a large fraction of the sky (*e.g.* ultraviolet excess, X–ray emission), the identification of new Sey–2 galaxies has been somewhat more fortuitous. Since the idea of a connection between interaction and activity is a long lasting one (*e.g.* Adams, 1977), a preferential selection of interacting objects could have created a strong bias for Sey–2 galaxies. The use of complete and/or flux-limited samples (as for instance that provided by the search for emission line galaxies by Wasilewsky, which was based upon the presence of prominent nebular [OIII]$\lambda\lambda$4959,5007 lines, believed to be complete up to $m_B = 15.7$) is necessary in order to establish whether the differences between Sey–1 and Sey–2 are real, but this is beyond the aim of the present work.

2.5 Implications

As outlined in Chapter § 1.4.2, the excess of companions among Seyfert galaxies means that a tidal force is probably able to induce a non–axisymmetric perturbation in the gravitational potential, which in turn may lead to accretion of matter onto the galactic nucleus.

Dahari (1984) defined a dimensionless *interaction parameter*, which measures the tidal strength of the encounter: $Q_D = (DD_{comp})^{1.5}/S^3$, where D and D_{comp} are the diameters of the Seyfert and of the companion galaxy, and S the projected separation. The strong dependence of the tidal strenght upon the linear separation hampers the study of any correlation between tidal strength and various indicators of the activity level (Dahari, 1985). The condition $\Delta m \lesssim 3$ does not introduce strong limitations on Q_D. Supposing that galaxies separated by less than $\frac{1}{4}D$ are considered isolate, because the companion will be so close that it would be masked by the Seyfert galaxy itself, and considering at a galaxy of the same magnitude of the Seyfert galaxy can be located at a distance from the observer ≈ 4 times that of the Seyfert, we have that $10^{-4} \lesssim Q_D \lesssim 20$, which covers the range spanned by the interacting Seyfert galaxies considered in the study of Dahari (1984). It is very difficult to set a more significant lower limit to Q_D. Although one would expect that it is more likely to find a fainter companion near to the Seyfert rather

than a galaxy of comparable luminosity at a large distance, because the luminosity function of normal galaxies is much steeper at high luminosities than that of Seyferts, a quantitative analysis would require the knowledge of the absolute magnitudes of the galaxies of our sample of Seyfert galaxies. This task cannot be easily accomplished from the data in the V85 catalogue. Although our search covers a wide range in the interaction parameter, we will loose objects which have experienced an hyperbolic encounter in the past. At the other extreme, *merging* galaxies would be equally lost, because of the difficulty of recognizing the remnants of the single components on the POSS prints. A compact companion of low mass can have a relevant effect, provided that it can reach the nuclear region of the galaxy before suffering tidal disruption. Therefore, our work should be coupled with a morphological survey based on large scale images, and on a careful analysis of the environment of each Seyfert galaxy beyond $3D$. To the best of our knowledge, no such a survey has been already completed. Seyfert galaxies do have in several cases amorphous morphologies in the inner disk (simkin *et al.*, 1980). This finding can be interpreted as evidence of large scale radial motions in the inner disk. Some Seyferts show also irregular envelopes, indicative of tidal distortion (Adams, 1977), although no systematic analysis has been done since then. If morphological peculiarities would be taken into account, the incidence of interaction in providing a *lighter* for activity may be much higher than that estimated from the present work. At present somewhat sparse (or even contradictory) evidence of peculiarities in the morphology of Seyfert galaxies has been collected.

Unclear is the relevance of *strong kpc*–sized stellar bars. Strong radial streaming of gas is possible in a barred gravitational potential. A bar is expected to form for some strong perturbations (Byrd *et al.*, 1986). Thompson (1981) has found a larger fraction of barred galaxies in the core of the coma cluster than outside. In isolated and paired galaxies the percentage of barred galaxies is 36 % and 50 % respectively (Elmegreen *et al.*, 1990).

Bars are long–lived structures, and would be observed in the galaxy also when the companion will be so far away to be lost in statistical searches. Simkin *et al.* (1980) discussed the morphology of several nearby galaxies ($cz < 5000\ km\ s^{-1}$), and found that barred galaxies are not significantly more frequent than among non–active galaxies. Probably, gas flow in a large scale stellar bar is stopped at ~ 0.1 of the bar radius (Shlosman *et al.*, 1989), so that further mechanisms should be at work to let the accretion flow reach the nucleus. If this is true, gaseous bars – which could be detected by observations of the CO emission (Combes, 1987) – would be of relevance. *Weak* stellar bars could be revealed in proximity of the nucleus by imaging in the near infrared ($\lambda \approx 1 \mu m$), where an evolved stellar population has its maximum emission. In these cases however, the appropriate definition of a control sample matching morphological types becomes of great importance.

In the next Chapter, we will show that tidal stripping of matter in the interacting system is occurring NGC 7592, and that matter is indeed infalling on the Seyfert nucleus, probably providing the fuel for nuclear activity.

This Chapter has been based on the following works:

1. Rafanelli P., Marziani P.: *Seyfert galaxies with close companions: a method of identification*, in *Morphological and Physical Classification of Galaxies*, Proceedings of the V^{th} *International Workshop of the Osservatorio Astronomico di Capodimonte.* G. Busarello *et al.* (Eds.), 1991. *In Press.*

2. Rafanelli P., Marziani P.: *The frequency of companions among Seyfert galaxies*, submitted for publication in the *Astronomical Journal.*

Chapter 3

The complex nature of the Seyfert galaxy NGC 7592

Abstract – In this Chapter we present a detailed analysis of the physical conditions and of the kinematical and dynamical properties of the system of interacting galaxies NGC 7592, the western component of which shows signs of Seyfert activity. Medium resolution long-slit spectra taken at different position angles along the nuclei show that the Hα, Hβ, [OIII]λλ4959,5007, [NII]λλ6548,6583, [SII]λλ6716,6731, and [OII] λλ3726,3729 emission lines are spatially extended over a size comparable to the size of the system. The aspect and the kinematics of the galaxies suggest that a prograde encounter between the eastern and the western component of the system is occurring. The large Hα luminosity indicates that all galaxies are undergoing a strong burst of star formation, with a very large global star formation rate ($\approx 20\ M_{\odot} yr^{-1}$). In the spectra of the nuclear and circumnuclear regions of the western component, the high ionization lines are redshifted by $\Delta v_r \approx 50$ km s^{-1} with respect to the low ionization lines, and their ratios indicate the simultaneous presence of thermally and non-thermally ionized gas. This is interpreted in terms of coexistence in the nucleus of the western component of Seyfert and Starburst activity, the last one being responsible for ≈ 75 % of the Hα line luminosity. In the contact region between the eastern and the western component of NGC 7592, the presence of gas whose radial velocity increases approaching the Seyfert nucleus has been revealed . We suggest that this could be due to gas stripped from the eastern component, and which is infalling on the Seyfert nucleus.

3.1 Introduction

Gravitational interaction can enhance the Star Formation Rate (SFR) in the disk and in the nuclear regions of galaxies, producing a starburst phenomenon in the most extreme cases, when the SFR can not be sustained for a time comparable with the age of the galaxy (*e.g.* Weedman, 1989). The link between the enhancement of SFR and interaction seems to be well established on a statistical basis, in the sense that interacting galaxies have larger emission line luminosity (Keel *et al.*, 1985), stronger

radio emission (Sulentic, 1976; Stocke, 1978; Heckman, 1982; Hummel, 1982) and higher far-infrared luminosity (Bushouse, 1987; Lonsdale *et al.*, 1984; Miley *et al.*, 1985; Lawrence *et al.*. 1989) *et al.*, 1989) than unperturbed and isolated galaxies. Moreover, the most powerful IRAS galaxies belong to interacting systems (Lawrence *et al.*, 1989). It is less clear the role that interaction may have in inducing non-thermal, Seyfert type, nuclear activity. The works of Adams (1977), Dahari (1984, 1985), Mc Kenty (1989) and of Rafanelli and Marziani (1991; Chapter 2) suggested that there is an excess of morphologically perturbed and interacting systems among Seyfert galaxies in comparison with a sample of non-active galaxies. Since the activity in Seyfert nuclei is believed to be powered by accretion onto a compact, massive object, it has been often suggested that:

1. gravitational instabilities produced by the interaction with a companion galaxy can lead the disk gas to move toward the nucleus of the galaxy (Simkin, Su and Schwarz, 1980; Byrd *et al.*, 1986),

2. the gas can be transferred from the companion to the active galaxy (*e.g.* Stockton, 1982; de Robertis, 1985). The observational evidence in favour of this is till now marginal: only one case has been considered explicitly (Arp 102b, de Robertis, 1985; UGC 3995A).

Kennicutt and Keel (1984), Keel *et al.* (1985), and Dahari (1985) have shown that interaction enhances both non thermal activity and nuclear star formation, but the statistical significance of this effect for the non-thermal activity is very limited (Dahari and de Robertis, 1988b). It is noteworthy that more than 70 % of the galaxies hosting an active nucleus do not show evident signs either of morphological peculiarities or interaction, since the percentage of interacting and morphologically peculiar objects is around, and probably less than 30 %.
On the other side, Starburst and nonthermal activity could be related phenomena. Emission line spectra of some low ionization objects suggest that they could be accounted for by a mixture of gas photoionized by both a thermal (as for HII regions) and a non-thermal contribution (as for active galactic nuclei; Keel *et al.*, 1985, Rafanelli, 1989). Furthermore, presence of circumnuclear star formation has been revealed in NGC 1068 (see Wilson *et al.* 1988, for detailed reference concerning this object). Several evidences suggest that the far-infrared luminosity of Seyfert galaxies should be at least in part due to thermal reradiation of dust heated by hot, young O-B stars (*e.g.* Neugebauer *et al.*, 1986; Rodriguez-Espinoza *et al.*, 1987). Dahari and de Robertis (1988a,b) in their comparative study of Starburst and Seyfert galaxies, pointed out that Starburst and Seyfert 2 galaxies have similar IRAS spectra, and similar Hα luminosity. However, Starburst galaxies have narrower line widths than Seyfert 2 nuclei (Feldman *et al.*, 1982; Balzano, 1983), implying that the kinematics and dynamics of the emission line regions are probably different in the two classes (*e.g.* De Robertis and Shaw, 1988).

Weedman (1983) has proposed an evolutionary link between the Starburst and Seyfert phenomenon. Since the gas velocity dispersion in the Starburst nuclei is probably too low for having equilibrium in the potential of the galactic bulge, remnants of star formation can collapse to a steady state configuration of radius $\approx$ 1 *pc*, and then be accreted by gas. Otherwise, mass loss during the later stages of the evolution of O-B stars could constitute a source of accreting matter for the central black hole (Norman and Scoville, 1988). Connections between the two phenomena have been barely exploited from the theoretical point of view, but also the observational evidence favoring a link remains until now sparse and circumstantial. If interaction is able to trigger a Starburst phenomenon in an otherwise normal galaxy, the study of interacting systems with an ongoing Starburst can provide constraints upon the geometry and dynamics of the encounter which are able at best to favor the occurrence and/or to strengthen the Starburst phenomenon. Intermediate objects, in which both a nuclear Starburst and a Seyfert nucleus may simultaneously coexist, are laboratories in which the proposed scenarios connecting the two phenomena can be tested.

In this Chapter we present a detailed analysis of the physical conditions and of the kinematical and dynamical properties of NGC 7592. NGC 7592 $\equiv$ VV 731 is a system of close interacting galaxies. It is described in the *2nd Reference Catalogue of Bright Galaxies* (de Vaucouleurs and de Vaucouleurs, 1954) as a *colliding pair of galaxies* and by Vorontsov-Velyaminov (1979) as *a pair of coalescents*, whose nuclei are nearly aligned along the east-west direction. Markarian and Lipovetskii (1977) identified the eastern component of the system as Mkn 928. Arkhipova *et al.* (1981) suggested that *the system actually comprises three components in a common envelope*, due to the presence of a third, smaller galactic body in the south. Arkhipova *et al.* (1981) noted that all nuclei of the three components show strong emission lines, and that the spectrum of the western nucleus is of Seyfert-type, with a broad component in Hα whose Full Width Half Maximum (FWHM) appeared to be $\gtrsim$ 1000 $km\ s^{-1}$FWHM. Further observations by Dahari (1985) did not confirm the presence of the broad component in Hα, suggesting the classification of the western nucleus as a Seyfert–2. Dahari and de Robertis (1988b) classified the same nucleus as intermediate between a Seyfert–2 and a Starburst nucleus. In addition, NGC 7592 is a strong IRAS source, whose far infrared flux is dominated by thermal emission (Bushouse, 1987).

3.2 Observations and data reduction

Images of NGC 7592 were taken on November 11, 1988 at the Cassegrain focus of the 1.82 m, F/9 telescope of the Asiago Observatory. The atmospheric seeing was typically $\approx$ 1.0" (FWHM). The Thompson CCD (pixel size 0.29") offered a field of view $\approx$ 2 *arcmin* $\times$ 3 *arcmin*. Long slit spectra of NGC 7592 were obtained from Sep. 26 to Sep. 29, 1989, using the Boller and Chivens spectrograph on the ESO 1.52 m telescope. The detector was a High Resolution RCA CCD (scale along the slit 0.68"/pixel), and was used for four settings with combined coverage 3350-7380 Å. The

slit was opened to a width of $\approx$ 2". Atmospheric seeing was estimated to be $\approx$ 1.0" - 1.5" (FWHM) during all the four nights of observation. On Sep. 26 1989 we used grating ESO Nr. 22 ruled at 1200 *lines* mm^{-1}, while on Sep. 27, we used grating ESO Nr. 19 at 2^{nd} order. Both settings gave a dispersion of 67 Å/mm, and a mean spectral resolution of 4 Å (FWHM). The spectral ranges covered were 6400–7400 Å on Sep. 26, and 4650-5550 Å on Sep. 27. The spectrograph slit was oriented at P.A.=100° in order to intersect the eastern and the western nucleus of the system . On Sep. 28 and Sep. 29 we used grating ESO Nr. 27 ruled at 600 *lines* mm^{-1} giving a dispersion of 129 Å/mm and a mean spectral resolution of 4 Å. The covered spectral ranges were 5440–7380 Å on Sep. 28 and 3550–5450 Å on Sep. 29. The slit was oriented at P.A.= 32° and P.A.=100° during both nights. Due to guiding errors, the spectrum taken on Sept. 29 at P.A.=100° is of poor quality. Its use has been limited to an estimate of the fluxes of the *strongest* lines of the nuclear spectra. The reduction of the data was performed using the VISTA program, developed at Lick Observatory (Terndrup, Lauer and Stover 1984). Bias levels were subtracted from all frames, which were then divided by flat field. No photometric calibration was applied to the images. The spectra were wavelength calibrated fitting third order polynomials to unblended emission lines in He-Ar comparison spectra recorded after each observation. RMS was always less than 0.1 Å. The spectra were then sky subtracted and extinction corrected. The spectral response of the detector was measured and the spectra were placed to an absolute flux scale using observations of standard stars from the lists of Stone (1977), performed each night after the observation of NGC 7592. Fluxes and positions of the lines were measured using the program RETICENT (Pritchet, Monacki and Yang, 1981). Line centroids were evaluated weighing each wavelength bin with a weight $\propto I^3$ over a range of width $\pm$ 1 FWHM, measured from the line center. The observed FWHM were corrected for instrumental width applying the relation $(\mathrm{FWHM})^2 = (\mathrm{FWHM})^2_{obs} - (\mathrm{FWHM})^2_{instr}$. The corrected line widths are reliable to $\pm$ 20 %.

3.3 Results

3.3.1 Morphology

The following analysis of the morphology of the NGC 7592 system is based on the R image, which is shown in Fig. 3.1. The V image is not presented here, because it is very similar to the R one, although a little less deep. For the sake of clarity, we will refer to the western galactic body as to NGC 7592 W, while NGC 7592 A will indicate its nucleus and the corresponding emitting region, identified on the spectra (see Table 1, section 3.2). Similarly, NGC 7592 E and NGC 7592 S will indicate the eastern and the southern component, while their nuclei will be called NGC 7592 B and NGC 7592 C. The nucleus A has a star-like appearance and it is surrounded by a nearly spheroidal envelope, with an extension in the west. This extension bends toward north joining a bright and large wing, which resembles a spiral arm or perhaps a tidal feature. A faint extension, similar to a spiral arm, is visible in the south. The envelope

around A is connected to a second galactic body, NGC 7592 E, whose nucleus (B), identified by Markarian and Lipovetskii (1976) as the nucleus of Mkn 928, is located at a distance $d_{AB} \sim 11$ *arcsec* ($\sim 4h^{-1}kpc$) from A at $P.A. = 100°$. The morphology of this component is peculiar. In the central region, B is linked to two knots which extend up to $d" \sim 4$ *arcsec* to the east. In addition, a smooth extension is detected along the direction (P.A.= 40°) joining B and C. An arc of condensations on the eastern side of NGC 7592E seems to be distorted in the direction of the nucleus of NGC 7592 S, located at $d_{BC} \approx 12.1$ *arcsec* ($\approx 4.1\ h^{-1}kpc$) from B at $P.A. = 212°$. A faint plume extends from the west side of NGC 7592 S, bending toward south.

3.3.2 Emission Line Regions

The Hα, Hβ, [OIII]$\lambda\lambda$4959,5007, [NII]$\lambda\lambda$6548,6583, [SII]$\lambda\lambda$6716,6731, and [OII] $\lambda\lambda$3726, 3729 emission lines have been found to be spatially extended. Their overall extension is $\approx$ 30 *arcsec* $\approx$ 10.5 $h^{-1}kpc$ at $P.A. = 100°$ and $\approx$ 28 *arcsec* $\approx$ 9.8 $h^{-1}kpc$ at $P.A. = 100°$. The size of the emitting regions is comparable with the size of the galaxies belonging to the system NGC 7592 as measured on their R image. A careful analysis of the Hα profile along the slit permits to isolate 6 different emitting regions (A1,A,A2,B2,B,B1) along $P.A. = 100°$ and 4 regions (C,B4,B,B3) along $P.A. = 212°$. The slit positions and the regions analyzed are marked in Figure 3.1. A quantitative information on the location and the extension of the emitting regions is provided in Table 1. Column 1 and 2 list the slit P.A. at which each emitting region was observed and its identification; column 3 and 4 quote their angular and projected linear size, while column 5 gives the identification of the nucleus (A or B) used as reference for the determination of the position angle and of the angular and projected linear distances quoted in columns 6 to 9. Column 10 reports the heliocentric radial velocities and their associated RMS, derived measuring the following low-ionization lines: Hα, Hβ, [NII]$\lambda\lambda$6548,6583, [SII]$\lambda\lambda$6716,6731 and also [OII]$\lambda\lambda$3726,3729, [OI]λ6300 and Hγ for A, B, and C. The observed fluxes of the emission lines are quoted in Table 2. For lines which were present in more than one spectrum, the mean of the observed fluxes is given. The fluxes of the strongest emission lines are good to $\pm$ 15 %, whereas those below $2\times 10^{-15} erg\ s^{-1}$ can be uncertain by a factor $\approx$2. The Balmer lines of NGC 7592 A show features typical of a Seyfert 1.9 nucleus (Fig. 3.2a, 3.2b). Line fluxes for NGC 7592 A are in satisfactory agreement with the values reported by Dahari (1985), who had classified this object as a Seyfert 2. The line fluxes of NGC 7592 B are reported in Table 2 both for P.A. =100° and P.A.=32°. They differ by $\approx$ 10–15 %, since at P.A.= 100° the profile along the slit shows a contamination produced by the knot on its eastern side, see Fig. 3.1. The flux of Hα had been already measured by Bushouse (1987), who obtained a value just in our results. Other line fluxes for NGC 7592 B and C are not available to our knowledge in literature. Extranuclear emitting regions located very close to the nuclei (as NGC 7592 A2 and B2) have continuum and line flux levels strongly sensitive to the variations of seeing, since they can be contaminated by the strong nuclear sources. We guess that the *absolute* flux calibration for these

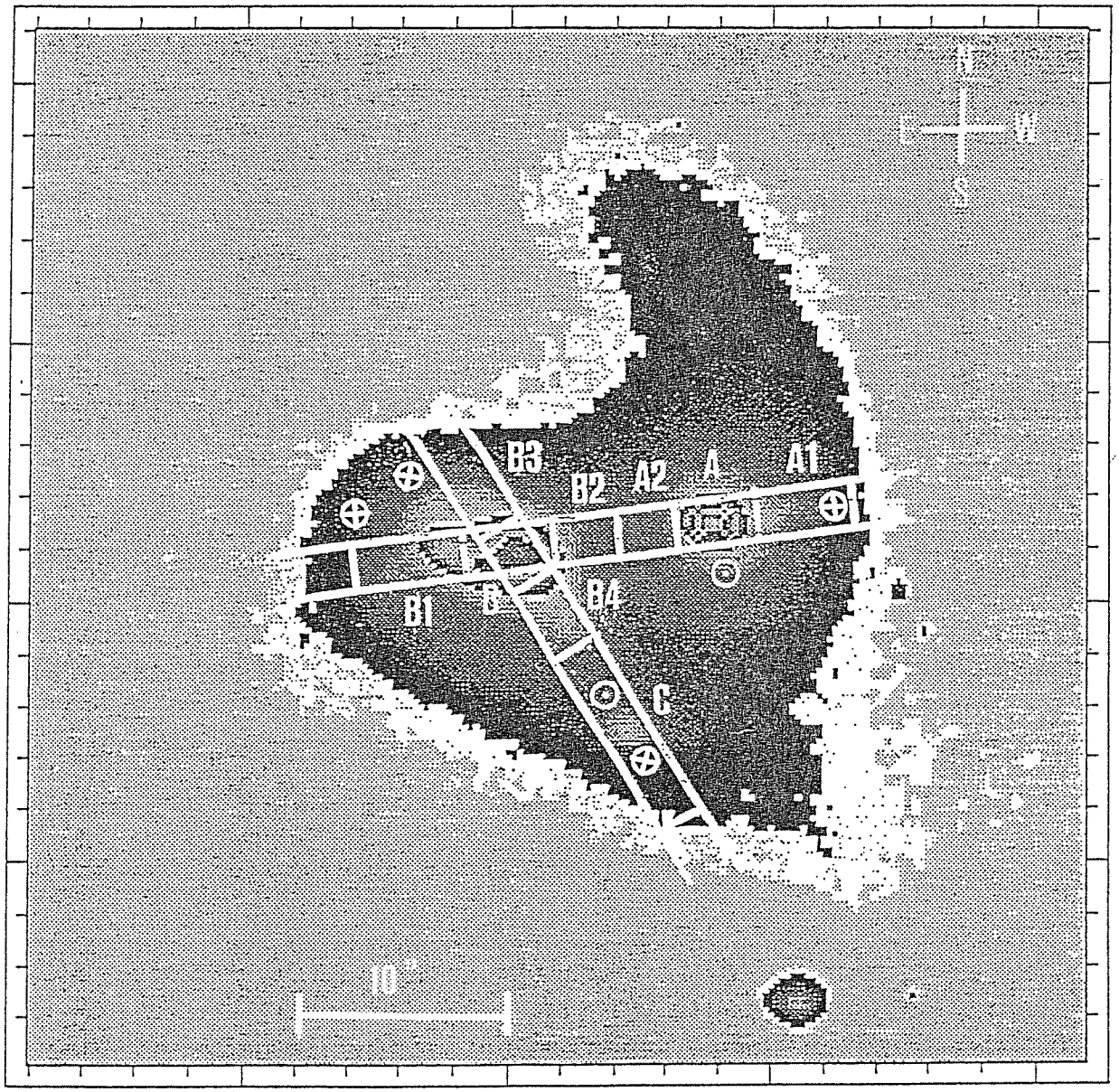

Figure 3.1: *R-band image of NGC 7592. North is to the top, east is to the left. Emission regions are marked as defined in Table 1.*

Table 1: Emitting Regions of the NGC 7592 system

Sp.	*P.A.*	*Ident.*	*Extension*		*Distance*				v_r
			arcsec	h^{-1} *pc*	*from*	*P.A.*	*arcsec*	h^{-1} *pc*	*km/s*
	100°	A1	7.5	2700	A	280°	5.8	2030	7362 ± 10
	"	A	3.4	1200	A	–	0.0	0	7330* ± 7
	"	A2	3.4	1200	A	100°	−3.4	−1200	7330* ± 10
	"	B2	4.1	1440	B	280°	4.1	1440	7300 ± 10
	"	B	4.1	1440	B	–	0.0	0	7320 ± 6
	"	B1	6.8	2500	B	100°	−5.4	−1900	7450 ± 10
	32°	B3	7.4	2630	B	32°	5.8	2020	7375 ± 10
	"	B	4.1	1430	B	–	0.0	0	7322 ± 10
	"	B4	4.1	1430	B	212°	−4.1	−1430	7285 ± 10
	"	C	11.6	4060	B	212°	−9.9	−3450	7225 ± 8

*see text

regions (A2 and B2) is accurate to within ± 30 % uncertainty. The diagnostic diagrams proposed by Veilleux and Osterbrock (1987) were used to analyze whether the ionization of the emitting regions in NGC 7592 is produced either by thermal sources (HII regions) or by nonthermal sources, as it is the case for Active Galactic Nuclei (AGN), Figures 3.3a,3.3b,3.3c. NGC 7592 A and A2 result to be ionized by a nonthermal source. All the other emitting regions can be classified as HII regions, with the exception of A1 for which a contribution to the ionization from NGC 7592 A cannot be excluded (see Fig. 3b). This classification has been also tested with the diagnostic diagrams based on the line ratios [OII]$\lambda\lambda$3726,3729/[OIII]λ5007, [OIII]λ5007/Hβ and [NII]λ6583/Hα (Baldwin, Phillips and Terlevich, 1981), which further allow to identify gas ionized by shock heating. It is confirmed that B, B3 B4 and C are typical HII regions, while A can be classified either as a *power-law galaxy* or as a *shock-heated galaxy*. Values of electron density, Balmer decrement and internal extinction for each emitting region are quoted in Table 3. The electron density n_e has been estimated from the ratio [SII]λ6716/[SII]λ6731, assuming an electron temperature $T_e \approx$ 10,000° K. The observation of a standard star right after each exposure of NGC 7592 allowed to remove with good accuracy the effect of the Fraunhofer B absorption band. Uncertainty in the density estimates is approximately a factor 2, for density values $\gtrsim$ 100 cm^{-3}. Balmer decrements have been computed after correction for galactic extinction, being E(B − V)$_{gal}$=0.015 (Burstein, 1986). The internal reddening c and the corresponding

E(B – V) has been computed using the Whitford reddening curve as parameterized by Miller and Mathews (1972). An intrinsic ratio Hα/H$\beta \approx$ 2.85 has been adopted for regions photoionized by thermal sources, while for regions whose ionization source is nonthermal, it has been assumed a ratio Hα/Hβ= 3.1 (Ferland and Netzer, 1983). Regions located in the outer parts of the galaxies NGC 7592 E and W (B1, B3 and B4 and A1) are characterized by very low electron density, $n_e \sim 10\ cm^{-3}$, and by narrow emission lines FWHM $\sim 140\ km\ s^{-1}$. The properties of the nuclear regions A,B and C and of the regions between B and A, B2 and A2, are discussed more extensively in the following subsections.

NGC 7592 A – Fig. 3.2a and 3.2b display the high resolution spectra of NGC 7592 A, which were used to measure the emission line widths and to analyze the line profiles. Most lines are asymmetric towards the red. The asymmetry is due to a semibroad component displaced to the red, which is present in the [OIII]$\lambda\lambda$4959,5007, [OI]λ6300, but not in Hβ and in the [SII]$\lambda\lambda$6716,6731 lines. The FWZI of the semi-broad component, measured on the [OIII]λ5007 lines is $\approx$ 1800 $km\ s^{-1}$, while the FWZI of Hβ is $\approx$ 850 $km\ s^{-1}$. A faint broad component is present below the system of lines [NII]$\lambda\lambda$6548,6583 and Hα. Fluxes were estimated employing a multicomponent fit with four gaussian curves modelling the narrow and broad components of Hα (NC and BC) and the [NII]$\lambda\lambda$6548,6583 profiles. Their values are reported in Table 2. However it should be remarked that a semibroad component below the Hα and [NII]$\lambda\lambda$6548,6583 lines could produce an apparent Hα broad component. This seems to be the case, since the upper radial velocity of the broad component is consistent with that expected for the semi-broad component of the [NII]λ6583 line. All emission lines (Hα, Hβ, [SII]$\lambda\lambda$6716,6731, [NII]$\lambda\lambda$6548,6583, [OI]λ6300, [OIII]$\lambda\lambda$4959,5007), show a double peaked core (see Fig. 3.4a and 3.4b, where the line cores of Hβ and [OIII]λ5007 are reproduced; hereafter we will refer to the lower and higher radial velocity component as to the *blue* and *red* component). The only possible exception is the [NI]λ5198 line, whose faintness does not allow any reliable consideration on its profile. The average heliocentric radial velocity of the blue component is $v_{r,B} = 7280 \pm 7\ km\ s^{-1}$ for all lines with the exception of [OIII]$\lambda\lambda$4959,5007, for which $v_{r,B} = 7330 \pm 10\ km\ s^{-1}$. The radial velocities of the red component of the [OIII]$\lambda\lambda$4949,5007 lines and the value averaged over all the other lines are $v_{r,R} \lesssim 7510\ km\ s^{-1}$ and $v_{r,R} = 7460 \pm 50\ km\ s^{-1}$ respectively. The extension along the slit of the red component of Hβ and Hα, and of the [NII] and [SII] lines (see Figure 3.5a and next section) suggests that this component corresponds to the red component seen in the [OIII] lines. The radial velocity of the blue peak of Hβ is on the contrary significantly lower than that measured for the blue peak of the [OIII]λ5007 line. Although the difference is small, $\Delta v_r \approx 50\ km\ s^{-1}$, it is also confirmed by the radial velocity measurements on the extended emitting regions (see next section). The measurement of the FWHM of the double peaked emission lines is then affected by the relative strength of their two components. FWHM values of [OIII]$\lambda\lambda$4959,5007 and [OI]λ6300 (490 and 280 $km\ s^{-1}$ respectively) are larger than those of the other lines ($\approx$ 200–220 $km\ s^{-1}$). This happens because red and blue component have similar peak intensity in the [OIII]$\lambda\lambda$4959,5007 and [OI]λ6300 lines, while the red component

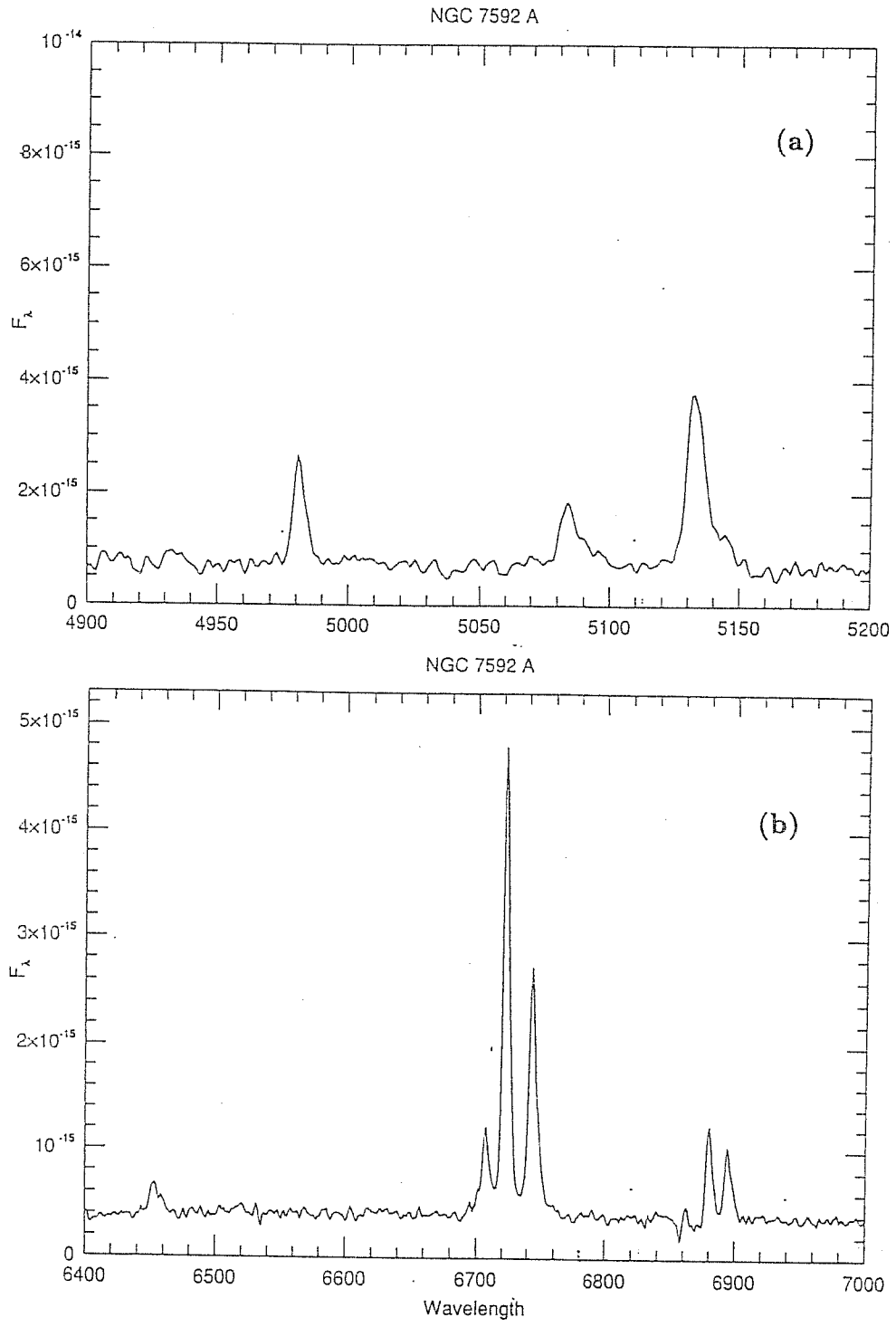

Figure 3.2: *High resolution spectra of NGC 7592 A: a) profiles of Hβ and of the [OIII]λλ4959,5007 lines; b) the Hα and [NII]λλ6548,6583 blend. Vertical scale is flux per unit wavelength (erg s^{-1} $Å^{-1}$), vertical scale is wavelength in Å.*

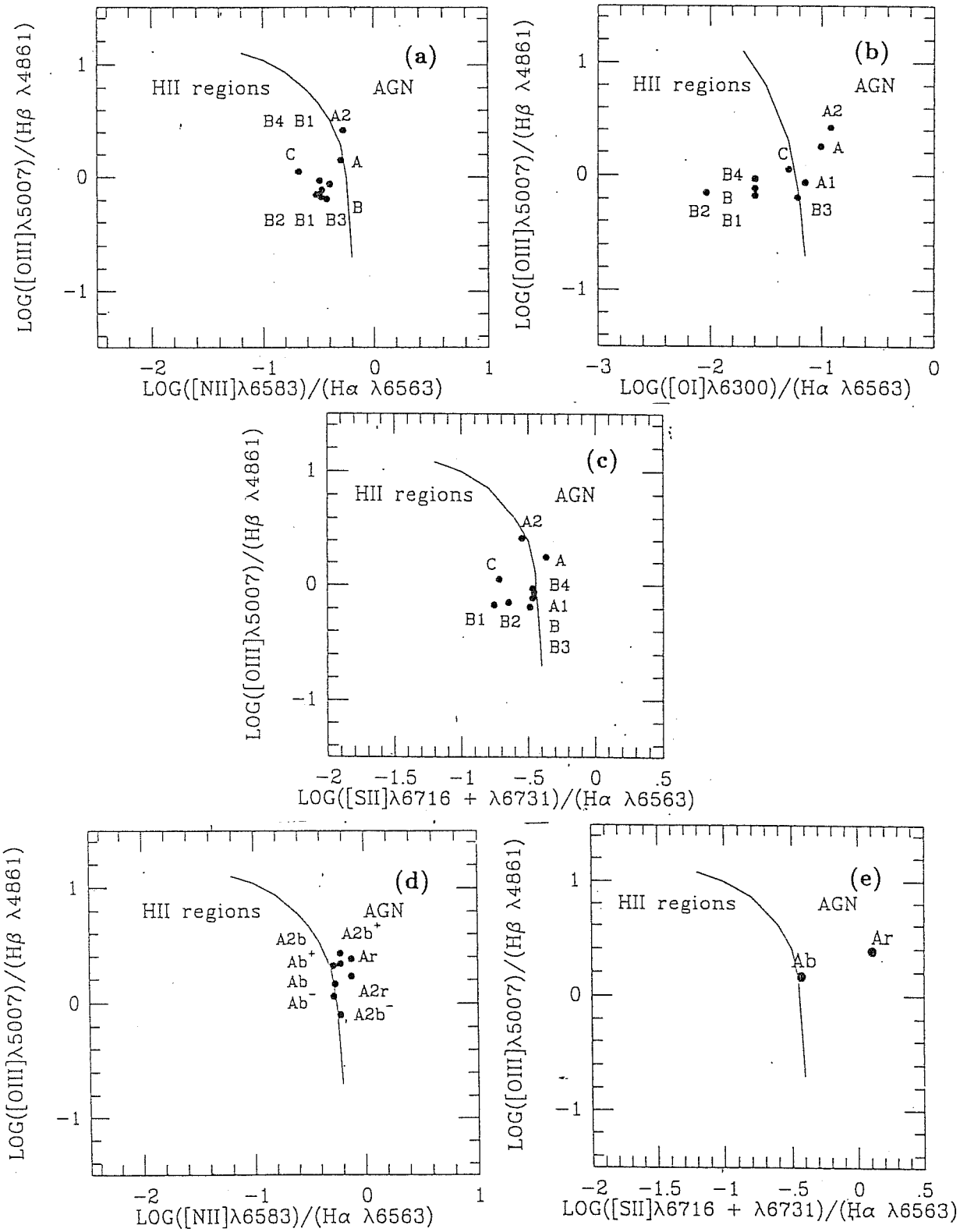

Figure 3.3: *a,b,c: Diagnostic diagrams applied to the line emitting regions of NGC 7592. d,e: Diagnostic diagrams applied to the red and blue line components resolved in A and A2 indicated as Ab, Ar and A2b and A2r. Ab^-, Ab^+, $A2b^-$ and $A2b^+$ indicate the ratios computed on the blue component at $v_r \approx 7280$ km s^{-1} (−), and at $v_r \approx 7330$ km s^{-1} (+).*

is fainter than the blue one ($I_R \lesssim 0.5\ I_B$) in Hα, Hβ, and [NII]$\lambda\lambda$6548,6583. The FWHM of Hβ, Hα, and [NII]$\lambda\lambda$6548,6583 should be therefore regarded as an estimate of the width of the *blue* component.
We have been able to separate the double-peaked profiles in the two core components and in the underlying semibroad component, and hence to report the line ratios of the core components separately in the diagnostic diagrams. The red component, indicated as Ar, is located among AGN in all the three diagnostic diagrams, while the blue one (Ab) has a more ambiguous location (see Figures 3.3d and 3.3e). An estimate of the flux values for each component is reported in Table 2a. The ionization degree of the red component ([OIII]λ5007/ H$\beta \approx$ 2.5) is higher than that of the blue component ([OIII] λ5007/H$\beta \approx$ 1.5). The electron density of the gas emitting the red component, $n_e \gtrsim 600\ cm^{-3}$, appears to be somewhat higher than that of the blue one, $n_e \lesssim 250\ cm^{-3}$.
The not univocal location of Ab in the diagnostic diagrams may imply that the emitting gas is either partly ionized by the same nonthermal source ionizing Ar, or by an internal nonthermal source. Support to the latter suggestion is provided by the radial velocity difference between the peaks of the blue components of [OIII] $\lambda\lambda$4959,5007 and Hβ. This implies that the blue component of the Balmer and [OIII] lines originates to some extent in different gaseous media, which are also in different kinematical conditions. If this is true, [OIII]λ5007 and Hβ are due to a mixture of contributions: the ratio of the intensities of the [OIII]λ5007 line and Hβ at a wavelength corresponding to $v_r \approx 7280\ km\ s^{-1}$, namely the peak velocity of the blue component of all lines but [OIII], is $\lesssim 1$, indicating the presence of low ionization emitting gas in the blue component. The same intensity ratio at $v_r \approx 7330\ km\ s^{-1}$, is >1, indicating the presence of highly ionized gas too. These results are confirmed by the [OIII]λ5007/Hβ intensity ratios at $v_r \approx 7280\ km\ s^{-1}$and $v_r \approx 7330\ km\ s^{-1}$ measured in the spectrum of the close extranuclear region A2 (see further details in the next subsection).
The Hα broad component can be accounted for by the blend of the semibroad components emitted by the [NII]$\lambda\lambda$6548,6583 doublet, and perhaps Hα. The upper radial velocity at which the broad feature is detected is consistent with the upper radial velocity of the [OIII]λ5007 semibroad component.
Although it is possible to estimate the contribution of the semibroad component in the [NII]λ6583 profile, it is not possible to use directly the diagnostic diagrams of Veilleux and Osterbrock, since the estimate of its flux contribution in Hα is too uncertain. We thus employed the ratio [OIII]λ5007/Hβ and the ratio [OI]λ6300/[NII]λ6583. A comparison with the values provided by Veilleux and Osterbrock (1987) suggests that the line ratios found for the semibroad component are rather typical of regions ionized by nonthermal sources.

The emission regions between A and B. – The spectrum of region A2 shows emission line profiles similar to those seen in the spectrum of the Seyfert nucleus, NGC 7592 A , but without the semibroad component. The [OIII]λ5007 and Hβ profiles are given in Fig. 3.4c and 3.4d. The line cores are double peaked, and the radial velocity of the blue component of [OIII]λ5007 is in this case higher than that of Hβ by $\Delta v_r \approx 100$

Table 2: Emission Line Fluxes[1]

Line Id.		A	A1	A2	B		B1	B2	B3	B4	C
					P.A.=100°	*P.A.*=32°					
[*SII*]	λ 6731	11.7	5.9	1.7	12.0	10.3	8.3	3.3	4.8	4.0	6.0
[*SII*]	λ 6717	14.8	9.0	2.0	15.6	13.0	11.6	4.5	7.2	5.0	7.3
[*NII*]	λ 6583	32.2	16.8	6.2	27.5	22.9	18.1	10.7	13.8	8.4	14.7
Hα (NC)	λ 6563	44.7	45.5	13.2	80.6	69.7	54.5	35.3	37.6	25.8	61.1
Hα (BC)	λ 6563	31.2	–	–	–	–	–	–	–	–	–
[*NII*]	λ 6548	10.7	6.3	2.6	9.3	7.6	6.0	3.5	4.6	2.6	5.6
[*OI*]	λ 6300	6.1	<3	1.5	2.5	1.5	1.5	0.5	2.5	~ 0.5	2.8
HeI	λ 5876	2.3	–	–	< 3	–	–	–	–	–	< 3
[*NI*]	λ 5198	1.5	–	–	–	–	–	–	–	–	–
[*OIII*]	λ 5007	32.2	7.9	8.3	12.9	11.0	9.9	7.2	5.6	4.5	15.4
[*OIII*]	λ 4959	11.2	2.7	2.8	4.3	4.0	3.4	2.6	2.2	1.5	2.2
Hβ	λ 4861	11.7	9.8	3.2	17.0	13.7	15.3	10.1	8.6	4.9	14.8
Hγ	λ 4340	4.6	n.a.	n.a.	6.0	4.6	n.a.	n.a.	4.4	–	5.6
[*OII*]	λ 3727	30.4	n.a.	n.a.	30.3	25.6	n.a.	n.a.	15.4	6.8	26.2

–: not detected

n.a.: not available

[1]Line fluxes are in units of $10^{-15} erg\ cm^{-2} s^{-1}$

Table 2a: NGC 7592A

Fluxes of line components(*)

Line	*Id.*	*Blue*	*Red*	*Semibroad*
[*SII*]	λ 6731	5.3	7.3	–
[*SII*]	λ 6717	6.3	7.3	–
[*NII*]	λ 6584	17	8.7	13.5
Hα	λ 6563	31.5	11.4	22.4(o)
[*NII*]	λ 6548	5.7(†)	2.9(†)	4.8(†)
[*OI*]	λ 6300	∼ 2.4	∼ 2.4	∼ 2.0
[*OIII*]	λ 5007	11.4	9.5	12.3
[*OIII*]	λ 4959	3.8	3.2	4.1
Hβ	λ 4861	7.8	3.9	2.4

(*) Line fluxes are in units of $10^{-15} erg\ cm^{-2} s^{-1}$

(o) Estimated as the difference between the total flux of the blend Hα + [NII] and the sum of all other lines

(†) assumed equal to 1/3 I([NII]λ6584)

$km\ s^{-1}$. Unlike NGC 7592 A, the ionization degree in NGC 7592 A2 is higher in the blue component ([OIII] λ5007/Hβ≈ 2.5 than in the red one ([OIII]λ5007/Hβ≈ 1.5). In the diagnostic diagram of Fig. 3.4d both components (labeled as A2b and A2r) are located among the non-thermally ionized regions.

The Hβ profile displays a minimum between the blue and the red component at the wavelength corresponding to the radial velocity $v_r \approx 7320\ km\ s^{-1}$, namely the peak velocity of the blue component of [OIII]λ5007. The [OIII]λ5007/Hβ intensity ratios at $v_R \approx 7320\ km\ s^{-1}$and $v_r \approx 7200\ km\ s^{-1}$, the latter value being the peak velocity as derived from the low ionization lines, are ≈ 0.9 and ≈ 3 respectively. This finding shows the coexistence of high and low ionization gas in the blue component.

The ratio [OIII]λ5007/Hβ measured on the red component decreases monotonically from NGC 7592 A towards NGC 7592B, and converges to a value $\lesssim 1$ in B2 where the red component is barely visible, and keeps this value up to B. Such decrease moves the point representing the extranuclear red component in the diagnostic diagrams towards the area occupied by the HII regions, indicating a decrease of the effects produced by the nonthermal nucleus at increasing distances from it. In practice the red component is not present in B2.

The line profiles are narrower in B2 than in 7592 A and A2: the mean FWHM is ≈ 150 $km\ s^{-1}$, and their peak velocity corresponds to the velocity of the blue component. It must be remarked that in B2, where the effects of ionization by a nonthermal source are

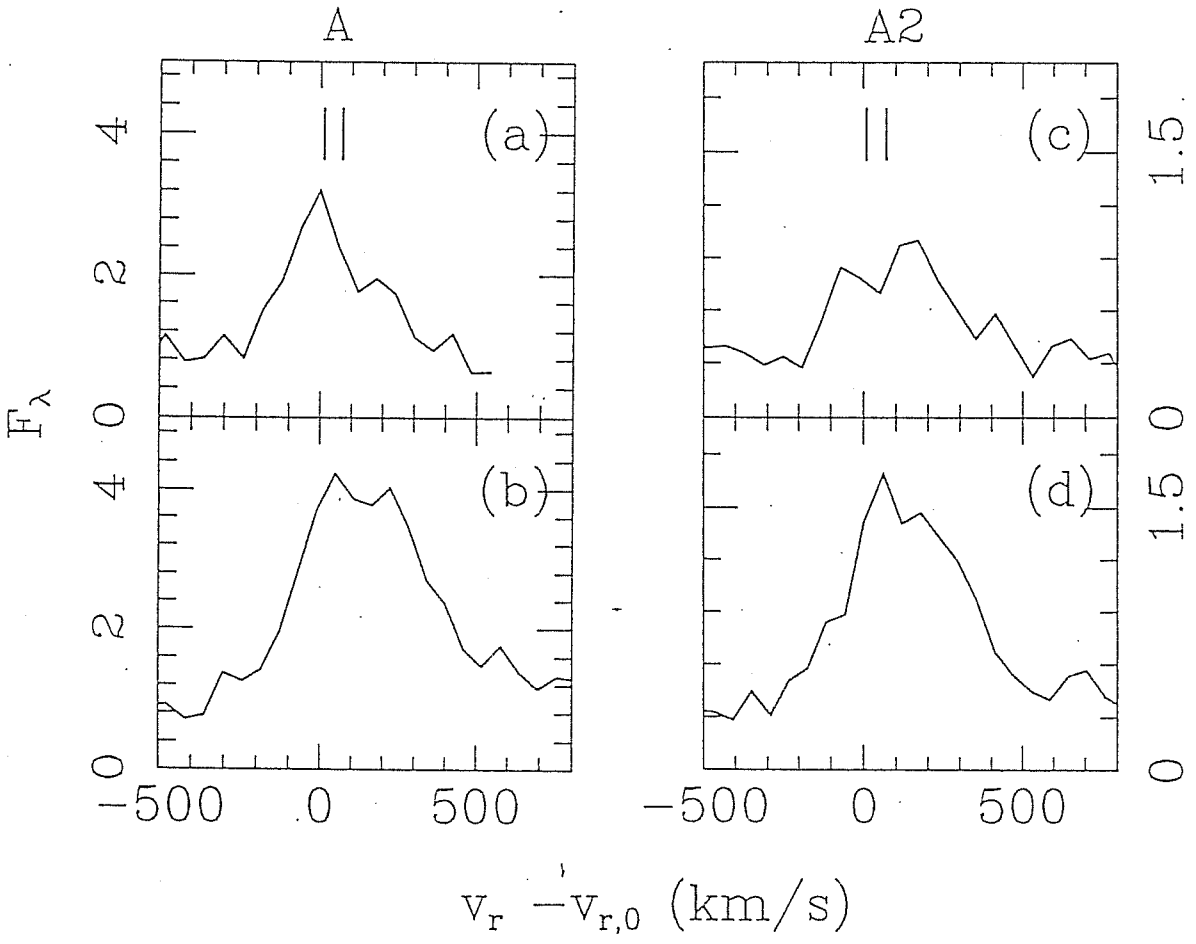

Figure 3.4: *Comparison of the Hβ and [OIII]λ5007 line profiles: a) and b) are for NGC 7592 A; c) and d) for region NGC 7592 A2. Vertical scale is flux per unit wavelength (erg* $s^{-1}cm^{-2}Å^{-1}$*); horizontal scale is radial velocity difference from the peak radial velocity of Hβ,* $\approx$ *7270* km s^{-1}*. The two thick marks indicate* $\Delta v_r = 0$ km s^{-1} *and* $\Delta v_r = 60$ km s^{-1}.

absent the peak velocity of the Hβ and [OIII]λ5007 lines are in good agreement, further suggesting that the shift in positions between Hβ and [OIII] in the blue component of A and A2 are due to the influence of the Seyfert nucleus.

NGC 7592 B $\equiv$ *Mkn 928* – The heliocentric radial velocity of B is 7320 $\pm$ 6 $km\ s^{-1}$, in good agreement with the value found from the HI 21 cm emission, 7311 $km\ s^{-1}$ (Bushouse, 1987). Since NGC 7592 B is also the brightest nucleus of the system, we will assume in the following the position and the radial velocity of B as references.
The radial velocities of the [OIII]$\lambda\lambda$4959,5007 lines and of the low ionization lines show no significant discrepancy. Emission line profiles appear to be rather narrow, without differences between Balmer and [OIII]$\lambda\lambda$4959,5007 lines: the FWHM of Hα and Hβ are $\approx$ 200 $km\ s^{-1}$, while the FWHM of the [OIII]$\lambda\lambda$4959,5007 lines is $\approx$ 210 $km\ s^{-1}$. These values are close to those found for the low-ionization lines in NGC 7592 A.

NGC 7592 C– NGC 7592 C corresponds to the third *condensation* revealed by Arkhipova. The Hα luminosity is comparable to that of B, although the continuum is much fainter than that of B. the equivalent width of Hα is W(Hα) $\approx$ 154 Å, two times larger than the value of B. Line profiles are very narrow, and have a mean FWHM $\approx$ 100 $km\ s^{-1}$.

3.3.3 Emission line structure and velocity curves

The spatial emission line structure at P.A. = 100° is shown in the isophotal maps reported in Fig. 3.5 a,b,c for the Hα, [NII]$\lambda\lambda$6548,6583, Hβ and [OIII]λ5007 lines. Velocity curves are shown in Fig. 3.6a (for P.A.=100°) and in Fig. 3.6b (for P.A. = 32°), for both the low ionization (Hα, Hβ, [NII]$\lambda\lambda$6548,6583,[SII]$\lambda\lambda$6716,6731), and high ionization lines ([OIII]$\lambda\lambda$4959,5007). Angular distances and radial velocities are referred to the position and to the heliocentric radial velocity of B.
On the eastern side of NGC 7592 B, the radial velocity increases and flattens at around 6 *arcsec* from B. Between A and B, gas motions appear to be peculiar. The radial velocity curve is separated in two tails, which correspond to the blue and red component described in the previous sections. On the lower tail, the radial velocity curves derived from low ionization and [OIII]$\lambda\lambda$4959,5007 lines differ by about 40–50 $km\ s^{-1}$on the western side of B, at locations corresponding to A and A2, while they agree within the measurement uncertainties in all other regions. The upper tail is due to gas turning to higher radial velocities (the red component seen on A, A2 and marginally on B2), contributing to both the Balmer and [OIII]λ5007 emission up to the position of A, and whose v_r increases from $\approx$ 7300 $km\ s^{-1}$ to $\approx$ 7500 $km\ s^{-1}$. Due to the small separation between the blue and red peak of the [OIII]$\lambda\lambda$4959,5007 lines, values reported for the red component of [OIII]$\lambda\lambda$4959,5007 are upper limits. On the western side of A, the velocity curve turns swiftly toward higher radial velocities. At P.A.= 212° no systematic differences are found between the velocity curves computed from the low ionization and the [OIII]$\lambda\lambda$4959,5007 lines (Fig. 3.6b). The velocity curve is approximately linear from $\approx$ –7 to $\approx$ 3 *arcsec* from B and flattens beyond both edges of the linear part.

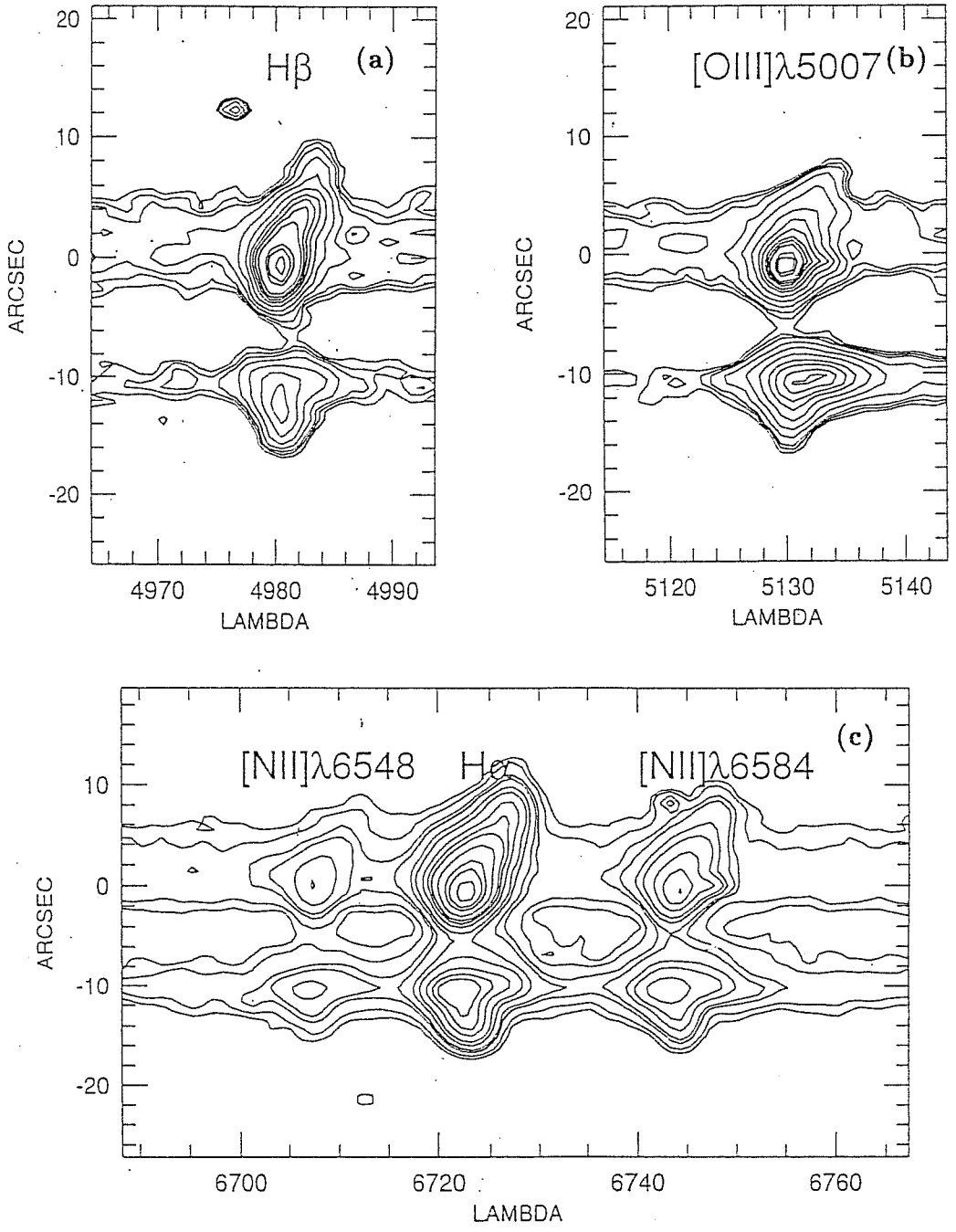

Figure 3.5: *Spatially extended structure of Hβ (a), [OIII]λ5007 (b), Hα and [NII]λλ6548,6583 (c). Horizontal scale is wavelength in Å, vertical scale is angular distance from B in arcsec.*

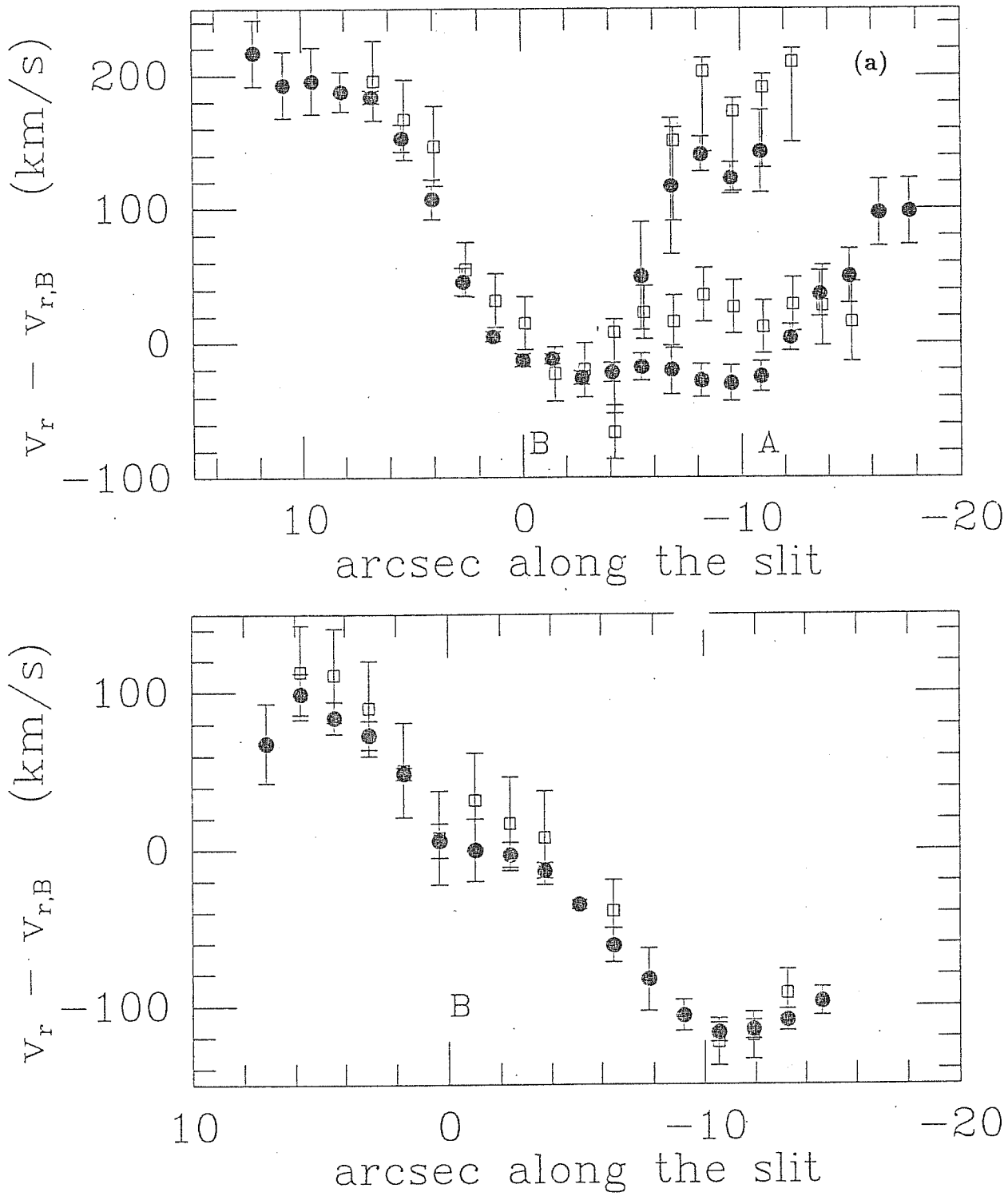

Figure 3.6: *Radial velocity curves at P.A. = 100° (a) and at P.A. = 32° (b) for low ionization (filled circles) and high ionization ([OIII]λλ4959,5007) lines (open squares). Horizontal scale is angular distance from NGC 7592 B in arcsec; vertical scale is radial velocity difference from the heliocentric radial velocity of NGC 7592 B ($v_r \approx 7280$ km s^{-1}).*

Table 3

	A	A1	A2	B		B1	B2	B3	B4	C
				P.A.=100°	*P.A.=32°*					
n_e (cm^{-3})	550	$\lesssim$ 10	180	150	–	40	70	$\lesssim$ 10	180	210
Hα/Hβ/Hγ	3.8/1.0/0.39	4.6/1.0/–	4.0/1.0/–	4.7/1.0/0.35	5.05/1.0/0.335	3.6/1.0/–	3.4/1.0/–	4.3/1.0/–	5.25/1.0/–	4.1/1.0/0.38
c	0.25	0.59	0.32	0.62	0.71	0.29	0.21	0.51	0.76	0.45
E(B–V)	0.19	0.45	0.24	0.43	0.55	0.22	0.16	0.39	0.59	0.35
$L_c(H\alpha)\cdot h^2$ ($erg\ s^{-1}$)	4.5×10^{40}	8.0×10^{40}	1.5×10^{40}	1.35×10^{41}	1.5×10^{41}	5.7×10^{40}	3.2×10^{40}	5.8×10^{40}	6.0×10^{40}	8.5×10^{40}
S.F.R ($M_\odot yr^{-1}$), M > 10 $M_\odot$	0.046	0.11	0.20	0.19	0.20	0.077	0.046	0.08	0.085	0.12
S.F.R. ($M_\odot yr^{-1}$), total	0.28	0.71	0.13	1.20	1.3	0.51	0.29	0.51	0.53	1.33
Projected Area (pc^2h^2)	8.3×10^5	1.84×10^6	8.33×10^5	1.00×10^6	1.0×10^6	1.7×10^6	1.0×10^6	1.8×10^6	1.0×10^6	2.84×10^6
SFR/area ($M_\odot yr^{-1}pc^{-2}$)	3.4×10^{-7}	3.8×10^{-7}	1.6×10^{-7}	1.2×10^{-6}	1.3×10^{-6}	3.0×10^{-7}	2.9×10^{-7}	2.8×10^{-7}	5.3×10^{-7}	2.7×10^{-7}

3.4 Discussion

3.4.1 Physical and kinematical conditions in NGC 7592 A

In this section, we will further discuss the ionization mechanism of the blue component detected on NGC 7592 A and A2. In section 3.2.1, we suggested that the location in the diagnostic diagrams of NGC 7592 Ab could be accounted for by the existence of two distinct kinematical components of different ionization degree. Although the ionization mechanism of these components cannot be directly proved, since its presence is revealed only by a slight displacement of the line center of [OIII]$\lambda\lambda$4959,5007 lines, we can give some insight to its ionization mechanism from the following analysis.
If the ionizing source is non thermal, the gas can be either shock heated or photoionized by a nonthermal source. A contribution from shock-heated gas seems unlikely for explaining the [OIII]$\lambda\lambda$4959,5007 components peaking at $v_r \approx 7330$ $km\ s^{-1}$. If shock-heating plays a role in the ionization, high electron temperature ($T_e \sim 10^5$ °K) is needed in order to have collisional ionization of O^+. In this case, also the strength of lines originating in ions of ionization potential lower than that of O^+ should be enhanced, and in particular the [NI]λ5198, [OII]$\lambda\lambda$3726,3729, [NII]$\lambda\lambda$6548,6583, [OI]λ6300, [SII]$\lambda\lambda$6716,6731 (Shull and McKee, 1979; Binette, Dopita and Tuohy, 1985). We tested whether the blue components of the strongest low ionization lines ([NII]$\lambda\lambda$6548,6583,[SII]$\lambda\lambda$6716,6731) showed radial velocity consistent with that of the [OIII]$\lambda\lambda$4959,5007, but we did not reveal any significant difference between the radial velocity of these lines and that of the blue peak of the Balmer lines.
We reported the intensity ratios [OIII]λ5007/Hβ and [NII]λ6583/Hα computed at $v_r \approx$ 7280 $km\ s^{-1}$ (Ab^-) and at $v_r \approx 7330$ $km\ s^{-1}$ (Ab^+) in the diagnostic diagram of Fig. 3.4d. The higher ionization degree at $v_r \approx 7330$ $km\ s^{-1}$ definitely locates Ab^+ in the zone of the nonthermally ionized regions.
Therefore, the [OIII]$\lambda\lambda$4959,5007 line component peaked at $v_r \approx 7330$ $km\ s^{-1}$ is probably being photoionized by an AGN-type non-thermal continuum. We note in addition that a mixture of gas photoionized by thermal and a nonthermal source can account for the observed line ratios of the blue component. The observed [NII]λ6548/Hα and [OIII]λ5007/Hβ ratios can be reproduced assuming that the gas whose ionization source is non-thermal emits a spectrum with [OIII]λ5007/H$\beta\sim$ 5–10, and [NII]λ6583/Hα $\sim$ 1, that the spectrum of the thermally ionized gas is characterized by line ratios [OIII]λ5007/H$\beta\sim$ 1 and [NII]λ6583/H$\alpha\sim$ 0.4, and that the percentage of contribution of the non-thermally ionized gas to the luminosity of the lines is between 10 % - 30 %.

As far as the view suggesting the presence of a mixture of thermally and nonthermally ionized gas is correct, the luminosity in the blue component of the Balmer lines should be essentially due to thermal sources. Assuming that the luminosity of the red component is *entirely* due to nonthermal sources, the *total* (both blue and red component) Balmer line luminosity of the gas whose ionization source is nonthermal, is less ($\lesssim$ 35 %) than that of the gas photoionized by thermal sources.

Table 4

	12 + log(O/H)	log(N/O)	log(S/O)
B	8.86	−1.16	−1.58
B3	8.85	−1.20	−1.52
B4	8.87	−1.15	−1.60
C	8.75	−1.15	−1.61
Adopted Solar	8.82	−1.14	−1.52

The centroids of the profiles along the slit of [OIII]λ5007, of Hβ, and of their nearby continuum are coincident to within the measurement uncertainties (0.2 *arcsec*) in all the spectra. This implies that the maximum of the [OIII]λ5007 and Hβ emission lines originates in a spatially unresolved region
coincident with the optical nucleus. Furthermore, we did not find evidence of displacement in the centroid along the slit of the red and blue component. Henceforth, we suggest that thermally and nonthermally ionized gas is simultaneously present in the nucleus and in the nuclear environment of NGC 7592 W.
Another point of interest is that the width of the lines emitted by the non-thermally ionized gas are comparable to those of the low ionization, blue line components ($\lesssim$ 180 $km\ s^{-1}$).
The definition of a local standard of rest from the emission lines of the Seyfert nucleus is not clear: we suggest that the Narrow Line Regions (NLR) of the active nucleus should be associated to the high-ionization gas revealed at $v_r \approx 7330 km\ s^{-1}$, the value reported in Table 1. Although we can only guess that the [OIII]$\lambda\lambda$4959,5007 peak at $v_r \approx 7330\ km\ s^{-1}$is due to an
additional, nonthermal component, it is difficult to think that the NLR is be associated with the red component which is redshifted by $\approx 200\ km\ s^{-1}$ with respect to the radial velocity of the galaxy, $v_r \approx 7280\ km\ s^{-1}$(*e.g.* Wilson and Heckman, 1985). The radial velocity $v_r \approx 7280\ km\ s^{-1}$ is appropriate as the systemic velocity of the underlying galaxy, since it does probably not suffer from the peculiar motions that could take place in the NLR.

The ambiguity in the definition of the local standard of rest based on the NLR could be responsible for the large differences for the red-shift values reported in literature. The v_r value found by us is significantly different from that given by Arkhipova *et al.* (1981), ≈ 7400 $km\ s^{-1}$. The agreement is not satisfactory also with the value $v_r = 7255$ $km\ s^{-1}$ found by Dahari (1985). The lower resolution (≈ 13 Å) of Dahari's spectra did not allow to separate the blue and red line components, thus probably shifting the line center toward the stronger, blue, low ionization component.

3.4.2 Geometry of the encounter and dynamical masses

The detection of the plume toward west revealed on NGC 7592 S, and the distortion in the arc of condensations in the south of NGC 7592 B add suggest that NGC 7592 S is indeed a third galaxy physically interacting with NGC 7592 W and E.
In order to gain further clues to the geometry of the system, we need to actually explain the two extensions seen on NGC 7592 W as origins of two spiral arms. If spiral arms are trailing, NGC 7592 W should rotate clock-wise, and since in the western part of the galaxy the gas is receding the observer (see Fig. 3.6a), it follows that the wing is in foreground with respect to the galactic bulge. In this case, NGC 7592 W can be described as a rather unperturbed galaxy, probably of morphological type Sa, located behind NGC 7592 E and whose southern spiral arm is hidden by the galactic body of NGC 7592 E. Identification of a spiral structure in NGC 7592 E is hampered by the perturbed morphology of this galaxy. It is not possible to state with reliability whether the arc of condensations described in section 3.1 can be assimilated to a spiral arm. Another possibility would be to consider it as the remnant of a ringed structure. However, if the interpretation of the morphology of NGC 7592 W is correct, the south-eastern part of NGC 7592 E should be closer to the observer than the north-western edge. In this case, the radial velocity curve at P.A.=100° allows to state that gas in the contact region between NGC 7592 E and W rotates in opposite directions.
We have pointed out earlier that it is difficult to unambiguously define a standard of rest for NGC 7592 A, but that the radial velocity deduced from the blue component of the low-ionization lines, $v_r \approx 7280$ $km\ s^{-1}$is probably related to the underlying galaxy. The radial velocity of the nucleus of NGC 7592 B slightly exceeds that of NGC 7592 A, by $\Delta v_r \approx 40$ $km\ s^{-1}$. Henceforth, the orbital motion of NGC 7592 W appears to be in the same sense of the rotational motion of NGC 7592 E, suggesting that a prograde encounter is taking place. The inclination of NGC 7592 E can be computed from the ellipticity of the arc of condensation. We estimated i$\approx$ 44°. The position angle of the nodal line ϕ can be estimated with good accuracy by the comparison of the radial velocities observed at P.A.= 32° and P.A.= 100°. Following the procedure of Burbidge, Burbidge and Prendergast (1960), we obtained $\phi \approx 91°$. The rotational velocity v_{rot} is thus ≈ 270 $km\ s^{-1}$ at a deprojected distance from B $d \approx 3.0$ $h^{-1}kpc$. The value of the rotational velocity is typical of galaxies of morphological type Sa/Sab (*e.g.* Rubin *et al.*, 1984). We estimated the mass contained within this radius M(R) = G^{-1} R v^2_{rot}(R) $\approx 5.0 \times 10^{10}$ $M_\odot$. It is very difficult to get a reliable estimate of the

inclination of NGC 7592 W, but the general appearance suggests that it is seen rather face-on. Conversion to true rotational velocity (and hence mass estimate of NGC 7592 W using the dynamical method) for the radial velocities observed on the western side of A is hampered by the large uncertainty in the inclination estimate, and by the lack of a certain criterion for evaluating the position angle of the nodal line ϕ. However, we note that on the western side of A, radial velocity increases up to $v_r \approx 150$ $km\ s^{-1}$, suggesting that rotational velocities could be as high as or even higher than for NGC 7592 E. The small size and the intrinsic faintness of the stellar continuum of NGC 7592 S indicates that this component has probably a mass much lower than that of NGC 7592 E and W. An estimate of the mass of NGC 7592 W is anyway possible analyzing the gas motions in the contact region of NGC 7592 E and W.

Between NGC 7592 A and B: infall or outflow?

We have shown that the spatially extended emission line gas in the region between the nuclei of NGC 7592 E and W, and in the nucleus of NGC 7592 A, is made up of two principal components. The blue component is probably emitted in the nuclear and disk star forming regions of the system, with a contribution to the ionization from a nonthermal source. The red component is red-shifted with respect to the systemic velocity of NGC 7592 W and is due to high-excitation gas, photoionized by a nonthermal source (see section 3.2).

It appears that the motions of the red component can not be readily explained in terms of rotation. The geometry of the system NGC 7592 could indicate that the gas receding the observer, emitting the red component, is moving toward NGC 7592 W, located behind NGC 7592 E. An alternative hypothesis is that the gas is outflowing from NGC 7592 A. In this case, we should be able to see gas moving on the far side of NGC 7592 W, regardless of the geometry of the system. One has moreover to explain why the gas seems to converge to the radial velocity of the low ionization gas, in correspondence of B, and to find a suitable mechanism for matter ejection up to a projected distance of ~ 5 h^{-1} kpc. Both circumstances seem to be rather unlikely. In addition, the blue component suffers a stronger reddening (E(B–V) ≈ 0.24) than the red one (which is nearly unreddened). This further indicates that the gas emitting the red component is probably located in foreground with respect to the gas emitting the blue component. Thus we believe that the most reasonable assumption is that the gas emitting the red component is infalling toward NGC 7592 A.

Under this assumption, we can compute the mass of the attracting galaxy. The maximum radial velocity with respect to the Seyfert nucleus is $v_r \approx 200$ $km\ s^{-1}$, and it is reached at a (projected) distance of ≈ 500 pc. Applying a correction factor for the projected velocity $\sin i \approx \sqrt{2}/2$, we obtain a lower limit to the mass of NGC 7592 W, $M \approx 4.8\times\ 10^9\ M_\odot$.

3.4.3 Star formation

A comparison of the Hα luminosity of the emitting regions of NGC 7592 with the Hα luminosity function for starburst galactic nuclei published by Kennicutt *et al.* (1989) shows that the Hα luminosity of B and C are typical of this class of objects and that they would be extremely high for disk HII regions. The Hα luminosity of Ab, although lower than that of B by a factor ~ 2, is still common among starburst nuclei. The Hα luminosity of the extranuclear regions (Tab. 2) are also located on the high-luminosity tail of the Hα luminosity function for disk HII regions of Kennicutt *et al.* (1989).

The star formation rate (SFR) can be computed from the reddening corrected Hα luminosity, with a suitable choice of the Initial Mass Function (IMF). Adopting an extended Miller-Scalo IMF, where $\Psi(M) \propto M^{-1.4}$ for 0.1 $M_\odot$ < M < 1 $M_\odot$ and $\Psi(M) \propto M^{-2.5}$ for 1 $M_\odot$ < M < 100 $M_\odot$, and following Kennicutt (1983) we obtain the results reported in Table 3 for the high mass (M > 10 $M_\odot$) SFR, and for the total SFR. For NGC 7592 A, we compute the SFR taking the thermal contribution of the Hα luminosity, which corresponds, as an upper limit, to the Hα luminosity of Ab, about 3/4 of the total Hα luminosity. SFR per unit of projected area (SFR/area) has the largest values in NGC 7592 E in correspondence of the nucleus B, according to the finding that SFR/area is usually larger in the nuclear regions than in the circumnuclear and disk regions (Bushouse, 1987). It is interesting to note that this is not true for the thermal contribution in NGC 7592 A, whose lower limit to the SFR/area is comparable to that of A1, which is probably made up by unresolved disk HII regions. Far infrared fluxes (between 25μm and 100 μm) of the whole system allow an independent estimate of the SFR. NGC 7592 is known as an IRAS source, whose SFR appears to be very high also among interacting galaxies (Bushouse, 1987), being SFR $\approx 21\ M_\odot \mathrm{yr}^{-1}$. This value is much larger than the values found employing the reddening-corrected emission line luminosity ($\approx 5.7\ M_\odot yr^{-1}$). The discrepancy arises probably because the latter values refer only to the area covered by the spectrograph slit, while IRAS fluxes are to be referred to the whole system, whose angular extension is much smaller than the slit aperture of IRAS. We therefore refined the computation of the SFR from the Hα luminosity assuming that the star formation is spread over the areas of high surface brightness of the system. We used as SFR/area in NGC 7592 E the values computed from the SFR/area of B1 and B3 (namely $\approx 3.0\times10^{-7}$ $M_\odot$ $\mathrm{yr}^{-1}pc^{-2}$), assuming that they are valid over the region encircled by the arc of condensations, with the exception of B. Similarly, we computed the SFR/area for NGC 7592 W from region A1, ($\approx 3.8\times 10^{-7}$ $M_\odot$ $\mathrm{yr}^{-1}pc^{-2}$) and then used this value to estimate the total SFR of the galaxy over a region of radius $\approx 1.5kpc$ centered on A (A excluded). Values for A and C have been separately added. In this way, we derived a value of the total SFR ($\approx 20\ M_\odot \mathrm{yr}^{-1}$) which is in very good agreement with the value deduced from the IRAS data. It is interesting to compute the age over which the Starburst phase can be sustained at the present SFR, *e.g.* the time needed to completely exhaust the gas reservoir of the galaxy. The total HI mass of NGC 7592 is $M_{HI} \approx 3.85 \times 10^9\ h^{-2}\ M_\odot$ (Bushouse, 1987). The gas masses were obtained by multiplying the total HI mass by a factor

2.0 to account for Helium and molecular gas and by 1.25 to account for recycled gas, following Larson, Tinsley and Caldwell (1980). Assuming that the SFR for the whole system is $\approx$ 20 $M_{\odot}\mathrm{yr}^{-1}$, we computed a value for the depletion time scale $\approx 1.9 \times 10^8$ yr. This value (only approximately 10 life-times of an O–B star, $t_{OB} \sim 2{\times}10^7$ yr) underlines the temporary character of the star formation events occurring in NGC 7592.

3.4.4 Chemical composition

Emission line fluxes were corrected for internal reddening according to the color excess E(B–V) tabulated in Table 3. We then employed the extragalactic HII regions abundance sequence build by Dopita and Evans (1986), and the method recommended by these authors for computing the abundance of oxygen, nitrogen and sulfur. Computation of the elemental abundance has been limited to the regions B, B3, B4, C, for which reliable [OII]$\lambda\lambda$3726,3729 fluxes are available. The method of Dopita and Evans (1986) could not be applied in region A, for which the contribution of the non-thermally ionized gas can be separated in all the relevant lines but not for the [OII]$\lambda\lambda$3726,3729 doublet. Results are reported in Table 4. The oxygen abundance of the B, B3 and B4 regions are the same to within the uncertainties, and approximately 15 % larger than the solar values. Conversely, the oxygen abundance for the C region is significantly lower, namely $\approx$ 10 % below the solar values. Nitrogen and sulfur abundances relative to oxygen are not different from the solar value, within the uncertainties.

3.4.5 The nature of the semi-broad component of [OIII]$\lambda\lambda$ 4959,5007

Recent work outlines that red asymmetries are indeed present in the [OIII]$\lambda\lambda$4959,5007 lines, although at present the percentage of known object showing a blue asymmetry is higher (Busko and Steiner, 1989). This view is clearly different from that of a few years ago, when it was commonly believed that red asymmetries had never been observed (*e.g.* Wilson and Heckman, 1985). The strong red asymmetry found in the [OIII]$\lambda\lambda$4959,5007 lines
of NGC 7592 A is not a unique feature, although it is not common. The asymmetry index, defined following Whittle (1985), is $A.I. = -0.3$, and would place the profile at the limit of the asymmetry index distribution for the [OIII] lines in the sample of Busko and Steiner (1989). There is one object (at least) showing an [OIII] line profile very similar to that observed on NGC 7592 W, namely NGC 4388 (Iye and Ulrich, 1986). In the previous sections we have outlined the evidence suggesting that the red component of NGC 7592 W is due to gas ultimately infalling toward NGC 7592 A. Since the radial velocity and the ionization degree (*e.g.* the [OIII]λ5007/ Hβ ratio) appear to increase steadily approaching the Seyfert nucleus, it is plausible that the semi-broad component could be also due to gas in-falling toward the central core of the galaxy. Although we can not prove this suggestion, we can show that the ionization source can be provided

by the Seyfert nucleus itself, and that the increase of the ionization degree is consistent with the gas experiencing a stronger photoionization because of its location closer to the Seyfert nucleus. Emission of the semi-broad component is not spatially resolved, so that it should arise in a region contained within approximately $\pm$ 180 pc from the very center of NGC 7592 W. Moreover, we are able to estimate a lower limit to the ratio [OIII]λ5007/H$\beta \gtrsim$ 5 taking the intensity ratio at $\Delta v_r \approx 450$ $km\ s^{-1}$from the blue peak of the [OIII]λ5007 line, where the emission in [OIII]λ5007 begins to be due only to the semi-broad component. The analysis of section 3.2 suggests that the heating mechanism of the gas emitting the semibroad component is provided by a nonthermal source. In the following, we further suggest that the emitting gas is able to see the ionizing continuum from the Seyfert nucleus, and that the ionization degree should be higher in comparison to that of the gas emitting the red component. Under the assumption of photoionization, the ratio [OIII]λ5007/Hβ is sensitive, for a fixed metallicity, mainly to the ionization parameter $\Gamma = Q(H)/4\pi R^2 n_e c$, where R is the distance from the photoionizing source, and Q(H) is the number of ionizing photons. In order to compute Γ, Q(H) can be estimated from the reddening corrected value of the Hα luminosity, taking the non-thermal contribution ($\approx$ 25 % of the total line luminosity). It results that $Q(H)_A \sim 1.0\times10^{52}\ h^{-2} photon\ s^{-1}$. Then, a lower limit to Γ is $\approx 1.5\times10^{-4}$, if the gas is located at $R \approx 200pc$ from the central source. Ferland and Netzer (1983) computed the dependence upon Γ of several line ratios. According to their diagrams, a ratio [OIII]λ5007/H$\beta \approx$ 5 implies a value of the ionization parameter of $\approx 3.5 \times 10^{-4}$, in the case of solar metallicity. This value of Γ is comparable with that computed directly, suggesting that the nucleus can be the ionization source for the semibroad line region. The FWZI of the semibroad component allows the computation of the central mass, $M_c = R_{min} v^2_{max}/\ 2\ G$, where R_{min} is the minimum distance reached from the Seyfert nucleus. Since $v_{max} \approx 1200\ km\ s^{-1}$, $M_c \approx 1.74\times\ 10^8\ R_{min}(pc)\ M_\odot$. Since the ionization parameter could be as high as $\sim 10^{-3}$–10^{-2}, but the density can not greatly exceed the critical density for the [OIII]$\lambda\lambda$4959,5007 lines, we can assume that $\Gamma n_e \sim 10^{4.5} - 10^{3.5}$. Hence, $R_{min} = [Q(H)/4\pi c(\Gamma n_e)]^{1/2} \sim 0.37$–$1.2\ pc$. The central mass is thus $M_c \sim 6.5\times10^7 - 2.1\times10^8\ M_\odot$, a reasonable value for Seyfert galaxies.

3.5 Implications of NGC 7592

Interaction is able to trigger star formation in a more *direct* way than nuclear activity, as it seems to be the case from several evidences partly reviewed in the introduction of this Chapter and in Chapter 1. The insurgence of *strong* Seyfert activity in interacting systems could be delayed by the time necessary for the gas to accrete the core, while Starbursts could be produced in earlier stages of interaction. Assuming an attracting mass $\sim 10^{11}\ M_\odot$(a reasonable value for NGC 7592 W), and that gas is located initially at $\approx$ 3.5 kpc from A, a lower limit to the time needed for the gas to reach the Seyfert

nucleus from the vicinity of B is given by the free-fall time (from rest),

$$t_{ff} = \sqrt{\frac{3\pi}{32G\rho}} \approx 1 \times 10^8 yr. \tag{3.1}$$

This is more than the life-time of a generation of O–B stars, $t_{OB} \sim 2{\times}10^7$ yr. The slightly over solar chemical abundances obtained for NGC 7592 E indicate that we are observing a generation of O–B stars later than the first one. We suggest that transfer of matter is taking place between NGC 7592 E and W, in the sense that gas is moving toward the Seyfert galaxy, and it is (possibly) accreting the central core of the nucleus. Since infall and tidal stripping of matter can be actually promoted, further evidence is added that interaction is *physically sufficient mechanism* for triggering nuclear activity. Our analysis has shown that the gas has already reached the Seyfert nucleus while the Starburst is still occurring. This means that interaction is probably able to drive inflow of gas at a wide range of radii, since τ_{ff} is too long compared to the lifetime of a Starburst generation. Rotational period at a few hundred parsecs from the nucleus is $\tau_{dyn} \sim 3 \times 10^7 yr$. If the gas clouds require a few rotational periods to reach the central *parsec* in dissipative flow, then $\tau_{dyn} \gg \tau_{OB}$, and the Starburst and AGN phases should be separated in time (DeRobertis and Shaw, 1988). If interaction can supply enough gas at all radii nearly simultaneously, then one would expect also a simultaneous occurrence of non–thermal activity and Starburst, and this is indeed what we observe. Once the gas has reached a few hundred of *pc* in radius, as effect of radial motions induced for instance by a stellar bar,the gas can become unstable again and, under certain conditions, flow inward until it joins the outer regions of the accretion disk where turbulent viscous process control the angular momentum transport (Shlosman *et al.*, 1989).

In principle, the Starburst could thus not be related to the nuclear activity. DeRobertis and Shaw (1988) emphasized that Starbursts do not seem to be confined in the galactic nuclei, and that they are spread over a *kpc*–sized scale. Since the velocity curves of these galaxies are consistent with a normal rotational velocity field of spirals, they argue that the Starburst is rotationally supported, so that collapse of a large mass in the nucleus of a Starburst galaxy cannot take place. Extensive star formation in the disk may diminish the flow of gas able to reach the nucleus (Olson and Kwan, 1990). However, as far as the *nuclear* Starburst is concerned, there is no theoretical reason to avoid collapse of gas and stars, due to the deep gravitational well and the high viscosity of the gas (Bailey, 1980; Norman and Scoville, 1988).

We have found evidence in NGC 7592 A of a nuclear starburst occurring simultaneously with Seyfert type activity. This is not an unique case among Seyfert galaxies: NGC 7469, studied by Wilson *et al.* (1986), also shows a nuclear starburst in addition to Seyfert characteristics. In this and in other known cases (Chapter 1) the luminosity of the Seyfert component usually overswamps the luminosity of the nuclear starburst. An interesting feature of NGC 7592 is that the emission line luminosity of the nuclear starburst in A is apparently much larger than that due to the Seyfert type activity, $\approx$ 75 % of the total Hα line luminosity. It is moreover interesting to note that the

high ionization gas responsible for the Seyfert character of the line spectrum shows line widths comparable to those of the low ionization HII-gas. The width of the single [OIII]$\lambda\lambda$4959,5007 line components is probably less than 100 $km\ s^{-1}$, which is an extremely low value for Seyferts, but which is common among Starbursts. We note moreover the star formation rate per unit area in the Seyfert nucleus is less than that deduced for A1, unlike the case of *truly* starbursting and interacting system, for which the SFR/area is strongly peaked near to the center of the galaxy (Bushouse, 1987), as is the case of NGC 7592 E. This may suggest that the Seyfert activity could arise from the same conditions from which the Starburst phenomenon is formed, and may indicate that the insurgence of the non–thermal activity is related to the fading of the nuclear SFR. These lines of evidence confirm the possibility of a direct connection between the Starburst and the non–thermal activity.

The evolution of a nuclear Starburst is unclear. Weedman (1983) proposed that the remnants of high mass evolution (white dwarf, low mass black hole), can concentrate in a small nuclear volume, and eventually act as separate accretors leading to an AGN phase. An important prediction is that the AGN phase should follow the Starburst after $\sim 10^8\ yr$, which is not the case of of NGC 7592. Another hypothesis is that supernova blasts would lead to an outflowing wind, which in turn would let starve any central black hole (*e.g.* Heckman *et al.*, 1987). Outflowing *bubbles* are indeed observed in several Starburst galaxies. However, the case of NGC 7592 demonstrate that Starburst and AGN can co–exist, and hence that outflowing winds may become perhaps more important in later stages.

If a black hole of $\gtrsim 10^8\ M_\odot$ was already present, the strong mass loss of the coeval cluster produced by the Starburst (which will return to the interstellar medium nearly 1/4 of the cluster mass in $\sim 10^8 yr$; the accretion may take place at a rate 1 $M_\odot\ yr^{-1}$ if a cluster of $10^8\ M_\odot$in the innermost few pc is considered, Norman and Scoville (1988)), could probably give rise to a strong *flare* ($L \sim 10^{45}\ erg\ s^{-1}$) of duration $\sim 10^8 yr$. In this case the luminosity of the AGN would had to become much larger than the Starburst in a very short time scale $\sim 10^7 yr$. We suggest that a massive black hole may be at present *forming* as a direct consequence of the Starburst, and that its mass should be lower than that estimated for powerful Seyfert galaxies.

What seems unlikely is that a large mass concentration is being collected at the very center of NGC 7592 A in rather short times $\sim 10^8\ yr$. The reddening corrected luminosity of the thermal component of NGC 7592 A is $4.1\times10^{40}\ \ erg\ s^{-1}$(Table 3). The mass produced is $M \sim 10^7 (S.F.R) t_7$, where t_7 is the duration of the starburst in units of $10^7 yr$. We have estimated earlier that the maximum duration of the Starburst should be $2\times10^8 yr$. If the present SFR is sustained over this time, the mass production would be $M_{HI} \sim 1\times10^7\ M_\odot$ and $M_{tot} \sim 7\times10^7\ M_\odot$. We believe that the estimate of the masses in NGC 7592 A poses some problems to the models requiring the existence of very massive ($\sim 10^{10}\ M_\odot$) and dense clusters of stars in order to feed the AGN (*e.g.* Norman and Scoville, 1988). There is no evidence of a very large mass concentration in the core of NGC 7592 W, the dynamical mass being $M_c \lesssim 2\times10^8\ M_\odot$. Thus, the total mass at the end of the Starburst should be around $3\cdot10^8\ M_\odot$.

Concluding, the simplest view emerging from this view is perhaps that a central (not too massive) black hole is accreting matter directly channeled to the core of the nucleus via a bar–like instability. Several lines of evidence suggest however that the AGN is *closely* mixed with the Starburst component. The dynamical properties of this extremely interesting system could be responsible for the ongoing exchange of matter and for the location and intensity of the star formation events. NGC 7592 E and NGC 7592 W are undergoing a prograde encounter. If NGC 7592 S is indeed a third galactic body, it most probably experienced a star formation history different from NGC 7592 E and W, since the O/H ratio is less than solar and significantly different from that of NGC 7592 E. The fact that probably three galaxies are present in the system, that they are nearly equidistant from each other, and that the mass of the two main components are similar and much larger than that of the third allows to draw an analogy with the restricted three body problem. This could be a good premise for a complete theoretical modelling able to explain the morphological peculiarities and the ongoing transfer of matter.
In Chapter 4, we will find some evidence against models which do not suppose the existence of a massive compact object and explain the Seyfert type activity *only* in terms of Star formation.
The second part of this thesis, which begins with the next Chapter, will be mainly devoted to search – on the basis of emission line profiles – for a signature of the accretion disks around massive black holes in AGN.

This Chapter has been based on the following work:

1. P. Rafanelli, P. Marziani, *The complex nature of the interacting system NGC 7592*, *Astronomical Journal*, *in press*

Chapter 4

Line Emission from Accretion Disks

Abstract – The possibility that the Balmer lines are emitted by accretion disks is investigated considering at first AGN with very broad and peculiar emission line profiles. We analyze in detail the case of Akn 120, considered one of the most likely candidate for disk emission. Constraints to the disk illumination model are set if the disk emission is switched on *in the high luminosity phase of this object (Alloin et al., 1988). Then, a comparison is made between the predictions of the disk models and the largest available sample of line profile parameters. The comparison, made at three different profile heights, shows little agreement with the theoretical predictions. The models imply that all or most profile asymmetries will be red (i.e. excess of emission on the long wavelength side of the profile). In fact, many blue asymmetries are observed. Perhaps the most significant conclusion from the comparison is that the disk must not be the dominant source of line radiation in most AGN (or be almost heavily obscured). The data suggest that the remarkable agreement between theory and observations for Arp 102b is probably an example of a very rare class of AGN with the* entire *low ionization broad line emission arising directly from the accretion disk. We propose a parametric scheme which extends the one suggested by Sulentic (1989) and which can in principle reveal whether a disk contribution is masked from an additional emission component.*

4.1 Introduction

In the past few years attention has been given to the idea that an accretion disk around a supermassive black hole could be responsible for the broad Balmer line emission in some Seyfert 1 and Broad Line Radio Galaxies (BLRG). The outer regions of hypothesized disks are probably at a distance from the central source, estimated for the broad line region (BLR), $d \sim 1$ *light month*. The theoretical work of Dumont and Collin-Souffrin (1990a,b) further suggests that the outer regions of the disk are at conditions suitable for the emission of the low ionization lines (LILs, comprising HI Balmer lines, FeII, Mg IIλ2798). In this view the High Ionization Lines (HIL: CIV]λ1549, CIII]λ1909)

arise from clouds ($n_e \lesssim 10^9 cm^{-3}$) directly illuminated by a UV and soft X–ray continuum, while the LIL arise, most likely, from a disk ($n_e \gtrsim 10^{11} cm^{-3}$) illuminated by backscattered hard X–ray radiation. As outlined in Chapter 1, this model is attractive for reasons other than providing an explanation for the kinematic difference between HIL and LIL:

1. it provides an high density ($n_e \gtrsim 10^{12} cm^{-3}$) environment which may account for the strong Fe II LIL features often observed (Collin Souffrin *et al.*, 1980; Collin–Souffrin and Dumont, 1989), and

2. it may solve the energy budget problem.

Systemic blueshifts ($\lesssim 10^3$ $km\ s^{-1}$) of the BLR HIL with respect to the BLR LIL, in the same object (Gaskell, 1982; 1985), has been interpreted as evidence in support of a disk origin of the LIL emission (Collin– Souffrin *et al.*, 1980; Collin–Souffrin, 1987). The radio objects in the Sulentic (1989) sample generally support this correlation in the sense that relatively narrow symmetric profiles tend to be radio core dominated sources, and broader asymmetric type profiles are the opposite. There is however no general correlation between FWHM(Hβ) and profile type in that sample.
Further support for the idea that we are observing disk LIL emission (at least in radio QSOs) comes from a possible correlation between the FWHM of Hβ and the ratio of core–to–extended component flux density at 5 GHz (Wills and Browne, 1986). If one assumes that LIL emission line gas is confined in a plane perpendicular to the radio axis, such a correlation arises quite naturally from a relativistic beaming model.
The Balmer line profiles of Arp 102b (Chen *et al.*, 1989), and 3C332 (Halpern, 1991) are a good match to models where the emission originate from an accretion disk for which relativistic effects are non negligible (§ 4.2.2). An analysis of the profile variations in Akn 120 (Alloin *et al.*, 1988), NGC 5548 and NGC 3783 (Stirpe *et al.*, 1988) indicate that the Broad Line Region (BLR) in these galaxies is made up of at least two parts, one of which emits a double– peaked contribution to the Balmer lines, as expected from a disk-like structure. It is not clear whether the same considerations can be applied to other objects, since the expected profiles of lines emitted by a rotating disk cannot readily explain the generality of observed profile shifts and asymmetries (Sulentic *et al.*, 1990; see § 4.4.1). Seyfert 1 and broad line radio galaxies (BLRG) are good prospects for finding further candidates for line emitting disks, especially when they show irregular and very broad Balmer line profiles. We are carrying out a spectroscopic survey of these objects aimed to obtain high resolution and intermediate ($\approx 2 - 4$ Å FWHM), high S/N spectra of these objects. This survey has a twofold utility, since:

1. analysis of the profiles and profile variations may be useful for understanding gas kinematics in the BLR (although it is generally suggested that radial motions are dominant, it is yet unclear whether infall or outflow is taking place);

2. they could provide additional support for and, possibly, constraints on models for the central source in AGN. The most widely accepted model (i.e. accretion

in a disk around a supermassive black hole) has observational support until now limited to the existence of the so-called Big Bump (see Chapter 1).

It is remarkable that the study of emission line profiles is in principle a powerful tool for testing the presence of the accretion disk. The keplerian velocity field of the gas allows to formulate *strong* predictions for the shape and variations of emission line profiles, and hence a comparison between observations and theory can be less ambiguous than in other cases. In this Chapter we present at first our results and a discussion extended to data available in the literature of several Seyfert 1, BLRG and one low redshift quasar with very broad or irregular Balmer line profiles. In the second part, we present a comparison between the predictions of the disk models and the largest available sample of line profile parameters.

4.2 Double horned profiles

As outlined in the previous section, good prospect for finding further evidence of line emitting disks are Sey–1 and BLRG with the broadest and most irregular Balmer line profiles. We think that the study (currently underway) of small groups of objects with peculiar and variable profiles (as is the case for Akn 120 and IC 4329a; 3C 390.3 and 3C 382; Arp 102b and 3C 332 and some others) may help to settle some fundamental questions concerning the BLR and the nature of the central engine, at least whether a unique geometrical model is able to explain the BLR, or whether one should expect the presence of different geometries in different object classes. The importance of studying objects with very similar profiles stems from the possibility that they have similar kinematics/geometry/orientation to the line of sight. Detailed study may lead to the discovery of other similarities (or differences) in key parameters related to the physical conditions in the BLR. It could provide a starting point for the search for global correlations between various AGN parameters and profile classes.
We present and discuss extensively our results on OQ 208, Akn 120, IC 4239a and a brief outline of the results on Arp 102b, 3C332, 3C390.3, 3C382, OX 169, NGC 5548. For each object basically the same mechanisms will be discussed – emission from disk, binary BLR, biconical BLR. We will exclude at first that the substructures observed in the line profiles are due to transient light–echoes, since the substructures are long lasting ($\gtrsim$ 10 yr) in comparison with the light travel time for the BLR.

4.2.1 Observations

The Journal of spectroscopic observations is reported in Table 1.
3C 390.3 (1845+79), 3C382 (1833+32), Arp 102b (1717+49), and NGC 5548 (1415+25) were observed at the 1.82m telescope of the Asiago Observatory, equipped with a Boller and Chivens spectrograph. We employed a $600/gr/mm$ grating which yielded a dispersion $\approx$ 120Å$/mm$, and a spectral resolution $\approx$ 3.5 Å FWHM. The detector was a Thomson CCD (pixel size $23\mu m \times 23\mu m$, which allowed the coverage of $\approx$ 1100

Å. Spectral ranges were approximately centered on Hα and Hβ and are quoted in the Journal of Observations.
IC 4329a (1346–3003), Akn 120 (0513–0012), OQ 208 (1404+28) and OX 169 (2141+17) were observed with the 1.52 m ESO telescope at La Silla. It was equipped with a Boller and Chivens spectrograph and a high resolution (pixel size $15\mu \times 15\mu$) RCA CCD detector. The slit width employed was ≈ 2 *arcsec* during all nights of observation. The dispersion used were (1) 67 Å/mm, allowing a spectral resolution of ≈ 1.8 Å FWHM (the spectral ranges covered were 6400–7400 Å and 4650–5550 Å). (2) 120 Å/mm, yielding a spectral resolution of ≈ 3.5 Å FWHM. Recorded spectral ranges were 5440–7380 Å and 3550–5450 Å.
A spectrum of OQ 208 was collected on Feb. 19, 1991 with the 2.1 *m* telescope at Kitt Peak National Observatory (KPNO).
Spectra were bias subtracted, flat-field corrected and wavelength calibrated using a third order polynomial on unblended emission lines in a FeAr (Asiago) and HeAr (ESO) comparison source recorded after each observation. The rms was always less than 0.1 Å. Flux calibration was obtained from nightly observations of a standard star from the list of Stone (1977). Fluxes are believed to be accurate within $\pm$ 15 % (ESO and KPNO) and $\pm$30 % (Asiago).

4.2.2 Arp 102B and 3C332

The suggestion that an accretion disk around a supermassive black hole could produce the Broad Balmer lines is some Seyfert 1 and Broad Line Radio Galaxies (BLRG) has found observational support mainly in the good match between the line profiles of Arp 102b and 3C332 and the model prediction. The weak BLRG Arp 102b has been already quoted as an example of a galaxy *stripping* gas from a gas rich companion (de Robertis, 1985). The Hα profile is shown in Fig. 4.1.

Chen and Halpern (1989) were able to fit in a spectacular way the broad Hα profile of Arp 102b employing a relativistic disk model with $R_{in} = 175R_g$, $R_{out} = 500R_g$, $i = 32°$, with a power law emissivity of spectral index $q = 3.2$, and with a local broadening (due to electron scattering) $\nu = 850\ km\ s^{-1}$. The enhancement of the blue peak and the slight red displacement of the line basis due to gravitational plus transverse redshift are accounted for in a quantitative way.
3C332 is a faint ($m_{V} \simeq 16.5$) BLRG. The Hα profile of 3C332 is very similar to that of Arp 102b, although somewhat broader. A smaller disk is required: a detailed fit (Halpern, 1991) yields $R_{in} \simeq 88$ and $R_{out} \simeq 260R_g$, and the same considerations made by Chen *et al.*(1989) on Arp 102b apply to 3C332 as well.
The remarkable stability of the peak wavelengths rules out the suggestion that the double peaked structure is due to a *binary BLR* for Arp 102b, as suggested at a first instance, unless the central masses have unplausibly large values (Halpern and Filippenko, 1988; Gaskell (1988). The interpretation of the Balmer lines arising in a relativistic disk has been questioned by Miller and Peterson (1991). A spectrum obtained in 1982 shows a profile different from those published by Chen *et al.*(1989):

Journal of observations

Object	Date	U.T.	*Exp. Time*	Tel.	Disp. Å/*mm*	Sp.Range Å
3C390.3	Jul. 6, 1988	0^h34^m	50^m	1.82*m* As.	120	6050–7200
	Jul. 7, 1988	23^h23^m	50^m	1.82*m* As.	120	4260–5420
3C382	Jul. 7, 1988	0^h23^m	43^m	1.82*m* As.	120	6050–7200
	Jul. 8, 1988	0^h39^m	50^m	1.82*m* As.	120	4260–5420
Arp 102b	Mar 25, 1989	2^h00^m	50^m	1.82*m* As.	120	5850–7000
		3^h02^m	50^m	1.82*m* As.	120	5850–7000
	Mar. 26, 1989	2^h32^m	35^m	1.82*m* As.	120	5850–7000
	Mar. 27, 1989	3^h19^m	50^m	1.82*m* As.	120	4750–5900
NGC 5548	Mar. 24, 1989	2^h54^m	35^m	1.82*m* As.	120	5850–7000
	Mar. 27, 1989	1^h02^m	50^m	1.82*m* As.	120	4750–5900
Akn 120	Sep. 26, 1989	8^h51^m	50^m	1.52*m* ESO	120	6250–7250
	Sep. 27, 1989	8^h48^m	40^m	1.52*m* ESO	60	4600–5600
	Sep. 29, 1990	9^h23^m	15^m	1.52*m* ESO	120	6380–8330
	Apr. 1, 1990	23^h48^m	40^m	1.52*m* ESO	60	6250–7250
	Apr. 2, 1990	23^h43^m	50^m	1.52*m* ESO	60	4510–5510
	Apr. 3, 1990	23^h30^m	30^m	1.52*m* ESO	120	3550–5450
	Apr. 4, 1990	23^h48^m	40^m	1.52*m* ESO	60	5450–7350
IC 4329a	Apr. 2, 1990	7^h18^m	50^m	1.52*m* ESO	60	6250–7250
	Apr. 3, 1990	7^h47^m	60^m	1.52*m* ESO	60	4510–5510
	Apr. 4, 1990			1.52*m* ESO	120	3550–5450
	Apr. 5, 1990	4^h48^m	50^m	1.52*m* ESO	120	5450–7350
OX 169	Sep. 28, 1989	1^h57^m	60^m	1.52*m* ESO	120	5400–7300
OQ 208	Apr 4, 1990	6^h32^m	50^m	1.52*m* ESO	120	5450–7350
	Feb. 19, 1991	11^h26^m	60^m	2.1*m* KPNO	60	4600–5900

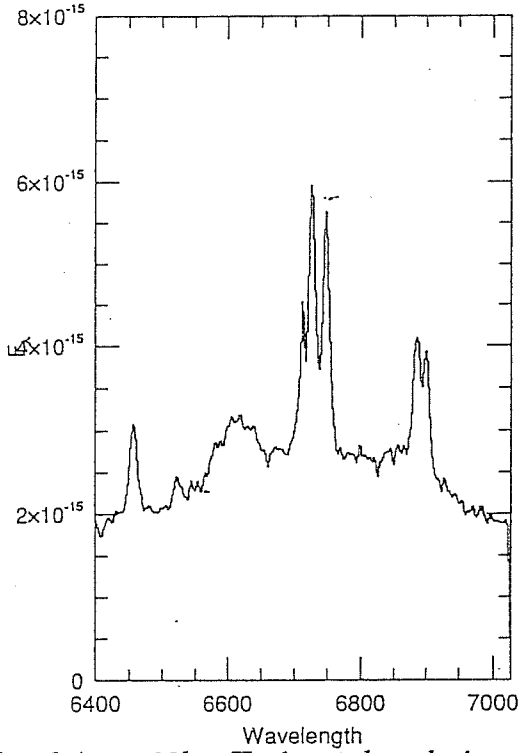

Figure 4.1: *Hα profile of Arp 102b. Horizontal scale is wavelength, vertical scale is specific flux (erg s^{-1} cm^{-2})*

the strength of the red peak at that epoch was a bit stronger, or at least comparable to the blue one. Accepted at face value this result would rule out the disk origin of the Balmer lines in Arp102b, unless an additional probably infalling component is invoked (see the discussion in § 4.2.4 for OQ 208). We suggest however that the change should be confirmed by independent observations, since: 1) the spectrum of Miller and Peterson (1991) is of very low resolution, and the red peak is contaminated by the strong [SII]λλ6717,6731 lines and by the B–band absorption; 2) if radiation is polarized, as expected for disk emission, variation in the peak strength could be due to the dependence on the direction of the polarization vector of the transmission of the spectrograph grating. Recently, Chen and Halpern (1991) have suggested that only a tiny fraction of the flux emerging from a relativistic disk with an atmosphere dominated by electron scattering should be polarized: $\sim$ 0.5 % for the small inclination of the disk in Arp102b. They also predict that the polarized profile should have a red peak stronger than the blue one, the contrary of which is observed in non–polarized light. The percentage of polarization expected from theory is too small to explain a change of $\simeq$ 20 % in the relative strength of the two peak. Another possible mechanism able to affect the relative strength of the peak could be variation in the optical depth for electron scattering.

The disk fitting of Arp 102b and 3C332 suggests that the outer boundaries of the BLR are much closer as expected from standard photoionization models. Results on emission line variability for NGC 4151 confirm that the inner boundary of the BLR is

probably located at $\simeq 350R_g$ (M $= 10^7 M_\odot$). The location of the inner boundary so close to the central black hole raises the problem of the disk illumination. Chen and Halpern (1989) suggested that the emitting region of the disk could be illuminated by hard X ray radiation produced via inverse Compton scattering of IR radiation emitted by an ion torus. These authors pointed out that the energy budget is satisfied only for a limited range for the ratio between the effective radius of the ion torus r_0 and the inner radius of the disk. The covering factor of the disk is inversely proportional to r_{in}/r_0. Chen and Halpern suggest that the disk could not intercept enough flux unless there is a very abrupt transition between the ion torus and the thin disk, that is $r_0/r_{in} \sim 0.5-1$. The important requirement is that any scattering medium – above an internal thick structure – should extend at least near to the inner edge of the accretion disk, as demonstrated in § 4.2.3. For the sake of the energy budget of the BLR, models are favoured if the scattering medium is also *above* the accretion disk (e.g. Stirpe *et al.*, 1988, for NGC 5548).

4.2.3 IC 4329a and Akn 120

Although IC 4329a is a rather bright and nearby Seyfert galaxy, absolute optical spectrophotometry has only been recently published (Morris and Ward 1988; Fricke and Kollatschny 1989). Spectra of IC 4329a were also published by Wilson and Penston (1979). The latter authors did not do accurate spectrophotometry, but pointed out that variations in the emission line fluxes were plausible. This suggestion was later confirmed by Morris and Ward (1988).
We confirm the existence of variations in the Balmer line profiles. We demonstrate that the variation, analyzed using new spectrophotometric data and previously published spectra, is very similar to that seen in the well studied Seyfert 1 galaxy Akn 120. Spectral variability in Akn 120 was first noted by de Bruyn (1980) and Schulz and Rafanelli (1981). Unlike IC 4329A, Akn 120 has been extensively studied in the optical by several authors (*e.g.* Peterson *et al.*, 1983; Alloin *et al.*, 1988). Last, consequences and constraints of our comparison of Akn 120 and IC 4329a on the BLR structure and central source models are discussed.

Results

Line profiles – The profiles of Hβ and Hα are shown in Figures 4.2a,b and 4.2c,d for IC 4329a and Akn 120 respectively. They have very similar shapes and the profiles would *ideally* be classified (assuming the zero peak was an NLR component) as type AB,R (blue asymmetric profile with red displaced peak) in the scheme proposed by Sulentic (1989), see § 4.3. Neither object was included in that study of Hβ profile shape and asymmetry that included 61 AGN. *In fact*, using the definitions for asymmetry and displacement defined in Sulentic (1989), both objects are classified as SR (symmetric and redshifted). Neither the blueshifted peak nor the red asymmetry of the base are strong enough to affect a classification based upon measures at 3/4, 1/2, and 1/4

intensity. The peculiar structure is concentrated in the upper 1/4 of the profile. SR profiles are quite common while AB,R profiles were found to be rare in the Sulentic (1989) study with only one AGN (IZw1) assigned that type. Perhaps an extension of the classification scheme is needed in order to quantify peculiarities of the kind found in Akn 120 and IC 4329a. This would be appropriate when larger samples of (FeII decontaminated) spectra with sufficient resolution and S/N become available. We are restricted for the present to comparisons of the kind presented in this Chapter. The profile similarity between Akn 120 and IC 4329a is very striking, with Hα and Hβ in the two galaxies having nearly identical FWHM $\approx$ 15,000 $km\ s^{-1}$and FWZI $\approx$ 30,000 $km\ s^{-1}$. These values are extremely large for Seyfert 1 galaxies. There was no general trend in profile shape among the very broad profile objects included in the Sulentic (1989) study. A weak blue wing is detected out to –18,000 $km\ s^{-1}$ in Hα (its detection in Hβ is hampered by the presence of FeII and HeIIλ4686 lines on the blue side of that profile). The Hβ profiles clearly show two peaks: 1) a peak or shoulder displaced to the red by $\sim$ 1800 $km\ s^{-1}$(hereafter the *red* peak) and 2) a peak near the redshift of the narrow lines (hereafter the *zero* peak).
Emission line fluxes are presented for IC 4329a and Akn 120 in Table 2. The last rows indicate the heliocentric redshift, the observed Hβ luminosity, the reddening E(B–V), and the reddening corrected Hβ luminosity. We suspect a small ($\Delta v \approx 50\ km\ s^{-1}$) blueshift of the *zero* peak in Hβ relative to the [OIII] lines for IC 4329a (a similar value was derived at a low level of confidence by Wilson and Penston (1979)). Akn 120 shows a much larger ($\Delta v = 300\ km\ s^{-1}$) blueshift of this feature. This result coupled with the greater width of the *zero* peak suggests that it is another BLR component rather than a narrow line (NLR) contribution as had often been assumed. Further support for this interpretation comes from suspected variability in this feature. The NLR redshift is assumed to be the same as the systemic velocity of the host galaxy derived from absorption line measures. The situation for Hα is more confused (due to [NII] emission) but the same general structure appears to be present. The red peak has always (in all published spectra) been less prominent in the Hα line suggesting that the Balmer decrement is less steep for this component.

Emission line variability – A comparison with the spectra published by Wilson and Penston (1979) and with the fluxes published by Morris and Ward (1988) and Fricke and Kollatschny (1989) suggests that the Balmer lines in IC 4329a go through a high and low luminosity phase. Broad line fluxes (Hα and Hβ) decreased in the period of time from June 1975 to June 1977, but they increased again in 1984, when IC 4329a was observed by Fricke and Kollatschny (1989). The observations of Morris and Ward (1988) suggest that the object in 1985 was still in the high phase, but probably fading. Fluxes were considerably lower in 1990, when our observations were made.
Hence, at that time IC 4329a was near to the low phase. Peterson *et al.* (1983) and Alloin *et al.* (1988) previously suggested that it was appropriate to consider a *low* and a *high* luminosity phase for Akn 120. The Hβ flux of Akn 120 changes by a factor of $\approx$ 2–3 on a timescale of several months – one year, in response to changes in the continuum.

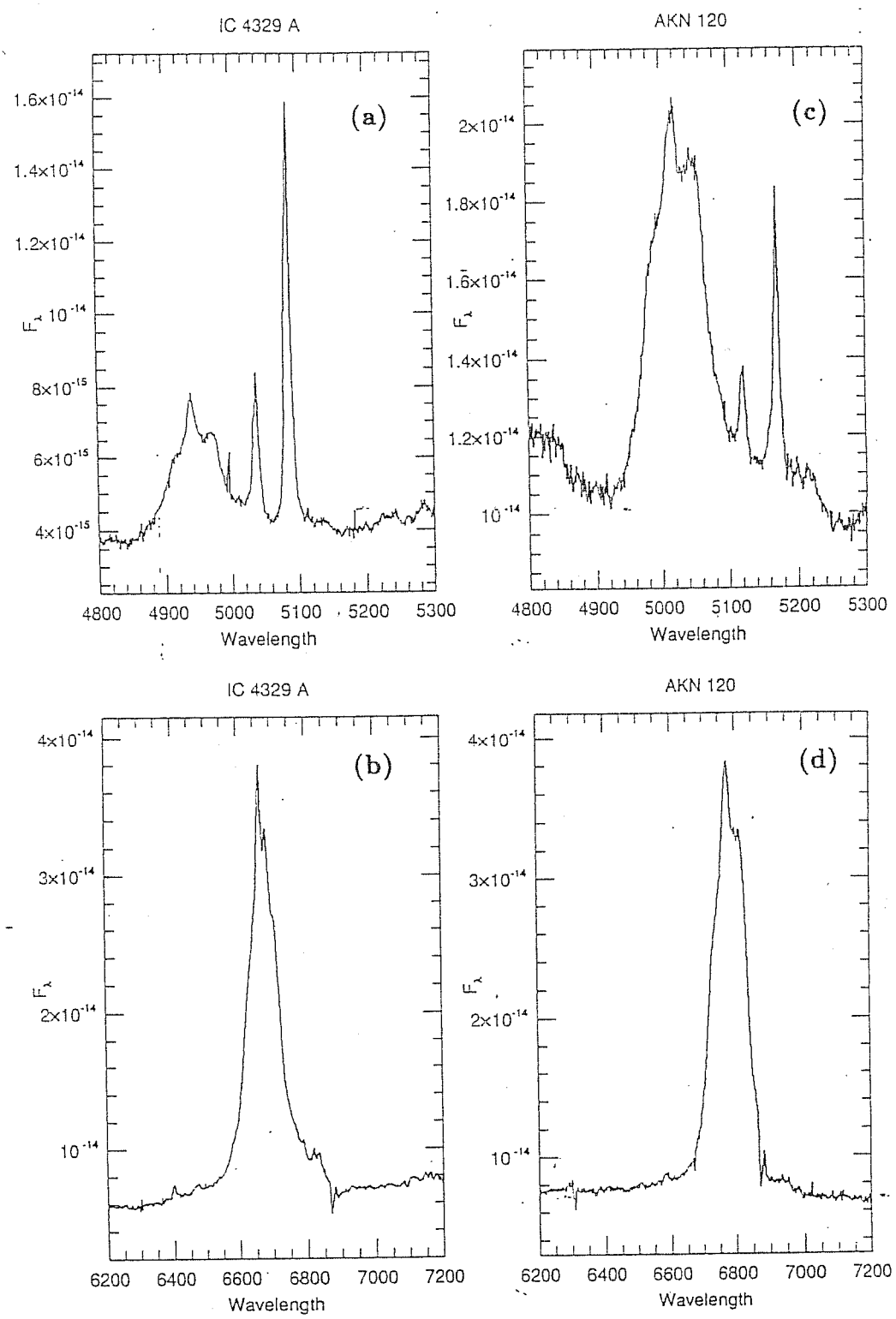

Figure 4.2: *Line profiles of IC 4329a: (a) Hβ, (b) Hα, and of Akn 120: (c) Hβ, (d), Hα. Horizontal and vertical scale is as for Fig. 1*

One gets the impression that the red peak of Hβ in both objects, is more prominent during the high luminosity state but this is difficult to verify quantitatively. If one compresses the bright phase spectrum to the same scale as the low phase one, the similarity remains remarkable. The general shape of the profile does not change significantly as measured by the half width at different levels or the asymmetry index. The tendency for profiles to preserve the same shape during variations was noted in Sulentic (1989). The details of the Hβ profile in Akn 120 show changes. A high S/N spectrum published by Foltz *et al.* (1983), for example shows that the red peak is almost as strong as the zero peak. In the past there was some confusion about the identification of the peaks. The Hβ profile of Akn 120 has even been described as double peaked with displaced red *and* blue components. In only one published spectrum was a blue peak possibly seen (Foltz et al. 1981). The low S/N of this spectrum, lack of confirmatory data and width of the feature make this detection suspect. The so–called *blue* peak has instead been observed as an inflection on the blue side of the Hβ profile. Our spectra for both objects suggest that the blue shoulder is increasing in strength relative to older spectra. The difference spectrum for Akn 120 published by Alloin et al. (1988) is the strongest evidence for an underlying double peak component to the Balmer profiles. Unfortunately a convincing double peaked structure is only seen in the Hα profile. This raises questions about the reality of a distinct double peak component. Hβ is a cleaner feature for generating a difference spectrum and it suggests that the profile retained the same general shape during the variations. Since it is believed that the Balmer decrement in the red component is flatter than for the central emission, the double structure should be more distinct at Hβ. Hα is confused by the presence of the narrow [NII] emission feature in addition to the zero peak. Since the difference spectrum was produced from data taken with different equipment, small difference in resolution could affect the width of the narrow emission components. In addition, if the two spectra were slightly mismatched in wavelength at Hα, a further error in the subtraction might result. It is very difficult to prove that only the shoulders of the Balmer lines are varying in these objects. This is especially true because of the zero peak. It is often assumed to be a true NLR component arising in the same region as the forbidden lines. This impression is reinforced in our spectra because it appears as a distinct component with clear inflection points on both sides. As pointed out earlier, this interpretation is not consistent with the observed width of the zero peak in both objects. It appears distinctly broader than the [OIII] lines: $\gtrsim$ 15 Åcompared to $\sim$ 7 Å at the same fractional intensity. It was also broader than the red peak during the times when this feature rivaled it in intensity. If the zero peak is an independent variable component arising in the BLR, it would make interpretation of the difference spectrum very dangerous.

Multifrequency continuum – The continuum fluxes for IC 4329a and Akn 120 in the range from 20 cm to 10 keV are plotted in Figures 4.3 a and 4.3 b respectively. Data sources are listed in the caption of Figure 4.3. Present data cannot offer a simultaneous view across the continuum, but flux values at different epochs are reported, in order to (at least) illustrate the range in the variations of the ionizing and optical continuum.

We can quantify the level of variation in IC 4329a from EXOSAT spectra where a factor of $\approx 1.6 \sim 2$ is observed in the hard X-ray range (2 keV < E <10 keV). The same observation shows that the flux in the soft X ray range (0.05 < E < 2 keV) did (probably) not vary (Grandi *et al.*, 1991). Akn 120 is also known to be variable by a factor o f ≈ 2 at UV wavelengths (Turner and Pounds, 1989). Perhaps the most striking feature in the IC 4329a continuum is the impressive decrease of the continuum at optical and UV wavelengths. No UV continuum is detected above the noise level in the short wavelength range of IUE, while in the long wavelength range, only faint emission steeply decreasing from 3100 Å to 2800 Å is present. The large extinction in IC 4329a (E(B–V)$\approx$ 0.97 from the Balmer decrement) is most probably due to the near edge on orientation of the galaxy, and thus probably affects in the same way continuum and emission lines. We note in passing that, since the galaxy is seen
nearly edge-on, the value of E(B–V)$\approx$ 1 provides an estimate of the reddening due to the passage of light from the nucleus through one half galactic disk, for a galaxy of morphological type around Sa. The ultraviolet spectrum of Akn 120 is rather typical of Seyfert 1 galaxies, while no emission lines are detected in the IUE spectra of IC 4329a. If we assume an intrinsic ratio of Lyα and CIVλ1459 to Hα comparable to the values for Akn 120, the reddening E(B–V) = 0.97, will reduce the line fluxes below the noise level of the IUE spectra. The strong absorption at UV wavelengths makes it difficult to constrain the *Big Bump*, whose shape in active galaxies is usually inferred from the continuum shape in the (rest) wavelength range 1200-2500 Å.

FeII emission – FeII lines vary appreciably in response to continuum variation, following the same behavior as the Balmer lines. Although FeII lines enhance the red wing of the Hβ profile, they are not responsible for all of its emission: the broad wing persists also when the FeII nearly completely disappears, as is the case at the minimum luminosity phase in IC 4329a. FeII may slightly enhance the red peak, but the expected contribution from multiplets 36 and 42 is not able to account entirely for the feature. Foltz et al. (1983) argue that a broad [OIII]$\lambda\lambda$4959,5007 forbidden line component also contributes to the red shelf. The FeII emission is considerably stronger in Akn 120 than in IC 4329a. The difference in strength of the FeII features is, along with morphology of the host galaxies, one of the most prominent *differences* between the two objects: the ratio FeII(λ5250)/Hβ is $\lesssim 0.20$ for IC 4329a and ≈ 0.33 for Akn 120.

Discussion

The striking similarities between the Balmer line profiles and profile variations in Akn 120 and IC 4329a suggest a similar response to continuum changes by the BLR. This may be an indication that the profiles reflect very similar BLR kinematics/geometry. The similarity of IC 4329a and Akn 120 implies that some kind of *ordered* and *reproducible* phenomenon is taking place in the BLR. It argues against the idea that random motion in an ensemble of clouds is the main source of Doppler line broadening in the BLR. The reproducibility of peculiar emission line profiles poses difficulties for the idea that several independently accreting objects can account for the properties of the

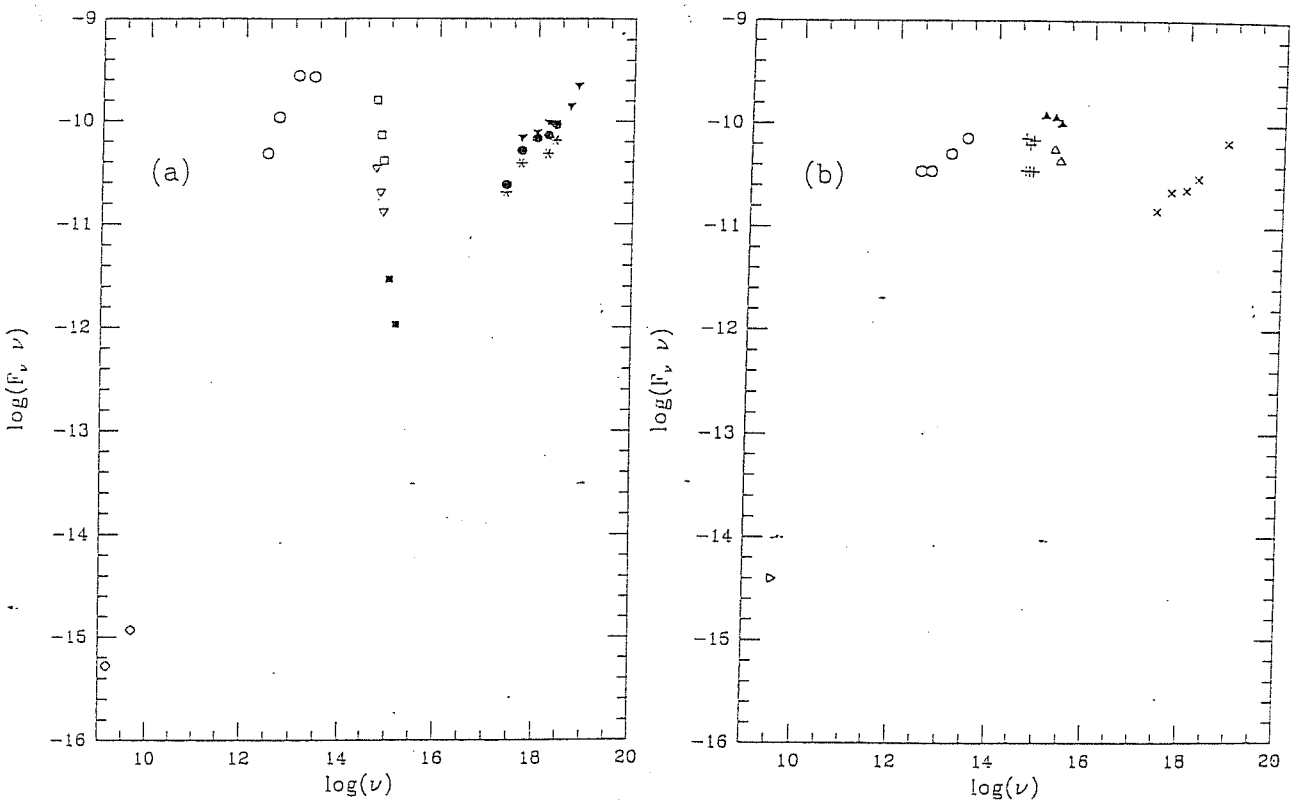

Figure 4.3: *Multifrequency continuum of IC 4329a (a) and Akn 120 (b). References:* ◇ *Dahari and de Robertis (1988);* ▷ *Mazzarella and Balzano (1986);* ○ *IRAS data as reported by Dahari and de Robertis (1988);* □ *Morris and Ward (1988): June 5, 19884;* ▽ *Kollatschny and Fricke (1989): Feb. 18, 1985;* + *Alloin et al. (1988);* ■ *archive IUE observations (unpublished);* ▲ *archive IUE observations: Mar. 14, 1982;* △ *archive IUE observations: Oct. 22, 1980;* ∗ *Turner and Pounds (1989): June 19, 1984;* • *archive EXOSAT spectra (Grandi et al., 1991): July 31, 1985;* ▼ *Yamauchi et al. (1991): Jul. 9, 1989;* × *Turner and Pounds (1989).*

Seyfert 1 spectra, as suggested by Weedman (1983). Although a link between starburst phenomena and nonthermal nuclear activity seems real (*e.g.* Wilson *et al.* 1986; Rafanelli and Marziani, 1991b), it is also difficult for models (*e.g.* Terlevich and Melnick, 1988) explaining the optical spectrum of Seyfert 1 galaxies as due to supernova explosions to account for the nearly identical profile variations over a timescale of a few years, as seen in the spectra of the two galaxies.
The parameters leading to similar BLR structures do not seem to depend strongly upon the morphology of the host galaxy, since IC 4329a is a spiral galaxy of type near Sa, while Akn 120 has an (amorphous) elliptical-like appearance. Similarly, the strength of FeII emission appears to vary considerably between objects with almost identical broad line profiles. If Akn 120 is indeed an elliptical galaxy, it is particularly interesting that it shows much stronger FeII than IC 4329a.
The profile similarity may reflect a similarity in some parameter related to the central engine, such as the bolometric luminosity, mass, Eddington ratio $\eta = L_{Bol}/L_{Edd}$, or even the line of sight orientation. The Eddington ratio is a very important parameter, since it governs the structure of the expected accretion disk: if $\eta \ll 1$, a geometrically thin disk is expected to be present, while if $\eta \sim 1$, a thick structure is expected to form (see *e.g.* Calvani *et al.*, (1989)). Perhaps the Balmer lines are being emitted by gas moving in a very ordered velocity field, as would be the case for a rotating disk. Another possibility is that the double peaks are the signature of a *binary BLR*.

Estimate of mass, L_{bol}, η – The mass of the central accreting object can be estimated (with reasonable accuracy) under the assumption that rotational or infall motions are dominating in the BLR. The mass in these two cases is $M = v^2 r/G$ and $M = v^2 r/2G$ respectively. The FWZI provides an estimate of the radial velocity for the gas near R_{in}, the innermost radius of the BLR. The value of R_{in} can be estimated from the number of ionizing photons emitted by the continuum source $\int_{\nu_0}^{\infty} L\nu d\nu/h\nu$, and the product of the ionization parameter Γ and electron density n_e, since

$$R_{in} = \left(\frac{\int_{\nu_0}^{\infty} \frac{L_\nu d\nu}{h\nu}}{4\pi c \Gamma n_e}\right)^{1/2}. \qquad (4.1)$$

We assume that $\Gamma \times n_e \approx 10^{9.6} cm^{-3}$, following Padovani and Rafanelli (1988). The number of ionizing photons has been computed by extrapolating the power-law index computed between 1 and 10 keV (namely $\alpha \approx 0.74$ for IC 4329a and 0.8 for Akn 120) over the range from 0.2 keV up to 120 keV. The *Big Bump* has been taken into account by modeling the spectrum as a power-law with spectral index $\alpha = 1.3$ between the Lyman limit and 0.2 keV. We estimate (assuming infall) $M \approx 1.21 \times 10^8\ M_\odot$ for IC 4329a and $M \approx 2.26 \times 10^8\ M_\odot$ for Akn 120. The bolometric luminosity has been computed for IC 4329a and Akn 120 after correcting the optical and UV continuum for reddening. We find $L_{bol} \approx 1.95 \times 10^{44} ergs^{-1}$ for IC 4329a, and $L_{Bol} \approx 2.60 \times 10^{44} ergs^{-1}$ for Akn 120. Since the Eddington luminosity is $L_{Edd} = 1.3 \times 10^{38} (M/M_\odot) erg\ s^{-1}$, both objects appear to radiate at a very sub-Eddington rate, $\eta \approx 0.015 - 0.020$. Changes in the ionizing flux by a factor ≈ 2 affect the bolometric luminosity by a factor ≈ 1.6.

Table 2

Line Id.		IC 4329a		Akn 120	
		Flux[1]	*E.W.(Å)*	*Flux*[1]	*E.W.(Å)*
[*SII*]	λ 6731	0.23	...	0.086	...
[*SII*]	λ 6717	0.19	...	0.098	...
Hα (BC)[2]	λ 6563	32.6	515	35.5	519
[*OI*]	λ 6300	0.072	...	0.12	...
[*FeVII*]	λ 6087	0.06	...	...	...
HeI	λ 5876	1.81	...	...	...
[*FeVII*]	λ 5721	0.145	2.5	...	...
FeII blends	λ 5250[3]	1.20	25	3.12	41
[*OIII*]	λ 5007	1.33	...	0.66	...
[*OIII*]	λ 4959	0.42	...	0.22	...
Hβ	λ 4861	3.68	90	10.5	118
FeII blends	λ 4570[4]	0.73	22	3.43	34
[*OII*]	λ 4363	0.28	...	0.42	...
Hγ	λ 4340	0.25	...	3.52	...
Hδ	λ 4101	...	...	1.44:	...
z		0.0159 ± 0.0001		0.0324 ± 0.0001	
$L_{H\beta}$	$(ergs^{-1})$	1.0×10^{41}		1.2×10^{42}	
$E(B-V)$[5]		0.98		0.16	
$L_{H\beta,redd.corr.}$	$(ergs^{-1})$	2.4×10^{42}		2.0×10^{42}	

[1]Fluxes are in units of $10^{-13}\ erg\ s^{-1}cm^{-2}$

[2]Including Hα Narrow Component and [NII]λλ6548,6583

[3]FeII blends measured from 5190 to 5320 Å.

[4]FeII blends measured from 4460 to 4700 Å

[5]Estimated from the ratio Hα/Hβ.

Hence the Eddington ratio remains $\ll 1$. Since these values of η are typical for Seyfert–1 galaxies, and no changes in the structure of the accretion disk are expected, it appears that these parameters (Mass, L_{bol}, η) alone cannot account for the peculiarities observed in the spectra. Although IC 4329a and Akn 120 are luminous Seyfert galaxies, their bolometric luminosities are not extraordinarily large. They are both near the nominal absolute magnitude (M_V= -23.0, H_0= 50 $km\ s^{-1}Mpc^{-1}$) boundary between quasars and Seyfert galaxies.We will discuss later the possibility that the central engine is being viewed at a peculiar orientation.

Accretion disk – Emission by an accretion disk is naively suggested by the *double peak* structure in the Balmer lines. It would however be difficult for a simple model of a rotating disk to explain the *entire* Hβ and Hα emission. In general, gravitational + transverse Doppler redshifts + Doppler boosting should be considered in order to explain the observed profiles. The most straightforward models predict a stronger blue peak and redshifted base for line emission originating from the disk (Chen *et al.*, 1989). At larger values of R_{out} these effects tend to diminish and the profile in general would show a red asymmetry with a possible small blue shift of the peak (AR, or AR,B in Sulentic (1989)). Since it is difficult to reconcile a strong displaced red peak with the simple radiative accretion disk model, no clear accretion disk signature can be readily isolated in these unusual objects. One possible scenario might involve a disk radiating at large R producing the central peak with a separate infalling component producing the red peak. Another possibility is that the red peak is an independent component, perhaps in a double stream configuration, and that its variations are uncorrelated with those of the *zero* peak.

Alloin *et al.* (1988) suggested that the BLR of Akn 120 is made of two regions, one of which corresponds to the accretion disk. Their suggestion is based upon the difference of the line profiles in the *high* and *low* luminosity phase. The difference spectrum of Hβ shows a double peaked profile, whose peaks are shifted by $\pm$ 2000 $km\ s^{-1}$ with respect to the radial velocity of the *zero* peak. The *zero* peak however does not correspond to the systemic velocity in Akn 120. We have discussed earlier possible problems with this spectrum.

We have repeated the same operation on the Hβ and Hα profiles of IC 4329a, taking as representative for the high state the spectrum of 1975 June published by Wilson and Penston (1979). We have been able to produce the same structure in the IC 4329a profile using the [OIII] lines as a fixed intensity reference. The peaks are shifted by -1950 ± 100 $km\ s^{-1}$ and by $+1950 \pm 100$ $km\ s^{-1}$with respect to the systemic velocity of IC 4329a. These values are similar to those found by Alloin *et al.* for Akn 120. In both cases, the blue peak of the difference spectrum appears as a shoulder on the blue side of Hβ, while the red peak of the difference spectrum corresponds to the red peak of the observed profile.

If a contribution from a disk is present, we must hypothesize that it is switched on as a consequence of particular events. This can have deep consequences upon the possibility of effectively revealing the disk, and will be discussed in a further study (Marziani *et*

al., 1991) and preliminarily at the end of this chapter. However, the two peaks revealed in the difference spectrum should vary in phase. The Hβ profile of Akn 120, taken on Dec. 27, 1987 clearly shows that this is not the case, since the blue shoulder is at the same intensity level as the red peak (P. Rafanelli, *private communication*). Older data support this contention. A spectrum of Akn 120 presented by Foltz et al. (1981) shows a possible *blue* peak that is stronger than the more commonly observed red feature.
Binary Black Hole – The Hβ profile observed in Akn 120 and IC 4329a are not as expected for a binary BLR: in this case a centrally peaked profile should be surrounded by two peaks symmetrically displaced with respect to the line center and located in the line wings, as is more the case for Arp 102b (see e.g. Halpern and Filippenko, 1988). The suggestion of a binary black hole could be saved if the two BLR are associated with the blue and the red peak in the difference spectrum (the former corresponding to the blue shoulder in the Hβ profile). The blue shift of the *zero* peak, as seen in Akn 120, may represent a serious problem for this idea.
As an ultimate test for the presence of a binary black-hole, monitoring of the line profiles should reveal a peak displacement due to the orbital motion of the two black holes around their center of mass. The remarkable stability of the wavelengths of the *red* and *blue* peaks over 15 years does not rule out the idea that the red and the blue components are emitted by a binary BLR (Halpern and Filippenko, 1988). No radial velocity shift has been detected (with an uncertainty of 100 $km\ s^{-1}$, for an 1800 $km\ s^{-1}$ *red* peak). Hence, the maximum change of orbital phase can be $2 \arccos 0.95 = 36°$, and a lower limit to the period is $P \approx 9.9\ yr$. The corresponding lower limit to the mass is $M \approx 3.5 \times 10^8 M_\odot$, which is reasonable for a Seyfert 1 galaxy.
An important implication of Akn 120 and IC4329a – Constraints to the interpretation of profile variations as due to the *lighting* of a disk contribution arise from considerations on the energy balance in the BLR. In the following, we will restrict our calculations to Akn 120, because of the less uncertain reddening estimate. Geometrical parameters for the best fit disk of the difference spectrum are $R_{out} = 2.2 \times 10^4 R_g$ and $R_{in} \approx 400 R_g$, assuming $\sin i = \sqrt{2}/2$. Dumont and Collin–Souffrin (1990,a,b) have suggested that the outer region of the accretion disk has physical conditions suitable for the emission of a low ionization spectrum, with prominent Balmer, FeII and MgIIλ2800 lines. Dumont and Collin–Souffrin pointed out that the disk should be illuminated by an external source in order to have emission of a line spectrum. They suggested two illumination models:

1. two point sources located at height A above the disk plane (*Point Source Model*, PSM). This provides an incident flux per unit area:

$$F_{inc} = f_i \frac{L_{ion}}{4\pi} \frac{A}{[R^2 + A^2]^{3/2}}, \tag{4.2}$$

where f_i is the fraction of continuum radiated toward the disk (we assume $f_i = 0.5$, as it is the case for two isotropically emitting sources). This equation is a rough approximation of Eq. 1b of Dumont and Collin–Souffrin (1990b);

2. a diffuse central source of radius R_{min}, giving an incident flux per unit area

$$F_{inc} = f_r \frac{L_{ion}}{4\pi R^2} [\frac{R_{min}}{R}]^g \tag{4.3}$$

where the fraction of flux scattered toward the disk is now f_r/g, if $g > 0$ (*Diffusion Model*, DM). We adopt $f_r = 0.4$ and $g = 0.8$ (see below for a discussion on the physical meaning of these parameters).

Variations in the Hβ luminosity assumed due to the disk are $\approx$ 2–3 times the total line luminosity in the low state. If the ionizing continuum changes *switch on* the illumination of the disk, we can compute the ionizing luminosity intercepted by the disk, by integrating over the disk area:

$$\int_{R_{in}}^{R_{out}} F_{inc} d\Sigma = f_i \frac{L_{ion}}{4\pi} \int_{R_{in}}^{R_{out}} \frac{A}{[R^2 + A^2]^{2/3}} 2\pi R dR = f_i \frac{L_{ion}}{4} A [\frac{1}{\sqrt{R_{in}^2 + A^2}} - \frac{1}{\sqrt{R_{out}^2 + A^2}}] \tag{4.4}$$

and

$$\int_{R_{in}}^{R_{out}} F_{inc} d\Sigma = f_r \frac{L_{ion}}{4\pi} \int_{R_{in}}^{R_{out}} \frac{1}{R^2} [\frac{R_{min}}{R}]^{0.8} 2\pi R dR = f_r \frac{L_{ion}}{2} \frac{R_{min}^g}{g} (\frac{1}{R_{in}^g} - \frac{1}{R_{out}^g}), \tag{4.5}$$

where R_{in} and R_{out} are as deduced earlier. Note that the right side of Equations (4) and (5) give the covering factor f_a of the disk times L_{ion}.
We adopt the values of R_{in} and R_{out} as deduced earlier. The number of ionizing photons needed to sustain the Hβ change can be computed once estimated the enhancement in the Hβ luminosity due to collisional processes is taken into account. These are most relevant in the extended *Partially Ionized Zone* (PIZ) which develops in the Compton heated part of the disk (see Chapter 1), and which should emit the most of the low ionization lines. According to Dumont and Collin-Souffrin (1990a,b), only little Lyα flux is produced in the disk. The ratio Lyα/Hβ depends on the illumination model, and has been estimated from Eq. 21 of Dumont and Collin- Souffrin (1990b) and from the graphs reporting various line intensities as a function of the radius (Fig. 3a–d of the same work). We consider the PSM model at first. The enhancement factor ε is $\varepsilon \approx 100$ if $A \sim 10^3 R_g$, and decreases when the height of the point sources is larger, to $\varepsilon \approx 30$ for $A \sim 10^4 R_g$ and $\varepsilon \approx 22$ for $A \sim 10^5 R_g$. The fraction of ionizing continuum photons intercepted by the disk would require that the height of the point sources is $A \gtrsim 10^3 R_g$, in order to match the required number of ionizing photons needed for the Hβ emission. This condition is unlikely to be satisfied, since the ionizing continuum is believed to be produced in a region which is contained within a radius $R < 100 R_g$. Furthermore, this estimate has been made assuming the most favourable conditions in order to increase the covering factor and hence to diminish A. More debatable is the possibility that $R_{min} \rightarrow R_{in}$. The case $g = 0.8$ corresponds to diffusion by a nuclear wind (Mardaljevic *et al.*, 1988). The collisional enhancement of Hβ in this case is $\varepsilon \approx 55$. It would require a diffusion sphere of radius $R \simeq 200 R_g$. However, a more

realistic value is considered $g = 0.5$. In this case, $R_{min} \simeq 650\ R_g$ would imply that the scattering medium extends beyond the inner radius of the disk. Thus we suggest that the DM is suitable to explain the variations in the Balmer line profiles of Akn 120 and hence of IC 4329a, particularly if the radiation is backscattered by medium located partly above the disk, unless:

1. the continuum variations are poorly constrained and are much larger than a factor ≈ 2;
2. the continuum is not emitted/scattered isotropically;
3. the correction for reddening applied to the lines is too high.

Although the first condition should be tested by X–ray monitoring of these objects, the latter two seem to be rather unlikely.

Further clues – Although self-absorption in the Balmer lines appears unlikely, since the dip is displaced by $\approx 1000 km\ s^{-1}$ with respect to line center (assuming that the rest frame of the galaxy is also that of the BLR). It is useful to recall that the central dip in the *profile difference* could be due to self-absorption in very high density gas, rather than a reflection of the rotational kinematics of the emitting gas. If density is as high as $n_e \approx 10^{12} - 10^{13} cm^{-3}$, as in stellar chromospheres, self–absorption in the Balmer lines should arise. This high density gas, located at the inner edge of the BLR (estimated as ≈ 2 *light months* for Akn 120), could have $\Gamma \approx 1 \times 10^{-4}$, and would thus be able to emit the observed low ionization spectrum. This view is supported by the decrease of the Balmer decrement between the low and high luminosity states.
Morris and Ward (1989) found that the OIλ8446 profiles are very similar in the two galaxies. The profile of the OIλ8446 line is in turn similar to the core of the Hβ profile. Since the OIλ8446 line is a fluorescence line produced only by gas very optically thick to the Lyman continuum, this confirms that the line cores are emitted by optically thick gas, as expected from photoionization models. Morris and Ward (1989) found moreover that Akn 120 and IC 4329a are the only two galaxies in their sample for which emission from optically thin gas is likely to contribute. For both object, the optically thin emission is present in the blue wing of the Balmer lines. Recently, Ferland *et al.* (1990) have suggested that optically thin gas could be responsible for the uniform screen covering the X–ray source in NGC 4151 and in some other galaxies. In the case of NGC 4151 nearly complete coverage of the central source is indicated by the fact that the soft X–ray flux remains approximately constant, while the hard X ray flux varies by a factor ≈ 2.
The reddening corrected luminosity of Hβ is rather high among Seyfert galaxies: from a comparison with the values provided by Padovani and Rafanelli (1988) it is found that Akn 120 and IC 4329 have the highest Hβ luminosities in their sample of Seyfert 1 galaxies. Since the BLR geometry is likely to be flattened (e.g. Osterbrock, 1983), existence of a preferential plane/axis is a rather likely possibility. This plane could be identified with the plane of the accretion disk, which cannot generally be identified

with the principal plane of the galaxy (Tohline and Osterbrock, 1982). Several forms of evidence suggest that at least some Seyfert 2 galaxies have a BLR hidden by a torus of cold obscuring matter (*e.g.* Wilson *et al.*1988; Miller, 1988). If the differences between Seyfert 2, intermediate Seyfert and Seyfert 1 galaxies are due only to a projection effect, continuity arguments would suggest that the central engines of Akn 120 and IC 4329a are oriented rather *face on* toward the observer. The rarity of Balmer line profiles like those seen in the Akn 120 and IC 4329a also points toward an unusual orientation or extremum in the viewing angle.
This is in agreement with the detection of optically thin gas. As Ferland *et al.* (1990) argue, the optically thin gas should be located between the inner edge of the BLR and the central continuum source. Analysis of the EXOSAT spectra suggest that IC 4329a does not vary in the soft X ray range, while the hard X ray flux increases by a factor ≈ 1.6, as is the case for NGC 4151. Thus, the detection of optically thin emitting gas – completely covering the central continuum source – could provide additional support for the idea that we are looking in a rather direct way at the central engine of these galaxies. This adds in turn further support also to the model of Ferland *et al.* (1990). The presence of such gas only in the blue wings of the lines suggests that it could be associated with an outflowing component. Zheng *et al.* (1990) have produced a good fit to the profile of Akn 120 using a model that assumes bi-conical outflow for the gas clouds.

Conclusions and further work

The profile variations occuring in IC 4329a and Akn 120 make these objects of great value for understanding the BLR structure. In particular, observations of the Paschen continuum should be performed in order to test whether optical depth effects in the Balmer lines are playing a role. IC 4329a deserves much more attention than it has had in the past. It is a good candidate for an extensive spectroscopic monitoring campaign. Akn 120 and IC 4329a are the best (known) candidates for testing the models of Dumont and Collin–Souffrin (1990a,b). If the illumination models of Dumont and Collin–Soffrin apply, we suggest that the *diffuse* illumination model is probably more appropriate. We finally suggest that the orientation of the flattened BLR should be rather face-on, and hence extremely favourable for having a direct look at the central engine in these objects.

4.2.4 OQ 208

Little attention has been paid in the literature to the optical spectrum of OQ 208 ($\equiv$ Mkn 668). Osterbrock and Cohen (1979) discussed this object b because of its redshift difference between narrow and broad emission lines (whose centroid was identified with the peak A in Fig. 1a). OQ 208 was further studied by Perez (1987, hereafter P87), who emphasized some variations of its Balmer line profiles. Gaskell (1983b) argued

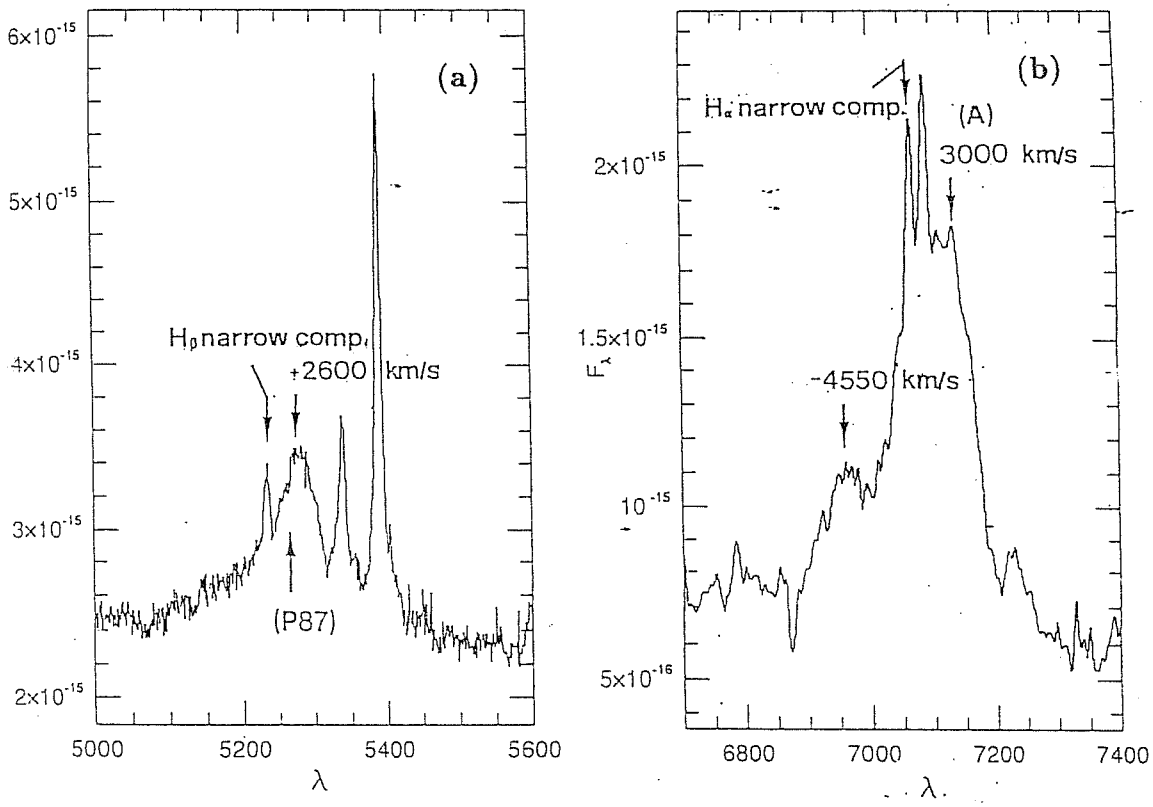

Figure 4.4: *Hβ (a) and Hα (b) profiles of OQ 208. Vertical and horizontal scales are as for Fig. 4.1*

that a weak blueshifted peak was also present, and suggested that OQ 208 may host a *binary* black hole, as a result of galactic merging.

Results

A strong variation (a factor ≈ 3) has occurred in the continuum level in the time elapsed between our observations of Hα in Apr. 1990 and of Hβ in Feb. 1991. A comparison with the spectra published by Osterbrock and Cohen (1979) and with those of P87 confirms the variability and suggests that this object goes through a *high* and a *low* luminosity phase. The existence of large variations and the short time scale (a few months) of the variations make OQ 208 one of the strongest optically variable object among BLRG and Seyfert galaxies.
The radial velocity shifts of the most prominent features attributed to the Broad Line Region (BLR) with respect to the Narrow Line Region (NLR) are quoted in Fig. 4.4 a and b. The broad Hα profile appears double–peaked: two broad *shelfs* are present on the blue and the red side of the narrow component of Hα. The shelf on the red side is by far the most prominent. The radial velocity of A ($v_{r,A} \approx 2450$ $km\ s^{-1}$) is in good agreement with that measured by Cohen and Osterbrock (1979).
In the Hβ profile, the *blue* shelf appears to be depressed with respect to the red one. A faint emission feature is visible on the blue side of Hβ (B, in Fig. 4.3). It is located at $v_r \approx -5500$ $km\ s^{-1}$, which corresponds to the edge of the *blue* shelf seen in Hα.
OQ 208 would be classified AB,R (blue asymmetric profile with red displacement) in the scheme proposed by Sulentic (1989). This appears to be an uncommon class. Of the 61 objects included in that study only I Zw I was assigned this type. OQ 208 is a much more dramatic example of a red displacement, with $\Delta v_r \approx 2400$ $km\ s^{-1}$ compared to 640 $km\ s^{-1}$ for I Zw I.
Emission line profiles are strongly variable in shape. The red shelf is much stronger in our spectrum than in those shown by P87. Furthermore, one gets the impression that it has been displaced toward the red (the position of the of the centroid of Hβ measured on the spectra of P87 is marked in Fig.4.3b). Noticeably, a faint emission feature is also visible on the blue side of the Hβ profiles in the spectra of P87. Its radial velocity is $-2500 km\ s^{-1}$with respect to the NLR.

Discussion

The observation of a *red* shelf much stronger than the *blue* one disagrees with the predictions of simple relativistic disk models (*e.g.* Chen and Halpern, 1989), making very difficult any attempt to explain the *entire* Balmer emission of OQ 208 as due to an emitting keplerian disk.
If *only* the *blue* shelf of Hα is interpreted as emitted by an accretion disk, a relativistic disk model profile (q=3.2, $R_{in} = 200R_g$, a relativistic disk model profile ($q = 3.2, R_{in} = 200R_g, R_{out} = 1250R_g, i = 37°$, that is, with the disk oriented rather face–on) plus an additional redshifted component (needed to explain the *red* shelf) provides a satisfactory reproduction of the broad component of Hα. The value of i would

be in agreement with the large value of the parameter R (Orr and Browne, 1982), which suggest that the radio source is also oriented pole-on (P87).
The reality of the faint emission feature revealed on the *blue* side of Hβ needs confirmation by further observations, so that only some preliminary and tentative considerations will be derived from its detection.
The enhancement, the variable centroid displacement toward the red of the shelf in the Hβ profile can be explained in several conflict ways:

1. The increased radial velocity of the red shelf with time may be used as a supporting evidence for *infall* motion of the emitting gas.

2. The centroid displacement may be due to the orbital motion of a binary black hole. In this case, variations of the centroid allow to obtain a lower limit to the mean black hole mass: $M \gtrsim 10^8 M_\odot$, which is a reasonable value for avoiding super–Eddington accretion. The corresponding period would be $\approx 15yr$. The strong prediction of periodicity of such a rather short time scale should help the observational confirmation of the binary black hole suggestion. A preliminary analysis of the published spectra made by us does however not favour this explanation.

3. One is tempted to draw an analogy with the satellite lines of CIVλ1549 detected in NGC 4151 by Ulrich *et al.* (1985). However, in this case the comparison of our data with those of P87 shows that the radial velocity of the red shelf of Hβ and of the (*assumed real*) B emission feature appears to increase with time (and with continuum luminosity). This is exactly the opposite of what is expected if the emitting gas were ballistically outflowing in a bipolar configuration. Radiative acceleration of the emitting gas could help to get out of trouble a model assuming bipolar outflow.

Concluding, our considerations suggest that the most likely explanation for the complex profiles of OQ 208 involves either a rotating disk (heavily obscured) plus an infalling component or bipolar outflow of the gas (probably radiatively accelerated).

4.2.5 3C390.3 and 3C382

The Hα profiles of 3C390.3 and 3C382 are shown in Fig. 4.5 a and 4.5 b respectively. Although little data have been published on 3C 382, the two galaxies can be probably regarded as BLR twins like Akn 120 and IC 4329a. It was proposed by Perez *et al.* (1988) that the Balmer lines of 3C390.3 are due to an accretion disk. A simple disk model was able to roughly account for the prominent double–peaked structure. However, from the spectrum of Fig. 4.5, taken on Apr. 15, 1988, it appears that the average of the peak position was displaced by $\simeq -450\ km\ s^{-1}$ with respect to the NLR, a result which is inconsistent with the disk hypothesis. A set of 38 spectra from 1974 to 1988 has been recently published by Veilleux and Zheng (1991a). The second panel of Fig.1 in their work clearly shows that the centroid of the blue *shelf* changed by ~ 20

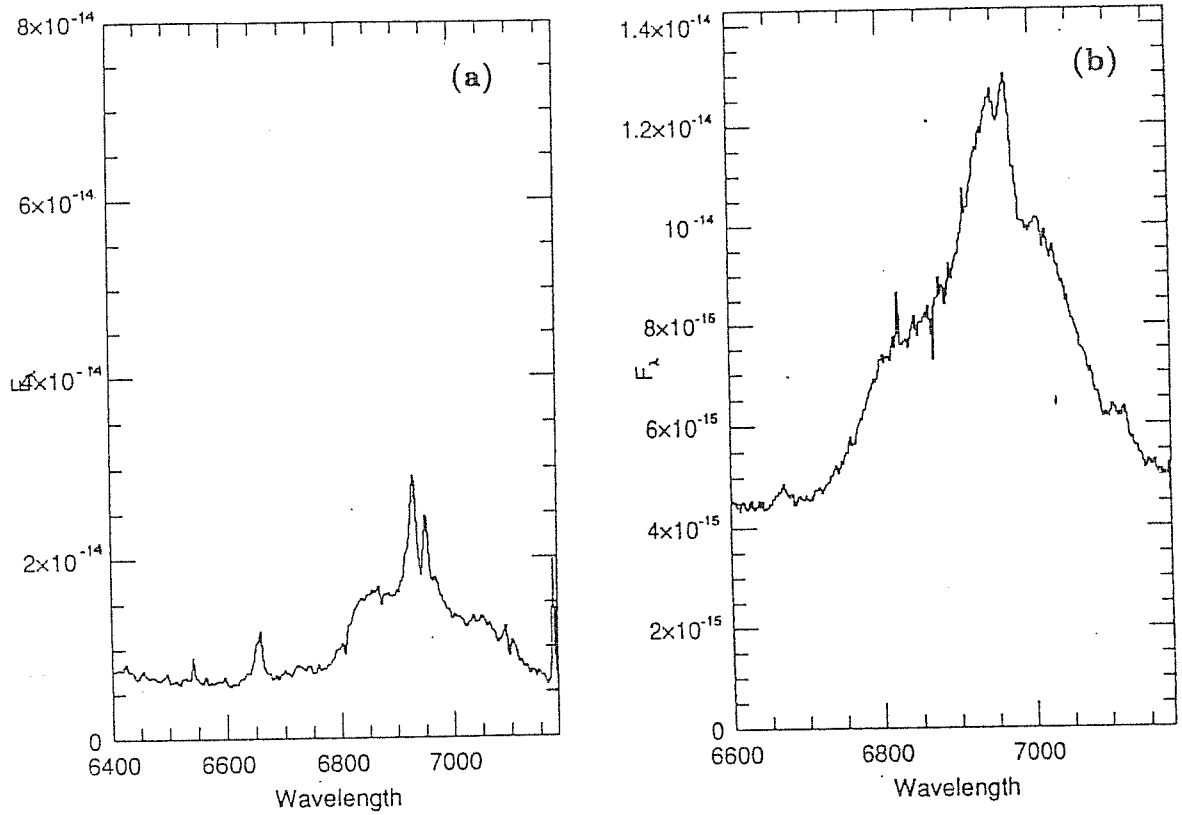

Figure 4.5: *Hα profile of 3C390.3 (a) and 3C382 (b). Horizontal and vertical scales are as for Fig. 4.1*

Å to the red from 1975 to 1980. The radial velocity of the blue peak seems to decrease when the continuum is fading. A rather similar behaviour was found by us for OQ 208. Note that the Hα profile of 3C390.3 at certain epochs – when the red shelf is stronger than the blue one – is very similar to that of OQ 208. In order to save the disk origin for the Balmer lines, an interesting possibility discussed by Veilleux and Zheng is that the shift of the peak could be due to inhomogeneities of the accretion flow. Another possibility that should be considered both for 3C390.3, 3C382 and OQ 208, is that the strength of one of the peaks is affected by accreting matter, impinging at the outer boundary of the disk and creating an *hot spot*. Veilleux and Zheng (1991b) reported that the ratio of the fluxes of the blue and red shelfs of the Balmer line behaved in very regular, nearly sinusoidal fashion. Their result are explained in the context of emission from an accretion disk and an hot spot which corotates with the disk.
The shift of the position of the blue shelf to larger wavelengths can be explained if the gas is disposed in a bipolar geometry, and if the luminosity distribution has changed such that it peaks at a radius where the gas velocity relative to the systemic velocity is smaller. As discussed for OQ 208, the increase of the shift when the continuum source brightens can probably indicate that the line emitting gas is accelerated outward under the influence of radiation pressure.

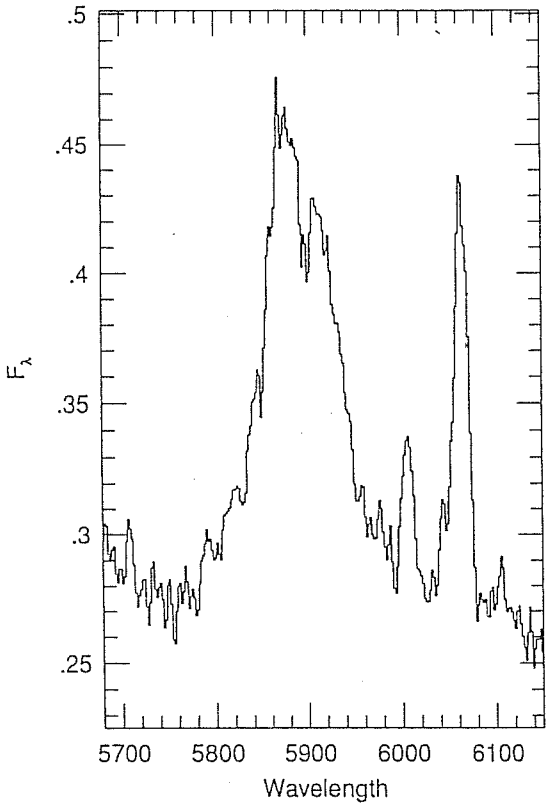

Figure 4.6: *Hβ profile of OX 169. Horizontal scale is wavelength in Å; vertical scale is arbitrary intensity units.*

4.2.6 OX 169

OX 169 is a fairly luminous low–redshift quasar ($z = 0.21$). The morphology is suggestive of a recent merger (Stockton and Farnham, 1991). It was noted by Smith (1980) because of its double peaked line profiles, with one peak having radial velocity roughly coincident with the NLR, and with another prominent peak to the red (Gaskell, 1981). If we look at the core of the Hβ profile (Fig. 4.6) there is a certain similarity with the Hβ profile of Akn 120. A measurement of the centroid of the peaks yields -300 $km\ s^{-1}$ and $+1400$ $km\ s^{-1}$ with respect to the rest frame defined by the NLR. It is interesting to note that the small blue displacement of the *zero* peak was found also for Akn 120, and that the peak separation is nearly the same. However the profile of OX 169 is more symmetric in the wings than that of Akn 120, without any shoulder or inflection on the blue side.

The Hβ profile of Fig. 4.6 cannot be fitted by an accretion disk model, for the same reasons explained in the case of Akn 120. Spectra taken in 1983 (Stockton and Farnham, 1991) show that the Hβ profile did change. In 1983, when the OX 169 was brighter the red peak appeared stronger than the blue one. The difference spectrum – single peaked and displaced to the red – computed by these author is in this case inconsistent with an accretion disk contribution.

4.2.7 NGC 5548

The Hβ and Hα profiles are shown in Fig. 4.7 a and 4.7 b respectively. Due to the weakness of the FeII lines in the ranges 5150–5300 Å and 4450–4700 Å, the profile of Hβ is probably not contaminated by FeII emissions. The profile of Hα and Hβ are rather smooth, with a weak asymmetry to the red. An inflection is visible on the blue side of the Hβ profile. The profile of Hβ is however composite: a distinctly narrower component is superimposed to the wings of Hβ. This component can not be due entirely to the NLR, since it is broader than the [OIII]$\lambda\lambda$4959,5007 lines at the same fractional intensity.
The Hβ profile reminds to the profiles obtained by Dumont and Collin–Souffrin (1990b) for the *diffusion* illumination model (see also §4.2.3). This object was studied by Stirpe (1989) and by Stirpe *et al.* (1989). Profile variations occur with the same sign on both sides of the emission lines, a result confirmed by the variability in the UV lines (Clavel *et al.*, 1990; Koratkar and Gaskell, 1991). This argues against the predominance of radial motions, since a delay between the responses of the two sides should be observed in that case. Stirpe *et al.* (1989) proposed to explain the profiles and the profile variations as due to a disk illuminated by a thin scattering medium above the disk. The disk model is anyway unable to account for the observed asymmetries, unless the presence of an additional component is invoked. Although the profile of Hβ appears symmetric at certain epochs as shown in Fig. 4.7 it is rather asymmetric at others, with a prominent blue shoulder. If both the red and blue side respond in the same way to the continuum changes, it seems nevertheless proved that the blue shoulder varies more than the red one in the Hβ profile. It is at present unclear whether a disk model is able to explain these features.
An interesting point is that the Balmer line profiles of NGC 5548 are not as peculiar as the profiles of the objects discussed previously. If a disk model were sophisticated enough to explain the profile variability in NGC 5548, probably it would be able to reproduce also profile changes in other, not extremely peculiar AGN. In section 4.4.1 we will investigate whether the range spanned by some parameters used to describe the line profiles is covered by the model predictions. Before turning to the description of a suitable parameterization of line profiles (§ 4.3), we will present some general consideration on the object showing double–horned profiles.

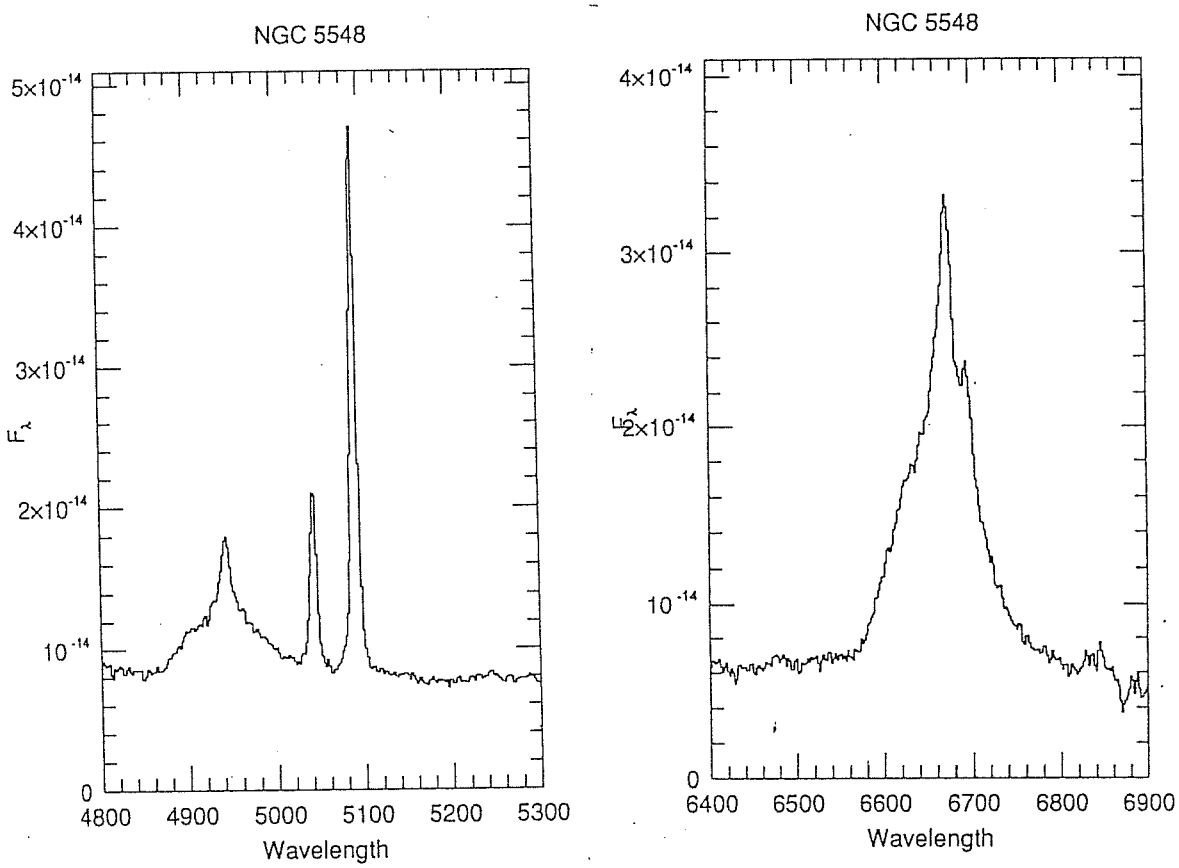

Figure 4.7: *Hβ and Hα profiles of NGC 5548. Horizontal and vertical scales are as for Fig. 4.1*

4.2.8 General considerations

From the analysis of the single objects it emerges that convincing evidence for disk emission is found only in the cases of Arp 102b and 3C332. In some other cases, the indroduction of a second emission line component is required to get even a rough agreement with the observations. An important point is that the Balmer decrement in the *blue* and *red* shelfs or peaks is not the same. Akn 120, IC 4329a, OQ 208, 3C382 as well as 3C390.3 (at certain epochs) have steeper Balmer decrement for the *blue* component. This fact can be explained in disk models with the somewhat *ad hoc* assumption that the disk is either non–uniformly illuminated or that its luminosity is greatly enhanced at a *hot spot*. This suggestion is particularly well suited for 3C390.3, beacuse of the variable strength of the *red* and *blue* peak. The different Balmer decrement for the *red* and *blue* peaks or shelfs is nevertheless easier described in a bipolar geometry.
Stockton and Farnham (1991) emphasized the peculiar morphology of OX 169, suggestive of a merger. It is intriguing for the binary black hole hypothesis that nearly all the galaxies studied show a morphology that could be proved as peculiar. 3C 332, 3C 382, 3C390.3 and (probably) Akn 120 are elliptical galaxies, Arp 102b is also elliptical, and belongs to a strongly interacting system. It is currently thought that at least some elliptical have been formed by the merging of two spiral galaxies (Barnes, 1988; and Schweizer, 1990, for a review). IC 4329a is a spiral whose nucleus is crossed by a dust lane. Are these peculiarities a *sign* of the fact that many peculiar galaxies are found among Seyfert galaxies, or does it mean that double horned profiles are due to a binary BLR (associated with a *binary* black hole? We think that the morphology of all these objects should be analyzed carefully in order to further test this idea.

4.3 A parametric study of emission line profiles

Sulentic (1989) has proposed a simple classification scheme for the broad line profiles. As a first step, he distinguishes between symmetric (S) and asymmetric (A) profiles. Symmetric profiles were splitted in two possible variety: those with displacements toward the red (SR) or blue (SB) relative to the [OIII]$\lambda\lambda$4959,5007 lines. Asymmetric profiles were described by a descriptor of the asymmetry (AR or AB for red and blue asymmetries) and after a comma, by a descriptor of the line shift that may be present (e.g. AR,R for a red asymmetric profile displaced to the red). The parameterization was applied to 25 objects from the Palomar Bright Quasar Survey (Schmidt and Green, 1963) with published spectral scans, and 36 Seyfert galaxies, BLRG and quasars selected from various literature sources. From the parametric study of these 61 AGN Sulentic (1989) found:

1. 35 objects showed a measurable wavelength shift relative to the NLR, with redshifts slightly more common than blueshift;

2. a large number of displaced profiles (15) are symmetric;

3. only 9 objects have symmetric and unshifted profiles;

4. 37 objects show an asymmetric profiles with red asymmetries more common than blue ones;

5. shifted profiles are very unlikely to have a blue asymmetry.

Taken as a whole, these results cannot be easily explained by a unique model of the BLR. The predominance of redshift may indicate that gravitational redshift affects the line profile. The effect of gravitational plus transverse redshift should increase from the top of the line to the line base: indeed, 20 of the 25 profiles for which the profile centroid at four profile heights is considered, show a behaviour which is consistent with an increase of the shift toward the line base. There is a clear paucity of objects having a redshifted peak or non–shifted base and a blueshifted line base.

4.4 Implications of Arp 102b and 3C332

The successful modelling of Arp 102b and 3C332, accepted at face value, suggests that the LIL emission arises directly from an accretion disk for which relativistic effects are not negligible. The differences between the HIL and LIL profiles in Arp 102B (as evidenced by Lyα, Chen *et al.*, 1989) also support the contention that the HIL region is kinematically distinct. To the best of our knowledge, no one has proposed that both LIL and HIL originate from a disk. The results of Chen and Halpern (1989) suggest that we can identify those AGN with LIL emission originating from a disk (*assuming Arp 102B is typical of the class*) on the basis of their (1) double horned and (2) redshifted base of LIL profiles. Further, as a result of Doppler boosting, we would expect to observe (1) an enhanced blue horn or a (2) blue displacement near to the profile peak if the horn are not resolved. Unfortunately, we observe very few profiles with these properties. No double horned profiles are seen in the large profile sample of Sulentic (1989). Is it possible that LIL arises from disks in many cases but that a double horned profile is not seen? Is Arp 102B one of an exceedingly rare group of AGN where we are able to see an emitting disk? The unsatisfactory nature of the latter possibility has led to various explanations for the rarity of the double horned profiles:

1. the central depression is filled in by the narrow line component (Calvani *et al.*, 1989) or by additional BLR emission, which is kinematically distinct; additional BLR contribution to the Hα profile is superimposed to the disk profile in the Hα profile of Arp 102B, and this could be also the case of the *zero* peak of Akn 120. If the peaks were not so widely spaced, the central depression would be cancelled.

2. the radius of the emitting region of the disk may typically favour profiles where the separation of the peaks is small resulting in blended, single peaked features (Chen and Halpern, 1989; Collin–Souffrin and Dumont, 1989);

3. one of the peaks is typically suppressed or obscured (Sulentic, 1989);

4. there is some kind of azimuthal variation of the emissivity, due to a non uniform illumination.

4.4.1 A comparison between theory and observations

The above results, particularly the apparent uniqueness of Arp 102B, call into question a disk origin for the LIL emission in any AGN. The conflict between the observations and the predictions of disk models has recently been the subject of some discussion (Chen and Halpern 1989; Collin–Souffrin and Dumont 1989; Dumont and Collin–Souffrin, 1989). Extensions of the models have been proposed to account for the discrepancies, mostly involving emission from larger disk radii. The modified profiles are able to produce profiles closer to the observed, particularly after allowance for turbulence.

The observation of redshift discrepancies among emission lines in AGN places a serious constraint on any model model of the emitting region. Ordinarily one distinguishes between two emission zones in an AGN: the BLR which show permitted features such as the Balmer series, and the NLR which show mostly forbidden lines produced by transitions following collisional excitation. Many AGN (Gaskell, 1982; 1983a; Wilkes, 1984) show significant velocity shifts among the BLR among the BLR lines and also shifts of the BLR relative to the NLR lines. A recent reanalysis of 61 AGN showed that over one half have BLR versus NLR velocity differences (Sulentic 1989). All evidence is consistent with small ($\lesssim$ 200 $km\ s^{-1}$) or nonexistent shifts of the NLR with respect to the systemic velocity (determined from 21 cm or absorption line measures).

We have performed a more general comparison of the domain of disk model predictions with that for the data. This could be, in principle, more useful than discussing agreement or disagreement between the models and any single AGN. There are at least two useful parameters for such a comparison:

1. the wavelength of the profile centroid at different profile heights [C(1/4), C(1/2), C(3/4)] measured with respect to [OIII] $\lambda\lambda$4959,5007 FWHM, and

2. the profile asymmetry index, here defined as

$$A.I. = \frac{C(3/4) - C(1/4)}{FWHM} \tag{4.6}$$

While the A.I. is constant for any object, the centroid value can change significantly. Figure 4.8 presents a comparison of the model predictions for these parameters and the observations. We have used a representative set of model parameters (inner and outer radii, inclination) that should effectively define the domain in shift–asymmetry space. The largest existing data sample (Sulentic 1989) is used for the comparison. This sample included all AGN with:

1. published spectra of moderate to high resolution ($\approx$ 10 Å);

2. weak/absent FeII optical emission or corrected for the presence of FeII emission.

The assumption is that the sample is large enough to allow us to characterize the observational LIL parameters for AGN (i.e., Seyfert galaxies, QSOs and BLRG).

We did not think that any accretion disk model was sophisticated enough to give exact prediction that could be directly compared to observations. We decided to use the simplest approach in evaluating theoretical line profiles since we are mainly concerned with general trends rather than with detailed fits.

We therefore decided (rather than using a fully general relativistic treatment (see e.g. Fabian *et al.*, 1989)) to use formula (14) in Chen *et al.* (1989), which takes into account all relevant general relativistic effects, but is correct only to first order im M/R and for inclination angles greater than $\sim 5°$. Near edge–on profiles generated from this expression produce a spurious third peak near the systemic velocity. In this way we obtained line profiles for r_{in}, r_{out}, and the inclination angle as free parameters (we fixed the exponent in the surface emissivity power law to be q = 3.2 [see Eq. (9) in Chen *et al.* (1989)]). Models were also generated with q = 2.2 but they do not alter the conclusion and therefore are not shown. From the plots we then evaluated the FWHM, C(3/4), C(1/2), C(1/4), the A.I., the peak ratio and separation. Moreover, in order not to rely on a single model, we did the same for the plots of Hβ presented by Dumont and Collin–Souffrin (1990b) for their models of an accretion disk illuminated by a central source of nonthermal radiation. These results for radiation from large disk radii occupy a small part of the total model domain near the origin. Data for both models are plotted for inclination angles of 15°, 25°, 45°, and 65°. we considered inner and outer disk radii in the ranges from 100 to 700 and 400 to 1900 r_g. We end up therefore with two sets of theoretical data to be compared with observations. The assumption here is that we have sampled a sufficiently large range disk radii and inclination values in order to effectively define the domain of disk models.

Each of the three profile measures has certain advantages and disadvantages for the comparison with the models. The 3/4 level is most sensitive to the Doppler boosting in the models. It is the only level where the models predicts significantly blueshifted profiles. The lowest (1/4) level in the profile is most sensitive to the gravitational + transverse redshift which decreases rapidly as the inner radius of the emitting region is increased in the models. The lower left–hand plot in Figure 4.8 illustrates this by by labeling the points corresponding to the different values for the inner radius of the emitting region. Observationally, the 1/4 level is the most difficult to measure accurately.

The data measures for 3/4 height show little correspondence with the models. We see no preference in the data for blue– shifted profiles. Numerous data points fall outside of the model domain entirely. The disagreement between models and data becomes even more striking at 1/2 level. The data show little preference for redshift or blueshifts while the models strongly favour redshifts. The best agreement is seen at the lowest 1/4 level where models and data favour redshifted profiles. Still there are a large number of profiles that show properties that fall outside of the domain of the models. The models strongly favour red asymmetries while the data show a distribution more symmetric around zero except for eight extremely asymmetric points. Even these

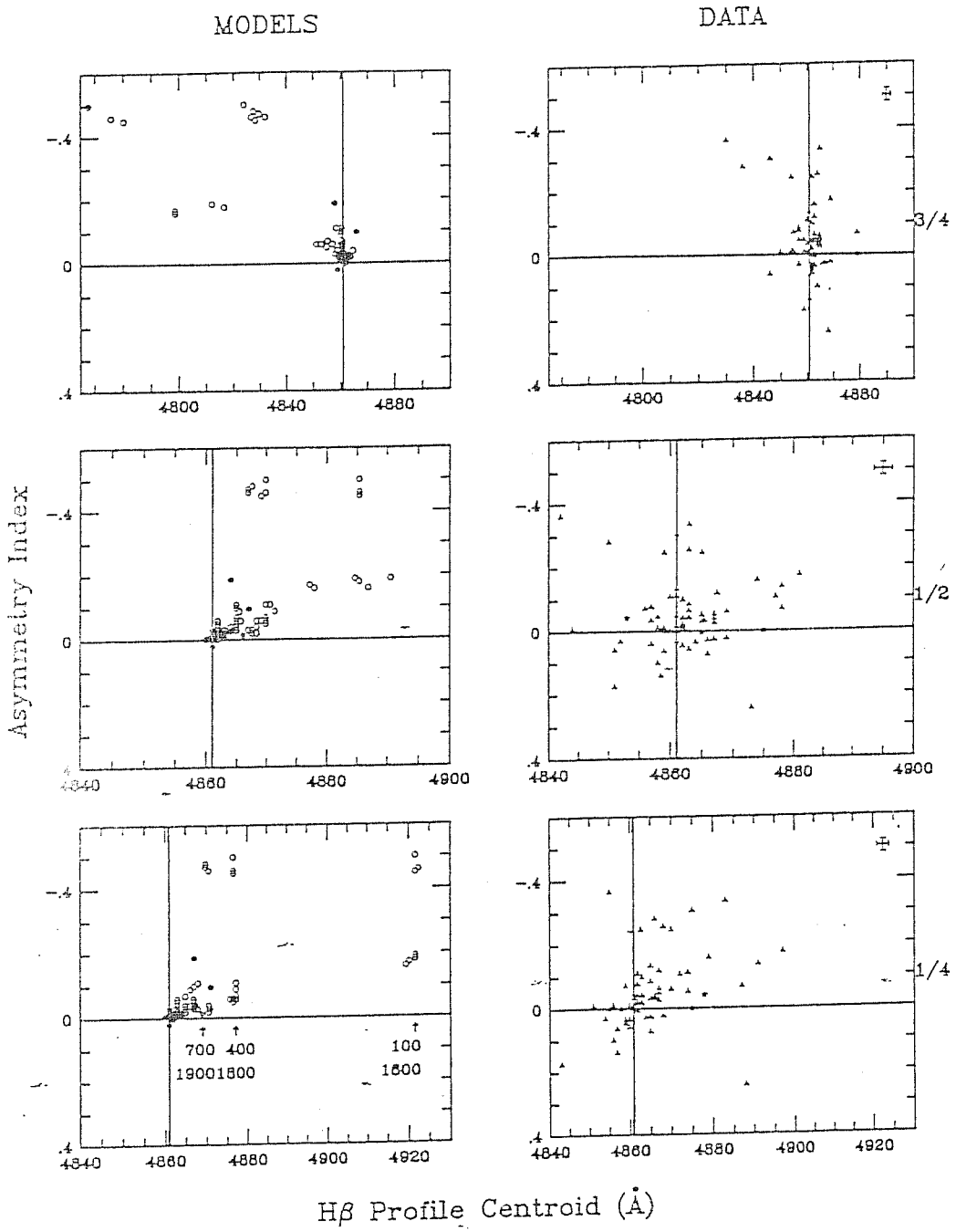

Figure 4.8: *A comparison of model predictions* (left column) *and observations* (right column – *1 σ error bars in upper right corners) for the Hβ profile. The abscissae are profile centroids in Ångstroms, and the ordinates are profile asymmetry index. The first, second and third rows present the comparison at 3/4, 1/2, and 1/4 profile height respectively. Models were derived from Chen and Halpern (1989)* (open circles), *and Collin–Souffrin and Dumont (1989)* (filled circles). *A random and representative set of disk inclinations and radii were used. The data sample was taken from Sulentic (1989). Vertical axis corresponds to rest wavelength for Hβ).*

extremely asymmetric profiles show equal numbers of red and blue centroid shifts.

The sample of Sulentic (1989) showed a tendency for the mean profile centroid to become increasingly redshifted as one goes from line peak to the base, a result, at first glance, consistent with the idea that the relatively blue peak of the profile is Doppler boosted and that the base is gravitationally redshifted. This was mostly the effect of a few outlier pulling the mean of the distribution to the red or blue. Removal of the outliers from the calculation of the means reveal a possible profile redshift of about 100 $km\ s^{-1}$at all profile heights (Sulentic, 1989). The distribution of centroids near the base of the profiles (1/4 maximum), however, reveals only a small number of cases where the redshift is similar to that for Arp 102B. 75 % of the Sulentic (1989) sample shows a measurable shift; redshifts are only slightly more common than blueshifts. Blueshifts close to 2000 $km\ s^{-1}$are observed. The mean for the full width at quarter maximum distribution of 61 profiles is 4865.1 Å, which corresponds to $\approx$ 200 $km\ s^{-1}$ redshift. The lack of bimodality in the centroid distribution (ignoring the eight extremely asymmetric profiles) suggests that a single *stochastic* process is responsible for shifts. Disk emission models would be forced to invoke at least two mechanism conspiring to produce the single smooth distribution of shift that is observed. If the *extreme* sample were the second disk–emitting population, we would expect profiles of class AR,B (in the system used by Sulentic, 1989) to be the most common, which is not observed. Ruling out a disk origin for the LIL emission in most AGN reinstates the problem of the kinematic difference between the HIL and LIL BLR regions. Accepting a disk origin for all, or most, of the nonblueshifted (at C(1/2) and C(1/4)) profiles raises the question of how the blueshifted ones arise. The existence of the blueshifts and blue asymmetries among so many LIL profiles must be considered a challenge to any model attributing the emission to an accretion disk.

The above results answer a question raised in Sulentic (1989). All basic profile types, symmetric (S), red or blue asymmetric (AR or AB), and *double–horned* show red and blue displacements. Profiles of type SB, AB, and AB,R or B, as defined there (representing respectively, asymmetric profile with blue asymmetric unshifted profiles and blue asymmetric profile with redshift or blue shift are virtually forbidden by the disk models. Other possibilities have been proposed to account for the complex, broad, double–horned or asymmetric profiles including (1) binary black holes Gaskell (1983a), and (2) conical or jet like configurations (Zheng *et al.*, 1991) for the BLR. The problem still remains in explaining a data distribution that, at this point, almost equally favors redshifted and blueshifted single peaked profiles. One possibility – not considered in the previous sections – is that the shift phenomenon arises by some other external mechanism. Such an effect would be necessary to resurrect a disk model for 3C390.3 (assuming the shift is the only impediment). One could then argue that the line shifts were due to some external cause while the profile shape was determined by the disk kinematics. An explanation for the blue profile asymmetries would also have been found. Wolf (1987) and Wolf *et al.* (1989) have shown that correlations in the fluctuations of a source distribution function can produce line shifts. This induced partial coherence could arise either directly from correlations between the elementary radia-

tors (BLR clouds?) or through a scattering process (in the NLR?). This mechanism is attractive because it could provide redshifts and blueshifts independent of the AGN kinematics. It also produces shifts that are of the order or less than the line width which is generally observed. A disadvantage of the mechanism is that the shifts would be frequency dependent. Another is, obviously, the lack of a mechanism for generating the required fluctuation in source or surrounding medium. Recent work (James *et al.*, 1990) suggests that appropriate scattering functions can be found in anisotropic radiation fields that result in frequency independent shifts. This results brings to mind the increasing evidence for both collimated particle and radiation fields in AGN. The existence of significant numbers of both red and blue profile shifts, with both blue and red asymmetries is surely one of the biggest challenges to the models of the BLR, and for any disk model in particular.

4.5 A more extended classification

As outlined in Chapter 1, densely and evenly sampled observations of Balmer line profiles would allow to solve for the velocity field of the BLR. The observational effort needed to obtain the two dimensional transfer function is however so large that it will be limited to a few objects. Useful informations could be gained extending the scheme by Sulentic (1989), using line parameters that (1) can be easily measured for a large number of objects; (2) different kinematical models occupy different regions in parameter space, and (3) variation in the line profiles can be effectively described by variations in the line parameters. A preliminary analysis (Marziani *et al.*, 1991) suggest that the following parameters are suitable: (1) the line peak radial velocity, which can give an indication of the entire line displacement; (2) a *global* asymmetry parameter defined as: flux on the red side minus flux on the blue side of the line divided by the total flux; (3) global curthosis parameter, defined as the flux emitted above the half maximum intensity divided by the flux below; (4) *blue* and *red* curthosis parameter, as at point (3), but evaluated for the *blue* and *red* part of the profile. These parameters are rather well suited for revealing, for instance, a variation of the intensity of the line core or of the intermediate line wings due to the switching on of a disk component.

This chapter has been based on the following works:

1. Marziani P., Calvani M., Sulentic J.W.: *Twin Peaks: IC 4329a and Akn 120.* Submitted for publication in the *Astrophysical Journal*, 1991.

2. Marziani P., Calvani M., Sulentic J.W.: *Observations of AGN with peculiar and very broad emission line profiles: OQ 208*, contributed paper presented at the meeting *Physics of the Active Galactic Nuclei*, held in Heidelberg, June 3–7, 1991. *In press.*

3. Sulentic J.W., Calvani M., Marziani P., Zheng W.: *Implications of Arp 102b: line emission from an accretion disk?*, *Astrophysical Journal* **355**, L15 (1990).

Chapter 5

The Effect of Anisotropic Emission from Thick Accretion Disks on the Luminosity Functions of AGN

Abstract – High-luminosity AGNs powered by accretion onto a massive black hole (or other compact object) may have bolometric luminosities dominated by thermal emission from a geometrically thick accretion disk. Radiation from these disks is strongly anisotropic, which has important consequences for the observed luminosity distribution, and therefore for systematic biases in flux-limited samples. We calculate the effect of anisotropic emission from an ensemble of AGN with randomly oriented thick disks radiating at or near the Eddington limit. Because of their higher luminosities, we predict face-on disks should constitute an increasing fraction of observed high redshift, high luminosity AGN. Comparison of our results with observed quasar luminosity functions suggests a narrow mass distribution with an upper limit of $\lesssim 10^9 M_\odot$ *for high redshift quasars.*

5.1 Introduction

It is well known that at accretion rates approaching the Eddington limit ($\dot{M}_{Edd} = \mathcal{L}_{Edd}/c^2$) the *standard* theory of accretion disks is no longer appropriate and possibly geometrically thick accretion disks should be considered (e.g., Frank *et al.* , 1985). In the past few years thick accretion disks have been actively investigated (see Abramowicz *et al.* 1987 for references) though they are not yet completely understood; remaining problems include the apparent arbitrariness of their angular momentum distribution, their unknown internal structure, and their stability properties. Nevertheless some basic properties can be stated:

1. thick disks can radiate above the Eddington luminosity by large factors (at least the radiation-supported disks can),

2. the largest fraction of the luminosity is radiated from the surface of a funnel around the rotation axis, the flux being highly anisotropic (Abramowicz, Calvani, and Nobili 1980), and

3. the hottest emission (UV and X–ray) originates in the funnels, partly because temperature increases with decreasing radius and partly because of reflection effects at the funnel walls (Madau 1988).

There is considerable circumstantial evidence in support of thick accretion disks in AGN (see Calvani *et al.* , 1989 for a recent review). Fits of thin accretion disk models to AGN spectral energy distributions suggest that the most luminous quasars are accreting at or above the Eddington limit (e.g., Sun and Malkan 1989). A similar conclusion was reached by Padovani (1989) based on the velocity of the broad-line clouds at a distance derived from photoionization models. Anisotropic radiation from the central engine in AGN, as evidenced by cones of ionizing radiation (Wilson *et al.* 1988; Tadhunter *et al.* 1989; Chambers *et al.* 1987; McCarthy, Spinrad, and van Breugel 1989), might be produced by a geometrically thick accretion disk (Acosta Pulido *et al.* 1990).
The consequences of anisotropic emission from thick accretion disks are analogous to the case of relativistic beaming (Urry and Shafer 1984, Urry and Padovani 1991); indeed, some unified schemes invoke both thick, obscuring torii and relativistic beaming simultaneously (e.g., Wills and Browne 1986, Barthel 1989). However, there are some important differences. First, the anisotropy is generally weaker for disks, with a face-on to edge-on enhancement of only a factor of ~ 20 rather than $\gtrsim 1000$. Among other things, this means there is less variation in observed properties like equivalent widths of lines, so that these properties can be traced continuously through the full range of orientation. Second, at an angle corresponding to the opening angle of the funnel in a thick disk, the rate of change of observed luminosity with angle greatly exceeds that for beaming (at any angle), making effects near that critical angle even more pronounced. Third, the radiation is not blueshifted, although for a given mass and disk size the peak emitted frequency depends on inclination.
It is important to take anisotropic radiation into account. Although one can define *post facto* samples based on intrinsic or isotropic properties, the selection effects on any flux-limited sample have already occurred. Once these effects have been specified quantitatively, working with flux-limited samples is straightforward.
In this Chapter we consider the effects of anisotropic emission from thick disks alone, in order to characterize and quantify the effect. Specifically, we examine the influence of orientation on the observed luminosity functions of high-luminosity AGN, and the consequences for flux-limited surveys. In § 5.2 we calculate the distribution of observed bolometric luminosities for an ensemble of accretion disks radiating at or above their Eddington limits, and with random orientations with respect to the observer. This is a general prescription appropriate to arbitrary populations of high-luminosity AGN (arbitrary distributions of central masses). In §5.3 we apply the calculation to two specific examples of AGN, Seyfert galaxies and radio-quiet quasars. (Radio-loud objects are excluded in order to minimize the importance of special relativistic effects from

radio jets.) In §5.4 we discuss our results and summarize the conclusions.

5.2 Method of Calculation

For a given intrinsic luminosity, the observed luminosity from thick accretion disks varies strongly with inclination angle. The effect on the observed luminosity function can be calculated from the dependence of L_{obs} on inclination plus the intrinsic distribution of Eddington luminosities (or equivalently, the distribution of central masses).

The dependence of observed bolometric luminosity on θ, the angle between the axis of the disk and the line of sight, was described by Madau (1988), who calculated the emergent spectrum from a thick, toroidal, super-Eddington accretion disk. The published calculation refers to a specific set of black hole and disk parameters: black hole mass $M = 10^8 M_\odot \equiv M_8$, ratio of gas pressure to total pressure in the disk $\beta = 3\times10^{-4}$, inner and outer disk radii $2.7r_g$ and $500r_g$ where r_g is the Schwarzschild radius, and specific angular momentum per unit mass with a power law radial dependence, $l(r) \propto r^{2-q}$. (The index of the latter is calculated self-consistently, and depends mainly on the outer radius of the disk.) For this case, the Eddington luminosity and dimensionless mass accretion rate are $\mathcal{L}_{Edd} = 4\pi GMm_p c/\sigma_T \sim 1.4\times10^{46} M_8$ ergs/s and $\dot{m} \equiv \dot{M}/\dot{M}_{Edd} \sim 100$, respectively, where $\dot{M}_{Edd} \equiv \mathcal{L}_{Edd}/c^2$.

The $L(\theta)$ appropriate for these parameters is plotted in Figure 9 of Madau (1988). It can be approximated by two functions: a shallow, cosine-function decrease at small angles ($\theta \lesssim 18°$) and an exponential decline at larger angles:

$$\frac{L(\theta)}{\mathcal{L}_{Edd}} = \begin{cases} Acos(\theta) & 0 \le \theta \le \theta_0, \\ Be^{-C\theta} & \theta_0 \le \theta \le \frac{\pi}{2}, \end{cases} \tag{5.1}$$

where the values for the constants are $A = 23.15$, $B = 51.78$, $C = 2.802$, and $\theta_0 = 17.42°$, and of course the function is continuous at $\theta = \theta_0$: $L(\theta_0)/\mathcal{L}_{Edd} = Acos(\theta_0) = Be^{-C\theta_0} = 22.09$.

This parameterization is essentially independent of $\mathcal{L}_{Edd}$, or (M); it depends only on the ratio of r_{out}/r_{in} (Abramowicz *et al.* , 1980). If the absolute size of the disk scales with mass (fixed r_{out}/r_{in}), the functional form of the angular dependence of bolometric luminosity (Eq. 5.1) will be scale-free. The angular momentum law will also be practically scale-free, since it depends primarily on the dimensionless outer radius (Madau 1988). The angular dependence of luminosity in a given wavelength band does vary with mass so we defer that problem for the moment.

If the thick accretion disks are randomly oriented on the sky, then the probability of observing a particular bolometric luminosity for a given Eddington luminosity $\mathcal{L}$ is $P(L_{obs}|\mathcal{L}) = P(\theta)\frac{d\theta}{dL_{obs}} = d(cos\theta)/dL_{obs}$. For convenience, we use L and $\mathcal{L}$ (dropping the subscripts) to represent the observed and Eddington luminosities, respectively, and

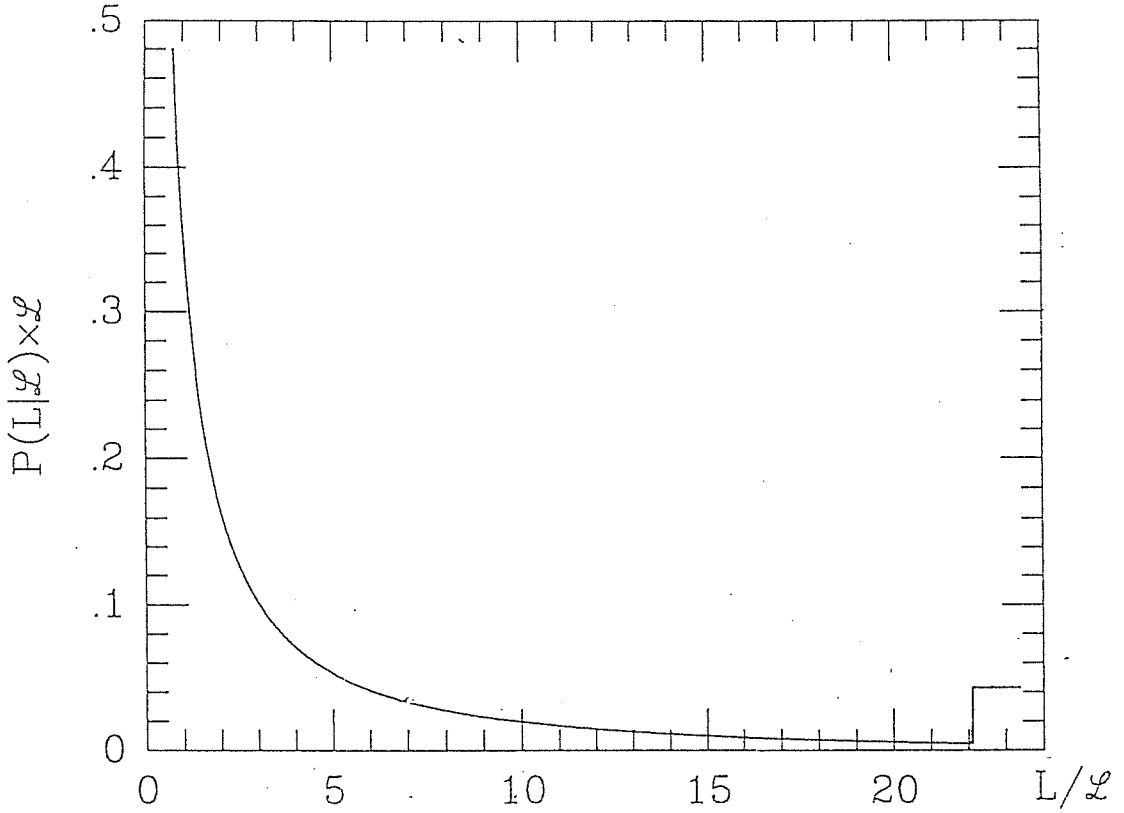

Figure 5.1: *The conditional probability, $P(L|\mathcal{L})$, of observing luminosity L given intrinsic Eddington luminosity $\mathcal{L}$, for radiation from a thick accretion disk (Eq. 5.2). The quantity $P(L|\mathcal{L}) \times \mathcal{L}$ is plotted as a function of L.*

we define $R_0 \equiv L(\theta_0)/\mathcal{L} = 22.09$ and $R_{min} \equiv L(\frac{\pi}{2})/\mathcal{L} = 0.6350$. Then

$$P(L|\mathcal{L}) = \begin{cases} \dfrac{1}{C\mathcal{L}} \sin\left[\dfrac{1}{C}\ln\left(\dfrac{L}{B\mathcal{L}}\right)\right] , & R_{min} \leq \dfrac{L}{\mathcal{L}} \leq R_0, \\ \dfrac{1}{A\mathcal{L}} , & R_0 \leq \dfrac{L}{\mathcal{L}} \leq A. \end{cases} \tag{5.2}$$

This function, shown in Figure 5.1, changes value discontinuously at θ_0, and is appreciable only at large angles ($L < L(\theta_0)$), where the solid angle is large, and at $\theta < \theta_0$ ($L > L(\theta_0)$), where the inside of the funnel suddenly becomes visible. These are therefore the preferred orientations; not surprisingly, the probability of finding the face-on configuration, where the luminous interior of the funnel dominates, is enhanced.
Given the intrinsic distribution of Eddington luminosities, $\Phi_{intr}(\mathcal{L})$, or equivalently the distribution of black hole masses, the observed luminosity distribution will be:

$$\Phi_{obs}(L) = \int d\mathcal{L} P(L|\mathcal{L}) \Phi_{intr}(\mathcal{L}(M)), \tag{5.3}$$

assuming all the emitted luminosity comes from the disk. This is not an unreasonable assumption for quasars, which have most of their bolometric luminosity in a large ultraviolet excess (e.g., Malkan 1983).

Table 1. Cases for Integration Limits

Case	Relative Values of Observed Luminosity	Relevant Regime
(i)	$L_{min} < L_1 < L_2 < L_3 < L_4 < L_{max}$	$1 < \frac{\mathcal{L}_2}{\mathcal{L}_1} < \frac{A}{R_0}$
(ii)	$L_{min} < L_1 < L_2 < L_4 < L_3 < L_{max}$	$1 \lesssim \frac{\mathcal{L}_2}{\mathcal{L}_1} \leq \frac{R_0}{R_{min}}$
(iii)	$L_{min} < L_2 < L_1 < L_4 < L_3 < L_{max}$	$\frac{R_0}{R_{min}} \leq \frac{\mathcal{L}_2}{\mathcal{L}_1} \leq \frac{A}{R_{min}}$
(iv)	$L_{min} < L_2 < L_4 < L_1 < L_3 < L_{max}$	$\frac{A}{R_{min}} \leq \frac{\mathcal{L}_2}{\mathcal{L}_1}$

The integral in Eq. 5.3 is straightforward to calculate providing one takes proper account of the integration limits, which depend on the relative values of $L_{min} \equiv R_{min}\mathcal{L}_1$, $L_1 \equiv R_{min}\mathcal{L}_2$, $L_2 \equiv R_0\mathcal{L}_1$, $L_3 \equiv R_0\mathcal{L}_2$, $L_4 \equiv A\mathcal{L}_1$, and $L_{max} \equiv A\mathcal{L}_2$, where $\mathcal{L}_1$ and $\mathcal{L}_2$ are the minimum and maximum values of the $\Phi_{intr}(\mathcal{L})$ under consideration. The four possible cases and the regions in which they are important are listed in Table 1. In practice, the first case pertains to an unrealistically small ratio of $\mathcal{L}_2/\mathcal{L}_1 \equiv M_2/M_1$ (~ 1) and the third to a rather restricted range of values, $34.7 < M_2/M_1 < 36.4$. The second and fourth cases are most likely, referring to narrow ($1.04 < M_2/M_1 < 34.7$) and broad ($M_2/M_1 > 36.4$) distributions of masses, respectively.

5.3 Results

In the previous section we outlined the effect of anisotropic emission from luminous thick accretion disks on the observed bolometric luminosity function. In order to illustrate our results, which must be calculated numerically from eq. 4.3, we consider two specific examples, Seyfert galaxies and radio-quiet quasars. The former are probably not radiating near the Eddington limit (*e.g.*, Padovani 1989) and so are unlikely to have thick accretion disks, but because their mass function has been estimated (Padovani *et al.* , 1990) the input to eq. 4.3 is not uncertain. Quasars, on the other hand, are more likely to have Eddington ratios near 1 and thick accretion disks, and so are more relevant for our purposes, but their mass function is unknown.

The mass distribution of Seyfert galaxies, based on a well-defined optically-selected sample, has recently been calculated by Padovani, Burg, and Edelson (1990). It can be approximated by the linear fit (neglecting their lowest mass point as it is due to a

single object):

$$\log \Phi(M) = 11.09 - 2.00 \times \log(\frac{M}{M_\odot}) \quad M_\odot^{-1}\ Gpc^{-3} \tag{5.4}$$

in the mass range $10^6 M_\odot < M < 10^8 M_\odot$. This is shown as a thin solid line in Figure 5.2, where mass has been converted to Eddington luminosity. The corresponding bolometric luminosity function after modification for the effects of anisotropic emission is shown as a thick solid line. For comparison, data representing the observed bolometric luminosity functions of Seyfert 1 galaxies ($z \lesssim 0.12$; filled circles), low-redshift quasars ($0.3 < z < 0.55$; open squares), and high-redshift quasars ($1.65 < z < 2.2$; filled squares) are also plotted. These were generated from the data of Cheng *et al.* (1985) and Boyle *et al.* (1987), respectively, using a bolometric correction appropriate to a power-law spectrum $F(\nu) = k\nu^{-\alpha}$ with $\alpha = 1$ from 100 μm to 20 keV. The assumed zero point flux for the B system was taken from Hayes and Latham (1975).

First we note that the input bolometric luminosity function (generated directly from the mass function) lies above the observed one by roughly a factor of 10. That is, they would agree very roughly for an Eddington ratio ~ 0.1 (this moves the function down and to the left), a result already implicit in the work of Padovani (1989). The computed luminosity function incorporating the effects of anisotropic emission from a thick disk (thick solid line) does not agree at all with the data regardless of Eddington ratio, which is not surprising since radiation-pressure-supported thick disks are unlikely for objects with low Eddington ratios.

To some extent the taxonomical distinction between broad-line Seyfert galaxies and quasars is arbitrary, especially at intermediate luminosities. The continuity of properties suggests they are related, perhaps in an evolutionary sense (the luminosity functions of Seyferts and low-redshift quasars are not very different; Boyle *et al.* 1987), or in some more parallel way (Cavaliere and Padovani 1988). In either case, quasars must accrete most of their mass at high redshifts (since that is where they are most luminous), and their mass function probably extends at least as far as that of Seyfert galaxies. Most estimates suggest masses $M \sim 10^{9-10} M_\odot$ and accretion rates $\dot{m} \gtrsim 1$ (Kriss 1988, Wandel and Mushotzky 1986, Cavaliere and Padovani 1988, Padovani 1989), based on broad-line widths, ultraviolet continuum spectra, etc., although these are highly uncertain because of a selection bias toward the high luminosity (and therefore high mass) quasars. Given these considerations, we tried approximating the quasar mass function with the Seyfert mass function extrapolated to higher masses by an order of magnitude. The extrapolation (dotted line) and the corresponding computed luminosity function (dot-dash line) are shown in Figure 5.2.

This extrapolated mass function does not match the quasar data at all; it spans much too wide a range, suggesting the assumed mass function is too broad. Nevertheless, this first calculation can be used to illustrate one of the results of this Chapter, the increasing fraction of face-on sources with increasing luminosity (Fig. 5.4a). The face-on orientation becomes important only at the highest luminosities, $\log L \gtrsim \log \mathcal{L}_2 = 45.42$, where the funnel begins to contribute, and reaches 50% (equal numbers of visible

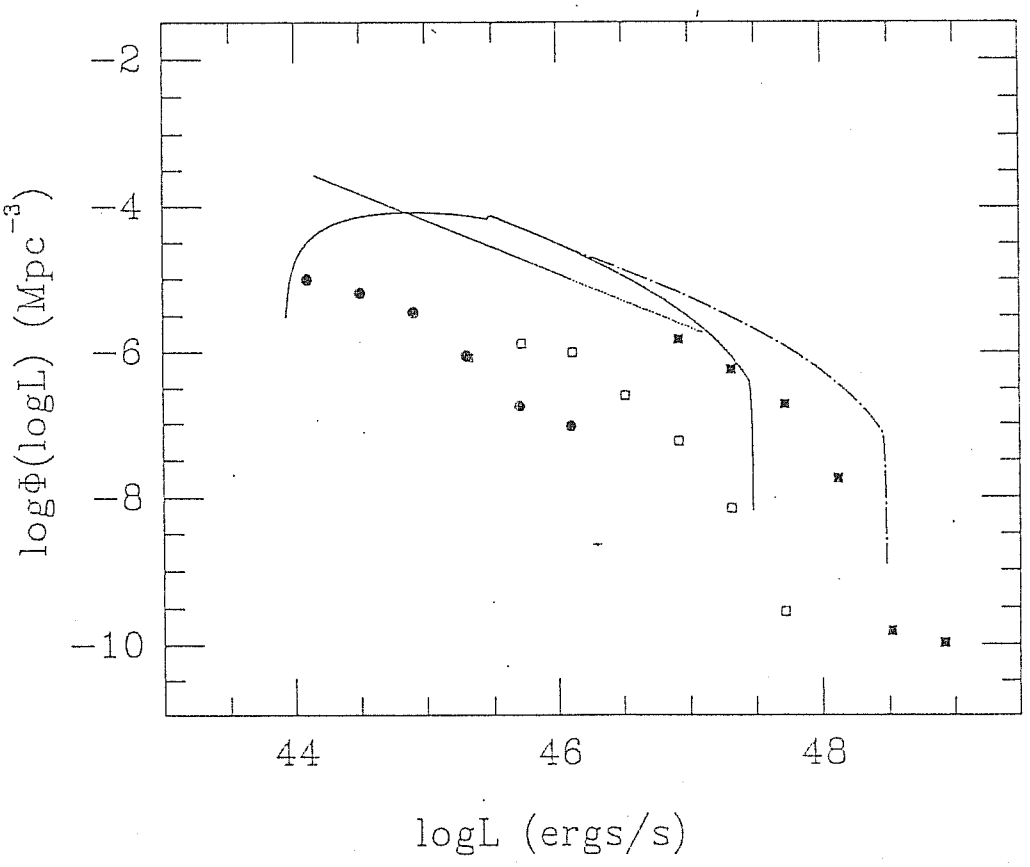

Figure 5.2: *The predicted bolometric luminosity distribution function (thick solid curve) for radiation from an ensemble of randomly oriented thick accretion disks with Eddington ratios equal to 1 and intrinsic bolometric luminosity functions described by a power law of slope 2 between* 1.3×10^{44} *and* 1.3×10^{46} *ergs/sec (thin solid line). The ordinate is shown as* $\log \Phi(\log L) = 2.303\ L\ \Phi(L)$ *vs.* $\log L$. *The dotted line shows the extension of the intrinsic luminosity function to* 1.3×10^{47} *ergs/sec and the dash-dot line the consequent extension of the predicted luminosity function. For comparison, three sets of observed bolometric luminosity functions are shown: Filled circles — Seyfert galaxies* ($z \lesssim 0.12$) *from Cheng et al. (1985) ; Open squares — low redshift* ($0.3 < z < 0.55$) *quasars from Fig. 7a of Boyle et al. (1987); Filled squares — high redshift* ($1.65 < z < 2.2$) *quasars also from Fig. 7a of Boyle et al.*

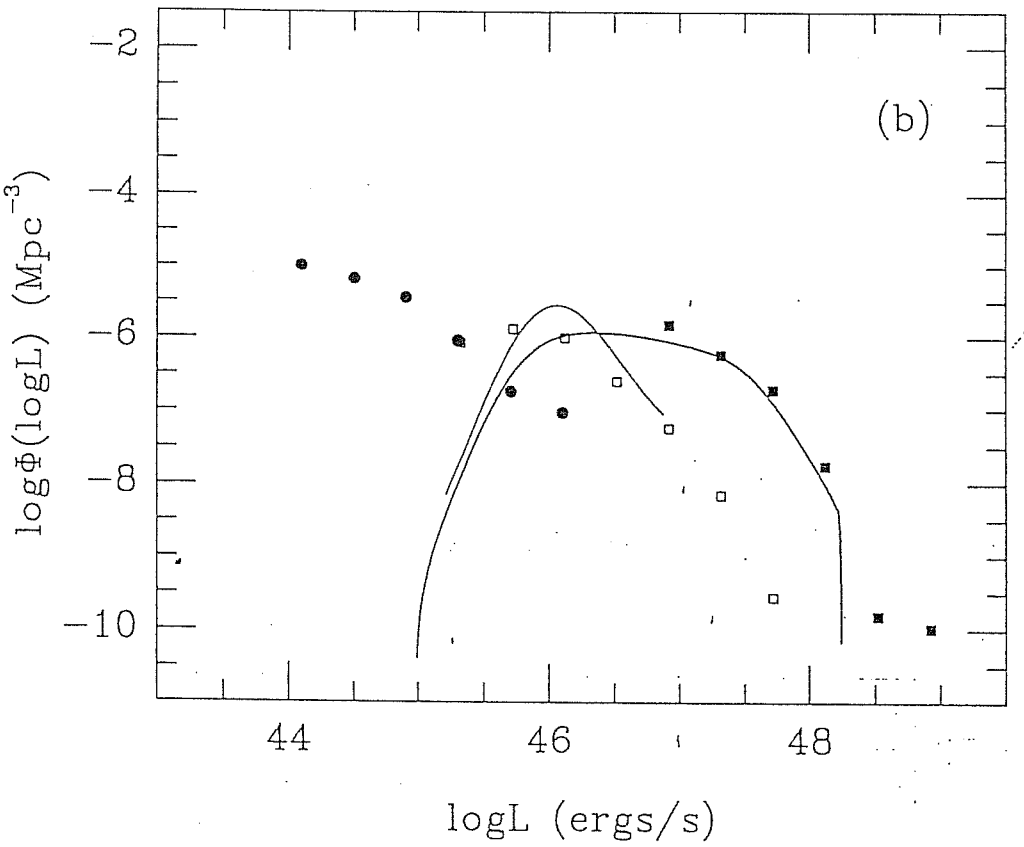

Figure 5.3: *Here the assumed intrinsic luminosity function (thin solid line) is a Gaussian given by Eq. 5.5 with M converted to $\mathcal{L}$, with peak luminosity 10^{46} ergs/sec and with $\sigma = 0.6$ between 1.5×10^{45} and 7.5×10^{46} ergs/sec. This gives a predicted bolometric luminosity function (thick solid line) that agrees well with the data for high redshift quasars (filled squares; all data as in Fig. 5.2)*

and invisible funnels) at $\log L \sim 47.3$. Disks at larger angles ($\theta > \theta_0$), for which the funnel interior is not seen and the observed luminosity is sub-Eddington, dominate at most luminosities because of the large solid angle available to inclined orientations. Matching the observed bolometric luminosity function of quasars seems to require a peaked or steep mass function. We tried a Gaussian function of the form

$$\log \Phi(M) = a_1 \exp\left[-\frac{(\log(\frac{M}{M_\odot}) - (\log(\frac{M_C}{M_\odot}))^2}{2\sigma^2}\right] - a_2 \quad M_\odot^{-1}\ Gpc^{-3}, \qquad (5.5)$$

where M_C is the central mass. The best fit to the observed high-redshift quasar data is obtained for $M_C = 7 \times 10^7 M_\odot$, distribution width $\sigma = 0.6$, integration limits $M_1 = 1.1 \times 10^7 M_\odot$ and $M_2 = 5.4 \times 10^8 M_\odot$, and normalization constants $a_1 = 3.4$ and $a_2 = 5.9$. The results are not terribly sensitive to the exact values of these constants

or the integration limits; indeed, only the half of the curve above the peak is really important, so most significant are the value of M_C and the fact that the small σ means the Gaussian function has a steep slope.

The input luminosity function corresponding to this mass distribution is shown in Fig. 5.3 as a thin solid line. As before, the observed bolometric luminosity function (thick solid line), incorporating the effects of anisotropic emission, is broader and extends to higher luminosities than the intrinsic bolometric distribution derived from the input mass function. In effect, the distribution of angles permits this range of luminosities. It reproduces quite well the break in the quasar luminosity function (which depends on the mass at which the Gaussian becomes steep) and the steep high-luminosity slope (which reflects the slope of the Gaussian).

The fraction of face-on sources again increases markedly at high luminosities, as shown in Fig. 5.4b. The funnel becomes visible at $\log L \sim 47$, and the fraction exceeds 50% for $\log L \gtrsim 47.9$. These orientations should dominate any high-redshift, flux-limited sample. Since only the highest luminosity sources are seen at high redshift, and since $L/\mathcal{L} \sim 20$ for face-on sources, we predict that objects in the steep part of the quasar luminosity function are almost all face-on.

It is interesting to note the contrast in mass functions implied by our results. As long as the Eddington ratio is ~ 1, the quasar mass function that we have derived is lower in number density (by roughly an order of magnitude), higher in mass, steeper, and narrower ($\sigma \approx 0.6$ compared to $\sigma \approx 1$) than the Seyfert mass function of Padovani *et al.* , (1990). Also, for quasars in this redshift range, the implied upper limit to the mass function is $\log M \sim 5 \times 10^8 M_\odot$ (see also Cavaliere and Padovani 1988), substantially lower than one would infer from equating the observed luminosity to the Eddington luminosity, by the factor of ~ 20, as already implicit in the results of Madau (1988). The mass function appropriate to the low-redshift quasars, derived in the same way, is a Gaussian centered at $L_C = 7.3 \times 10^{43}$ ergs/sec, with width $\sigma = 0.6$ and limits between 2.0×10^{43} and 7.3×10^{44} ergs/sec.

5.4 Discussion and Conclusion

If quasars are powered by accretion and if they radiate the bulk of their luminosity as thermal emission from a thick accretion disk, then orientation effects are important. Besides affecting observational characteristics in individual objects, they distort the perceived number density. This should be an important effect for quasars, which are among the highest luminosity AGN and which are thought to have large Eddington ratios.

The results of § 5.3 imply that the preferred orientation will change systematically with luminosity in flux-limited samples, biasing quasar samples toward systems with $\theta \lesssim \theta_0$, particularly at the highest luminosities, where systems will be preferentially face-on. The details may change for other accretion disk models if $L(\theta)$ differs, but this general result will be unchanged.

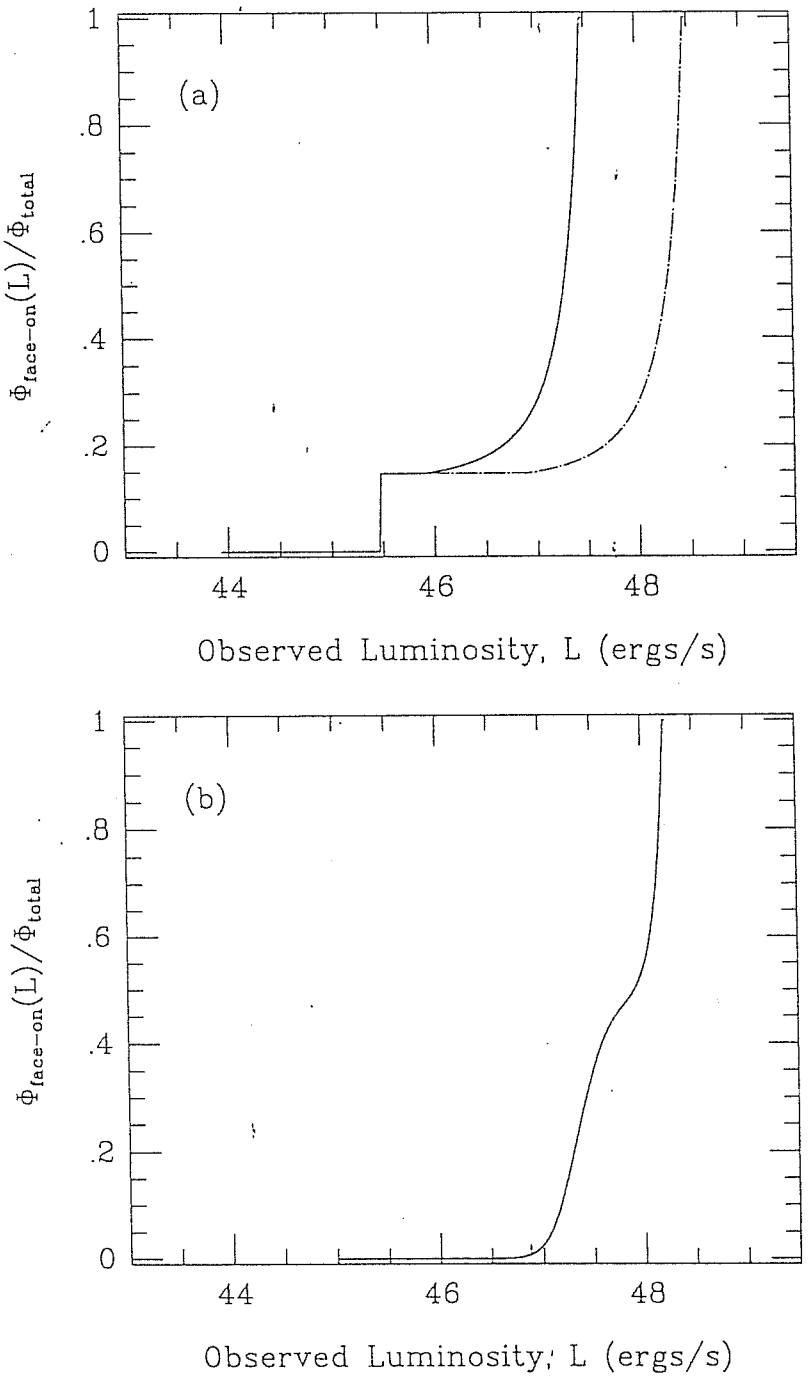

Figure 5.4: *The fraction of pole–on sources as a function of observed luminosity for (a)the calculations in Fig. 5.2, and (b)the calculation in Fig. 5.3. At high luminosities, face-on sources will dominate flux-limited samples.*

Some constraints on the mass function of high-redshift quasars can be gained from a comparison between the computed luminosity function and the data. The predicted luminosity function of anisotropic emitters is always broader and extends to higher luminosities than the intrinsic mass function. For a sharply peaked Gaussian centered near $7 \times 10^7 M_\odot$ and cut off at $M{=}5 \times 10^8 M_\odot$, the predicted luminosity function reproduces nicely the break in the high-redshift quasar luminosity function. (A steep power law would give similar results. For low-redshift quasars, the inferred mass function has a similar shape but lower mean mass.) Above the break, we predict that most quasars should be face-on. A range in Eddington ratio would broaden this break more than is observed, so if our model is correct, the range in Eddington ratio cannot be large. Similarly, a flat power-law mass function like that of Seyfert galaxies would produce a break that is not so sharp (Fig. 5.2), and can be excluded within the context of our model.

The fitted Gaussian mass function also predicts the luminosity function cutoff at low luminosities to be about half a decade below currently observed luminosities of high redshift objects (Fig. 5.3), which can be tested with deeper surveys. If the luminosity function extends to lower luminosities, the mass function must then extend to lower masses with a relatively flat curve.

The calculation presented here is meant to be suggestive of the importance of the orientation of thick accretion disks. Even for thin disks, if they puff up at the inner edge (e.g., Czerny and Elvis 1987), the sense of the present results will be the same (ignoring General Relativistic effects). We have deferred consideration of a number of important selection effects, most notably the wavelength dependence of the luminosity enhancement, that will influence any flux-limited sample, especially important since flux limits always apply to a specific waveband rather than to the bolometric luminosity. Proper treatment of the wavelength-dependent $L_\nu(\theta)$ involves a more complicated calculation because the functional form changes with mass. As it is, the intrinsic mass function is really not known for most classes of AGN. However, the wavelength-dependent effects should be, if anything, more pronounced (compare Figs. 7 and 9 of Madau 1988), so that our most important conclusion — that the highest luminosity [radio-quiet] AGN are heavily biased toward low-inclination systems — will still hold.

This chapter is based on the following paper:

1. C.M. Urry, P. Marziani, M. Calvani: 1991, *The effect of Anisotropic Emission from Thick Accretion Disks on the Luminosity Function of AGN*, *Astroph. J.***371**, 510.

Chapter 6

Final remarks

The way in which the accretion flow can reach the nucleus of a galaxy is strictly related to mechanisms operating on galactic scale. These mechanisms ultimately involve conditions on the structure and dynamics of galaxies which may control birth and evolution of AGN. We have shown that there is a strong excess of interacting systems among Seyfert galaxies. This evidence, together with theoretical considerations, is an indication that interaction with a nearby companion is able to trigger gravitational instabilities which may lead to the *lighting* of nuclear activity. Another important effect of interaction is the strong enhancement of the star formation rate in the nuclei and in the disks of interacting galaxies. Less clear is whether interaction, Starburst and Seyfert activity can be linked in an evolutionary scenario. The connection between interaction and Starburst is now well founded, both on an observational (more than half of Starburst galaxies are interacting; evidence of extreme star formation in merging galaxies), and a theoretical basis. Numerical simulations confirm that interaction is able to drive gas to a distance of ~ 100 *pc* from the nucleus. A link between Starburst and Seyfert type activity is appealing because mass loss from evolving high mass stars can provide either the matter supply to build up a massive black hole or fuelling matter if the black hole has been already formed (Norman and Scoville, 1988; Scoville and Norman, 1988).

The results of Wilson (1987), McKenty (1989), and Kollatschny and Fricke (1989) and our discussion on NGC 7592 suggest that interaction *may* act more direcly in enhancing the Star formation rate rather than in triggering the nuclear activity. The occurrence of AGN activity may be delayed because of the time needed for the gas to loose its residual angular momentum at $\lesssim 100$ *pc* from the very center of the galaxy, or, for the time needed to form a massive black hole. The case of NGC 7592 suggest that the accretion flow is driven at a wide range of radii. The latter explanation seems thus better suited to explain the low luminosity of the AGN in NGC 7592.

The phenomena occurring in the inner few hundred *pc* from the nucleus, that is in the NLR, are poorly known. The strong radiation field of the active nucleus, as well as presence of radio emitting plasma, the possibility of winds driven by supernovae, add many complications, and gas could be swept away rather than be accreted by the

nucleus, particularly in the latest stages of Starburst and of nuclear activity.

We have presented results on the gas kinematics of NGC 7592, suggesting that transfer of matter between the two main components of the system is taking place, a possibility early foreseen by Toomre and Toomre (1972). Probably, several galaxies of the Arp atlas are also experiencing transfer of matter from a gas rich companions, since they show filamentary structures connecting the central regions of one galaxy with the outer region of the companion. We have remmarked that the semibroad component of the [OIII]$\lambda\lambda$4959,5007 lines is probably due to gas ultimately infalling toward the central core of NGC 7592 A. The semibroad component gives rise to a strong redward asymmetry, which is not commonly observed. Observations of red asymmtries in the narrow lines – once thought to be rare – have been now widely found (Busko and Steiner, 1989), but it unclear at present whether they can be generally used as evidence of infall.

In order to set up an evolutionary sequence between Starburst and AGN in interacting intermediate objects an *age* indicator is needed. A comparison between N–body simulations aimed to reproduce the morphology and the aspect of observed paired interacting galaxies should provide a timing as well as an estimate of the orbital parameter of the encounter. In a suitable sample of interacting galaxies, one could study the location of the star formation site, the gas kinematics, any inner isophotal distortion in the near infrared, and the occurrence of non–thermal activity. Further indicators for the age of the Starburst (presence of absorption lines, shape of the radio continuum, Hα EW, chemical composition *etc.* can provide additional valuable information. It should be interesting to direct this search onto a sample of nearby Seyfert galaxies which are interacting and undergoing a burst of star formation. A great observational effort for each system (comparable to that needed for NGC 7592) is however necessary in order to reach the scientific goals.

Turning to the ultimate manifestation of the accretion flow, that is the accretion disk, our preliminary results do not favour the possibility that the *entire* flux of Balmer lines are emitted from the accretion disk itself. This is probably true at least as far as simple models for the line emitting disk are concerned. However, the similarity of the profiles of Akn 120 and IC 4329a implies that a reproducible phenomenon is taking place, and hence that the velocity field should be ordered. On the basis of energetic conciderations, we suggest that continuum radiation should be backscattered by medium located near the inner edge of the disk or even above the disk in order to be able to emit at least part of the low ionization lines. Although we can not reach a definite conclusion, we suggest that the study should be extended to a large sample of Seyfert galaxies and BLRG, applying the parametric scheme outlined at the end of Chapter 4. This would allow a tighter comparison between theory and observation without unaffordable requirements of telescope time. Recent results on profile variability rule out *pure* radial motions, but favour a composite BLR radially moving component plus a disk contribution. A point which may help to reveal the disk contribution is related to the wavelength shift between HIL and LIL. The shift has been studied only for intermediate redshift quasars, and it should be further studied separtely for Seyfert galaxies, BLRG and low–

redshift quasars. A difficulty is that HIL are in the far UV, unaccessible from space observations. IUE spectra have a large uncertainty in the wavelenght scale and a poor wavelength resolution, and are therefore not suitable for a study of this kind. Only the *Faint Object Spectrograph* mounted on Hubble Space Telescope offers the needed resolution and spectral coverage. An extensive study of wavelength shifts would help to an additional emission component which may introduce strong asymmetries in the line profiles, and hence mask the possible disk contribution.

References

Abramowicz M.A., Calvani M., Nobili L.: 1980, *Astrophys. J.* **242**, 772

Abramowicz, M., Calvani, M., and Madau, P. 1987, *Comments Astrophys.*, **12**, 67.

Acosta–Pulido J.: 1990, *Ph. Thesis, SISSA, Trieste*

Acosta–Pulido J., Perez–Fournon I., Calvani M., Wilson A.S.: 1989, *Astrophys. J.* **365**,

Adams T.F.: 1977, *Astrophys. J. Supp.* **33**, 19

Alloin D., Boisson C., Pelat D.: 1988, *Astron. Astroph.* **200**, 17

Angel J.R.P., Stockman H.S.: 1980, *Ann. Rev. Astron. Astroph.* **18**, 321

Antonucci R.R.J.: 1983, *Nature* **303**, 358

Antonucci R.R.J., Cohen R.D.: 1983, *Astrophys. J.* **271**, 564

Antonucci R.R.J., Miller J.S.: 1985, *Astrophys. J.* 297, 621

Arkhipova V.P., Afanas'ev V.L., Dostal' V.A., Zasov A.V., Karachentsev I.D., Noskova R.I.: 1979, *Soviet Astron.***25**, 277

Bailey M.E.: 1980, *M. N. R. astr. Soc.* **191**, 195

Bailey M.E.: 1982, *M. N. R. astr. Soc.* **200**, 247

Baldwin J.A., Phillips M.M., Terlevich R.: 1981, *Publ. Astr. Soc. Pac.* **93**, 5

Baldwin J.A., Wilson A.S., Whittle M.: 1987, *Astrophys. J.* **319**, 84

Balzano V.A.: 1983, *Astrophys. J.* **286**, 602

Barnes J.: 1988, *Astrophys. J.* **331**, 699

Barthel, P. D. 1989, *Astroph. J.*, **336**, 606.

Barthel P.D.: 1991, in *Physics of Active Galactic Nuclei*, Proceedings of the Conference held in Heidelberg, June 3–7, 1991. (Berlin: Springer), *in press*

Bechtold J., Czerny B., Elvis M., Fabbiano G., Green R.F.: 1987, *Astrophys. J.* **314**, 699

Binette L., Dopita M.A., Tuohy I.R.: 1985, *Astrophys. J.* **297**, 476

Binette L., Robinson A., Courvoisier T. J.-L.: 1988, *Astron. Astrophys.* **194**, 65

Binney J., Tremaine S.D.: 1987, *Galactic Dynamics.* (Princeton: Princeton University Press)

Blaes O.M.: 1987, *M. N. R. astr. Soc.* **227**, 975

Blandford R.D., McKee Chr. F.: 1982, *Astrophys. J.* **255**, 419

Blumenthal G.R., Mathews W.G.: 1975, *Astrophys. J.* **198**, 517

Blumenthal G.R., Mathews W.G.: 1975, *Astrophys. J.* **198**, 517
Blumenthal G.R., Mathews W.G.: 1979, *Astrophys. J.* **233**, 479
Boyle, B. J., Fong, R., Shanks, T., Peterson B. A.: 1987, *M. N. R. astr. Soc.* **227**, 717
Bregman J.: 1991, in *Variability of active galactic nuclei*, H.R Miller and P.J. Wiita (Eds.). (Cambridge: Cambridge University Press), p.1
Boroson T.D.: 1989, *Astrophys. J. Letters* **349**, L9
Browne I.W.A., Clark R.R., Moore P.K., Muxlow T.W.B., Wilkinson P.N., Cohen M.B., Porcas R.W.: 1982, *Nature* **299**, 788
Burbidge G.R., Burbidge E.M., Prendergast: 1960, *Astroph. J.* **131**, 282
Burstein D., Heyles C.: 1984, *Astroph. J. Suppl. Ser.* **54**, 33
Bushouse H.: 1987, *Astrophys. J.* **320**, 49
Busko I.C., Steiner J.E.: 1989, *Mon. Not. Royal Astr. Soc.* **238**, 1479
Byrd G.G., Valtonen M.J., Sundelius B., Valtaoja L.: 1986, *Astron. Astrophys.* **166**, 75
Byrd G.G., Sundelius B., Valtonen M.J.: 1987, *Astron. Astrophys.* **171**, 16
Calvani M., Marziani P., Padovani P.: 1989, in *Proceedings of the VIII Italian Conference on General Relativity and Gravitational Physics*, (Singapore: World Sci.). M. Cerdonio *et al.* (Eds.), p. 102.
Cavaliere, A., Padovani, P.: 1988, *Astrophys. J. Letters* **333**, L33.
Chambers, K. P., Miley, G., van Breugel, W. 1987: *Nature*, **329**, 604
Chen K., Halpern J.P.: 1989, *Ap. J.* **344**, 115
Chen K., Halpern J.P, Filippenko A.V.: 1989 *Astroph. J.* **263**, 79
Cheng, F. Z., Danese, L., De Zotti, G., Franceschini, A.: 1985, *M. N. R. astr. Soc.* **212**, 857
Clavel *et al.*: 1987, *Astrophys. J.* **321**, 251
Clavel J., Santos-Lleo M.: 1990, *Astron. Astrophys.* **230**, 3
Clavel *et al.*: 1990, *M. N. R. astr. Soc.* **246**, 668
Clavel *et al.*: 1991, *Astrophys. J.* **366**, 64
Cohen R.D.: 1983, *Astrophys. J.* **273**, 489
Cohen R.D., Rudy R.J., Puetter R.C., Ake T.B., Foltz C.B.: 1989, *Astrophys. J.* **311**, 135
Cohen R.D., Osterbrock D.E.: 1981, *Astrophys. J.* **234**, 81
Colgate S.A., Cameron A.G.W.: 1963, *Nature* **200**, 870
Collin-Souffrin S.: 1986, *Astron. Astrophys.* **166**, 115
Collin-Souffrin S.: 1987, *Astron. Astrophys.* **179**, 60
Collin-Souffrin S., Dumont A.M.: 1989, *Astron. Astrophys.* **213**, 29
Collin-Souffrin S., Dumont A.M.: 1990a, *Astron. Astrophys.* **229**, 292
Collin-Souffrin S., Dumont A.M.: 1990b, *Astron. Astrophys. Suppl. Ser.* **83**, 71
Collin-Souffrin S., Dumont A.M., Heidman J., Joly M.: 1980, *Astron. Astrophys.* **83**, 110
Collin-Souffrin S., Dumont A.M., Tully J.: 1982, *Astron. Astrophys.* **106**, 362
Collin-Souffrin S., Joly M., Pequignot D., Dumont S.: 1986, *Astron. Astrophys.* **166**, 27

Collin–Souffrin S., Dyson J.E., Mc Dowell J.C., Perry J.J.: 1988, *M. N. R. astr. Soc.* **322**, 539
Collin–Souffrin S., Lasota J.-P.: 1988, *Publ. Astron. Soc. of Pacific* **100**, 1041
Combes F.: 1987, in *Starburst and Galaxy evolution.* Editions Frontieres. T.X. Thuan, T. Montmerle, J. Tran Thanh Van (Eds.), p. 313
Combes F., Gerin M.: 1985, *Astron. Astrophys.* **150**, 327
Condon J., Condon M., Gisler G., Puschell J.: 1982, *Astrophys. J.* **252**, 102
Corbin M.R.: 1991, *Astrophys. J.* **371**, L51
Corbin M.R., Baldwin J.A., Wilson A.S.: 1988, *Astrophys. J.* **334**, 584
Corvoisier T.J.L., Clavel J:, 1991, in *Structure and Emission properties of accretion disks*, IAU Coll. No. 129. C.Bertout *et al.* (Eds.), p.75
Czerny B, Elvis M. : 1987, *Astrophys. J.* **321**, 305
Dahari O.: 1984 *Astron. J.* **89**, **966**
Dahari O.: 1985, *Astron. J.* **90**, 1772
Dahari O., de Robertis M.M.: 1988a, *Astroph. J. Suppl. Ser.* **67**, 249
Dahari O., de Robertis M.M.: 1988b, *Astroph. J.* **331**, 727
Davidson K., Netzer H.: 1979, *Review of Modern Physics* **51**, 715
de Bruyn A.G.: 1980, *Highlights of Astronomy* **5**, 631
De Robertis M.: 1985, *Astrophys. J.* **289**, 67
De Robertis M.: 1987, *Astrophys. J.* **316**, 597
Disney M.J.: 1973, *Astroph J.*, **181**, 55
Dopita M.A., Evans I.N.: 1986, *Astroph. J.***307**, 431
Dressler, A: 1989, in: *Active Galactic Nuclei*, IAU Symposium No. 134. D.E. Osterbrock and J.S. Miller (Eds.) , p.217
Dumont A.M., Collin Souffrin S.: 1990a, *Astron. Astrophys.* **229**, 302
Dumont A.M., Collin Souffrin S.: 1990b, *Astron. Astrophys.* **229**, 313
Edelson R.A., Krolik J.H.: 1988, *Astrophys. J.* **333**, 646
Elitzur M., Netzer H.: 1985, *Astrophys. J.* **291**, 464
Elmegreen D.M., Elmegreen B. G., Bellin A.D.: 1991, *Astrophys. J.* **364**, 415
Espey B.R. *et al.*: 1989, *Astrophys. J.* **342**, 666
Fabian A.C., Rees M.J., Stella L., White N.E.: 1989, *Mon. Not. Royal Astr. Soc.* **238**, 729 **77**, 75
Feldman F.R., Weedman D.W., Balzano V.A., Ramsey L.W.: 1982, *Astroph. J.* **256**, 427
Ferland G.J., Korista K.T., Peterson B.M.: 1990, *Astrophys. J. Letters* **363**, 121
Ferland G.J., Netzer H.: 1983, *Astroph. J.* **264**, 105
Ferland G.J., Shields G.A.: 1985, in: *Astrophysics of Active Galaxies and Quasi-Stellar Objects* Mill Valley: University Science Books. J.S. Miller (Ed.), p. 157
Filippenko A.V.: 1988, *Adv. Space Res.* **8**, 5
Filippenko A.V.: 1989, *Astron. J.* **97**, 726
Foltz C.B., Peterson B.M., Capriotti E.R., Byard P.L., Bertram R., Lawrie D.G.: 1981, *Astroph. J.* **250**, 508
Foltz C.B., Wilkes B.J., Peterson B.M.: 1983, *Astron. J.* **88**, 1072

Fosbury *et al.*: 1991, in *Physics of Active Galactic Nuclei*, Proceedings of the Conference held in Heidelberg, June 3–7, 1991. (Berlin: Springer), *in press*
Frank J., King A.R., Raine D.J.: 1985, *Accretion Power in Astrophysics.* (Cambridge:Cambridge University Press).
Frank J., Rees M.: 1976, *M. N. R. astr. Soc.* **176**, 633
Fricke K.J., Kollatschny R.F.:1989, *Astron. Astroph. Suppl. Ser.* **77**, 75
Fried J.W., Schulz H.: 1983, *Astron. Astrophys.* **118**, 166
Fuentes-Williams T., Stocke J.: 1988, *Astron. J.* **96**, 1235
Gaskell C.M.: 1981, *Astrophys. J.* **251**, 8
Gaskell C.M.: 1982, *Astrophys. J.* **263**, 79
Gaskell C.M.: 1983a, *Astrophys. J. Letters* **267**, L1
Gaskell C.M.: 1983b, in *Proc. Liège Conference on Quasars and Gravitational Lenses* (Liège: Institut d'Astrophysiques), p.473
Gaskell C.M.: 1985, *Nature* **315**, 386
Gaskell C.M.: 1988, in: *Active Galactic Nuclei*, Proceedings of the Conference held at Atlanta, Georgia, on October 28–30, 1987. H.R. Miller, P.J. Wiita (Eds.) , p. 61
Gaskell C.M., Sparke L.S.: 1986, *Astrophys. J.* **305**, 175
Gehrz R.D., Sramek R.A. Weedman D.W.: 1983, *Astrophys. J.* **267**, 551
Gerin M., Combes F., Athanassoula E.: 1990, *Astron. Astrophys.* **230**, 37
Goldreich P., Goodman J., Narayan R.: 1986, *M. N. R. astr. Soc.* **221**, 339
Grandi S.A.: 1983, *Astrophys. J.* **268**, 591
Grandi P., Tagliaferri G., Giommi P., Barr P., Palumbo G.C.G.: 1991, *Astrophys. J. submitted*
Gregory S., Ptak R., Stoner R.: 1982, *Astrophys. J.* **261**, 30
Guilbert P.W., Rees M.J.: 1988, *M. N. R. astr. Soc.* **233**, 475
Gunn J.: 1979, in *Active Galactic Nuclei*, C.Hazard and S. Mitton (Eds.), p. 213. (Cambridge: Cambridge University Press).
Haniff C.A., Wilson A.S., Ward M.J.: 1988, *Astrophys. J.* **334**, 104
Halpern J.P.: 1990, *Astrophys. J. Letters* **365**, L51
Halpern J.P., Grindlay J.E.: 1980, *Astrophys. J.* **242**, 1041
Halpern J.P., Filippenko A.V.: 1988, *Nature* **331**, 46
Harwit M., Pacini F.: 1975, *Astroph. J.* **200**, L127
Hayes, D. S., and Latham, D. W. A. 1975, *Ap. J.*, **197**, 535.
Hearnquist L.: 1989, *Nature* **340**, 687
Heckman T.M.: 1982, *Astroph. J.* **268**, 602
Heckman T.M.: 1983, *Astrophys. J.* **268**, 628
Heckman T.M.: 1987 in *Starburst and Galaxy evolution.* Editions Frontieres. T.X. Thuan, T. Montmerle, J. Tran Thanh Van (Eds.), p. 381
Heckman T.M. Armus L., Miley G.K.: 1987, *Astron. J.* **92**, 276
Heckman T.M., Armus L., Miley G.K.: 1990, *Astrophys. J. Supp.*74, 833
Heckman T.M., Lebofky M.J., Rieke G.H., van Breugel W.: 1983, *Astrophys. J.* **272**, 400

Holt S.S., Mushotzsky R.F., Becker R.M., Boldt E.A., Serlemitsos, P.J., Szymkowiak A.E., White N.E.: 1980, *Astrophys. J.* **241**, L13

Holt S.S *et al.*: 1990, in *Proceeding of the 23rd ESLAB Symposium on Two Topics in X-ray Astronomy*, Bologna, Italy Sept. 13–20, 1989, p.1105

Hummel E., Pedlar A., van der Hulst J.M., Davies R.D.: 1985, *Astron. Astroph. Suppl.* **60**, 293

Horne W.D., Welsh W.F.: 1991, in *Variability of active galactic nuclei*, H.R Miller and P.J. Wiita (Eds.). (Cambridge: Cambridge University Press), p.332

Hutchings J.B., Crampton D., Campbell B.: 1984, *Astrophys. J.* **280**, 41

Iye M., Ulrich M.H.: 1986, *Astroph. Space Sci.* **118**, 523

Jackson Browne I.W.A.: 1991a, *M. N. R. astr. Soc.* **250**, 414

Jackson Browne I.W.A.: 1991b, *M. N. R. astr. Soc.* **250**, 422

James D., Savedoff M., Wolff E.: 1990, *Astroph. J.* **359**, 67

Jones T.W., O'Dell S.L., Stein W.A.: 1974, *Astrophys. J.* **188**, 353

Jones T.W., Stein W.A.: 1990, *Astrophys. J.* **349**, 443

Joseph R., Wright G.: 1985, *M. N. R. astr. Soc.* **214**, 87

Karashentsev I.D.: 1972, *Catalogue of Isolated pairs of galaxies in northern emisphere. Soobshch. Spets. Astrfiz. Obs.* **7**, 3

Keel W.C.: 1987, in *Star Formation in Galaxies*, Proceeding of a conference held at Caltech, Pasadena, June 16–19, 1986. C.J. Lonsdale–Persson (Ed.), p.661

Keel W.C., Kennicutt R.C., Hummel E., van der Hulst J.: 1985, *Astron. J.* **90**, 708

Kennicutt R.C.: 1983, *Astrophys. J.* **272**, 54

Kennicutt R.C., Roettiger K.A., Keel W.C., van der Hulst J.M¿, Hummel E.: 1987, in *Star Formation in Galaxies*, Proceeding of a conference held at Caltech, Pasadena, June 16–19, 1986. C.J. Lonsdale–Persson (Ed.), p.401

Kennicutt R.C.: 1990, in *Paired and Interacting Galaxies*, IAU Coll. No. 124, J.W. Sulentic, W.C. Keel, C.M. Telesco (Eds.), p.269

Kennicutt R.C., Kent S.M.: 1983, *Astron. J.* **88**, 1094

Kennicutt R.C. Jr., Keel W.C.: 1984, *Astroph. J.* **279**, L5

Kennicutt R.C., Keel W.C., Van der Hulst J.M., Hummel E., Roettiger K.A.: 1987, *Astron. J.* **93**, 1011

Kennicutt R.C. Jr., Keel W.C., Blaha C.A.: 1989, *Astron. J.* **97**, 1022

Kollatschny W., Fricke : 1989, *Astron. Astrophys.* **219**, 34

Koratkar K.T., Gaskell C.M.: 1990, *Astrophys. J.* **345**, 637

Koratkar K.T., Gaskell C.M.: 1991, in *Variability of active galactic nuclei*, H.R Miller and P.J. Wiita (Eds.). (Cambridge: Cambridge University Press), p.339

Kriss, G. 1988, *Ap. J.*, **324**, 809.

Krolik J.H.: 1988a, in: *Active Galactic Nuclei*, Proceedings of the Conference held at Atlanta, Georgia, on October 28–30, 1987. H.R. Miller, P.J. Wiita (Eds.) , p.19

Krolik J.H.: 1988b, *Astrophys. J.* **325**, 148

Krolik J.H.: 1989, in: *Active Galactic Nuclei*, IAU Symposium No. 134. D.E. Osterbrock and J.S. Miller (Eds.) , p.285

Krolik J.H., Begelman M.C.: 1986, *Astrophys. J. Letters* **308**, L55

Krolik J.H., Begelman M.C.: 1988, *Astrophys. J.* **329**, 702
Krolik J.H., Kallman T.R.: 1988, *Astrophys. J.* **324**, 714
Krolik J.H., McKee Chr. F., Tarter C.B.: 1981, *Astrophys. J.* **249**, 422
Kruper J.S., Urry C.M., Canizares C.R.: 1990, *Astrophys. J. Supp.***74**, 347
Kundt W.: 1987, in *Astrophysical Jets and their engines.* W.Kundt (Ed.). (Dordrecht: Reidel), p. 1.
Kwan J.: 1984, *Astrophys. J.* **283**, 70
Kwan J., Krolik J.H.: 1979, *Astrophys. J. Letters* **233**, L91
Kwan J., Krolik J.H.: 1981, *Astrophys. J.* **250**, 478
Laor A.: 1990, *M. N. R. astr. Soc.* **246**, 369
Laor A., Netzer H.: 1989, *M. N. R. astr. Soc.* **238**, 897
Larson R., Tinsley B.: 1978, *Astrophys. J.* **219**
Larson R.B., Tinsley B.M., Caldwell C.N.: 1980, *Astroph.J.* **237**, 692
Lawrence A.: 1987, *Publ. Astron. Soc. of Pacific* **99**, 309
Lawrence A., Rowan-Robinson M., Leech K., Jones D.M.P., Wall J.: *Mon. Not. Royal Astr. Soc.* **249**, 329
Lightman A.P., White T.R.: 1988, *Astrophys. J.* **335**, 57
Lonsdale C.J., Persson S.E., Matthews K.: 1984, *Astroph. J.* **287**, 95
Madau P.: 1988, *Astrophys. J.* **327**, 116
Malkan M.A.: 1983, *Astrophys. J.* **268**, 582
Malkan M.A.: 1991, in *Structure and Emission properties of accretion disks*, IAU Coll. No. 129. C.Bertout *et al.* (Eds.), p.165
Malkan M.A., Sargent W.L.W.: 1982, *Astrophys. J.* **254**, 22
Maoz D., Netzer H.: 1989, *M. N. R. astr. Soc.* **236**, 21
Maoz D., *et al.*: 1991, *Astrophys. J. Letters* **351**, L75
Mardaljevic J., Raine D.J., Walsh D.: 1988, *Astroph. Lett. Communications* **26**, 357
Markarian B.E., Lipovetskii V.A., Stepanyan D.A.: 1977, *Astrophysics* **13**, 116
Marziani P.: 1989, *Magister Thesis, SISSA, TS*
Marziani P., Calvani M., Sulentic J.W.: 1991a, *Astrophys. J. submitted*
Marziani P., Calvani M., Sulentic J.W., Zheng W.: 1991b, *in preparation*
Mathews W.G.: 1982, *Astrophys. J.* **258**, 425
Mathews W.G.: 1986, *Astrophys. J.* **305**, 187
Mathews W.G., Blumenthal G.R.: 1977, *Astrophys. J.* **214**, 10
Mathews W.G., Capriotti E.R.: 1985, in: *Astrophysics of Active Galaxies and Quasi-Stellar Objects* Mill Valley: University Science Books. J.S. Miller (Ed.), p.185
Mathews W.G., Ferland G.J.: 1987, *Astrophys. J.* **323**, 456
Mathews W.C., Wrampler J.: 1985, *Publ. Astron. Soc. of Pacific* **97**, 966
Mazzarella J., Balzano V.A.: 1986, *Astroph. J. Suppl. Ser.* **62**, 751
McCarthy, P. J., Spinrad, H., and van Breugel, W. 1989, in: *Active Galactic Nuclei*, IAU Symposium No. 134. D.E. Osterbrock and J.S. Miller (Eds.) 543
Miley G.K., Miller J.S.: 1979, *Astrophys. J.* **228**, L55
Miley G.K., Neugebauer G. Soifer B.T.: 1985, *Astrophys. J.* **293**, L11

Miller J.S.: 1988, in: *Active Galactic Nuclei*, Proceedings of the Conference held at Atlanta, Georgia, on October 28–30, 1987. H.R. Miller, P.J. Wiita (Eds.) , p.112
Miller J.S., Antonucci R.R.J.: 1983, *Astrophys. J. Letters* **271**, L7
Miller J.S., Goodrich R.W.: 1990, *Astrophys. J.* **355**, 456
Miller J.S., Goodrich R.W., Mathews W.G.: 1991, *Astrophys. J. in press*
Miller J.S., Mathews W.G.: 1972, *Astroph. J.* **172**, 593
Miller J.S., Peterson B.M.: 1990, *Astrophys. J.* **361**, 98
Miller R.H., Smith B.F.: 1980, *Ap. J.* **235**, 421
Morris S.L., Ward M.J.: 1988, *Mon. Not. Royal Astr. Soc.* **230**,
Morris S.L., Ward M.J.: 1989, *Astrophys. J.* **340**, 723
Mushotzky R.F.: 1982, *Astrophys. J.* **256**, 92
Mushotzky R.F.: 1988, in: *Active Galactic Nuclei*, Proceedings of the Conference held at Atlanta, Georgia, on October 28–30, 1987. H.R. Miller, P.J. Wiita (Eds.) , p.239
Mushotzky R., Ferland G.J.: 1984, *Astrophys. J.* **278**, 558
Ne'eman Y.: 1965, *Astroph. J.* **141**, 1303
Netzer H.: 1982, *M. N. R. astr. Soc.* **198**, 589
Netzer H.: 1985a, *Astrophys. J.* **289**, 451
Netzer H.: 1985b, *M. N. R. astr. Soc.* **216**, 63
Netzer H.: 1987, *M. N. R. astr. Soc.* **225**, 55
Netzer H.: 1991, in *Structure and Emission properties of accretion disks*, IAU Coll. No. 129. C.Bertout *et al.* (Eds.), p.177
Netzer H., Elitzur M., Ferland G.J.: 1985, *Astrophys. J.* **299**, 752
Netzer *et al.*: 1990, *Astrophys. J.* **351**, 108
Noguchi M.: 1987, *M. N. R. astr. Soc.* **218**, 635
Noguchi M.: 1988, *Astron. Astrophys.* **203**, 259
Noguchi M., Isibashi S.: 1986, *M. N. R. astr. Soc.* **219**, 307
Norman C.A., Silk J.: 1983, *Astrophys. J.* **266**, 502
Norman C.A., Scoville N.Z.: 1988, *Astrophys. J.* **332**, 124
Oke J.B.: 1987, in *Superluminal Radio Sources*, Ed. J. Zensus and T. Pearson (Cambridge: Cambridge University Press), p. 267 **230**, 353
Olson K.M., Kwan J.: 1990, *Astrophys. J.* **361**, 4
Orr M.J.L., Browne I.W.A.: 1982, *M. N. R. astr. Soc.* **200**, 1067
Osterbrock D.E.: 1977, *Astrophys. J.* **215**, 733
Osterbrock D.E.: 1978, *Phys. Scripta* **17**, 137
Osterbrock D.E.: 1979, *Astron. J.* **84**, 901
Osterbrock D.E.: 1981, *Astrophys. J.* **246**, 696
Osterbrock D.E.: 1985, in: *Astrophysics of Active Galaxies and Quasi-Stellar Objects* Mill Valley: University Science Books. J.S. Miller (Ed.), p. 111
Osterbrock D.E.: 1989, *Astrophysics of Gaseous Nebulae.* (Mill Valley: University Science Books)
Osterbrock D.E., Cohen R.: 1979, *MNRAS* **187**, 61p
Osterbrock D., Koski A., Phillips M.: 1976, *Astroph. J.* **206**, 899
Ostriker J.P., Peebles P.J.E.: 1973, *Astrophys. J.* **168**, 467

Padovani, P. 1989: *Astron. Astrophys.* **209**, 27.
Padovani P., Rafanelli P.: 1988, *Astron. Astrophys.* **205**, 53
Padovani, P., Burg, R., and Edelson, R.: 1990, *Astrophys. J.* **353**, 438
Papaloizou J.C., Pringle J.E.: 1984, *M. N. R. astr. Soc.* **208**, 221
Pelat D., Alloin D.: 1982, *Astron. Astrophys.* **105**, 335
Penston M.V.: 1991, in *Variability of active galactic nuclei*, H.R Miller and P.J. Wiita (Eds.). (Cambridge: Cambridge University Press), p.343
Penston M.V., Perez E.: 1984, *M. N. R. astr. Soc.* **211**, 33P
Perez E.: 1987, *Ph.D. Thesis* (P87)
Perez E., Penston M.V., Tadhunter C., Mediavilla E., Moles M.: 1987 *M. N. R. astr. Soc.* **230**, 353
Perola G.C., Piro L., Altamore A., Fiore F., Boksenberg A., Penston M.V., Snijders M.A.J., Bromage G.E., Clavel J., Elvius A., Ulrich M.-H.: 1986, *Astrophys. J.* **306**, 508
Piro *et al.*: 1991, in *Variability of active galactic nuclei*, H.R Miller and P.J. Wiita (Eds.). (Cambridge: Cambridge University Press), p.
Peterson B.M.: 1987, *Astrophys. J.* **312**, 79
Peterson B.M.: 1988a, in: *Active Galactic Nuclei*, Proceedings of the Conference held at Atlanta, Georgia, on October 28–30, 1987. H.R. Miller, P.J. Wiita (Eds.) , p. 38
Peterson B.M.: 1988b, *Publ. A. S. P.* **100**, 18
Peterson B.M., Ferland G.J.: 1986, *Nature* **324**, 345
Peterson B.M., Foltz C.B., Byard P.L., Wagner R.M.: 1982, *Astrophys. J. Supp.***49**, 469
Peterson B.M., Foltz C.B., Miller H.R., Wagner R.M., Crenshaw D.M., Meyers K.A., Byard P.L.: 1983, *Astron. J.* **88**, 926
Peterson B.M., Foltz C.B., Crenshaw D.M., Meyers K.A., Byard P.L.: 1984, *Astrophys. J.* **279**, 529
Peterson B.M., Korista K.T., Cota S.A.: 1987, *Astrophys. J.* **312**, L1
Peterson B.M., Meyers K.A., Capriotti E.R., Foltz C.B., Wilkes B.J., Miller H.R.: 1985, *Astrophys. J.* 292, 164
Peterson B.M., Reichert G.A., Korista K.T., R.M.: 1990, Astroph. J. **352**, 68
Phillips M.M.: 1978, *Astrophys. J. Supp.***38**, 187
Phinney E.S.: 1985, in: *Astrophysics of Active Galaxies and Quasi–Stellar Objects* Mill Valley: University Science Books. J.S. Miller (Ed.), p. 453
Pogge R.W.: 1988, *Astrophys. J.* **328**, 519
Pringle J.E.: 1981, *Ann. Rev. Astron. Astroph.* **19**, 137
Pringle J.E., Rees M.J., Pacholczyk A.G.: 1973, *Astron. Astrophys.* **29**, 179
Pritchet C., Monacki S.: 1982, *Publ. Astr. Soc. Pacific* **84**, 733
Pronik I.: 1987, in: *IAU Symp. No. 121.* E. Ye. Khachikian, K.J. Fricke and J. Melnick (Eds.)., p. 169
Rafanelli P., Marziani P.: 1991a, *Astron. J., in press*
Rafanelli P., Marziani P.: 1991b, *Astron. j., submitted*

Rafanelli P., Marziani P., Birkle H., Thiele U.: 1991, *unpublished*
Raine D.J., Smith A.: 1981, *M. N. R. astr. Soc.* **197**, 339
Rees M.J.: 1984, *Ann. Review Astron. Astroph.* **22**, 471
Rees M.J.: 1991, in *Physics of Active Galactic Nuclei*, Proceedings of the Conference held in Heidelberg, June 3–7, 1991. (Berlin: Springer), *in press*
Reichert G.A., Mushotzky R.F., Petre R., Holt S.S.: 1985, *Astrophys. J.* **296**, 69
Rieke G.H.: 1987, in *Star Formation in Galaxies*, Proceeding of a conference held at Caltech, Pasadena, June 16–19, 1986. C.J. Lonsdale–Persson (Ed.), p.633
De Robertis M.M.: 1985, *Astron. J.* **90**, 998
De Robertis M.M., Shaw R.A.: 1988, *Astroph. J.* , 629
Robinson A., Binette L., Fosbury R.A.E., Tadhunter C.N.: 1987, *M. N. R. astr. Soc.* **227**, 97
Rodriguez–Espinosa J.M., Rudy R.J., Jones B.: 1987 *Astrophys. J.* **312**, 555
Rokaki E., Dumont A.M., Collin–Souffrin S.: 1991, *preprint*
Roos N.: 1981, *Astron. Astrophys.* **104**, 218
Rubin V.C., Burstein D., W.K. Ford Jr., Thonnard N.: 1984, *Astroph. J.* **289**, 81
Salpeter E.E.: 1964, *Astrophys. J.* **140**, 796
Sandage A.: 1961, *The Hubble Atlas of Galaxies.*
Sanders D.B., Phinney E.S., Neugebauer G., Soifer B.T., Matthews K.: 1989 *Astrophys. J.* **347**, 29
Sanders *et al.*: 1986, *Ap. J.* **305**, L45
Schmidt M.: 1963, *Nature Lond.* **197**, 1040
Schmidt M., Green R.: 1963, *Astrophys. J.* **269**, 352
Schulz H., Rafanelli P.: 1981, *Astron. Astroph.* **103**, 216 833
Schweizer : 1990, in: *Dynamics and Interaction of Galaxies.* Proceedings of the Conference held in Heidelberg, 29 May – 2 June, 1989. A.Toomre and R Wielen (Ed.), p.60
Scoville N.Z., Norman C.A.: 1988, *Astrophys. J.* **332**, 163
Seyfert C.: 1943, *Astrophys. J.* **97**, 28
Shakura N.I., Sunyaev R.A.: 1973, *Astron. Astrophys.* **24**, 337
Shields G.A.: 1978, in:*The Pittsburgh Conference on BL Lac Objects.* A.M. Wolfe (Ed.), p. 257
Shklovskii I.S.: 1960, *Soviet Astron.* 4, 885
Shapiro S.L., Teukolsky S.A.: 1985, *Astroph. J.* **298**, 58
Shlosman I.: 1990, in *Paired and Interacting Galaxies*, IAU Coll. No. 124, J.W. Sulentic, W.C. Keel, C.M. Telesco (Eds.), p.689
Shlosman I., Begelman M.C.: 1989, *Astrophys. J.* **341**, 685
Shlosman I., Frank J., Begelman M.C.: 1989, *Nature* **338**, 45
Shlosman I., Begelman M.C., Frank J.: 1990, *Nature* **345**, 679
Shuder J.M.: 1981, *Astrophys. J.* **244**, 12
Shuder J.M.: 1982, *Astrophys. J.* **259**, 48
Shull T.M., McKee C.F.: 1979, *Astroph. J.*, **178**, 623
Simkin S.M., Su H.J., Schwarz M.P.: 1980, *Astrophys. J.* **237**, 404

Soifer B.T., Houck J.R., Neugebauer G.: 1987, *Ann. Review Astron. Astroph.* **25**, 187
Smith H.E.: 1980, *Astrophys. J.* **241**, L137
Smith M.D., Raine D.J.: 1985, *M. N. R. astr. Soc.* **212**, 425
Stauffer J., Schild R., Keel W.C.: 1983, *Astrophys. J.* **270**, 465
Stella L.: 1990, *Nature* **344**, 747
Stirpe G.M.: 1989, *Ph.D. Thesis, Leiden University*
Stirpe G.M., de Bruyn A.G., Van Gröningen E.: 1988, *Astron. Astrophys.* **200**, 9
Stirpe G.M., de Bruyn A.G., Van Gröningen E.: 1989, *Astron. Astrophys.* **211**, 310
Stocke J.T.: 1978, *Astron. J.* **83**, 348
Stockton A.: 1982, *Astroph. J.* **257**, 33
Stockton A., McKenty J.W.: 1987, *Astrophys. J.* **316**, 584
Stockton A., Farnham J.: 1991, *Astrophys. J.* **371**, 525
Stone R.P.S.: 1977, *Astroph. J.* **218**, 767
Sulentic J.W.: 1976, *Astroph. J.* **213**, 327
Sulentic J.W.: 1989, *Astroph. J.* **343**, 54
Sulentic, J.W., Calvani, M., Marziani, P., and Zheng, W.: 1990, *Astrophys. J. Lett.* **355**, L15.
Sun W.–H., Malkan M.A.: 1989, *Astrophys. J.* **346**, 68
Tadhunter, C. N. *et al.*: 1989, *M. N. R. astr. Soc.* **235**, 403.
Tadhunter C.V., di Serego Alighieri S., Bland J., Danziger I.J., Goss W.M., McAdam W.B., Snijders M.A.: 1988, *M. N. R. astr. Soc.* **235**, 403
Tadhunter C.V., Tsvetanov Z.: 1989, *Nature* **341**, 422
Tarter C.B., Tucker W.H., and Salpeter E.E.: 1969, *Astrophys. J.* **156**, 943
Terlevich R., Melnick J.: 1981, *M. N. R. astr. Soc.* **195**, 839
Terlevich R., Melnick J.: 1985, *M. N. R. astr. Soc.* **213**, 841
Terlevich R., Melnick J., Moles M.: 1987, in: *IAU Symp. No. 121.* E. Ye. Khachikian, K.J. Fricke and J. Melnick (Eds.).497
Terlevich R., Melnick J.: 1988, *Nature* **333**, 239
Terndrup D., Lauer T.R., Stover R.J.: 1984, *Lick Obs. Tech. Rep.* No. 33
Thompson L.A.: 1981, *Astrophys. J. Letters* **244**, L43
Tohline J., Osterbrock D.E.: 1982, *Astroph. J. Lett.***252**, 49
Toomre A.: 1977, in *Evolution of Galaxies and Stellar populations*, B.M. Tinsley, R.B. Larson (Eds.), p. 401
Toomre A., Toomre J.: 1972, *Astrophys. J.* **178**, 623
Turner E.L.: 1976, *Astrophys. J.* **208**, 20
Turner T.J., Pounds K.A.: 1989, *M. N. R. astr. Soc.* **240**, 833
Turner T.J. T.J., Kunieda H., Mushotzsky R., Awaki H.: 1991, in *Variability of active galactic nuclei*, H.R Miller and P.J. Wiita (Eds.). (Cambridge: Cambridge University Press), p.260
Ulrich M.-H.: 1991, in *Structure and Emission properties of accretion disks*, IAU Coll. No. 129. C.Bertout *et al.* (Eds.), p.43
Ulrich M.-H., *et al.*: 1984, *M. N. R. astr. Soc.* **206**, 221

Ulrich M.-H., Altamore A., Boksenberg A., Bromage G., Clavel J., Elvius A., Penston M.V.: 1985, *Nature* **313**, 747 *M. N. R. astr. Soc.* **228**, 671
Ulvestad J.S.: 1982 *Astrophys. J.* **259**, 96
Ulvestad J.S., Wilson A.S.: 1984a, *Ap.J.* **278**, 544
Ulvestad J.S., Wilson A.S.: 1984b, *Ap.J.* **285**, 439
Ulvestad J.S., Wilson A.S.: 1989, *Astrophys. J.* **343**, 659
Urry C.M.: 1990, in *Multiwavelength Astrophysics*, F.Cordoba (Ed.), (Cambridge: Cambridge University Press), p. 249
Urry, C. M., and Padovani, P.: 1991, *Ap. J.*, in press
Urry, C. M. and Shafer, R. A.: 1984, *Ap. J.*, **280**, 569
van Gröningen E.: 1983, *Astron. Astrophys.* **126**, 363
de Vaucouleurs G., de Vaucouleurs A.: 1964, *2nd Reference Catalogue of Bright Galaxies.* Austin: The University of Texas Press.
Veilleux S., Osterbrock D.E.: 1987, *Astrph. J. Suppl. Ser.* **63**, 295
Veilleux S., Zheng W.: 1991a, *Astrophys. J. in press*
Veilleux S., Zheng W.: 1991b, in *Physics of Active Galactic Nuclei*, Proceedings of the Conference held in Heidelberg, June 3–7, 1991. (Berlin: Springer), *in press*
Veron-Cetty M.-P., Veron P.: 1985, ESO Sci. Report N. 4
Veron–Cetty M.–P., Veron P., Tarenghi M.: 1983, *Astron. Astrophys.* **119**, 69
Veron P., Veron M.–P., Bergeron J., and Zuidervijk E.J.: 1981, *Astron. Astroph.* **97**, 71
Vorontsov-Velyaminov B.: 1959, *Atlas and Catalogue of Interacting Galaxies*, Part I, Moscow University
Vorontsov-Veliaminov: 1979, *Astron. Astroph. Suppl. Ser.* **28**, 1
Wampler E.J., Gaskell C.M., Burke W.L., Baldwin J.A.: 1984, *Astrophys. J.* **276**, 403
Wandel A., Yahil A.: 1985, *Astrophys. J. Letters* **295**, L1
Wandel, A., and Mushotzky, R. F. 1986, *Ap. J. (Letters)*, **306**, L61.
Warwick R.S., Yaqoob T., Pounds K.A.: 1989, in: *Active Galactic Nuclei*, IAU Symposium No. 134. D.E. Osterbrock and J.S. Miller (Eds.) , p. 182
Weedman D.W.: 1983, *Astrophys. J.* **266**, 479
Weedman D.W.: 1987, in *Star Formation in Galaxies*, Proceeding of a conference held at Caltech, Pasadena, June 16–19, 1986. C.J. Lonsdale–Persson (Ed.), p.351
Whittle M.: 1985a, *Mon. Not. Royal Astr. Soc.* **213**, 1
Whittle M.: 1985b, *M. N. R. astr. Soc.* **213**, 33
Whittle M., Haniff C.A., Ward M.J., Meurs E.J.A., Pedlar A., Unger S.W., Axon D.J., Harrison B.: 1986, *M. N. R. astr. Soc.* **213**, 33
Whittle M., Pedlar A., Meurs E.J.A., Unger S.W., Axon D.J., Ward M.J.: 1988, *Astrophys. J.* **326**, 125
Wilkes B.: 1984, *M. N. R. astr. Soc.* **207**, 73
Wilkes B.J., Elvis M.: 1987, *Astrophys. J.* **323**, 243
Wills B.J., Browne I.W.A.: 1986, *Astrophys. J.* **302**, 56
Wills B.J., Netzer H., Wills D.: 1985, *Astrophys. J.* **288**, 94

Wills B.J., Wills D.: 1986, *IAU Symposium No. 119*, p.215. G.Swarup, V.K. Kapahi (Eds.)
Wilson A.S.: 1987, in *Star Formation in Galaxies*, Proceeding of a conference held at Caltech, Pasadena, June 16–19, 1986. C.J. Lonsdale–Persson (Ed.), p.675
Wilson A.S.: 1988, *Astron. Astroph.* **206**, 401
Wilson A.S: 1991, in *Physics of Active Galactic Nuclei*, Proceedings of the Conference held in Heidelberg, June 3–7, 1991. (Berlin: Springer), *in press*
Wilson A.S., Penston M.V.: 1979, *Astroph. J.* **232**, 389
Wilson A.S., Heckman T.M.: 1985, in: *Astrophysics of Active Galaxies and Quasi-Stellar Objects* Mill Valley: University Science Books. J.S. Miller (Ed.), p. 39
Wilson A.S., Baldwin J.A., Sun S.D., Wright A.E.: 1986, *Astroph. J.* **310**, 121
Wilson A.S., Ward M.J., Haniff Chr. A.: 1988, *Astrophys. J.* **334**, 121
Wolf E.: 1987, *Nature* **326**, 363
Wolf E., Foley J., Gori F.: 1989, *Journ. Opt. Soc. Am. A* **6**, 1142
Woltjer L.: 1959, *Astrophys. J.* **130**, 38
Yamauchi M., Piro L., Matsuoka M.: 1991, *Astrophys. J. in press*
Yee H.K.C.: 1980, *Astrophys. J. Letters* **241**, L133
Zamorani, G., *et al.*: 1981, *Astrophys. J.* **245**, 357
Zel'dovich Y.B., Novikov I.D.: 1964, *Sov. Phys. Dokl.* **158**, 811
Zepf S.E., Koo D.C.: 1989, *Astrophys. J.* **337**, 34
Zheng W., Binette L., Sulentic J.W.: 1990, *Astroph. J.* **365**, 115
Zwitter T., Calvani M., Bodo G., Massaglia S.: 1989, *Fund. Cosmic Phys.* **13**, 309